AN INVESTIGATION OF SWITCHING PHENOMENA IN AMORPHOUS SEMICONDUCTORS

by

John M. Robertson

Thesis presented for the degree of Doctor of Philosophy of the University of Edinburgh

February 1971

EX BIBL UNIV. EDINB GEN

ACKNOWLEDGEMENTS

I would like to express my appreciation for the help received from many of my colleagues in the Department of Electrical Engineering; also to thank Mr G. Angell, of the Department of Geology, who carried out the XRF analyses and Mr B. Flynn who helped to produce many of the thin film samples.

I am grateful to the Commissioners of the Royal Commission for the Exhibition of 1851 for providing me with a Research Fellowship.

Special thanks are due to Dr A. E. Owen, my supervisor, for his help and encouragement throughout this work; also to my wife for her support (moral and financial) and for typing this thesis.

SUMMARY

Switching occurs in many types of amorphous semiconductor but in this work the emphasis has been placed on devices made from chalcogenide glasses. There are two types of device: a memory switch and a threshold switch. The operating mechanism of the latter has been the subject of much controversy so most effort has been directed towards elucidating the mechanism involved.

Many theories and observations relating to switching have been published and the literature has been reviewed critically to assess mechanisms which may be applicable to chalcogenide glass switches. Only two processes, thermal breakdown and a space charge injection process appear to provide potential explanations of threshold switch behaviour. The experimental results obtained in this project were examined from the viewpoints of these two theories.

Switching devices must be made from thin films if low voltage working is required. When chalcogenide glasses are evaporated, dissociation occurs and the thin film composition differs from that of the starting material. The system AsTeSi was examined most extensively to establish the influence of evaporation technique on thin film composition and resistivity.

Threshold switching was examined in bulk glasses and in thin

films with both sandwich and coplanar electrode arrangements. In each case, the behaviour conformed to that predicted for reversible thermal breakdown. However, for thin film sandwich samples the explanation depends critically on the experimental observation that conductivity is field-dependent. Breakdown appeared to be localised and the switching and on-state characteristics were consistent with filament formation.

Memory switches were investigated briefly, but they share the same technology as threshold switches and threshold-type breakdown always preceeds memory switching.

CONTENTS

CHAPTER 1 INTRODUCTION

1.1. SWITCHING DEVICES

1.1.1. Classification of switching devices

When a high field is applied to some types of amorphous semiconductor, a rapid transition from a high resistance to a low resistance state occurs. This switching action has been most reliably observed in glasses of the chalcogenide type; those based on the elements S, Se and Te with additions of As, Ge and Si. The wide range of potential applications of switching devices has led to a great deal of interest in the basic properties of the chalcogenide glasses and the factors which affect switching performance. The work of this project was directed towards the latter.

Switches made from chalcogenide glasses are two-terminal devices and they have symmetrical current-voltage characteristics. The I - V relations may be classified as in fig. 1.1. into four basic types (1) :

a) A negative resistance device. There is an extended region of negative differential resistance. With a suitably large series resistor a quasi-stable operating point can be achieved in the negative resistance region.

b) A monostable or threshold switching device. There is no stable operating point between the high and low resistance

Fig. 1.1

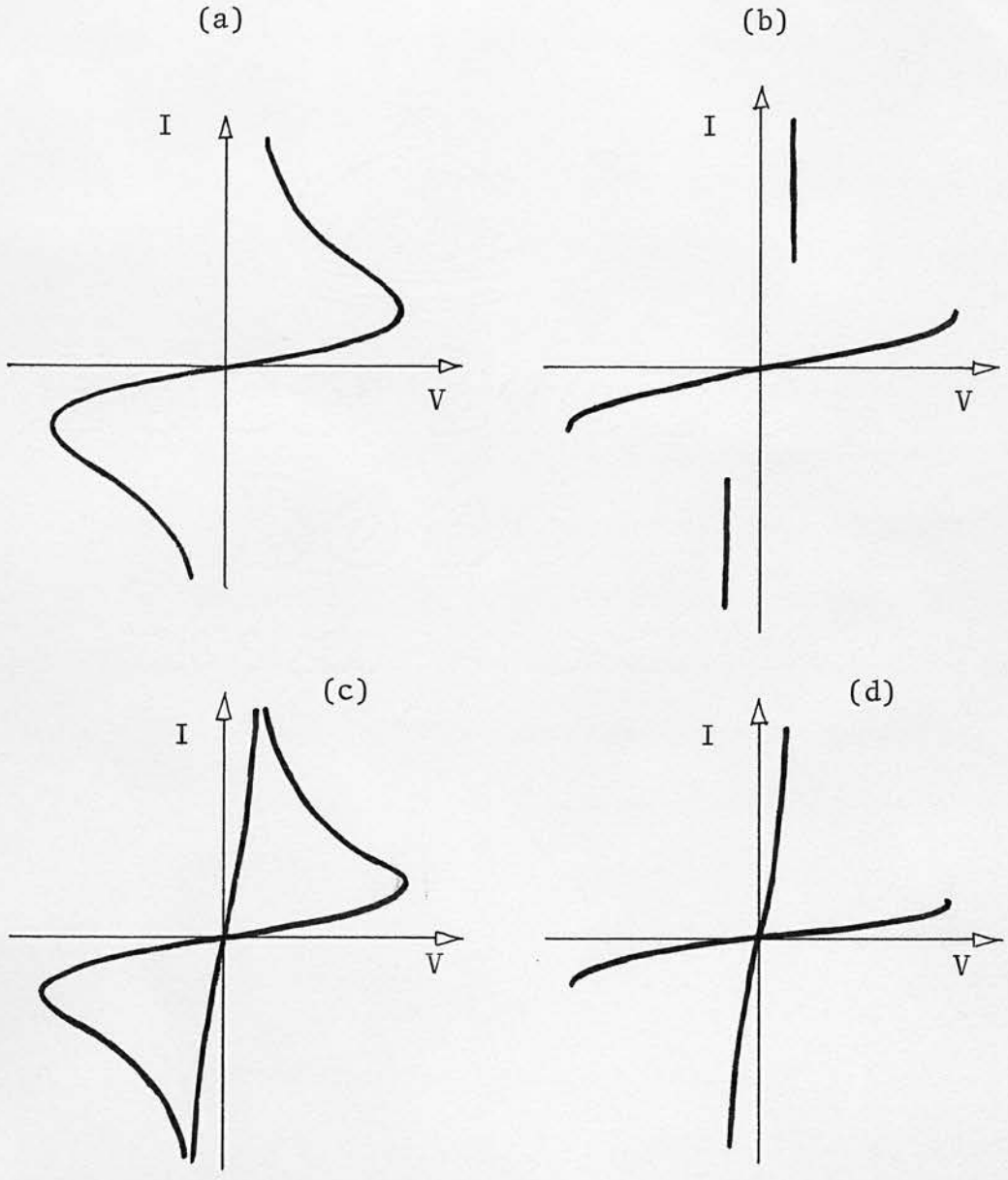

Basic switching characteristics.

states.

c) A negative resistance device with memory. This behaves as type a) but in the high current region, a stable low-resistance or on-state is established. This is maintained even when the supply voltage is reduced to zero.

d) A switching device with memory. There are two stable states and a direct transition occurs from the high resistance to the low resistance states.

The types b) and d) are those observed in thin films of chalcogenide glass and they are considered in detail in the following two sections.

The negative resistance characteristics of fig. 1.1. are current controlled (CCNR). Their dual is voltage controlled negative resistance (VCNR) which is associated with an I - V relation of the type shown in fig. 1.2. Characteristics of this form have not been observed with chalcogenide glasses, but another type of amorphous semiconductor, silicon monoxide, does exhibit VCNR and this is discussed in section 3.5.6.

1.1.2. Threshold switching behaviour

Detailed I - V characteristics of a monostable or threshold switch are shown in fig. 1.3. Only the positive quadrant is shown but the device is not polarity-sensitive. The off-state is characterised by a high resistance and below the threshold or switching voltage, V_{th}, the device behaves as a stable resistor. At voltages below roughly 0.4 V_{th} the characteristic is ohmic. Between 0.4 V_{th} and V_{th}, the current

Fig. 1.2

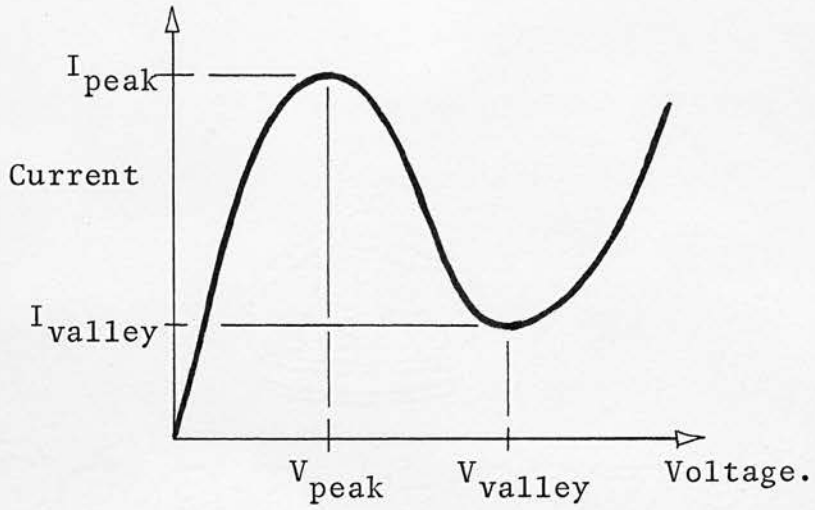

VCNR Characteristic.

Fig. 1.3

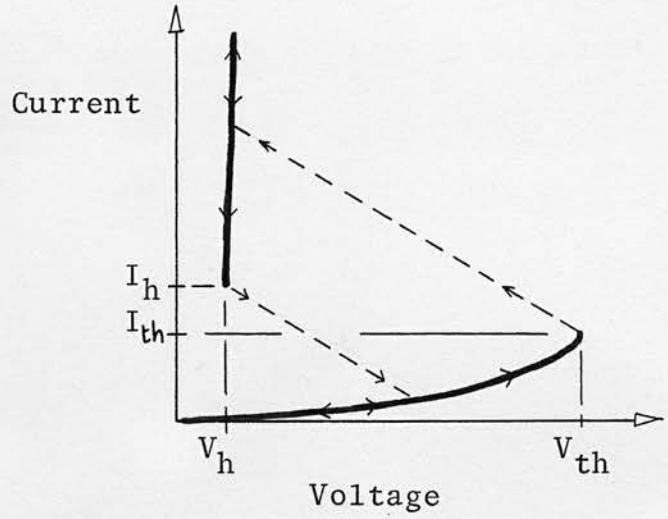

Threshold switch characteristic.

rises exponentially with voltage. Switching is very rapid, typically 1 ns or less, and a new stable operating point is achieved where the load line intersects the on-state characteristic.

The on-state has a dynamic resistance close to zero, i.e. the current rises almost vertically and the holding voltage, V_h, is almost constant. However, the on-state can only be maintained when the current exceeds a minimum holding level, I_h. If the current falls below I_h, the device switches off along the load line and regains the high resistance state. Thus the device always returns to the off-state when the voltage supply is reduced towards zero so the basic mode of operation is that of a monostable device.

When a square voltage pulse is applied and the pulse amplitude is greater than V_{th}, switching occurs, but there is a delay time, t_d, during which the device remains in the off-state. For typical thin film devices t_d is about 1 μs and the switching time, $t_s \leq 1$ ns. The delay time decreases rapidly as the voltage pulse amplitude is increased.

The off-state I - V characteristic is affected by the chalcogenide glass composition, resistivity, electrode area and separation, ambient temperature, electrode metal, the voltage duty cycle and waveform shape. By contrast the holding voltage and current are only slightly affected by any of these variables. This means that if the device is required to meet a specified condition, e.g. a certain on : off resistance or capacitance ratio, then it must be achieved by manipulation of the off-state characteristic.

1.1.3. Memory switching behaviour

In the off-state, a memory switch behaves very similarly to the threshold device. Memory glass compositions tend to have lower resistivity than threshold glasses so the off-state resistance may be lower, but the I - V relationship below V_{th} follows the same ohmic then exponential dependence as in the case of threshold switches.

Switching occurs along the load-line to the on-state operating point (fig. 1.4.). However, a forming time, t_f, of 1 - 10 ms is needed to establish the on-state. If the voltage supply is reduced after a shorter period than t_f, the device behaves as a threshold switch and when the current falls below I_h, it returns to the off-state. If the device is held in the on-state for a period longer than t_f, then a non-volatile memory state is established and the device remains in the conducting state even when the supply voltage is reduced to zero. Application of a high current pulse returns the device to the off-state.

The memory switch is a relatively slow device on account of the time needed to change state, but interrogation of the device to ascertain which state it is in is limited only by the RC time constant associated with the device. This time can be very short, of the order of 1 ns, so the memory switch is best suited to applications where a change of state is rarely required, i.e. it is a read-mostly memory (RMM) element.

Fig. 1.4

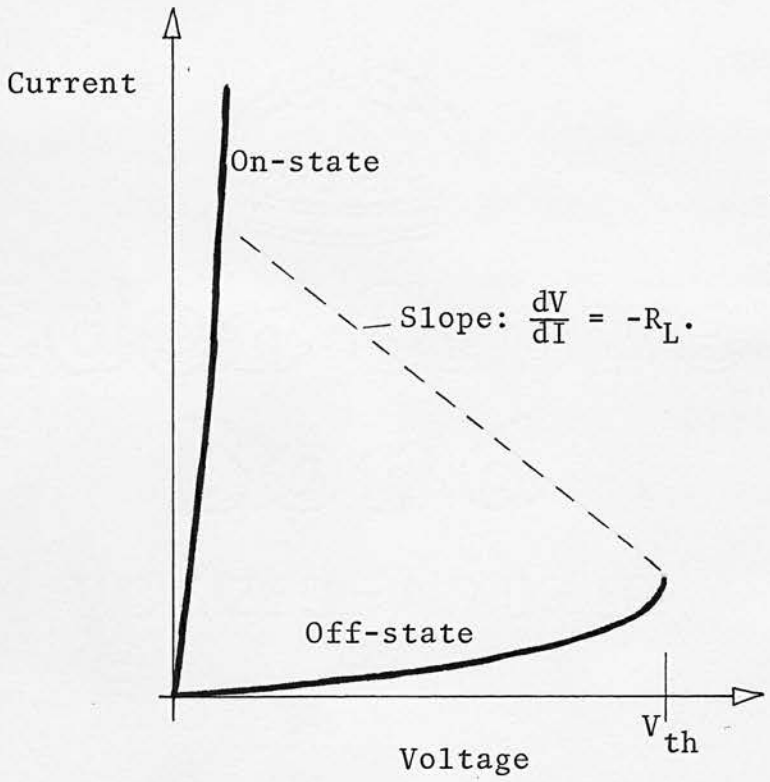

Memory switch characteristic.

1.2. APPLICATIONS

1.2.1. Applications of switching devices

A great deal of interest in amorphous switches has arisen because they represent a new class of semiconductor device. They do not depend on controlled doping of a very pure and perfectly ordered crystal as in the case of silicon or germanium. Indeed initial experiments with chalcogenide glass switches suggested that the device characteristics were not dependent on material purity. More recent work has confirmed this general feature but has also shown that resistivity can be very sensitive to composition changes and that some impurities, such as oxygen, can have a strong influence.

Most experimental work on chalcogenide switches has been done with discrete devices. They have proved very adequate for research into the operating modes of the devices. However, it is very unlikely that any new type of electronic device will succeed commercially unless it can fulfil two basic conditions:

1. It must be compatible with silicon integrated circuits. For most purposes this means low voltage, low current operation.
2. The process used to make the switches must be capable of producing large numbers of identical devices with only a few processing steps.

The low voltage requirement defines the electrode separation. In thin samples, switching occurs at a field value of about 10^7 V.m^{-1}. The electrodes therefore must be only 0.5 - 1μm apart. Films of this

thickness can be readily deposited by evaporation in a vacuum. This technique can also be used to produce large numbers of devices on a single substrate so it represents a potentially good production technique. Evaporation was used extensively in this project and the basic features of the experimental work are described in chapter 5.

Both memory and threshold switches are two-terminal devices. This makes their geometrical layout very simple: an electrode above and below a glass film or two surface electrodes separated by a narrow gap. The simple geometry means that it is easy to incorporate the devices into an array with access by X and Y strips to each electrode. With any two-terminal device however, the bias and control functions of the supply voltage are inextricably mixed. In turn this demands that the device characteristics, and in particular V_{th}, be repeatable from one device to another and also throughout the life of each device. Thus the mechanism by which switching is initiated should be elucidated and controlled.

Many possible applications have been suggested for amorphous switches but in the following sections only the most general applications are considered. They also represent the circumstances in which the switching devices are likely to be used most widely.

1.2.2. Threshold switches: application to displays

The cathode ray tube is very widely used as a cheap and efficient component of display systems. However, it does suffer from disadvantages of size, ruggedness and limited life and there is enormous potential for a solid state equivalent. One approach to this problem has been to use a threshold switch in series with an electroluminescent cell and a current limiting resistor (2) as shown in fig. 1.5.

The electroluminescent cell may be treated as a capacitor with a high leakage current. If the capacitor is initially uncharged and the a.c. supply voltage is just below V_{th} then almost all the supply voltage is dropped across the switch - assuming it has a higher (off-state) resistance than that of the resistor or the electroluminescent cell. There is then no light output. If the capacitor is initially charged and the supply voltage reinforces the voltage on the switch, then switching will occur when V_{th} is exceeded. The capacitor discharges and charge builds up with opposite polarity. However, if the leakage resistance of the capacitor is too high to allow the switch holding current to flow after the capacitor has been charged,then the switch will return to the off-state. In the next half cycle the process is repeated but with opposite voltage polarity. Thus there is a level of supply voltage where bistable operation may occur; the electroluminescent cell may or may not emit light depending on the initial conditions.

Small experimental alphanumeric displays have been made. The basic unit shown in fig. 1.5. (but without the variable resistor) exists at

Fig. 1.5

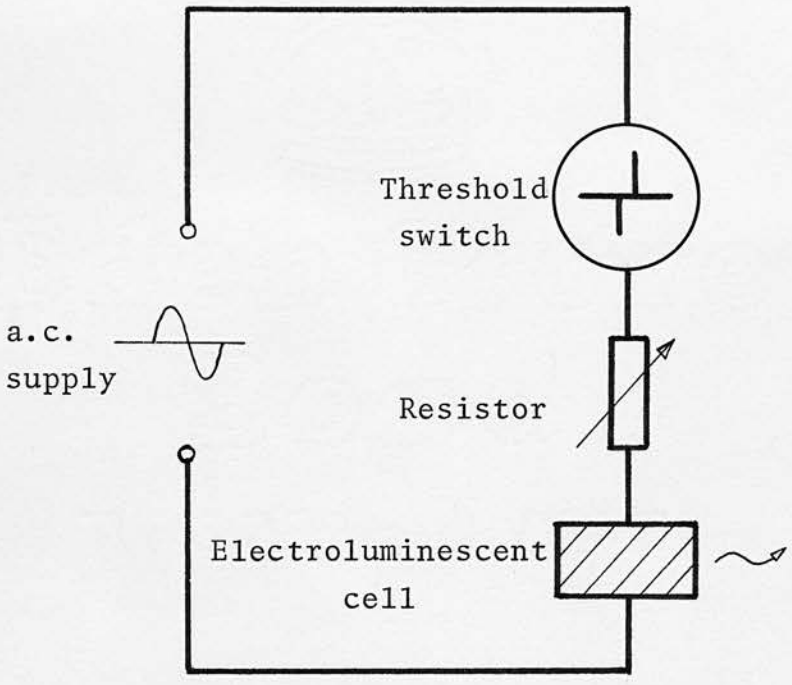

Display element incorporating a
threshold switch.

each crosspoint of an array and a constant amplitude a.c. signal is applied to each unit. To switch on any element, extra pulses are applied along the appropriate X and Y lines so that the voltage on the required threshold switch exceeds V_{th}. Switch-off is accomplished in a similar way by applying a pair of pulses to reduce the voltage across a device to the point where even with the potential on the capacitor, the switch cannot fire.

The whole process is an attractive one for obtaining solid state displays, but one of the principal difficulties lies with the electroluminescent material. Doped ZnS phosphors have been used; they are cheaply and easily deposited over large areas but operate at high voltages, usually 100 - 200 volts. Thus high voltage threshold switches are required. These are difficult to prepare in thin film form and have a relatively slow switching speed. Films about 25 μm thick can be prepared by a thick film screen-printing and firing process and this may prove to be the most efficient technique to use for the production of high voltage switches.

Other applications which have been investigated for threshold switches have been linear amplifiers and 3-level logic systems (3).

1.2.3. Wire-access memory arrays

Semiconductor memories have been extensively developed to provide cheap and reliable memory elements. The two basic types have serious disadvantages; either they are volatile in which case all information is

lost if the power is shut off, or else they are of the read-only type where the information pattern is determined by the metallization layer which interconnects the devices. This is non-volatile, but there is a commitment to the memory pattern when the unit is made and this may be expensive for small numbers.

A memory array has been developed which overcomes the greatest disadvantage of the read-only memory (ROM) (4). By using amorphous memory devices, the whole array is programmable but since the write/erase sequences are slow, the unit is envisaged as a read-mostly memory (RMM).

The RMM comprises a simple X - Y array. At each crosspoint there is a memory switch and an isolating element to eliminate spurious shunt paths between crosspoints. The isolation element may be either a threshold switch or a simple p-n diode. Operation with the threshold switch is rather slow (access time several μs) and the technology of the device has not yet been fully evaluated. Diodes on the other hand only limit the interrogation time by the RC product in the devices and access lines. Access times of about 20 ns have been achieved in a 16 x 16 array.

The use of isolating diodes allows one address line, isolation between the lines and the diodes themselves all to be diffused into a slice of silicon. The amorphous semiconductor is then deposited over the diode top contact and a final address line applied. In this form RMM arrays have been the first units incorporating amorphous switching devices to be seriously evaluated.

1.2.4. Electro-optic access memories

One of the most important factors which limits the packing density of the RMM described in the previous section is the space needed for access lines and their isolation. One of the attractive features of amorphous switches is that optical techniques can be used for read, write and erase functions of the memory and potentially fast-access high-density memories are possible.

To change the state of a memory switch, a controlled amount of energy must be supplied over a specified time period. The time-energy conditions derived for electrically alterable devices (4) are shown in fig. 1.6. To each switch-on condition, there corresponds a switch-off condition (marked by X). It is also possible to achieve the write and erase (switch-on and switch-off) energy conditions from a laser. The operation of memory switches is reviewed in chapter 4, but clearly with laser controlled systems high storage capacity should be possible, perhaps up to 10^{10} bits. m^{-2}.

There are several possible techniques which may be used to read the information pattern of the memory. The reflectivity of chalcogenide glass differs between on and off states and so also do the near infra-red transmission characteristics. Another process which has been suggested is analagous to the Xerox process. If a large enough resistance change occurred between on and off states an electrostatic charge pattern could be stored on a chalcogenide glass plate and used as the basis for a Xerox-type printing operation.

Fig. 1.6

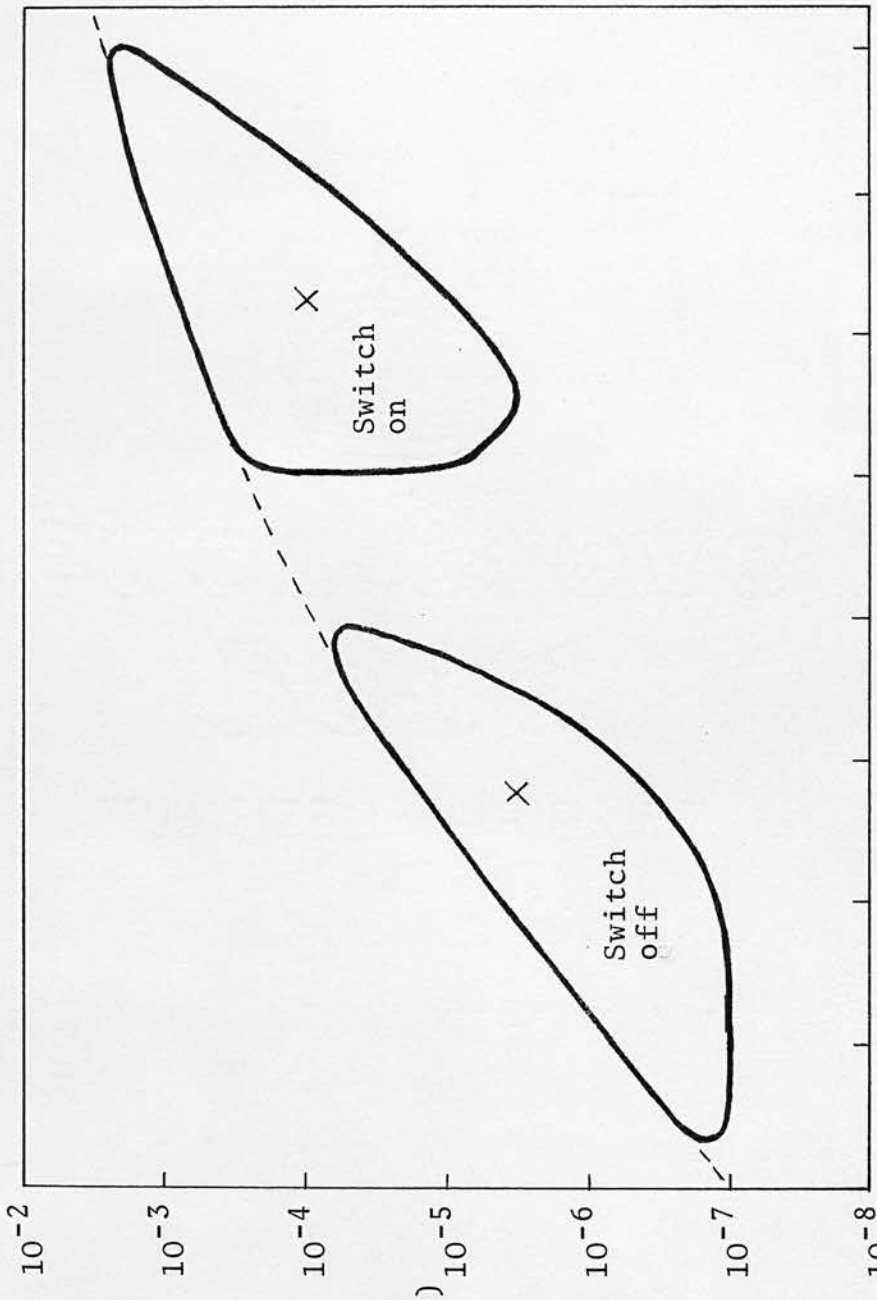

Energy and time conditions for memory switching.

1.2.5. Comment on device evaluation

There are many other applications of amorphous switches apart from the three considered in the previous sections. However, if any new type of device is to make much progress commercially it must first of all have a unique application, i.e. not duplicate any existing device. Only in this way is it possible to justify the large expenditure which is necessary to establish any new technology.

Amorphous switches have several unique features; they do not depend on perfect structural order and hence the need for tedious and difficult crystal growing; they are not sensitive to minor impurities; there are no junctions, only simple 2-terminal devices and most metals appear to provide good ohmic contacts. Against this, however, must be set the considerations that from the viewpoint of solid state physics, chalcogenide glasses are poorly understood; there is little depth of reliable experimental data and the precise mechanisms responsible for switching are the subject of much controversy.

Against this background, chalcogenide switches only make sense commercially in terms of unique and widespread applications which are not likely to be realized by current semiconductor technology. It is only in this way that sufficient time will be gained to assess amorphous switches in detail.

1.3. ORGANIZATION OF THIS PROJECT

Switching has been observed in a large number of different materials. In chapter 3 the possible mechanisms which can give rise to switching are reviewed. In most cases the conditions for a particular mechanism to be applicable are fairly clear, e.g. it may require a certain band structure or perhaps fields in excess of 10^8 V.m^{-1}. There are also experimental variables such as ambient temperature and device geometry which have an influence on switching and their affects can also be derived for each possible mechanism and compared with experimental results.

A great deal of interest has been aroused in amorphous switching devices in the past 2 - 3 years and consequently much parallel but independent experimental work has been done. Where this applies to the work done as part of this project, it is indicated as such. In the interpretation of experimental data, many of the concepts are well developed but have not been previously applied to amorphous semiconductors. The historical development of switching and the present state of the art are reviewed in chapter 4 in terms of the possible mechanisms considered in chapter 3.

The technology associated with the production of amorphous switches is not well defined nor is it described in any detail in the literature. Chapter 5 describes the investigation made into methods of preparing thin films of chalcogenide glass, composition and contact effects and other factors which influence film resistivity. This basic

work is inherent in the establishment of any new technology in a research group but the understanding and control it gives is essential for gaining meaningful experimental data on devices.

Most controversy over the operating mechanism of switches concerns the threshold or monostable device, therefore most experimental work has been concentrated on the threshold switch: chapter 6. The experimental work on the memory switch is treated in chapter 7. An alternative description of switching is that the mechanism by which current is limited in the off-state changes very rapidly to the current-limiting process which characterises the on-state. They may simply be different aspects of the same conduction mechanism or they may be completely different. The experimental work was aimed at resolving this question and identifying the mechanism(s) involved.

CHAPTER 2 GLASSES, IN PARTICULAR THE CHALCOGENIDES.

2.1. GENERAL FEATURES OF GLASSES

Bulk glasses are made by fusing together appropriate elements or compounds and allowing the melt to cool rapidly so that no crystallization occurs. This requires a progressive increase in viscosity as the melt is cooled and no discontinuous changes in first-order thermodynamic properties such as volume, heat content or entropy.

Transformation from properties which are characteristic of those of a liquid to those of a solid occurs over a temperature range about a temperature, T_g, which is known as the glass transition temperature. Unlike the thermodynamic melting point of a crystal (T_m), T_g is not a uniquely defined temperature; it depends on the cooling rate during glass formation. In general, the glassy state may be considered as unstable and the ease with which devitrification can occur depends both upon the glass composition and the thermal conditions under which the glass was formed.

Since the glassy state is continuous with the liquid state, it has essentially a disordered 'liquid-like' structure. During the quenching process the relative atomic positions of the melt are 'frozen-in'. Direct information about short range order in glasses is derived from X-ray, electron or neutron diffraction. The volume which interacts with

the incident radiation is much greater than the volume over which some order exists and the diffraction pattern corresponds to that of an isotropic body. All structural information must therefore be presented as a radial distribution function. This gives the probability of finding an atom at a given distance from an arbitrary central atom. The distribution function for vitreous As_2S_3 is shown in fig. 2.1. (5). The first peak represents nearest-neighbours to the (arbitrary) reference atom. It is well-defined and at a distance which to a first approximation is the same as that for nearest-neighbour separation in the corresponding crystalline material. The second and subsequent peaks of the distribution function gradually become less distinct and merge with the parabola $4\pi r^2 dr$ which is characteristic of a random structure.

The original description of the 'random-network' model of glass structure was made by Zachariasen in 1932 (6) for the case of silicate glasses. The atoms in the glass form an extended 3-dimensional network but unlike the perfect periodicity of a crystal, there are distorted bond lengths and angles in a glass so that beyond the first few coordination shells, all regularity is lost. A 2-dimensional representation of this 'random-network' model is shown in fig. 2.2. The hypothetical compound M_2X_3 may exist as a crystal or as a glass with a triangle MX_3 as the basic unit in each case. The lack of any long-range periodicity in a glass also means that it is a structure which can be formed for a wide range of compositions. The disorder shown in fig. 2.2.(b) is configurational. With multicomponent glasses another

Fig. 2.1

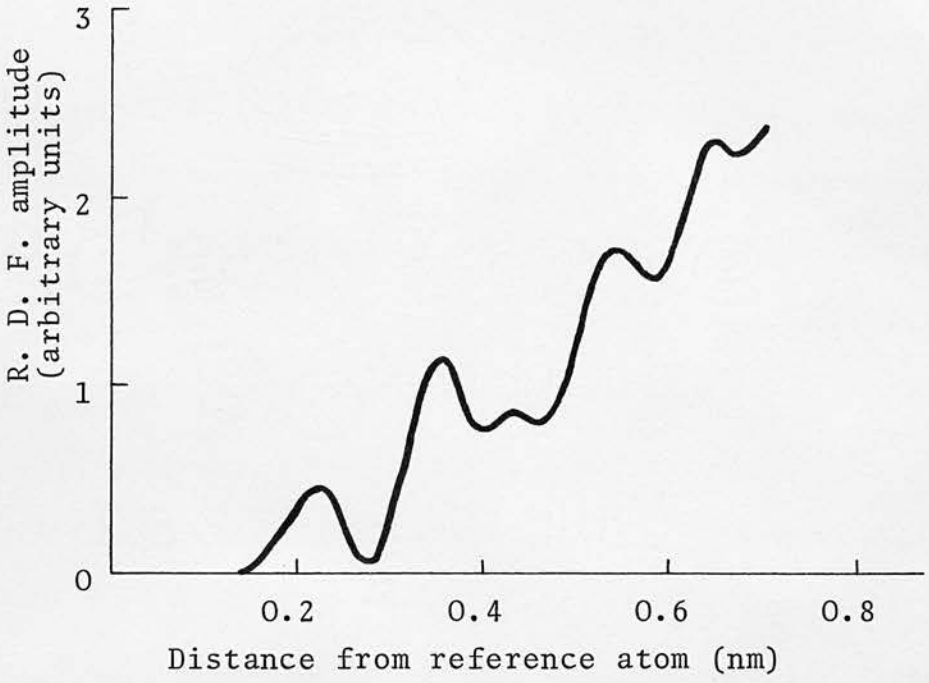

Radial distribution function for amorphous As_2S_3.

Fig. 2.2

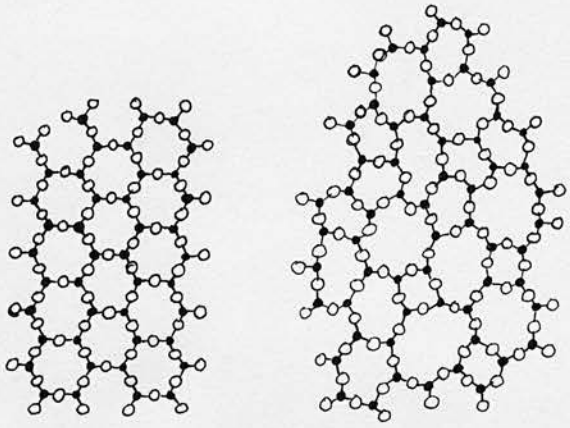

(a) Crystal (b) Glass

2-dimensional representation of crystal and glass structures.

degree of disorder may be introduced by local composition differences.

Although the 'random-network' representation of fig. 2.2. serves as a basic model for glass structure, it is nevertheless possible to recognise several types of local order in glasses, e.g. tetrahedra in $CdGeAs_2$, layers in As_2Se_3 and rings and chains in Se. In multicomponent glasses there is also the possibility of metastable separation (liquid-liquid or liquid-crystal) into two or more phases (7).

Disordered materials can be produced by evaporation. In terms of atomic arrangement they are amorphous and probably very similar to materials of the same composition produced by quenching from a melt. However, to preserve any distinction, evaporated films are described as 'amorphous' and the terms 'glassy' or 'vitreous' are applied to materials which have a specifiable relationship to the liquid state.

The common glasses such as those based on simple oxides, e.g. Na_2O, CaO and SiO_2, are ionic conductors; the charge carriers are the small relatively mobile alkali ions, e.g. Na^+. The glasses may therefore be considered as solid electrolytes. Electronic conduction is observed in the variable-valency transition metal oxide glasses and in chalcogenide glasses. Switching has been observed in both types of glass but the work of this project is based on chalcogenide glasses and they are considered in detail in the following sections.

2.2.1. Composition of chalcogenide glasses

The chalcogenide glasses are formed from compounds of S, Se and Te (the chalcogens) with a variety of elements, e.g. P, Sb, Bi, Tl, Pb, Ge and Si. In the binary systems As - S and As - Se, the compounds As_2S_3 and As_2Se_3 readily form glasses which may be regarded as prototypes for the whole range of chalcogenide glasses. Other binary glass-forming systems are: Si - S, Ge - S, Ge - Se, Si - Te and Se - I. An even larger number of ternary glasses can be formed. Fig. 2.3. shows some of the ternaries in which glass-formation is known and indicates the approximate extent of the glass-forming region for each. If the size of the glass-forming region is taken as a measure, the differences in tendency towards glass-forming ability for the different elements are (8):

S > Se > Te

As > P > Sb

Si > Ge > Sn

When four or more components are considered, the range of compositions clearly becomes very large.

Most chalcogenide glasses can be prepared by cooling from the melt. It may be necessary to melt the glass in an inert atmosphere or under vacuum to avoid oxidation of the component elements. The glass-forming region can be extended by very rapid cooling techniques or by deposition from the vapourphase by techniques such as evaporation or sputtering, e.g. As_2Te_3 is amorphous when evaporated, but only very small quantities can be prepared in the glassy state by quenching. However, if As_2Te_3

A	B	C																			
		Ia			IIa			IIIa				IVa		Va				VIa		VIIa		
		Cu	Ag	Au	Zn	Cd	Hg	B	Ga	In	Tl	Sn	Pb	P	As	Sb	Bi	Se	Te	Cl	Br	I
As	S	X	X	X	X	X	X		X	X	O	X	X	X		▨	X	●	▨	X	▨	●
	Se	O	O	X	O	O	O	O	X	X	▨	O	X	▨		▨	X		▨			▨
	Te										▨										X	▨
Ge	S				X				X	O		X		●	●				X			
	Se					X				X	O	X	X	▨	●	▨	X		X			
	Te													O	▨							
Si	S															▨						
	Se														▨	▨						
	Te													▨	▨							

Key: X very small region
O small
▨ moderate
● large.

Glass formation in the ternary system A-B-C.

Fig. 2.3

is alloyed with 20% or more of As_2Se_3, it can easily be made as a bulk glass.

Details of the glass-forming regions of the bulk glasses used in this project and the problems associated with their evaporation are given in chapter 5.

2.2.2. Electrical properties of chalcogenide glasses

The resistivity of a chalcogenide glass depends on its composition but a very wide range of values exists: from $10^{14}\,\Omega.m$ for As_2S_3 to $10\,\Omega.m$ for $As_2Te_3.Tl_2Se$. From a device point of view such a resistivity range is very useful since it means that the device characteristics can be tailored to a particular application by selection of a suitable glass composition. Resistivity changes steadily with composition. In the system As_2Te_3 + Si which is discussed in detail in chapter 5, the resistivity increases steadily by one order of magnitude for each 7% silicon added up to about 45% Si which is the limit of the glass-forming region.

See p. 26

The chart in fig. 2.4. shows typical glass compositions which are required for a specified resistivity value (8). In general, resistivity tends to decrease when larger atomic weight elements are used, e.g. Ge in place of Si or Te in place of Se.

Ionic effects may be present at high temperatures but at normal ambient values there is no evidence of ionic transport in chalcogenide glasses (9).

Fig. 2.4

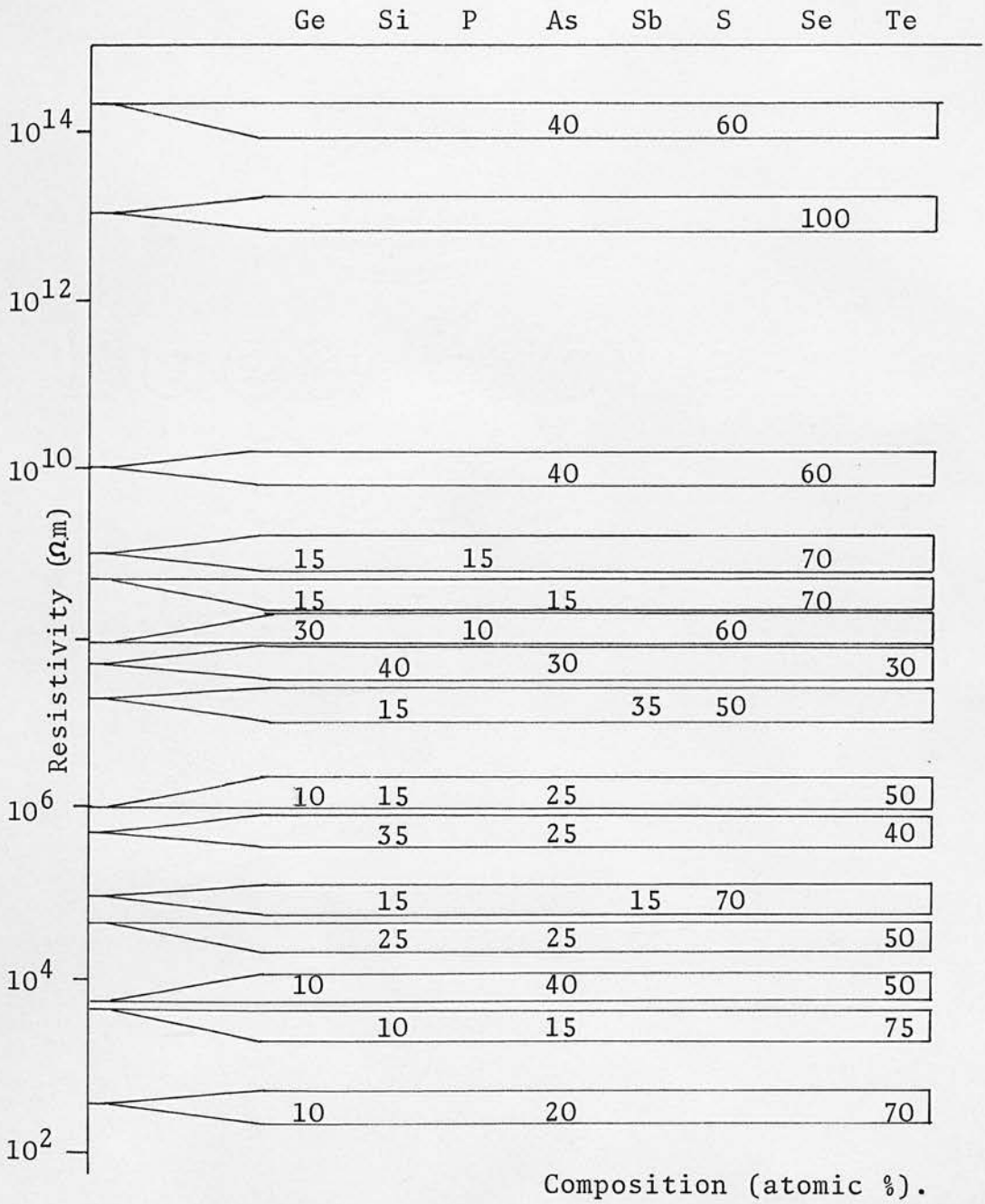

Resistivity of some chalcogenide glass compositions.

Conductivity increases with pressure and the occurrence of photoconductivity, a small but measurable Hall-effect and a thermoelectric effect, all indicate that conduction is predominantly due to the movement of electrons and/or holes. The sign of the charge carriers is in some doubt. The thermoelectric power has been measured in many chalcogenide glasses and always found to be positive. Its magnitude is of the order of $mV.K^{-1}$ which is typical for crystalline semiconductors. The Hall effect has been measured in a few of the more conducting chalcogenide glasses and has always been found to be negative. There has not been any adequate explanation why the sign should be different from that of the Seebeck coefficient. The mobility values derived from Hall coefficients are low - around 10^{-6} $m^2.V^{-1}.s^{-1}$. Measurement of a trap-limited drift mobility in chalcogenide glasses is difficult, but a low-field value of 5.10^{-11} $m^2.V^{-1}.s^{-1}$. has been estimated for holes in As_2Se_3 (10).

2.2.3. Physical and optical properties

Optical absorption in chalcogenide glasses is characterised by an absorption coefficient, α, which increases exponentially with photon energy. Saturation occurs at high values of α ($\sim 10^6$ m^{-1}.) The upper limit of the exponential tail can be used to define an optical energy gap E_{opt}. For photon energies greater than E_{opt}, the experimental absorption data fit the standard formula for indirect-allowed transitions in semiconductors (11). This implies a relaxation of the momentum

(k)-conservation rule, but not that for energy conservation. Values of E_{opt} change steadily with composition, e.g. As_2Te_3 0.95eV, As_2Se_3 1.90eV and As_2S_3 2.65eV (all measured at $\alpha = 10^6$ m^{-1} (12)).

The dielectric constant depends on glass composition, but typical values lie between 10 and 20. The density varies between 4 and 6×10^3 $Kg.m^{-3}$. The range of values of thermal conductivity, κ , is 0.3 - 2 $W.m^{-1}.K^{-1}$ (13) and of heat capacity, C, $1 - 3 \times 10^6$ $J.K^{-1}.m^{-3}$.

The glass transition temperature, T_g, is particularly important since it defines the upper temperature limit to which a glass can be taken without any drastic change in its structure or properties. A detailed map of T_g values for bulk glasses from the ternary system As - Te - Si is shown in fig. 5.1. For this system, values of T_g between 500°C and 120°C can be obtained. This serves to illustrate the general feature of all multicomponent chalcogenide glasses; a wide range of compositions is possible and by suitable choice of glass, any required properties (within a reasonably wide range) can be obtained.

2.3. CONDUCTION IN CHALCOGENIDE GLASSES

The low-field d.c. conductivity of nearly all chalcogenide glasses obeys the equation:

$$\sigma = \sigma_0 \exp\left(-\frac{\Delta E}{kT}\right) \qquad \ldots\ldots 2.1$$

The activation energy, ΔE is usually in the range 0.4 - 0.8 eV and the pre-exponential term, σ_0, in the region 10^3 - 10^4 $(\Omega.m)^{-1}$. Equation 2.1 is characteristic of that for an intrinsic semiconductor with a band gap $2\Delta E$. In general, the conductivity of chalcogenide glasses is not sensitive to impurities and this also suggests intrinsic conduction.

The effect of structural disorder in the band model for an amorphous semiconductor is to introduce 'tails' of localized states in the gap above and below the conduction and valence bands. Thus only a pseudogap exists as shown in fig. 2.5.(a). In simple glasses, a strong local atomic ordering may persist beyond the first coordination sphere and the effects of broken bonds, local inhomogeneities, etc., would be to introduce well-defined defect energy levels as in the case of a crystal. This is shown in fig. 2.5.(b). With multicomponent chalcogenide glasses, compositional as well as configurational disorder exists. This has the effect of broadening the tails of localized states and they may overlap appreciably as shown in fig. 2.5.(c). Structural defects are less probable and when they do exist they are less well defined spatially, so the tails may be taken to be approximately monotonic.

The Fermi level is fixed by the requirement that the number of empty states in the tail of the valence band above the Fermi energy must

Fig. 2.5

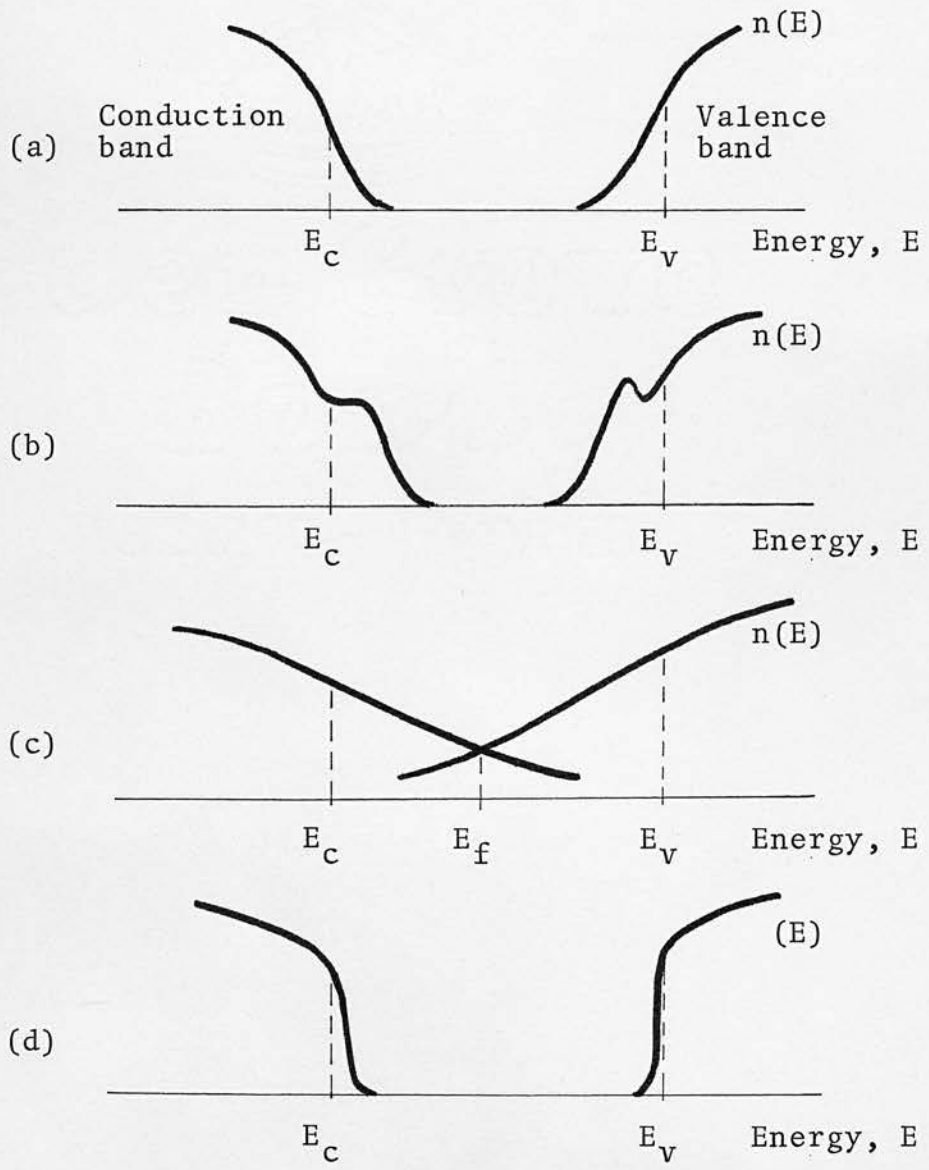

Energy diagrams for the development of the mobility-gap model for conduction in amorphous semiconductors.

equal the number of occupied states in the tail of the conduction band. Although there may be detailed differences in the shapes of the conduction and valence band tails, the Fermi level is assumed to be located approximately in the middle of the'gap' and good compensation exists.

The overlapping tails mean that a large density of states can exist at the Fermi level. This may be as high as 10^{25} - 10^{26} states.m^{-3}.eV^{-1}. (14) and consequently the depletion or enhancement layer depth around any source of charge imbalance is very small, e.g. 2 - 3 nm. When contacts are made to a glass, the tunnel current density through such a thin barrier region is very large and all metals should act as ohmic contacts (provided there is no chemical reaction or diffusion).

The model developed in fig. 2.5.(c) has a continuous density of states across the 'gap'. To reconcile this with the widespread applicability of equation 2.1, Cohen et al. (15) have introduced the concept of a mobility gap. In crystalline semiconductors there is a well-defined band edge at the critical energies E_c and E_v. In amorphous semiconductors, however, the states change their character at E_c and E_v from extended to localised. Well above E_c and below E_v, transport is characteristic of band conduction. A mean free path can be defined and its lower limit, the electron quantum wavelength, sets a lower limit to the carrier mobility of about 5.10^{-4} $m^2.V^{-1}.s^{-1}$. In the localized states, conduction is by phonon-assisted hopping and the mobility is about three orders of magnitude lower than that in the conduction and valence bands. The mobility edge as proposed by Cohen is shown in fig. 2.5.(d)

and the sharp mobility change occurs within an energy range kT about E_c and E_v.

In the region in between, transport is considered to involve extended (band) states in which the mean free path tends to the limiting value determined by the average interatomic spacing. The carriers are continuously under the influence of scattering centres so that the process is characteristic of Brownian motion (14).

The equation for conductivity in an intrinsic semiconductor given by equation 2.1 holds over the approximate temperature range 200 - 500 K. Beyond these limits, however, there is some departure from equation 2.1. This is shown in fig. 2.6. The curves marked 'Male' and 'Croitoru' are those measured by these authors for the composition $As_{30}Te_{48}Ge_{10}Si_{12}$ (16) (17). Fagen's data is for a glass of similar room-temperature resistivity but with composition $As_{35}Te_{28}S_{21}Ge_{16}$ (18). There is no discontinuity in conductivity at the softening point of either glass.

For temperatures above room temperature, Male's results have been replotted in fig. 2.7. as $\log \sigma$ against temperature. For comparison, an equation with a constant activation energy is also shown. Up to 500 K, conductivity accurately described by an equation of the form:

$$\sigma = \sigma_1 \exp(aT) \qquad \ldots\ldots 2.2$$

where σ_1 and 'a' are constants. Alternatively, the conductivity may be described in terms of its room temperature value, σ_a, and the temperature rise $\Delta T = T - T_a$:

$$\sigma = \sigma_a \exp(a \Delta T) \qquad \ldots\ldots 2.3$$

Fig. 2.6

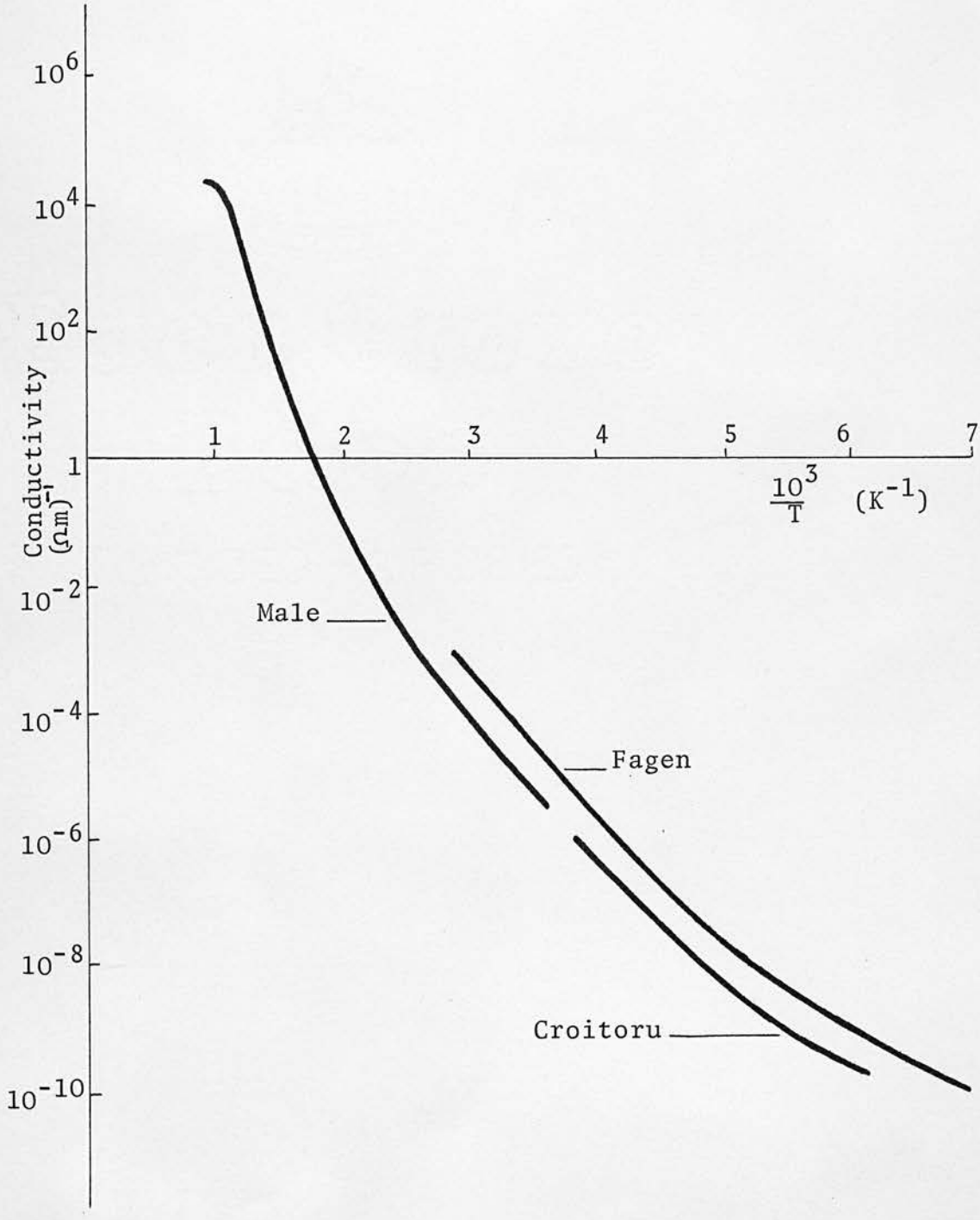

Variation of conductivity with temperature in chalcogenide glasses.

Equation 2.3 is shown in fig. 2.7. with a = 0.04.

When temperatures in excess of 100°C are encountered, equation 2.3 provides a more accurate description of the conductivity - temperature relation than equation 2.1. Equation 2.3 is also more convenient to use for analysis since it can be easily integrated. On occasions, however, it is useful to retain the concept of an activation energy so both equations 2.1 and 2.3 are used in later sections. For small temperature increases they can be used interchangeably.

The a.c. conductivity of chalcogenide glasses increases with frequency. This is most marked for high resistivity samples, e.g. as shown for As_2S_3 in fig. 2.8. (11). Up to about 1 MHz, σ increases as $\omega^{0.8}$. This is good but not unambiguous evidence for hopping between a random distribution of sites. The influence of frequency-dependent conductivity is not very great in glasses which are used for switching devices. Their d.c. conductivity is too high to be affected by the a.c. component and device operation is limited to frequencies below about 1 MHz by the delay and recovery times of the switching cycle. A hopping conductivity mechanism may, however, be responsible for the decrease in activation energy of conductivity at low temperatures (fig. 2.6.). If devices were operated in that temperature region, then it is also likely that their off-state resistance would be dependent on the measuring frequency.

Fig. 2.7

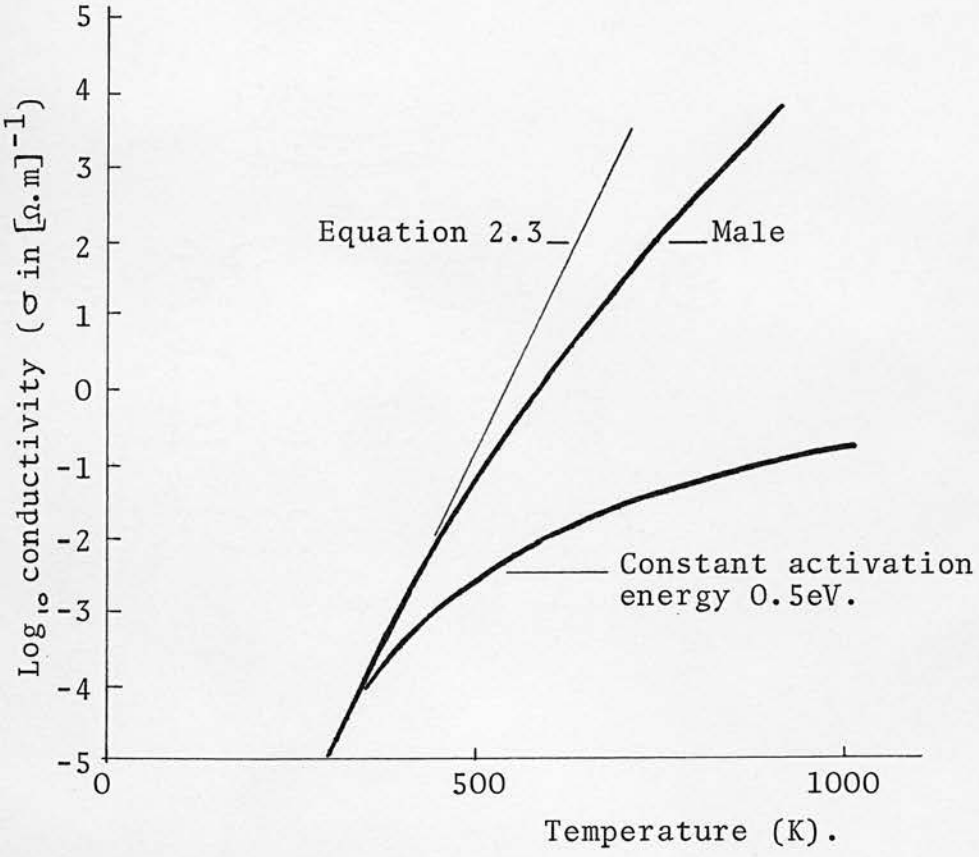

Comparison of conductivity-temperature expressions with Male's experimental results.

Fig. 2.8

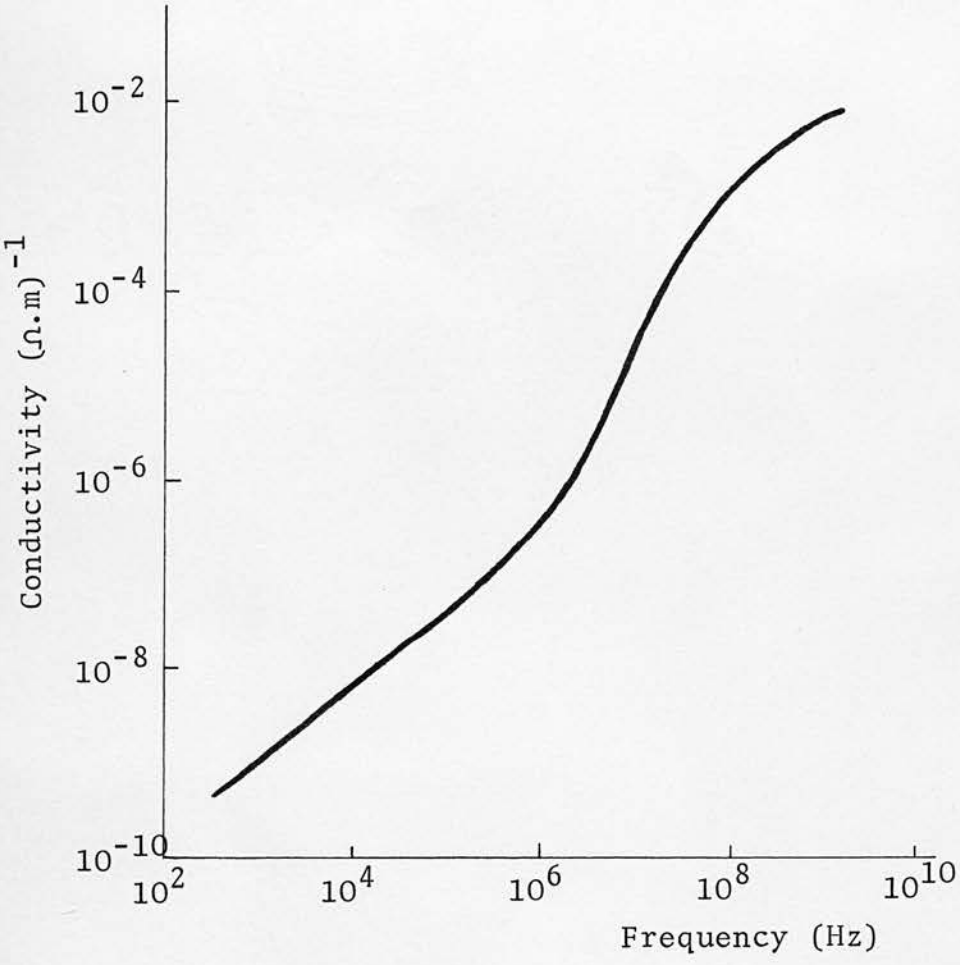

Frequency variation of conductivity for As_2S_3.

CHAPTER 3 MECHANISMS WHICH COULD BE USED TO EXPLAIN SWITCHING

3.1. SWITCHING AS A FORM OF DIELECTRIC BREAKDOWN

All dielectrics show some form of breakdown under high field conditions. Usually breakdown is catastrophic and permanent physical damage results. Under some conditions, however, it may be reversible; no permanent change occurs and when the high field is removed, the dielectric may return to its original insulating state. Superficially, this is the threshold switch behaviour. In the case of a memory switch, a second input of energy is required to return the dielectric to its original state.

In this chapter, the principal models of dielectric breakdown are reviewed. For each case, the principal features of the mechanism are derived and their possible relevance to switching considered. Some models have already been used to describe memory or threshold switching in chalcogenide glasses; others describe similar behaviour in different classes of materials. The overall objective of the chapter is to show which models could be applicable and then to assess them in detail in the discussions on published results (chapter 4) and experimental results of this project (chapters 6 and 7).

3.2. GENERAL THERMODYNAMIC APPROACH

The existence of a region of bulk negative resistance implies a degree of electrical instability. If the negative resistance is to be observed under steady-state conditions the material, initially homogeneous, must become heterogeneous in an attempt to reach stability. As well as satisfying the conditions for electrical stability, the material must also satisfy the general thermodynamic condition that stability implies a condition of minimum entropy production. Ridley (19) has treated this problem for the two types of negative resistance: voltage controlled and its dual, current controlled negative resistance. The I - V characteristics have already been described in chapter 1. Ridley's treatment considers the consequences of the existence of a region of negative differential resistance. Only the current-controlled case will be treated in detail in this thesis.

In order to consider the thermodynamic stability of a material with characteristic shown in fig. 3.1., assume that it is initially electrically homogeneous and a voltage V produces a field E_o and current density J_o in the negative resistance region. To investigate the stability of the material in this condition, separate a small current filament with an area a fraction 'b' of the total cross section. If the current density in the filament is higher than in the remaining material, two processes will occur:

1. The electrical bias conditions will either reinforce the deviation from homogeneity or damp it down.

Fig. 3.1

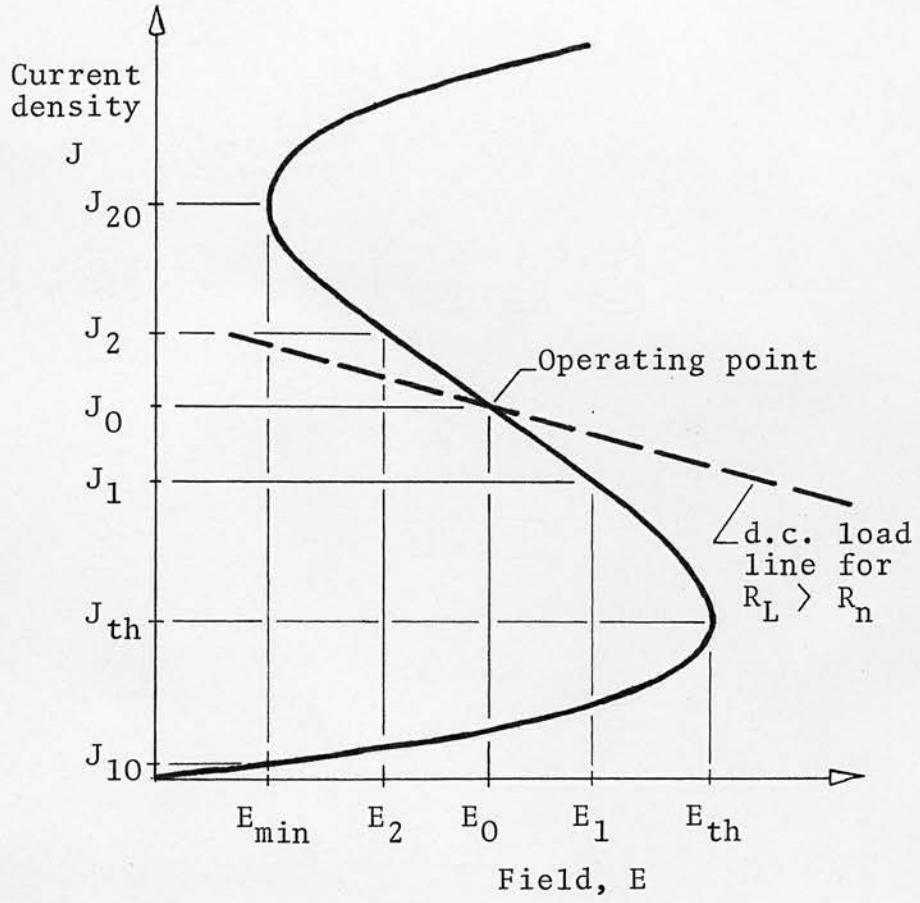

I - V characteristic with a negative resistance region.

2. There will be a change in the entropy production rate for the material as a whole. If the total entropy is reduced by filament formation then the heterogeneous arrangement will be favoured.

For steady state conditions, diffusive effects at the filament boundaries may be neglected and the entropy production rate $\dot{s}$ is given by:

$$\dot{s} = \dot{s}_1(1 - b) + \dot{s}_2 b \qquad \ldots\ldots 3.1$$

where the subscripts 1 and 2 refer to the area outwith the filament and to the filament respectively. Under steady state conditions, the total rate of entropy change arises from the electrical energy input:

$$\dot{s}_1 T = E_1 J_1 \qquad \ldots\ldots 3.2$$

$$\dot{s}_2 T = E_2 J_2$$

Substitution of equation 3.2 in 3.1 gives:

$$T\dot{s} = E_1 J_1(1 - b) + E_2 J_2 b \qquad \ldots\ldots 3.3$$

The current and field conditions in the filament and remainder of the material may be described by incremental relations:

$$J_1 = J_0 + \Delta J_1 \qquad \ldots\ldots 3.4$$

$$J_2 = J_0 + \Delta J_2$$

and

$$E_1 = E_0 + \frac{dE}{dJ} \cdot \Delta J_1 \qquad \ldots\ldots 3.5$$

$$E_2 = E_0 + \frac{dE}{dJ} \cdot \Delta J_2$$

with the average E_0, J_0 condition remaining constant, so:

$$J_1(1 - b) + J_2 b = J_0 \qquad \ldots\ldots 3.6$$

$$\Delta J_1(1 - b) + \Delta J_2 b = 0 \qquad \ldots\ldots 3.7$$

If equations 3.4 - 3.7 are substituted into equation 3.3, the entropy production rate is given by:

$$T\,\Delta\dot{s} = \frac{(1 - b)}{b} \cdot \frac{dE}{dJ} \Delta J_1^{\,2} \qquad \ldots\ldots 3.8$$

i.e. the sign of $\Delta\dot{s}$ is the same as dE/dJ so the formation of a current filament in the negative resistance region is consistent with a reduction in the rate of entropy production and is therefore a thermodynamically favourable condition. Equation 3.8 also shows that $\Delta\dot{s}$ is minimised for conditions of minimum Joule heating.

For a current density J_0 there are many possible stable states, each characterised by a filament of area b and field E. The entropy production rate is:

$$T\dot{s} = J_0 E = \left[J_1(1 - b) + J_2 b\right] E \qquad \ldots\ldots 3.9$$

The most favourable steady state will be that for which the field is a minimum. If J_{20} and J_{10} represent the values of current density at E_{min} in fig. 3.1., then for any other level of current density, J_0, the filament area will be given by:

$$b = \frac{J_0 - J_{10}}{J_{20} - J_{10}} \qquad \ldots\ldots 3.10$$

This means that as the current increases through the negative resistance region the filament area increases steadily and when the differential

resistance reaches its upper positive region, the filament has spread over the whole device area.

The electrical stability of a device with the characteristic shown in fig. 3.1. is dependent also on the conditions imposed by the external circuitry. For stable d.c. operation, the device can only be biased in the negative resistance region if the load resistor R_L is greater than the negative resistance at the operating point, R_n. A typical load line which satisfies this condition is shown in fig. 3.1.

Under a.c. conditions, however, the power dissipated by the external resistance must be greater than that generated in the negative resistance. For small voltages, V, and neglegible reactance, this means that for a.c. stability:

$$\frac{V^2}{R_L} > \frac{V^2}{R_n}$$

$$\text{i.e.} \quad R_L < |R_n| \qquad \ldots\ldots 3.11$$

Thus, although filament formation is thermodynamically favourable under conditions of minimum Joule heating and negative differential resistance, stable conditions in the negative resistance region with respect to d.c. and a.c. operation are likely to be difficult to achieve.

3.3. THERMAL BREAKDOWN

3.3.1. Conditions for negative resistance

In all semiconductors or insulators, conditions may occur where the self-generated Joule heat may exceed the capacity of the system to dissipate it without a large rise in temperature. Current increases with temperature; this leads to more Joule heating and consequent thermal runaway if no current limit is provided. The whole process may be reversible; if no physical changes occur in the high temperature state, the sample may return to its original characteristics when allowed to cool.

Chalcogenide glasses have large negative temperature coefficients of resistivity and low thermal conductivities, so thermal runaway must always be considered as a possible breakdown mechanism at high fields. Even if it is not the dominant mechanism which gives rise to switching, thermal effects are likely to be present and their influence must be understood.

The current-voltage characteristic for a device in which thermal breakdown occurs is similar to that of fig. 3.1. Below a voltage V_{th} (or the corresponding field, E_{th}), steady conditions of V, I and ΔT can be maintained where ΔT is the difference between the sample internal temperature and the ambient value. Beyond V_{th}, current and temperature increase rapidly so the voltage across the device drops. A stable d.c. operating point within the negative resistance region requires a large load resistance as shown in fig. 3.1.

To assess the differential resistance at any point on the characteristic, consider a d.c. signal (subscript 0) with a small superimposed a.c. signal (subscript 1) (20). The practical difficulties which occur when the device is biased in the negative resistance region were mentioned in section 3.2. but they do not affect the validity of the analysis. The small signal power dissipation is approximately given by :

$$P_1 = V_1 I_0 + V_0 I_1 \qquad \ldots\ldots 3.12$$

This gives rise to a temperature change, T_1 :

$$P_1 = \Gamma T_1 \qquad \ldots\ldots 3.13$$

where Γ is the thermal conductance between the device and ambient. Current is a function of voltage and temperature:

$$I_1 = gV_1 + hT_1 \qquad \ldots\ldots 3.14$$

where

$$g = \left.\frac{\delta I}{\delta V}\right|_{T_0}$$

$$h = \left.\frac{\delta I}{\delta T}\right|_{V_0}$$

and in general, both h and g are functions of T_0, the temperature associated with the d.c. bias conditions, V_0 and I_0.

If P_1 as derived from equation 3.13 is substituted in equation 3.12 and the resulting expression for T_1 put into equation 3.14, then the differential impedance, Z, is given by :

$$Z = \frac{V_1}{I_1} = \frac{\Gamma + hV_0}{g\Gamma + hI_0}$$

i.e. $$\frac{dV}{dI} = R_0 \cdot \frac{1 - y}{x + y} \qquad \ldots\ldots 3.15$$

where $R_0 = V_0 / I_0$, $x = R_0 \left.\frac{\partial I}{\partial V}\right|_{T_0}$, $y = \frac{V_0}{\Gamma} \cdot \left.\frac{\partial I}{\partial T}\right|_{V_0}$

x and y are dimensionless and are the representative parameters of the isothermal characteristic at the operating temperature and the temperature coefficient of current respectively.

Sectors of positive and negative differential resistance in the x - y plane are separated by the lines y = 1 and x + y = 0. For chalcogenide glasses, and most other semiconductors, $y > 0$. The influence of the frequency of the a.c. signal on differential impedance is considered in section 3.3.9.

3.3.2. General treatment

When a field, E, is applied to a dielectric, the equation for energy balance is :

$$C \frac{\partial T}{\partial t} = \text{div} (\kappa \text{ grad } T) + \sigma E^2 \qquad \ldots\ldots 3.16$$

where C is the specific heat per unit volume

κ is the thermal conductivity

σ is the electrical conductivity

In addition, σ and κ may be variables:

$$\kappa = \kappa (T)$$

$$\sigma = \sigma (E, T, t)$$

The current continuity equation must also hold throughout the sample:

$$\text{div } (\sigma \bar{E}) = 0 \qquad \ldots\ldots 3.17$$

Because of the widespread occurrence of thermal breakdown, many solutions of equations 3.16 and 3.17 have been produced over the past 50 - 60 years (21) (22) (23). For application to switching, conditions appropriate to chalcogenide glasses must be considered. The thermal conductivity, K , can usually be taken as a constant with respect to temperature. The low-field conductivity as a function of temperature was described in chapter 2. Two forms of equation may be used:

$$\sigma = \sigma_0 \exp\left(-\frac{\Delta E}{kT}\right) \qquad \ldots\ldots 3.18$$

$$\sigma = \sigma_a \exp(a \Delta T) \qquad \ldots\ldots 3.19$$

where σ_0 is a constant, ΔE is an activation energy, usually about 0.45 eV, σ_a is the conductivity at ambient temperature T_a or some other reference temperature, ΔT is the deviation from T_a and a is a constant : a = 0.04. It was shown in chapter 2 that for temperatures in the range 300 - 500 K, equation 3.19 is more accurate than 3.18. Under high field conditions ($> 10^6$ V.m^{-1}), the conductivity may also be field-dependent. In the analysis of thermal breakdown, it is therefore convenient to consider first a conductivity equation such as 3.19 and then repeat the analysis with an appropriate field-dependent conductivity equation.

To obtain equations which describe thermal breakdown in chalcogenide glasses, it is useful to consider three time regions for which the general energy balance equation (3.16) can be solved:

1. The steady-state case. This gives the d.c. thermal breakdown

condition. If current increases are made slowly, heat loss always balances heat produced and the time derivative term in equation 3.16 may be neglected.

2. Impulse breakdown. Application of a very short voltage pulse produces an adiabatic condition where all electrical energy supplied goes towards heating the sample. The sample temperature falls to the ambient value in the interval between pulses.

3. A.C. breakdown. The breakdown strength depends on the frequency of the applied field with cases 1 and 2 as extremes. This is an important practical case since switching devices may be required to operate at high frequencies.

Each of these three cases is analysed in some detail to demonstrate which factors affect the breakdown process. Where possible, specific equations are derived so that their quantitative predictions can be compared with the experimental data of chapters 4 and 6.

3.3.3. D.C. thermal breakdown for $\sigma = \sigma(T)$

Under steady-state breakdown conditions, the time derivative in equation 3.16 is zero and the energy balance equation is reduced to:

$$\text{div}(\kappa \ \text{grad}\ T) = -\sigma E^2 \qquad \ldots\ldots 3.20$$

The thermal conductivity, κ, is usually taken to be independent of temperature. The device dimensions in the plane of the area, A, are normally much greater than the electrode separation, d, so only the

temperature distribution along the x - axis need be considered. (This is also the direction of current flow). The energy balance equation is therefore:

$$K \frac{d^2T}{dx^2} = -\sigma \left(\frac{dV}{dx} \right)^2 \qquad \ldots\ldots 3.21$$

This equation may be solved with that for σ (equation 3.19) for appropriate thermal boundary conditions.

The analysis follows that developed for thermistors (24) (25) (26). The simplest boundary condition to consider initially is that the electrodes are massive enough to remain at ambient temperature under all conditions. The temperature in the middle of the sample is ΔT above ambient and in general, the temperature gradient between an electrode and the mid-point is non-uniform. This implies a non-uniform distribution of resistivity and field within the sample. The boundary conditions are:

$\Delta T = 0$ at the electrodes, i.e. $x = 0$ and $x = d$

$\frac{dT}{dx} = 0$ in the middle, i.e. at $x = d/2$.

The solution of equations 3.19 and 3.21 results in a temperature distribution which is given by : (27)

$$\frac{\Delta T}{\Delta T_{max}} = \frac{\cosh i\xi\Lambda - \cosh i\Lambda}{1 - \cosh i\Lambda} \qquad \ldots\ldots 3.22$$

where $\xi = 2x/d$

$\Lambda = V \left(\frac{\epsilon \sigma}{K} \right)^{\frac{1}{2}}$

ϵ is the temperature coefficient of resistance of the semiconductor

or insulator

ΔT_{max} is the value of temperature increase at $x = d/2$.

The distribution of equation 3.22 is shown in fig. 3.2 as a function of current, i, and the dimensionless parameter, Λ .

For $i\Lambda = 0$, the temperature distribution is parabolic. In fig. 3.2 the solid line represents equation 3.22 and the points are derived from an equation:

$$\frac{\Delta T}{\Delta T_{max}} = 4\left(\frac{x}{d}\right) - 4\left(\frac{x}{d}\right)^2 \qquad \ldots\ldots 3.23$$

The other extreme condition, $i\Lambda = \infty$, results in a rectangular temperature distribution with a discontinuous increase in temperature from $\Delta T = 0$ to ΔT_{max} at $x = 0$ and $x = d$. For thin film or small bulk samples, typical values of $i\Lambda$ are small and usually $i\Lambda \ll 1$. The parabolic temperature distribution given by equation 3.23 is therefore the most realistic.

The resistivity distribution for $i\Lambda = 0$ is shown in fig. 3.3. Resistivity has been expressed in terms of the average value across the sample. Since current is not a function of x, the voltage distribution is the same as that for resistivity and its slope represents the field distribution. This is also shown in fig. 3.3. In the relatively high resistivity regions near the electrodes the local field may be up to three times greater than the average field across the sample. If conditions are such that $i\Lambda > 1$ then the field near the electrodes may

Fig. 3.2

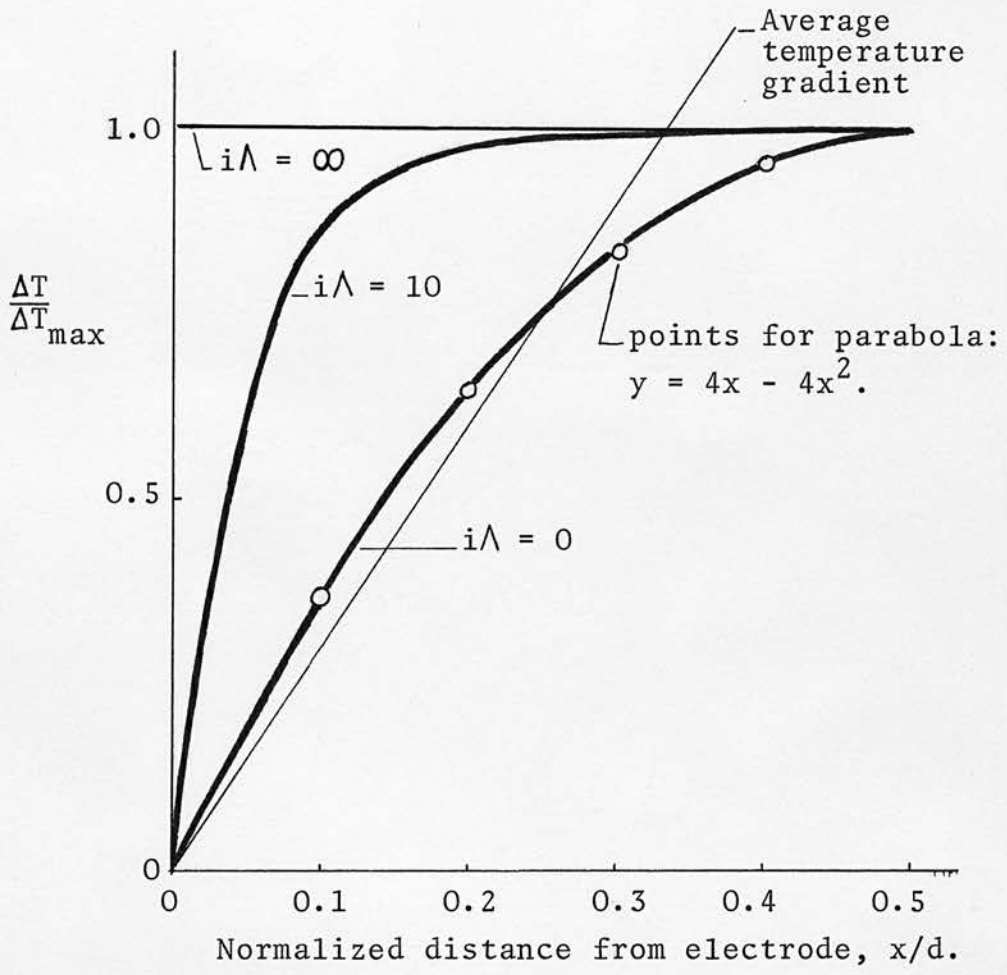

Influence of iΛ on the temperature distribution across a sample.

be considerably greater. At very high fields ($\sim 10^8$ V.m^{-1}) other forms of dielectric breakdown such as avalanche ionization or internal field emission may occur. These mechanisms are treated separately in section 3.4 but the purpose of fig. 3.3. is to show that they may also be involved in cases of thermal breakdown.

The rate of heat dissipation as derived from equation 3.21 is:

$$VI = \kappa A \frac{dT}{dx} \qquad \ldots\ldots 3.24$$

As shown in fig. 3.2., dT/dx does not depend on ΔT_{max} and it varies throughout the sample. For $i\Lambda = 0$, the average value of dT/dx occurs at x = 0.25 d and the non-uniform temperature gradient may be represented by the average value shown in fig. 3.2. :

$$\left\langle \frac{dT}{dx} \right\rangle \doteq \frac{\Delta T}{0.33\,d}$$

If equation 3.24 is expressed in terms of a thermal conductance, Γ:

$$VI = \Gamma \Delta T \qquad \ldots\ldots 3.25$$

The thermal conductance to both electrodes is given by:

$$\Gamma = \frac{3 \kappa A}{2 d} \qquad \ldots\ldots 3.26$$

for the parabolic case, $i\Lambda = 0$.

The variation in the mean resistance of a sample is shown in fig. 3.4. as a function of temperature for the two limiting temperature distributions of fig. 3.2., (i.e. those given by $i\Lambda = 0$ and $i\Lambda = \infty$). The mean resistance is expressed in terms of the resistance of the sample when $\Delta T = 0$. It has been assumed that the constant 'a' in the conductivity equation (3.19) is a = 0.04, i.e. equivalent to an activation energy $\Delta E \doteq 0.5$ eV.

Fig. 3.4

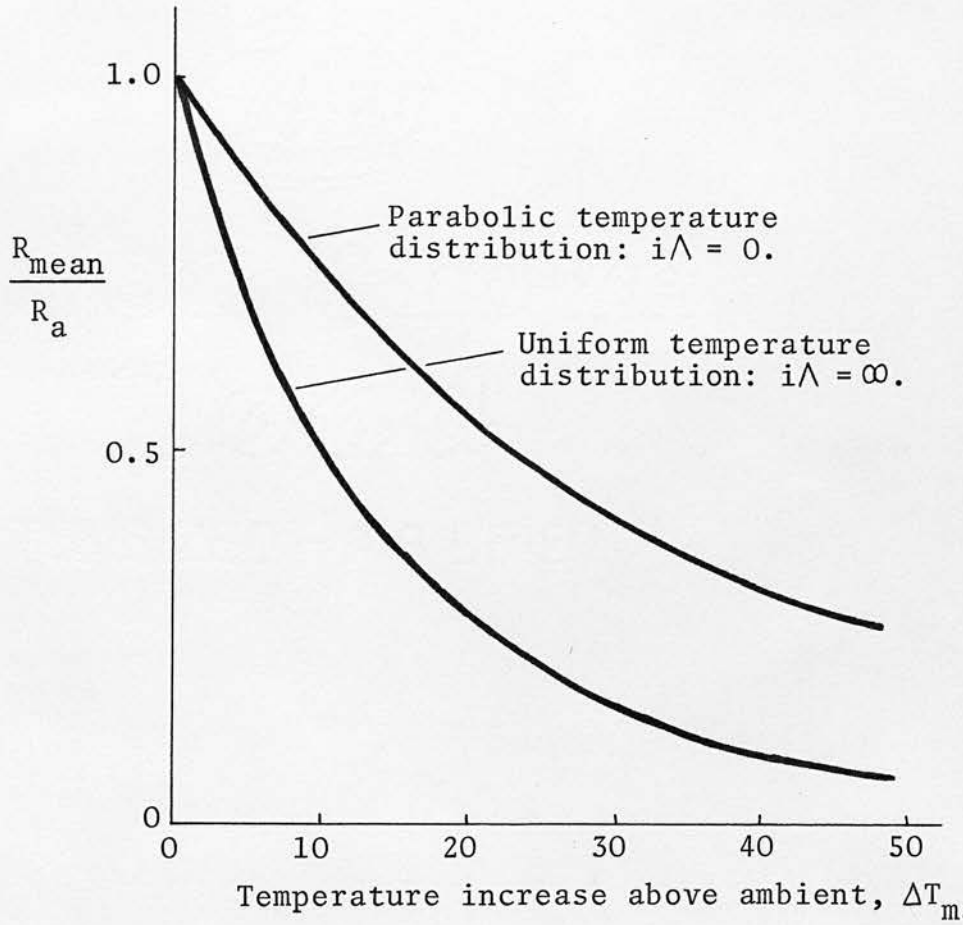

Variation of mean resistance with temperature distribution and maximum internal rise in temperature, (ΔT_{max}).

For any value of ΔT_{max}, fig. 3.4 gives a mean resistance or voltage : current ratio . Equation 3.25 must also be satisfied and for a specified temperature increase this can only occur at unique current and voltage values. The solution of equation 3.25 with the appropriate resistance expression is best done graphically to obtain an I - V characteristic. This is shown in fig. 3.5. The line R_{20} represents the resistance when $\Delta T = 20$ K and the temperature distribution is parabolic. The constant power line appropriate to $\Delta T = 20$ K (derived from equation 3.25) is also shown in fig. 3.5. and marked as P_{20}. The intersection of the R_{20} and P_{20} lines gives the current and voltage values appropriate to $\Delta T = 20$ K. Since fig. 3.5. shows log I against log V, constant resistance and power lines are orthogonal. The method of solution is therefore quick and straightforward. The constants used in the derivation of fig. 3.5. are: $R_a = 10$ MΩ , $a = 0.04\ K^{-1}$ and $\Gamma = 0.3\ mW.K^{-1}$. The thermal conductance is that for a sample 0.2 mm thick with $A = 4.10^{-8}\ m^2$ and $\kappa = 1\ W.m^{-1}.K^{-1}$.

The current-voltage characteristic of fig. 3.5. is ohmic at low voltages then non-linear up to a voltage V_{th} where $dV/dI = 0$. The characteristic has been plotted as log I against V in fig. 3.6. Most of the non-ohmic region can be described by an equation of the form

$$I = I_0 \exp \frac{V}{V_0} \qquad \ldots\ldots 3.27$$

where I_0 and V_0 are constants at any specified temperature. Fig. 3.6 also shows I - V curves at two temperatures above T_a. They were derived by the method shown in fig. 3.5.

Fig. 3.5

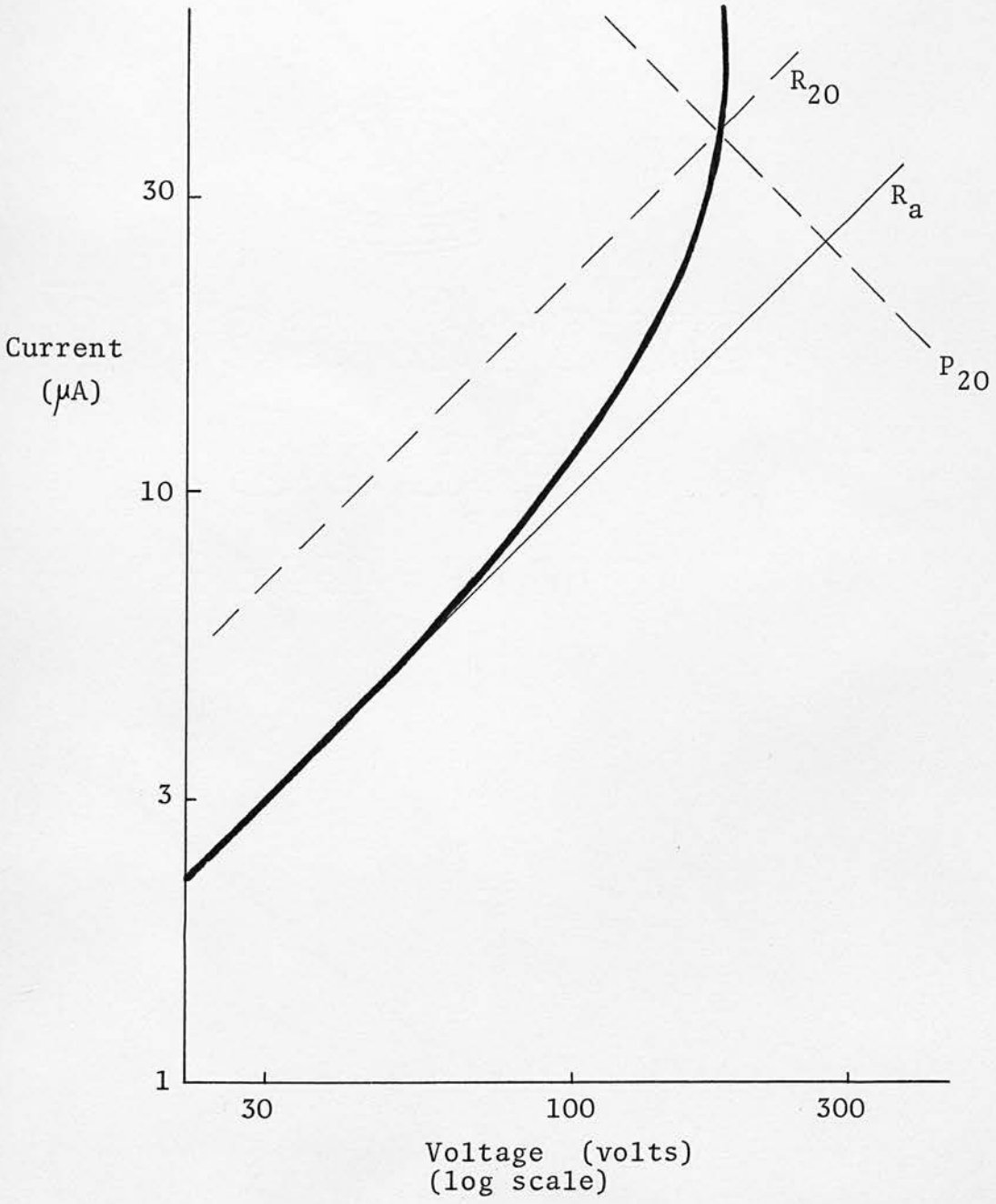

Construction of pre-thermal breakdown current-voltage characteristic.

Fig. 3.6

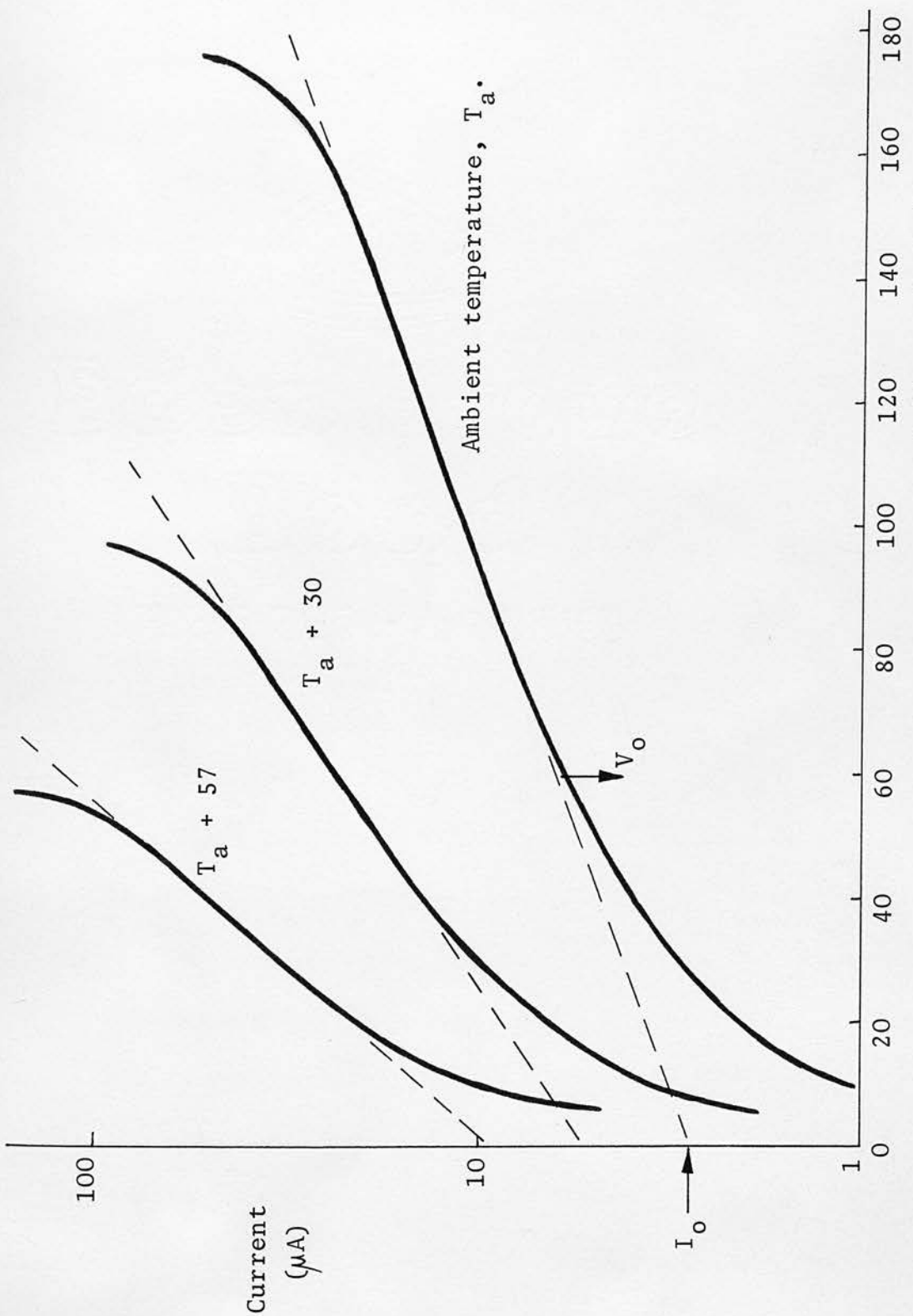

Theoretical thermal breakdown characteristics as a function of temperature

I_0 and V_0^{-1} increase with temperature. V_0 represents the point of transition from an ohmic to exponential I - V relation and switching occurs at $V_{th} \doteq 3V_0$ for each of the curves in fig. 3.6. Thus V_0 and V_{th} have the same temperature dependence.

The shape of experimental current-voltage characteristics in the pre-breakdown region is treated in chapter 6 for several different geometries.

3.3.4. D.C. thermal breakdown for $\sigma = \sigma(T, E)$

The conductivity of a dielectric frequently depends upon the field as well as temperature. The precise σ - E relation depends on the material and conduction mechanism. For a field-assisted hopping process such as the poole-Frenkel effect, σ is given by:

$$\sigma = \sigma_0 \exp - \frac{e}{kT}\left[\phi_1 - \left(\frac{eE}{\pi K_i \epsilon_0}\right)^{\frac{1}{2}}\right] \qquad \ldots\ldots 3.28$$

where σ_0 and ϕ_1 are constants.

K_i is the dielectric constant of the insulator.

An equation of this form has been used by Sze (28) to explain thermal breakdown in silicon nitride. More complex expressions for σ, such as that suggested by Hartman for SiO (29) may also be used:

$$\sigma = \frac{\alpha d}{E} \cdot \exp\left(\beta E^{\frac{1}{2}} - \frac{\gamma}{kT}\right).(1 - \exp \beta^2 E) \qquad \ldots\ldots 3.29$$

where $\beta = \left(\frac{\psi}{kT} + \phi\right)$

ψ, ϕ, α and γ are constants.

Manipulation of these equations is rather difficult in any analysis of thermal breakdown. It is more appropriate and convenient to anticipate the results of chapter 6 and use the equation:

$$\sigma = \sigma_a \exp(a\,\Delta T) \exp\left(\frac{E}{E_0}\right) \qquad \ldots\ldots 3.30$$

This equation was derived from experimental measurements of current-voltage characteristics of thin chalcogenide films. The form of equation 3.30 is <u>not</u> a result of Joule-heating within the sample; it may therefore be used to calculate self-heating effects. The temperature dependent term in equation 3.30 is the same as that used in the previous section. In the field-dependent term, E_0 is a constant; its experimental value is $3.3.10^6$ $V.m^{-1}$. for the samples discussed in chapter 6. An expression similar to equation 3.30 has been observed by Klein (30) for SiO.

The equation for conductivity may be substituted into the steady-state heat balance equation (3.25) :

$$V I = \Gamma \Delta T$$

i.e.
$$\sigma_a A d E^2 \exp\left(\frac{E}{E_0}\right).\exp(a\,\Delta T) = \Gamma \Delta T \qquad \ldots\ldots 3.31$$

The left side of equation 3.31 represents the rate of heat generation; the right side represents its rate of dissipation. At the turnover voltage, both rates are equal, i.e. the derivatives of each side with respect to temperature are equal:

$$\sigma_a A a d E_{th}^2 \exp\left(\frac{E_{th}}{E_0}\right).\exp(a\,\Delta T_{th}) = \Gamma \qquad \ldots\ldots 3.32$$

where the subscript 'th' represents the appropriate value at threshold conditions. If equation 3.32 is substituted in equation 3.31 :

$$\Delta T_{th} = \frac{1}{a}$$

i.e. self-sustaining thermal runaway occurs when the internal temperature has risen about 25 K above the ambient value since $a \doteq 0.04$ for typical chalcogenide glasses used in switching devices. This value of ΔT_{th} in equation 3.32 gives:

$$E_{th}^2 \exp\left(\frac{E_{th}}{E_0}\right) = \frac{\Gamma}{A e a d \sigma_a} \quad \ldots\ldots 3.33$$

or

$$V_{th}^2 \exp\left(\frac{V_{th}}{V_0}\right) = \frac{\Gamma d}{A e a \sigma_a} \quad \ldots\ldots 3.34$$

where $V_{th} = E_{th}.d$ and $V_0 = E_0.d$. Equation 3.34 may also be used in cases where conductivity is not field dependent, i.e. $V_{th} \ll V_0$, so the term $\exp(V_{th}/V_0)$ reduces to unity.

3.3.5. Factors which influence steady-state thermal breakdown

There are many factors which influence thermal breakdown in chalcogenide glasses. Among the more important are glass composition, sample geometry and ambient conditions. The glass composition determines the magnitude of the terms in the conductivity equation and other fundamental constants such as thermal conductivity. Temperature is the most important of the ambient conditions; along with sample geometry, it may be used to give a quantitative description of the

breakdown characteristics.

The breakdown equation derived in the previous section may be used to demonstrate how V_{th} may be controlled:

$$V_{th}^2 \exp\left(\frac{V_{th}}{V_0}\right) = \frac{\Gamma d}{A e a \sigma_a} \qquad \ldots\ldots 3.34$$

There are three sets of conditions for which V_{th} shows significantly different behaviour.

1. Thick samples Equation 3.33 shows that E_{th} decreases with increasing sample thickness. In the case of 'thick' samples $E_{th} \ll E_0$. It was also shown in section 3.3.3. (equation 3.26) that in thick samples, the temperature distribution may approach the uniform gradient condition, and

$$\Gamma = \frac{1.5\ K\ A}{d}$$

Thus, equation 3.34 reduces to:

$$V_{th}^2 = \frac{1.5\ K}{e a \sigma_a} \qquad \ldots\ldots 3.35$$

i.e. V_{th} is not geometry-dependent. It does, however, depend on glass composition and ambient temperature through the term σ_a. If the conductivity term were described by an equation with an activation energy - e.g. equation 3.18, then V_{th} would also have an activation energy, but it would be only half that for resistivity.

2. The constant Γ case. As in the 'thick sample' case, $V_{th} \ll V_0$

and the term $\exp(\frac{V_{th}}{V_0})$ reduces to unity. For some geometrical arrangements, the rate of transfer of Joule heat from dielectric to ambient may not be limited by the thermal conductance of the dielectric layer. The effective value of Γ may then be determined by the thermal properties of the electrodes or substrate. In such a case, Γ is independent of the electrode separation, d. The expression for V_{th} is then:

$$V_{th}^2 = \frac{\Gamma d}{A e a \sigma_a} \qquad \ldots\ldots 3.36$$

Breakdown voltage varies with electrode separation as: $V_{th} \propto d^{\frac{1}{2}}$. The variation of V_{th} with temperature is the same as in case 1: it may be described by an activation energy which is half that of the sample resistivity.

This constant Γ case represents the thermistor-type analysis. It provides the simplest conditions for evaluation of current-voltage relations. Becker et al. (24) have solved the equations :

$$VI = \Gamma(\Delta T)$$

$$V = IR_a \exp(\frac{\Delta E}{kT} - \frac{\Delta E}{kT_a})$$

for the case of a thermistor where $R_a = 5.10^4 \Omega$, $\Gamma = 5.10^{-4}$ W.K^{-1}. and $T_a = 300$ K. The result is shown in fig. 3.7. There are two limiting regions of positive differential resistance and their ratio depends on the activation energy, ΔE. A region of negative resistance only exists if $\Delta E > 0.12$ eV.

3. Thin samples. Breakdown fields are higher for thin samples than

Fig. 3.7

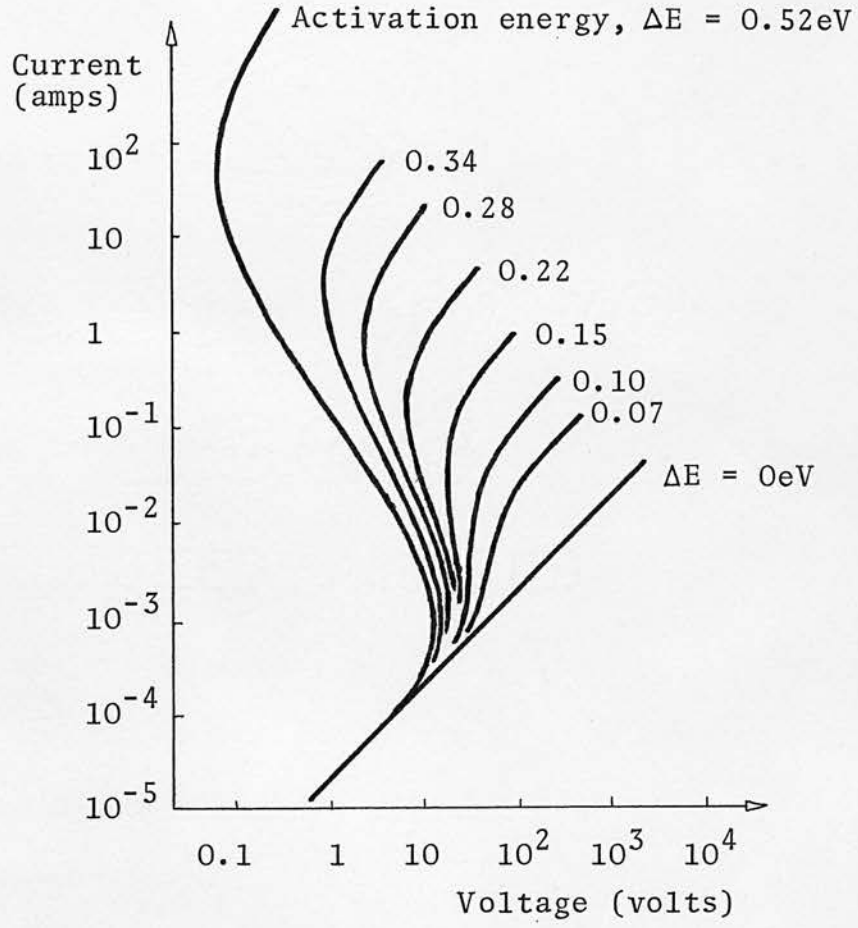

Thermistor I - V characteristics.

thick and conditions may be such that $V_{th} > V_0$. When the $\exp(\frac{V_{th}}{V_0})$ term in equation 3.34 is dominant, then:

$$V_{th} = V_0 \text{ Log } (\frac{\Gamma d}{A e a \sigma_a} V_{th}^2) \quad \ldots\ldots 3.37$$

This means that V_0 has a much greater influence on V_{th} than any of the terms in the Log expression. Thus, the variation of V_{th} with thickness should be approximately the same as that for V_0, i.e. $V_{th} \propto d$, since V_0 is derived from a field E_0 which is constant for any particular glass composition (chapter 6). Only temperature has a strong effect on the magnitude of the Log expression in equation 3.37 since :

$$\sigma_a = \sigma_{a0} \exp (a \Delta T)$$

where σ_{a0} is the conductivity when ΔT is zero.

Thus, the temperature dependence of V_{th} is approximately given by:

$$V_{th}(T) \propto V_0(T).(-a \Delta T) \quad \ldots\ldots 3.38$$

For the thin chalcogenide films described in chapter 6, V_0 may be expressed as:

$$V_0(T) = V_{01} \exp (\frac{\psi}{kT}) \quad \ldots\ldots 3.39$$

where the activation energy, ψ is about 0.1 eV.

The variation of V_{th} with temperature described by equations 3.38 and 3.39 is shown in fig. 3.8.

If $\psi = 0$ then V_{th} decreases linearly as ΔT is increased.

Fig. 3.8

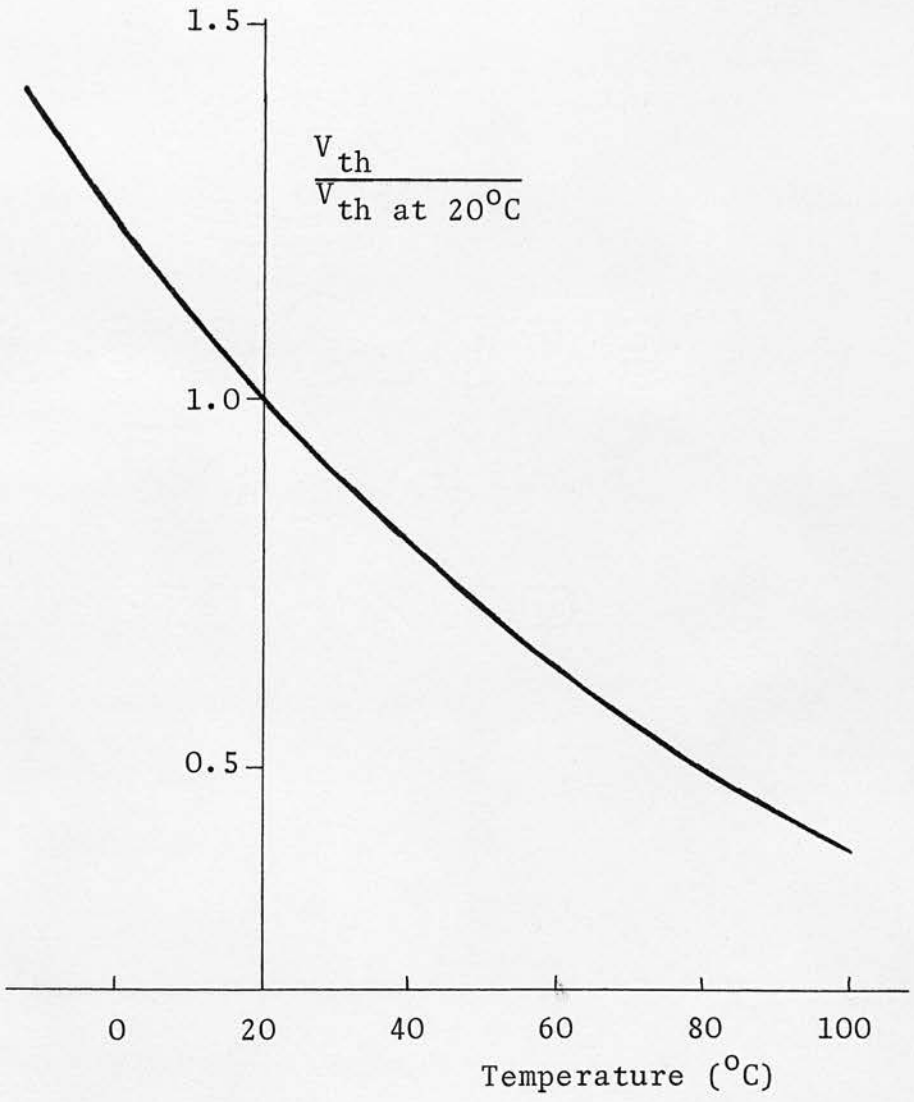

Thermal breakdown with $\sigma = \sigma(T,E)$:
variation of threshold voltage
with temperature.

The relative importance of each of these three cases on the value of thermal breakdown voltage may be summarised in a graph of V_{th} against sample thickness : fig. 3.9. Constants typical of chalcogenide glasses have been used: $a = 0.04$, $\sigma = 10^{-5}\ (\Omega.m)^{-1}$, $A = 10^{-7}\ m^2$, $\Gamma = 2.10^{-3}\ W.K^{-1}$ and $E_0 = 3.3.10^{-6}\ V.m^{-1}$. The inclusion of a field term in the conductivity equation has most influence in thin films. For thicker samples where E_{th}/E_0 is less significant, the occurrence of a uniform temperature gradient leads to a constant V_{th} for $d \gtrsim 1$ mm. Thus as sample thickness is increased, on the basis of a thermal breakdown mechanism , there should be a steady change from a constant breakdown field to a constant breakdown voltage.

3.3.6. Filament formation

The shape of the current-voltage characteristic for thermal breakdown has been derived (fig. 3.5.) from the solution of the equations:

$$VI = \Gamma\ (\Delta T) \qquad \ldots\ldots 3.40$$

$$\frac{V}{I} = \frac{d}{A} \cdot \rho\ (T) \qquad \ldots\ldots 3.41$$

At low voltages the characteristic is ohmic; this is followed by a non-linear region with $I \propto \exp V$ approximately. Beyond V_{th} there is a negative resistance region and the characteristic approaches a constant power line.

Fig. 3.10(a) shows the generalised I - V characteristic (solid line). It has the same shape as the characteristic drawn in fig. 3.5. Fig. 3.10(b) shows the slope, dV/dI, as a function of current for the curve of

Fig. 3.9

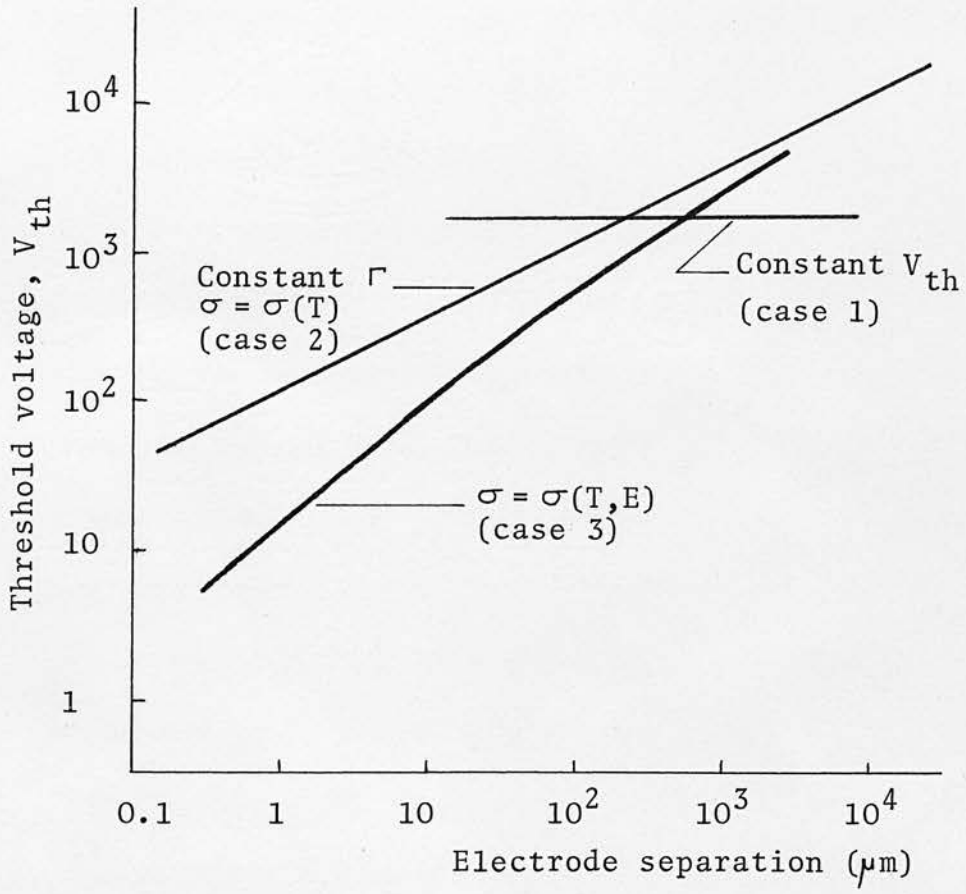

Variation of thermal breakdown voltage with electrode separation: influence of Γ and σ expressions.

fig. 3.10(a). For all current values, even in the negative resistance region, $\frac{dV}{dI} < R_L$ where R_L is the load resistor in series with the device. This means that a stable d.c. operating point can in principle be maintained on any part of the I - V characteristic.

The analysis of Ridley, described in section 3.2. showed that filament formation in a current-controlled negative resistance region is thermodynamically favourable. The physical consequence of filament formation in conjunction with thermal breakdown is that the effective sample area decreases while the internal temperature continues to rise. If the thermal conductance between the sample and ambient is area-dependent, then the formation of a filament may cause the power dissipated to rise more slowly with temperature than was the case for the pre-breakdown region (equation 3.40). The instantaneous resistance (V / I) as given by equation 3.41, is dominated by the $\rho(T)$ term and continues to decrease rapidly in spite of the reduction in area.

The effect of filament formation on the I - V characteristic is shown schematically by the dashed line in fig. 3.10(a). The magnitude of the negative differential resistance is increased and it may exceed $-R_L$: fig. 3.10(b). The region of the characteristic marked ABC in fig. 3.10(a) is not accessible in terms of a stable operating point, so filament formation implies rapid switching from point A to point C.

In the region beyond point C, an increase in current may involve an increase in internal temperature or an increase in filament area or, more likely, both effects. When the current is reduced, stable conditions

Fig. 3.10

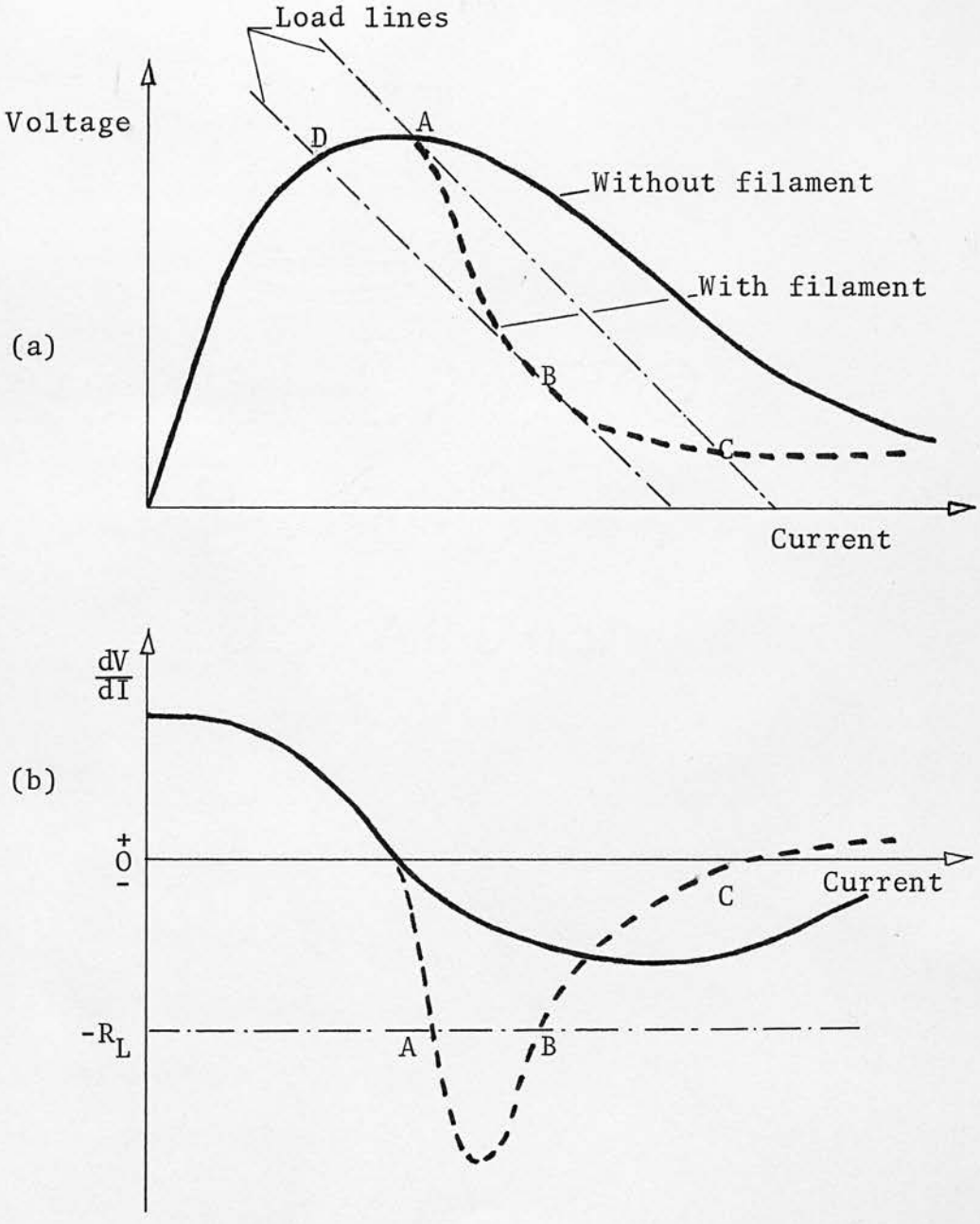

V - I and $\frac{dV}{dI}$ - I characteristics showing schematically the effects of filament formation.

can be maintained down to point B. This represents the minimum power level at which a hot filament can be sustained. If the current is reduced below the level at B, switching along the load line occurs to a stable point on the off-state characteristic : D.

This argument is qualitative, but it does indicate the principal effects of filament formation associated with steady-state thermal breakdown. There would be no accessible negative resistance region close to V_{th}; the I - V characteristic would show considerable hysteresis; there would be a minimum holding current associated with a constant minimum holding power below which the device could not be maintained in the on-state and there would be a small region of negative resistance just before switch-off. All of these features are observed in the experimental characteristics of amorphous chalcogenide switches.

3.3.7. Impulse thermal breakdown

When very short pulses of constant voltage, V_p, are applied to a sample all the energy can be considered as contributing to the heating of the sample, i.e. during the pulse there is negligible heat loss via electrodes, etc. The pulse repetition rate must also be low enough to make each pulse an isolated event; the sample cools to ambient temperature between pulses.

For this adiabatic condition, the energy balance equation (equation 3.16 in section 3.3.2.) becomes:

$$J E_p = C \frac{dT}{dt} \qquad \ldots\ldots 3.42$$

The case which is of interest occurs when V_p is large enough to produce thermal breakdown. Solution of equation 3.42 then gives the time taken to establish a thermal runaway condition.

The general approach used to derive the equations which describe dynamic breakdown follows the pattern of sections 3.3.3. and 3.3.4. for the steady-state case. Conductivity is a function of both temperature and field; the relative importance of each variable depends on device geometry and ambient conditions and these are treated in the following section.

When the conductivity equation:

$$\sigma = \sigma_a \exp(a \Delta T) \exp\left(\frac{E}{E_0}\right) \qquad \ldots\ldots 3.43$$

is substituted in equation 3.42, integration may be carried out:

$$\int_0^t \frac{E_p^2}{C} dt = \int_0^{\Delta T} \frac{dT}{\sigma} \qquad \ldots\ldots 3.44$$

The limits of integration are set by the condition that after a time, t, the sample internal temperature has risen ΔT above the ambient value, T_a.

$$E_p^2 \exp\left(\frac{E_p}{E_0}\right) . \frac{\sigma_a t}{C} = \int_0^{\Delta T} \exp(-a \Delta T)\, dT$$

$$= \frac{1}{a} \left[1 - \exp(-a \Delta T) \right]$$

i.e. $$E_p^2 \exp\left(\frac{E_p}{E_0}\right).t = \frac{C}{a}\left(\rho_a - \rho_T\right) \quad \ldots\ldots 3.45$$

where ρ_T is the sample resistivity at a temperature, T, which is ΔT above T_a.

By analogy with steady-state breakdown, thermal runaway occurs when ΔT is 20 - 50 K above T_a, but because the resistivity varies strongly with temperature, the condition for breakdown may be taken as $\Delta T = \infty$, i.e. $\rho_T = 0$. If this occurs after a time t_d, the delay time, then:

$$E_p^2 \exp\left(\frac{E_p}{E_0}\right).t_d = \frac{C\rho_a}{a} \quad \ldots\ldots 3.46$$

If equation 3.45 is divided by equation 3.46:

$$\frac{t}{t_d} = 1 - \frac{\rho_T}{\rho_a} \quad \ldots\ldots 3.47$$

On the assumption of a uniform temperature throughout the sample, ρ_T may be calculated for any value of ΔT. In fig. 3.11. the temperature rise is plotted as a function of time normalized to $t_d = 1$. The current density, calculated from ρ_T and E_p is also shown in fig. 3.11. as a function of time. J_a is the current density when ΔT and t are both zero.

A similar analysis of impulse breakdown has been produced by Burton and Brander (31) and Brander (32). However, they did not consider field-dependent conductivity and they used an activation energy

Fig. 3.11

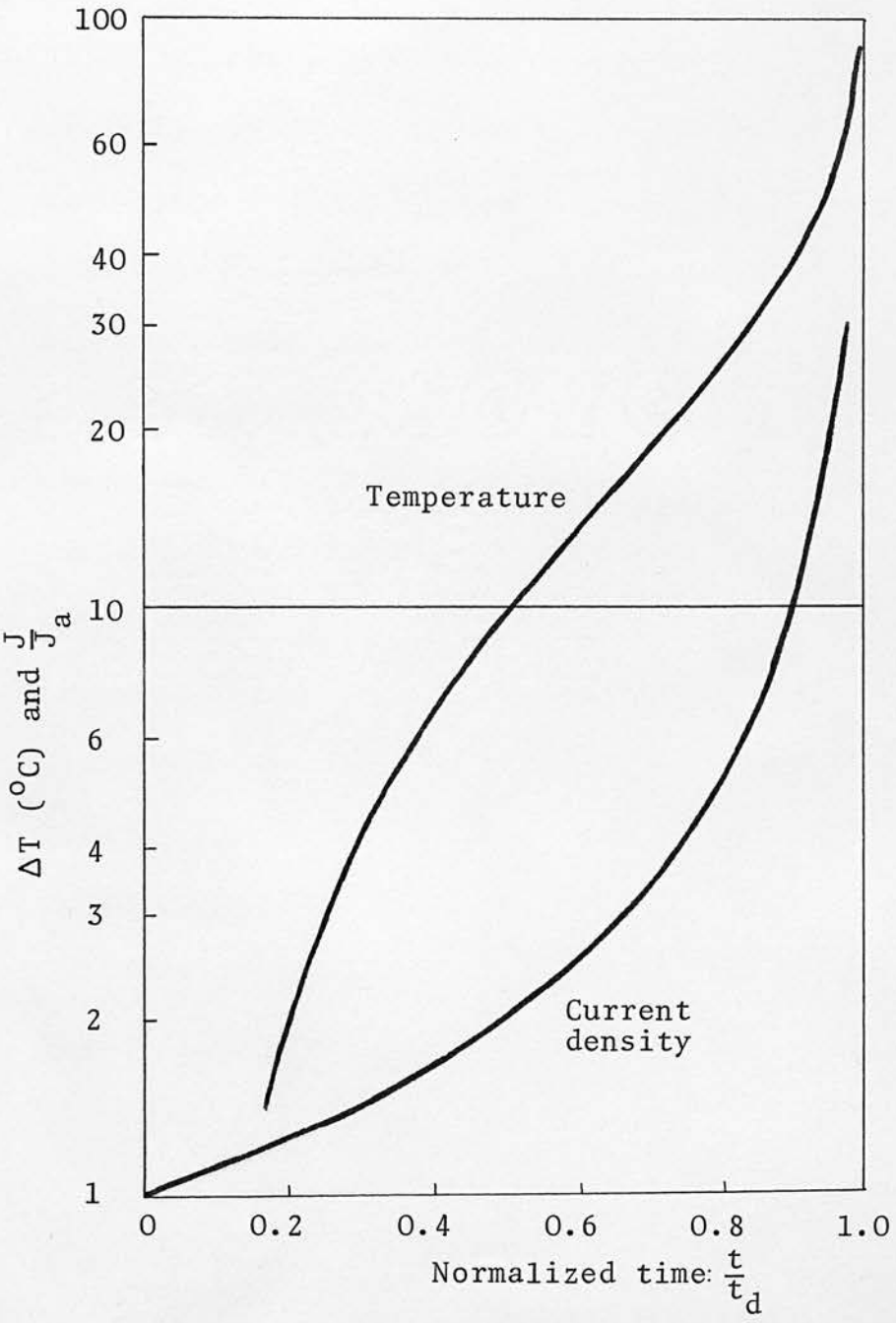

Current and temperature increase during the delay time.

to describe the dependence of ρ on T. This makes the manipulation of the equations much more difficult but produces the same result as equation 3.45.

It was assumed at the beginning of this section that no heat was lost to the surroundings; it all contributed to raising the sample temperature. This will only be true for short pulses. An assessment of how short the pulses would have to be may be made by considering a slab of chalcogenide glass. If the temperature at the surfaces is suddenly changed, the temperature in the middle of the slab rises (or falls) to half the difference temperature in about 0.2 μs for a slab 1 μm thick (33). This is the order of time to produce a significant temperature change in a thin glass film. The time to produce a corresponding temperature change in a metal electrode is much shorter. Experimental conditions usually require that pulses of 1 μs duration or more be used to study impulse breakdown in glasses. Heat loss via electrodes is therefore significant.

Klein (34) has studied impulse thermal breakdown in silicon monoxide. He obtained a machine solution:

$$V^2 \exp\left(\frac{V}{V_0}\right) = \frac{dKB}{a\sigma_a H} \qquad \ldots\ldots 3.48$$

where H is the substrate thickness

K is the thermal conductivity of the substrate

B is a function of the pulse length.

For the case of a sandwich sample, the substrate is provided by the

electrodes. Equation 3.48 gives the minimum voltage for impulse breakdown in a given pulse time. If a larger voltage is applied, the delay time is reduced in the same way as implied by equation 3.46.

The overall effect of heat loss via electrodes is to increase the delay time before breakdown occurs, but if a filament is formed when $\Delta T \doteqdot 25$ K as in the steady-state case (section 3.3.6.), the delay time is shortened. The two effects tend to cancel each other and equation 3.46 therefore gives a reasonable assessment of t_d.

3.3.8. Factors which influence impulse breakdown

The influence of device geometry and ambient conditions on impulse thermal breakdown can be assessed in the same way as for steady-state breakdown (section 3.3.5.). The general relation between pulse voltage amplitude and delay time may be derived from equation 3.46 :

$$V_p^2 \exp\left(\frac{V_p}{V_0}\right).t_d = \frac{C \rho_a d^2}{a} \qquad \ldots\ldots 3.49$$

The relative importance of V_0 depends on the electrode separation, d, and equation 3.49 can be studied for two cases : thin samples where $V_p > V_0$ and thick samples where $V_p \ll V_0$. The distinction between these two cases for steady-state breakdown is shown in fig. 3.8. Since equation 3.49 was derived for circumstances of no heat loss, it represents experimental conditions where $V_p > V_{th}$ and the pulse length is shorter than the thermal time constant for heat dissipation via the

electrodes and substrate. The influence of geometry and ambient on thermal conductance, Γ , therefore need not be considered.

1. Thick samples. With $V_p \ll V_0$, equation 3.49 may be simplified to:

$$V_p^2 t_d = \frac{C \rho_a d^2}{a} \qquad \ldots\ldots 3.50$$

This means that the delay time, t_d, is proportional to d^2 and V_p^{-2}. The temperature dependence of t_d arises wholly from its dependence on ρ_a. Thus:

$$t_d \propto \exp\left(\frac{\Delta E}{kT}\right)$$

or $$t_d \propto \exp(-a\,\Delta T).$$

2. Thin samples. As in the case of steady-state breakdown, when $V_p > V_0$, the $\exp(V_p/V_0)$ term is more significant than V_p^2. Equation 3.49 may be expressed as :

$$\exp\left(\frac{V_p}{V_0}\right).t_d \propto \frac{C \rho_a d^2}{a} \qquad \ldots\ldots 3.51$$

The delay time, t_d, is exponentially dependent on V_p, i.e. $\log t_d$ varies linearly with V_p. The slope of the line is $-V_0^{-1}$. The dependence of t_d on electrode separation involves two terms: d^2 and V_0 since V_0 is derived from a constant field, E_0. Thus:

$$t_d \propto d^2 \exp\left(-\frac{1}{d}\right)$$

for constant values of V_p.

Temperature influences t_d through the terms ρ_a and V_0 in equation 3.51.

$$t_d(T) \propto \rho(T) \exp\left[-\frac{1}{V_0(T)}\right] \quad \ldots\ldots 3.52$$

V_0 decreases with increasing temperature (chapter 6) so its overall effect on equation 3.52 is to make t_d a more sensitive function of temperature than is the case for thick samples where $t_d(T)$ depends on $\rho(T)$ only.

3.3.9. A.C. thermal effects

The two cases of thermal breakdown which have been considered so far have represented the limiting conditions. In the steady-state case, thermal equilibrium always exists (unless filament formation occurs). Under impulse conditions, no thermal equilibrium is established. Between these two extremes the influence of thermal time constants for heating and cooling must be considered.

The analysis of the a.c. admittance of a temperature-dependent circuit element follows that developed in section 3.3.1. to show the conditions required for negative resistance. It has been developed most generally by Burgess (35).

If a d.c. voltage V_0 with a small superimposed a.c. signal of amplitude V_1 is applied to a sample, then the time-variation of current I, power P, and temperature increase ΔT, are given by:

$$V = V_0 + V_1 \exp j\omega t$$

$$I = I_0 + I_1 \exp j\omega t$$

$$P = V_0 I_0 + (V_1 I_0 + V_0 I_1) \exp j\omega t$$

$$\Delta T = \Delta T_0 + \Delta T_1 \exp j\omega t$$

If the expressions for power and temperature are substituted into the energy balance equation:

$$VI = CAd \frac{d(\Delta T)}{dt} + \Gamma (\Delta T)$$

then the steady-state and time-variant portions are:

$$V_0 I_0 = \Gamma (\Delta T_0)$$

and

$$P_1 = V_0 I_1 + V_1 I_0 = \Delta T_1 \left[j\omega CAd + \Gamma_1 \right]$$

where Γ_1 is the value of thermal conductance at the mean temperature increment ΔT_0. This is only necessary if Γ is temperature-dependent. The total thermal admittance $\Gamma_\omega = P_1 / \Delta T_1$ is frequency-dependent. The effective thermal time constant is

$$\tau = CAd / \Gamma_1 \qquad \ldots\ldots 3.53$$

As in section 3.3.1. the alternating current may be expressed as:

$$I_1 = gV_1 + hT_1$$

where $$g = \left.\frac{\delta I}{\delta V}\right|_{T_0}$$

$$h = \left.\frac{\delta I}{\delta T}\right|_{V_0}$$

and the a.c. admittance is then:

$$Y(\omega) = \frac{g\Gamma_\omega + h I_0}{\Gamma_\omega - h V_0} \qquad \ldots\ldots 3.54$$

At zero frequency, equation 3.54 reduces to:

$$Y(0) = \frac{g\Gamma_1 + h I_0}{\Gamma_1 - h V_0}$$

Since Γ_1 is real, $Y(0)$ has no reactive component and is a constant, G_0, which represents the slope of the steady-state I - V characteristic.

At infinitely high frequencies, equation 3.54 gives:

$$Y(\infty) = \frac{g + \frac{hI_0}{\Gamma_\infty}}{1 - \frac{hV_0}{\Gamma_\infty}}$$

i.e. $Y(\infty) = g.$

Therefore, in this case too, the admittance is a pure conductance. g is the isothermal conductance, i.e. because of the thermal inertia of the device and its associated time constant, τ, there is no thermal response to very high frequency signals.

To examine the thermal behaviour at intermediate frequencies,

substitute

$$\Gamma_\omega = j\omega C_1 + \frac{C_1}{\tau} \qquad (C_1 = CAd)$$

into equation 3.54 then separate $Y(\omega)$ into its real and imaginary parts. In terms of resistance and reactance, this gives:

$$R(\omega) = \frac{g\omega^2 C_1^2 + (\frac{C_1}{\tau} - hV_0)(\frac{C_1 g}{\tau} + hI_0)}{\omega^2 C_1^2 g^2 + (\frac{C_1 g}{\tau} + hI_0)^2}$$

$$X(\omega) = \frac{\omega C_1 h(gV_0 + I_0)}{\omega^2 C_1^2 g^2 + (\frac{C_1 g}{\tau} + hI_0)^2} \qquad \ldots\ldots 3.55$$

For semiconductors such as chalcogenide glasses, h is always positive. $X(\omega)$ is therefore inductive and the effect of thermal inertia is to simulate an inductive effect with the current lagging the voltage signal. The locus of the tip of the I - V characteristic is an ellipse. This is shown in fig. 3.12. The thermal admittance may be represented by an equivalent circuit composed of resistors and an inductor. This is done in chapter 6 with experimental results.

Under a.c. conditions, dielectric loss may be sufficient to give rise to significant heating effects. This has been analysed by Klein and Levanon (36) for the case of silicon monoxide. The chalcogenide glasses which are used in switching devices have much lower resistivities than SiO ($10^4\ \Omega$.m rather than $10^8\ \Omega$.m) and at frequencies below τ^{-1}, heating due to dielectric loss is neglegible.

Fig. 3.12

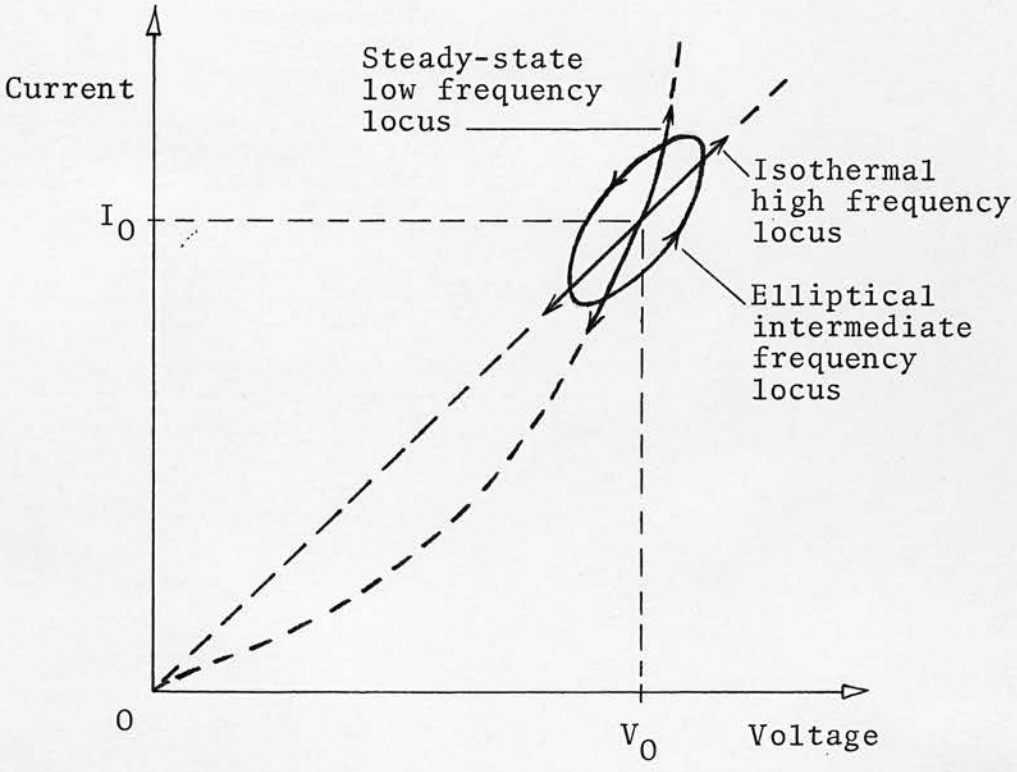

Influence of frequency on small-signal a. c. I - V characteristics.

3.4. DIELECTRIC BREAKDOWN BY ELECTRONIC PROCESSES

3.4.1. Introduction

In the study of breakdown in dielectrics, three basic modes are usually considered. Thermal breakdown has been treated in 3.3. The other two are usually described as Intrinsic and Electric breakdown. Both depend on the interaction between carriers or carrier and host material so they are considered together in this section. In the literature, some theories are closely associated with certain classes of materials, sometimes for experimental convenience and sometimes because of unique properties of these materials. Where it has been possible in this section, the application of a breakdown mechanism to chalcogenide glasses is considered.

Three classes of electronic breakdown are described in the following sections. They are:

1. Collective breakdown. With a high electron density and large number of collisions between electrons, the equilibrium electron temperature may rise without limit, (as opposed to a rise in the lattice temperature only for the case of Joule heating).
2. Avalanche breakdown. Collision with atoms of the dielectric by high energy electrons may lead to ionisation and an avalanche effect rather like a gas discharge.
3. Internal field emission. For very high fields, carrier tunnelling between bands may occur. This is Zener breakdown. In some cases, field assisted emission of trapped carriers may also occur.

Each of these breakdown modes has optimum conditions for occurrence. One general model may be used to demonstrate collective and avalanche breakdown so it is described in this section. The two variations are developed in the following sections.

In a dielectric under steady-state conditions, electrons gain energy, $\mathcal{E}$, as a result of the electric field. The rate of energy transfer from field to electron, A, is given by:

$$A = e \mu(\mathcal{E}) E^2$$

where $\mu(\mathcal{E})$ is the electron mobility which may be energy dependent. The rate of change of A with energy is shown schematically in fig. 3.13. (37).

The interaction between an electron and lattice vibrations involves either the emission or absorption of a phonon of energy $h\nu$ where h is Planck's constant and ν is the phonon frequency. The average number of lattice quanta with energy $h\nu$ is:

$$N_\nu = \left[1 + \exp\left(\frac{h\nu}{kT_0}\right)\right]^{-1} \qquad \ldots\ldots 3.56$$

and the ratio of probability of phonon absorption to emission is $N_\nu / 1 + N_\nu$. Thus only one out of $(2N_\nu + 1)$ collisions leads to a net energy loss. If equation 3.56 is expanded, the rate at which electron-phonon energy transfer occurs is approximately:

$$B = \frac{h\nu}{\mathcal{T}(\mathcal{E})(2N_\nu + 1)} \left(1 - \frac{kT_0}{\mathcal{E}}\right)$$

Fig. 3.13

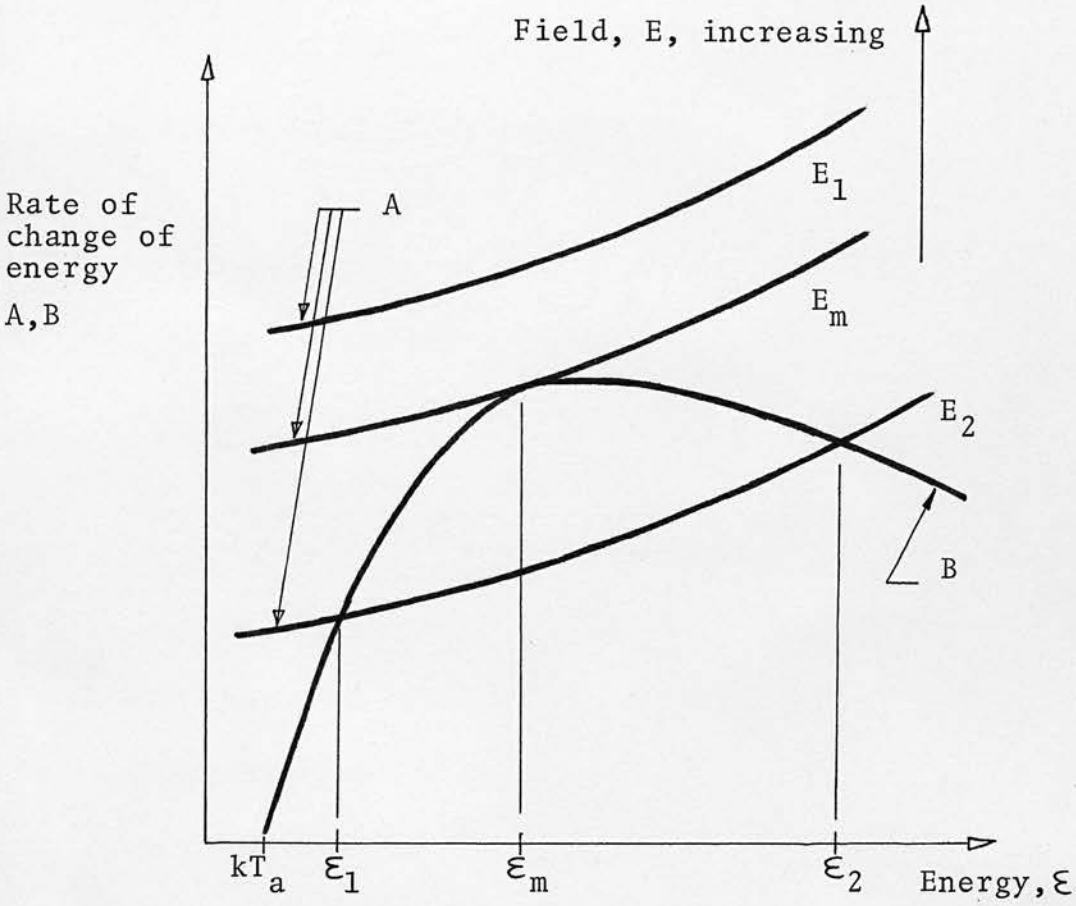

Energy conditions for electronic breakdown.

where $\tau(\mathcal{E})$ is the relaxation time associated with the electron-lattice collisions and T_0 is the lattice temperature. The value of $h\nu$ in equation 3.56 is an average over the phonons which can interact with an electron of energy $\mathcal{E}$. The variation of B with energy is shown schematically in fig. 3.13.

Three conditions can exist with respect to the relative values of A and B. They are shown in fig. 3.13.

1. For field E_1, A > B. There are no stable conditions. The electrons continue to acquire energy until breakdown occurs.
2. At field E_m there is a single stable state: A = B. Any increase in field produces breakdown. E_m was defined by von Hippel as the breakdown field.
3. For any field below E_m, two solutions are possible at energies $\mathcal{E}_1$ and $\mathcal{E}_2$ (B > A). An electron with energy $\mathcal{E}_1 < \mathcal{E} < \mathcal{E}_2$ loses energy until $\mathcal{E}$ approaches $\mathcal{E}_1$. Similarly if $\mathcal{E} < \mathcal{E}_1$ the electron will gain energy from the lattice until it reaches $\mathcal{E}_1$, the position of stable equilibrium. However, if $\mathcal{E} > \mathcal{E}_2$ the electron energy increases indefinitely even for very low values of field. Thus $\mathcal{E}_2$ represents a point of unstable equilibrium. To achieve stable conditions for $\mathcal{E} > \mathcal{E}_2$ additional mechanisms are needed which will transfer energy from the high energy electrons. If the electron density is high, electron-electron collisions may provide this mechanism. This leads to collective breakdown. At lower electron densities, collisions with atoms

of the dielectric may lead to ionization and hence avalanche breakdown.

3.4.2. Collective breakdown

When the electron density is sufficiently high, electrons with energy greater than $\mathcal{E}_2$ can collide with lower energy electrons so the whole system can remain in equilibrium with a mean energy only slightly in excess of $\mathcal{E}_1$. With a high collision rate and a rate of energy exchange due to electron-electron collisions greater than that due to electron-phonon interactions, the electron energy distribution function is Maxwellian with a mean temperature T above the ambient dielectric temperature, T_a. This means that the energy rate of change terms, A and B, can be averaged over the distribution function. These averaged values, $\bar{A}$ and $\bar{B}$, have a similar functional dependence on energy to A and B so von Hippel's general picture in fig. 3.13 remains valid but for averaged values, so only energies up to $\mathcal{E}_m$ need be considered.

This description has a strong analogy with thermal breakdown. In this case it is the steady-state electron temperature which rises until at a critical value no equilibrium is possible and breakdown occurs. The increased electron-phonon energy transfer near E_m implies, however, an increase in the internal temperature of the dielectric so thermal runaway follows and will always be associated with collective breakdown.

The electron density necessary for collective breakdown has been

calculated by Stratton (37). This turns out to be 10^3 - 10^4 times greater than the low field electron density. In amorphous semiconductors the pre-switching I - V characteristic implies that the maximum electron density could only be about 40 times the low field value so collective breakdown is unlikely to be important as an explanation for switching.

When the ambient temperature is increased, this has a greater effect on the effective electron temperature than on phonon energy. Thus the average functions $\bar{A}$ and $\bar{B}$ are moved to the right in fig. 3.13., but the relative displacement of $\bar{A}$ is greater than that for $\bar{B}$ so their intersection occurs at lower values of A and B, i.e. an increase in ambient temperature results in an increase in breakdown field. This is opposite to the observed T_a - E_{th} behaviour in chalcogenide switches.

Collective breakdown is a function of electron density. All calculations and relationships associated with fig. 3.13. have no functional dependence on sample dimensions. This too contrasts with chalcogenide switches (and thermal breakdown).

Collective breakdown has been applied successfully to alkali halide crystals. More complex relations can be derived for application to covalent materials or solids with a high proportion of defects or impurities. However, the theory still retains its basic features and is therefore unlikely to be important in any explanation of switching in glasses.

3.4.3. Avalanche breakdown

If the electron density is low, a high energy electron may have a negligible collision rate with other (lower energy) electrons. Instead, a collision with an atom of the dielectric may produce an ion and two low-energy electrons. This has been described by Frohlich as a high energy criterion (38) since it only applies to electrons with energies high enough to produce ionization.

A similar treatment was developed by Seitz (39) and has become known as the "40 generations theory". He considered a single electron having i ionizing collisions as it crossed the dielectric producing 2^i free electrons in a cone spread through the dielectric. If 10^{12} electrons were produced in a sample 1 cm thick and area 10^{-9} m^2, the temperature rise would be enough to give a thermal breakdown condition. Since $10^{12} \doteq 2^{40}$, 40 collisions are the approximate condition for avalanche breakdown.

O'Dwyer has pointed out a serious objection (40). After the final collision, 10^{12} electrons over an area of 10^{-9} m^2 move towards the anode, effectively acting as a sheet of negative charge. The immobile holes act as a sheet of positive charge at a distance of d/40. This arrangement acts as a capacitor but the field between the plates is of the order 10^{13} $V.m^{-1}$. which is clearly unrealistic. O'Dwyer's solution to this problem was to derive expressions for field and potential throughout the sample. The distribution of mobile electrons and stationary ions has to satisfy Poisson's equation and local continuity

of electron current was also imposed.

This theory was applied successfully to NaCl and Al_2O_3, and it was found that the avalanche field decreased very quickly with increasing sample thickness ($\frac{1}{E_{max}} \propto \log d$). For films 10 μm thick E_{max} was $\sim 4.10^8$ V.m^{-1}. Forlani and Minnaja (41) derived $E_{max} \propto d^{-\frac{1}{2}}$ but at 10 μm their numerical value of E_{max} was almost the same as O'Dwyer's.

To achieve an avalanche effect as described by Seitz or O'Dwyer, field strengths of the order of 10^8 V.m^{-1} are needed. In (relatively) narrow gap materials such as chalcogenide glasses, thermal breakdown occurs at average fields much lower than those needed for avalanche. It was shown in section 3.3.3., however, that during thermal breakdown high field regions can exist near the electrodes and avalanche breakdown could occur there. This is discussed in section 3.3 and in chapter 4.

One of the most important applications of avalanche breakdown is to p-n junctions. It provides a limit to diode reverse bias voltages or to transistor collector voltages, and this form of breakdown has therefore been studied in considerable depth.

The first experimental studies of avalanche effects in junctions were by McKay (42) (43) and were explained on the basis of a theory akin to that used for discharge in gases (44). The observed multiplication factor M was related to α, the ionization rate or number of electron-hole pairs produced by a carrier per unit length in the direction of the uniform field:

$$\alpha = \frac{(1 - M^{-1})}{d}$$

where d is the effective junction barrier width. This equation assumes that the ionization rate is the same for electrons and holes. Chynoweth established that the rates are slightly different (45) and that they are field dependent (46):

$$\alpha = \alpha_{\infty} \exp\left(-\frac{b}{E}\right)$$

The theoretical basis for this equation was later established by Baraff (47).

There are several important features of avalanche breakdown in p-n junctions. The most important is that breakdown is localised and the small regions of avalanche are described as microplasmas. Light is emitted due to electron-hole recombination so the spatial location and density of microplasmas could be studied (48). The I - V characteristics of single microplasmas have been studied by Senitzky (49). The multiplication rate varied with current level and there was a region of unstable negative resistance. However, a steady state can exist if carrier generation within the filament is balanced by the radial diffusion of carriers (50). This in turn demands uniform avalanche conditions which are difficult to achieve experimentally.

Rose (51) estimated that the temperature rise in a microplasma was in the range 15 - 40 K. A more recent treatment by Martirosov (52) puts it at $\sim$ 100 K (depending on current density).

As in the case of a gas discharge, the formation of microplasmas is a statistical process. The probability that an electron will have enough energy to produce an avalanche is strongly dependent on field.

An increasing field produces first an increase in the on : off time of microplasma current and then superposition of several microplasma currents. Beyond this level there is strong interaction between microplasmas (53) (54).

The statistical occurrence of microplasma current pulses has two important consequences.

1. If a high voltage is applied, there is a time lag before any avalanche occurs. This delay time decreases with increasing voltage (55) and shows strong similarities to the delay time which occurs with thermal breakdown (discussed in section 3.3.7.).
2. The on : off fluctuations of microplasma current at fields below the overall breakdown field result in a very characteristic form of high level current noise. Because of the importance of avalanche effects in electronic devices, the associated current noise has been studied extensively (56) (57) (58) (59). Current noise has been measured in the chalcogenide glass As_2Se_3 at fields of up to 5.10^6 $V.m^{-1}$ with no evidence of any avalanche microplasma features (60). However, preliminary measurements on a more conducting chalcogenideglass film composed of AsTeGeSi indicated that current noise increased considerably when the sample was biased close to its switching voltage, V_{th}. This could be due to localized avalanche breakdown in regions of the sample where the field was much greater than the average value,

e.g. as a result of Joule heating.

The effect of ambient temperature on avalanche breakdown voltage is shown in fig. 3.14. for abrupt silicon junctions (61). An increase in T_a reduces the mean free path between electron-phonon collisions. This increase in scattering also means that electrons lose more energy to the lattice and a higher field is needed to produce an avalanche. In amorphous switches an increase in T_a results in a reduced value of breakdown voltage so although some avalanche effects may be present, they do not represent the principal mechanism which gives rise to switching processes.

3.4.4. Internal field emission

In p-n junctions with very high impurity densities, high fields can exist and carriers can tunnel directly between bands. This process becomes more significant than avalanche breakdown for diodes with a turnover voltage below about 10 volts. (62). An increase in ambient temperature slightly increases the tunnel current density so the field necessary for breakdown is reduced.

A similar situation may also exist at a metal-semiconductor junction or for the case of a very thin dielectric layer sandwiched between two electrodes. This is closer to a situation which may arise for chalcogenide glass switches. The tunnel current density increases rapidly as thickness is decreased as is shown in fig. 3.15. (63) for the case of a rectangular barrier.

Under the thermal breakdown conditions of section 3.3.3., a

Fig. 3.14

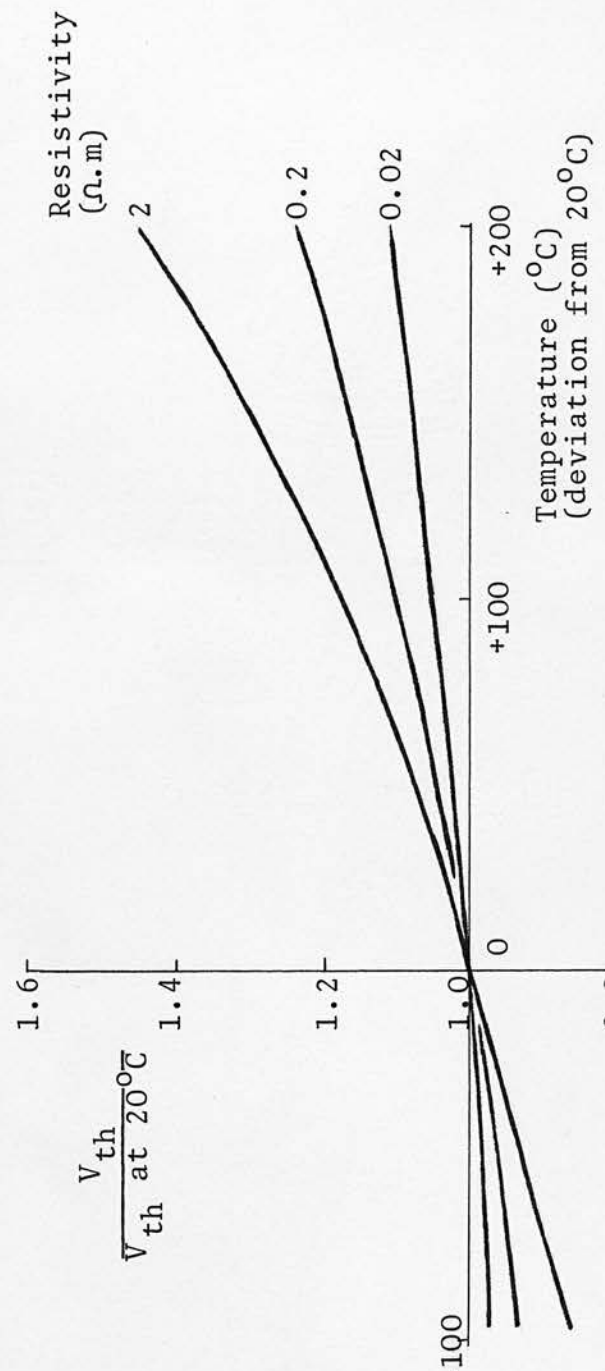

Avalanche breakdown in abrupt silicon junctions: variation of breakdown voltage with temperature.

Fig. 3.15

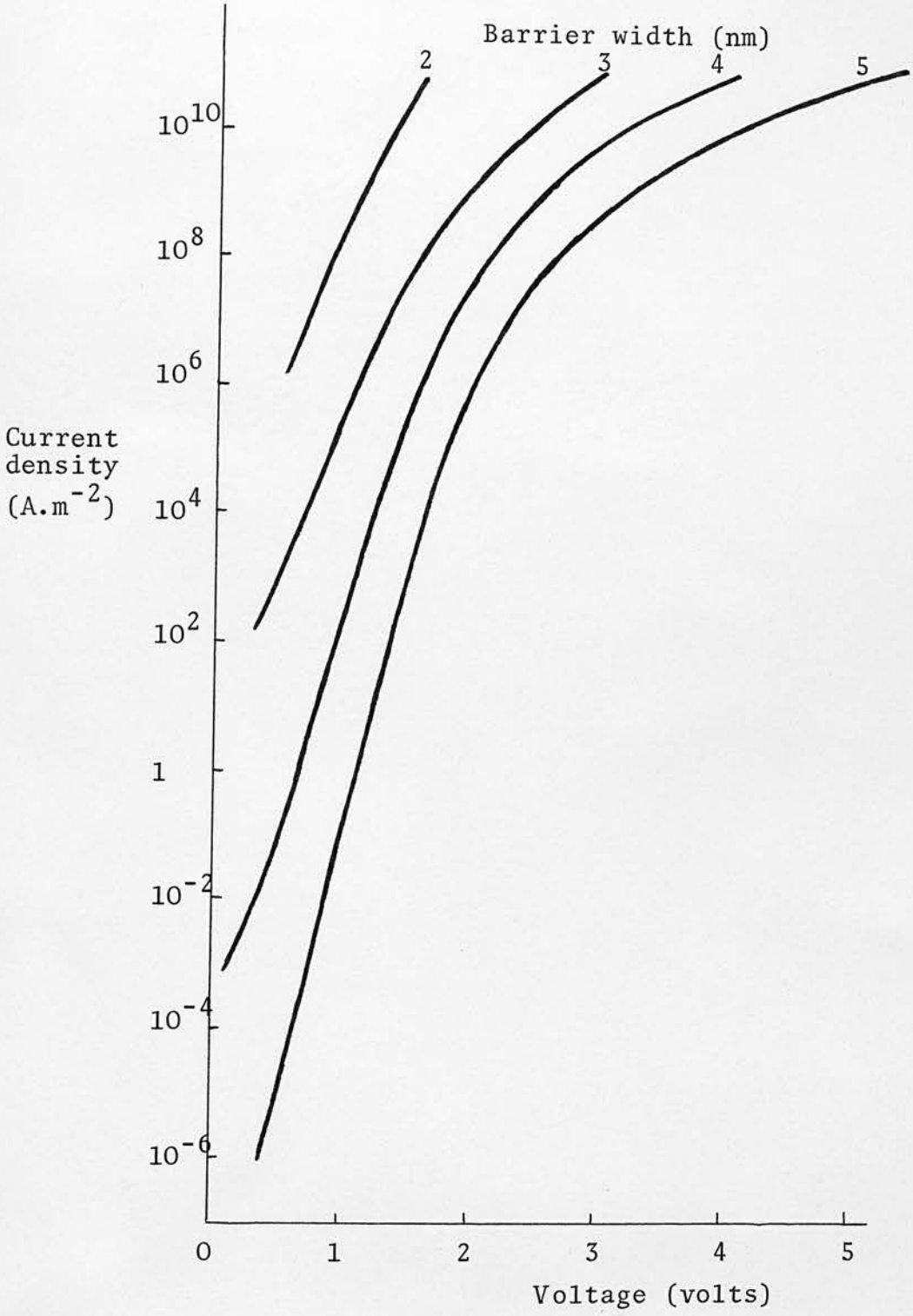

Tunnel current density as a function of voltage and barrier width.

relatively cool high resistivity region may exist at each electrode. Fig. 3.15. shows the voltage and thickness conditions needed for appreciable tunnelling.

A process related to internal field emission is field-assisted emission of carriers either over a contact energy barrier or from a coulombic potential well. These are the Schottky and Poole-Frenkel processes respectively. Poole-Frenkel emission is considered in detail in chapter 6 as a possible conduction mechanism in thin films of chalcogenide glasses.

3.5. DIELECTRIC BREAKDOWN AND ITS APPLICATIONS TO DEVICES

3.5.1. Avalanche injection diodes

If a high field can be established in a semiconductor without a high level of carrier injection, collision ionization may occur. The basic features of this process were discussed in section 3.4.3.; here its applications are reviewed.

The device off-state is characterised by a high resistance. The current noise due to self-extinguishing microplasmas increases as the voltage increases to the breakdown value, V_{th}. Beyond V_{th} the device can operate in a sustained avalanche mode. It was demonstrated by Gunn (64) that this could result in a region of negative differential resistance. Furthermore, the switching interval between the pre- and sustained avalanche modes should be of the same order as the collision ionization time. This may be as short as 10 ps.

Impact ionization diodes were first studied extensively with devices made from Ge cooled to 4 K (65) (66) (67). At this temperature the free carrier density is low but so too is scattering so the carriers have a high mobility. The low thermal energy of the system also means that the field required for avalanche by impact ionization is low; for Ge it is about 10^3. $V.m^{-1}$.

A switching diode based on this mechanism was proposed by McWhorter and Rediker (68). They called it a cryosar and its I - V characteristic is shown in fig. 3.16. Several features resemble

Fig. 3.16

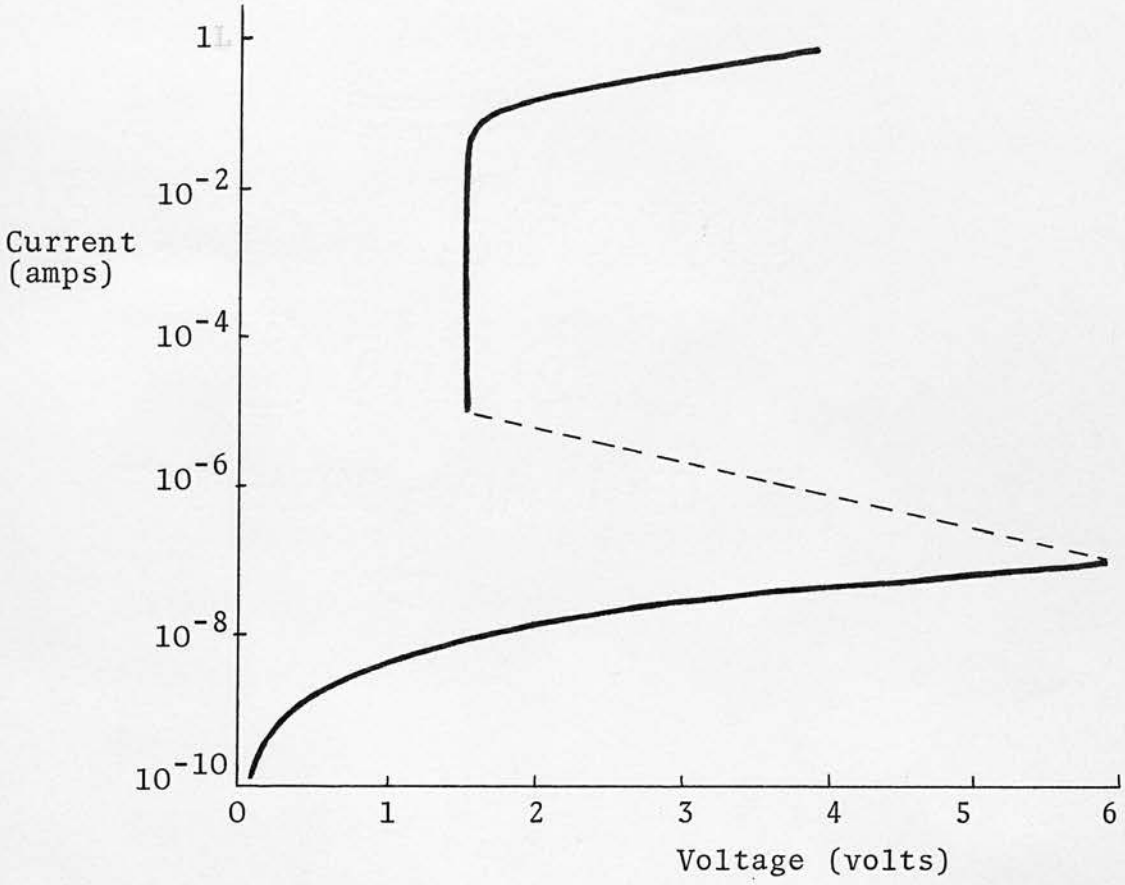

Cryosar I - V characteristic.

those for chalcogenide switches: the off state I - V relation is of the form: $I \propto \exp V$.; the holding voltage is $\sim 1\frac{1}{2}$ volts; the material has a high resistivity - 10^7 Ω .m at 4 K and is highly compensated; when a voltage pulse is applied there is a well-defined delay time before breakdown occurs. This delay time is strongly field dependent. These features also arise from the thermal breakdown mechanisms discussed in section 3.3. It is possible therefore that thermal runaway may assist or take over from impact ionization in cryosars. The discussion of switching mechanisms and their relation to experimental chalcogenide switches (chapter 4) can also be applied in some measure to cryosars.

3.5.2. Negative resistance transit-time devices

If an alternating voltage is applied to a two-terminal device and the resulting current waveform lags the voltage by more than 90°, the device has an effective negative resistance. If the phase lag is 180° the device acts as a pure negative resistance with no reactive component. For normal semiconductor resistivity and device geometry, the reactive current arising from device capacitance is neglegible.

Shockley (69) suggested that the finite transit time of carriers through a device could be used to introduce a phase lag between current and voltage but if a voltage pulse is applied to a device the current waveform at the output is much more diffuse due to scattering and diffusion as the carriers drift through the sample. The requirement

for a very sharp source of carriers was met by the structure proposed by Read (70).

The basic Read diode comprises four layers of silicon to give a p^+nin^+ structure. A typical doping profile is shown in fig. 3.17 (a) and fig. 3.17 (b) shows the resulting field distribution. The field in the p^+ and n^+ regions is neglegible. The field at the p^+n junction is higher than in the intrinsic region and the n region is narrow enough to ensure a uniform change between the two field values. If the d.c. bias is such that the field at the p^+n junction is close to the critical avalanche field, then a small alternating voltage superimposed will give avalanche breakdown. Since the ionization coefficient is very sensitive to field, a very narrow sheet of charge is produced. This is slightly out of phase with the voltage waveform and a further phase lag is introduced by the time taken for the carriers to drift across the intrinsic layer. The field in the intrinsic layer is such that the carriers drift with constant velocity. Fig. 3.16 (c) shows the ionization coefficient, α , as a function of distance and the area under the spike represents the total charge produced by the avalanche.

The Read diode is the prototype of a family of IMPATT devices (IMPATT is derived from IMPact ionization, Avalanche and Transit Time). Their basic features are determined by the avalanche conditions:

1. High local fields are necessary $\sim 5.10^7$ V.m^{-1}.
2. The pre-avalanche current noise is characteristic of self-extinguishing microplasmas (71).

Fig. 3.17

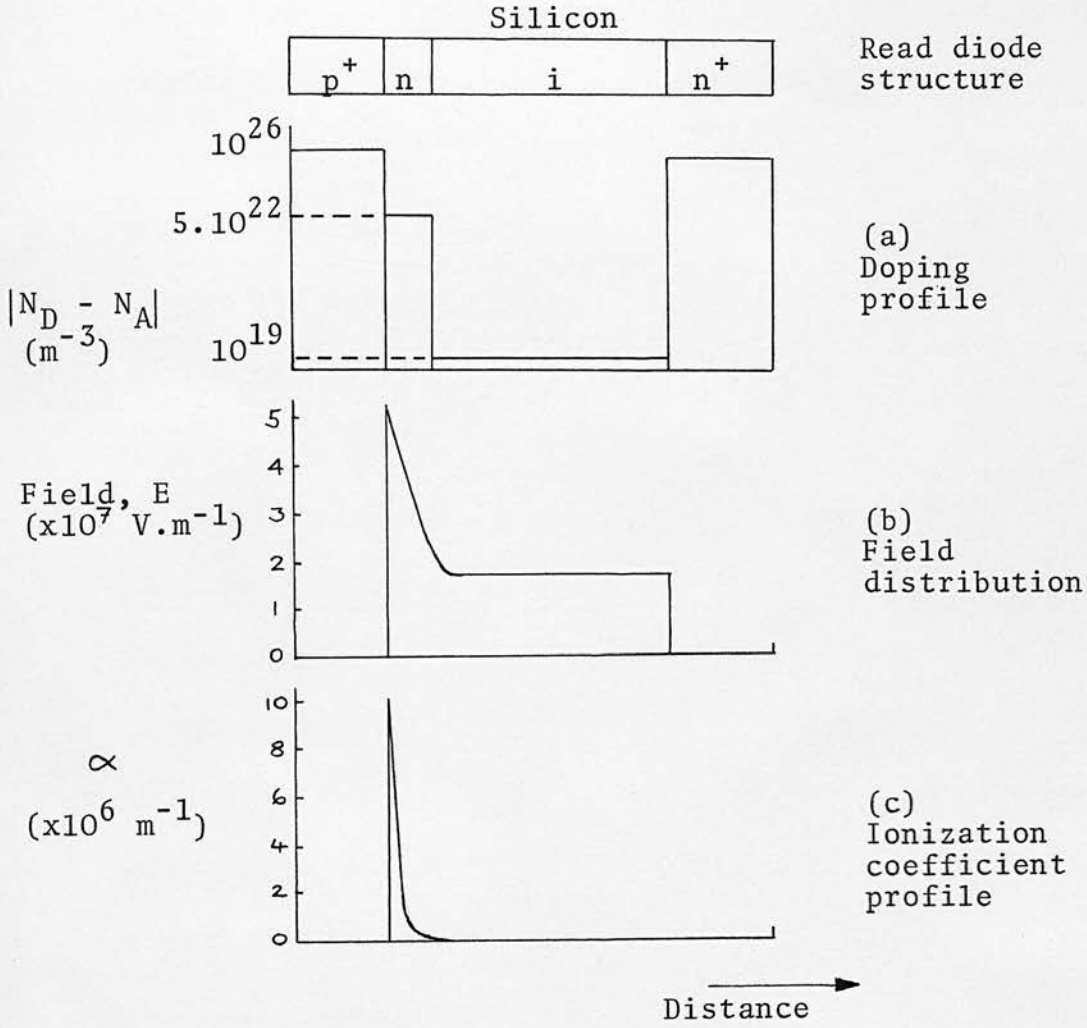

Operational features of a Read diode.

3. The frequency range over which the device has an effective negative resistance is determined by the carrier transit time.

Although Read's original model was proposed in 1958, it was not realized until 1965 when a junction with uniform ionization rate across a large area was produced (72). Defects and non-uniformities in a junction tend to give rise to local avalanche breakdown and microplasmas. These are unstable, have a very high local power density and ultimately fail, often by thermal breakdown.

3.5.3. Double injection

One-carrier space charge limited currents (SCLC) in semiconductors have been widely studied. Theoretical studies by Lampert (73) and Rose (74) indicated that at high injection levels, two-carrier conduction could be significant and the current would be recombination-limited rather than space charge limited. This change in current limiting mechanism could be very rapid and give rise to a current controlled negative resistance (CCNR) characteristic. Since this broadly resembles switching in chalcogenide glasses, this section examines the conditions and consequences of double injection.

Lampert's simplest treatment refers to a semiconductor with one electron and one hole injecting contact and a very small density of thermally generated (as opposed to injected) free carriers. A single set of recombination centres lies below the Fermi level. They are therefore fully occupied by electrons and the capture cross-section for

holes, σ_p is much greater than that for electrons, σ_n. At low injection levels, holes are trapped by the recombination centres close to the anode but electrons have no such limit, so the current is electron, trap-free SCLC. As the field across the device is raised, holes can penetrate further into the semiconductor before trapping occurs. Finally, when the hole transit time becomes as short as the hole lifetime, all the recombination centres are neutralized and the space charge limit to the electron current is removed. Current can then rise to a much higher value which is recombination limited. The increase in free hole lifetime which accompanies the neutralization of the recombination centres allows holes to cross the device at lower voltages, so the overall I - V characteristic has a region of negative resistance.

Pre-breakdown one-carrier SCLC may be of the simple trap-free type discussed in the model above, but in most materials it is dominated by the trap distribution above the Fermi level where trapped carriers are in thermal equilibrium with those in the conduction band. There are four distinct cases, and the establishment of one of the four is an important preliminary condition for the application of double injection theory to a switching process.

1. Trap-free SCLC. The total space charge which can be accommodated within a semiconductor is:

$$Q_{sc} = CV$$

where capacitance $C = \dfrac{\kappa_i \epsilon_o A}{d}$

for area A, thickness d, dielectric constant κ_i.

The approximate transit time τ_t is:

$$\tau_t = \frac{d^2}{V\mu}$$

where μ is the free carrier mobility.

The current is then approximately Q_{sc}/τ_t:

i.e.

$$J = \frac{\kappa_i \epsilon_o \mu V^2}{d^3}$$

This differs by a factor of 9/8 from the more rigorously derived equation of Mott and Gurney (75) but serves to illustrate the origin and functional interdependence of the terms.

2. Shallow traps. With a uniform density of shallow traps at a well-defined energy, E_t, below the conduction band edge, the trapped and free carriers are in thermal equilibrium. For a typical semiconductor the traps can be deep enough to allow the trapped charge density, n_t, to exceed the free charge density, n :

$$\frac{n}{n_t} = \frac{N_c \exp(-E_t/kT)}{g N_t} = \theta$$

where N_c is the density of states at the bottom of the conduction band

N_t is the trap density

g is the degeneracy factor for the traps

The overall effect of the shallow traps is to reduce the effective free carrier mobility to a value $\mu\theta$. The SCLC equation is of the same

form as that for the trap-free case, but the trap-limited mobility value, $\mu\theta$ is used in place of μ (76) and may be several orders of magnitude smaller.

3. Uniform energy distribution of traps. i.e. the trap density is constant throughout the forbidden gap. The free : trapped charge ratio, θ , is no longer a constant as in the single shallow trap case, but is a function of voltage (77). This results in an exponential I - V relation:

$$J = \frac{9}{8} \sigma_a \, E \, \exp(t_1 E)$$

where σ_a is the low field conductivity

$$t_1 = \frac{C}{A \, e \, N_t \, kT}$$

and C = sample capacitance with area A

N_t = trap density per eV of band gap.

I - V characteristics of this form have been reported by Hartke for films of amorphous selenium (78).

4. Trap density falls off exponentially with energy into the gap. This case most closely resembles the models used for amorphous semiconductors. It is an extension of the uniform energy distribution and the I - V relation is of the form (77):

$$I \propto \frac{V^{m+1}}{d^{2m+1}}$$

where $m = T_c/T$

and T_c is a parameter with the dimensions of temperature and which characterises the shape of the trap distribution.

There have been a number of detailed modifications to Lampert's theory, e.g. Ashley (79) showed that the limiting space charge could in some cases be dominated by the charge on the recombination centres. However, the existence of SCLC in one of its forms is a useful identification feature for pre-breakdown double injection.

The most extensive experimental studies of double injection have been with silicon p i n diodes (80) (81). Many elements can be used to give deep recombination levels, e.g. In, Hg, Au, Cd, Tl, Pt and Zn. (82) (83). In the pre-breakdown region the current noise spectrum is characterised by a single relaxation time (84). This has been interprete as arising from fluctuations in the occupancy of recombination centres.

Lampert's theoretical analysis gives a simple relation between the maximum and minimum voltage turnover values which define the limits of the negative resistance region:

$$V_{min} = \frac{\sigma_n}{\sigma_p} V_{max}$$

An initial condition for the model is that the electron and hole capture cross-sections should be very different with $\sigma_p \gg \sigma_n$ so $V_{max} \gg V_{min}$.

The effect of an increase in ambient temperature would be to decrease the hole trapping rate and thus decrease the voltage needed to drive the holes across to the cathode, i.e. reduce the voltage needed for onset of recombination-limited current flow. An exact value for V_{max} is difficult to obtain analytically, but Iida (85) has obtained a

numerical situation for the case of a single deep recombination level. This is shown in fig. 3.18. as a function of temperature together with V_{min} and some experimental data for compensated silicon diodes (86) (87) (88). Although the numerical values and detailed shapes vary considerably, V_{max} is more sensitive to temperature than V_{min} and at 'high' temperatures they approach the same numerical value. V_{max} decreases as the ambient temperature is increased.

Most of the features of double injection are similar to those for chalcogenide switching devices. In section 6.4., pre-switching characteristics of thin chalcogenide films are related to SCLC and double injection mechanisms to assess whether there is reasonable quantitative and functional agreement.

3.5.4. Electronic switching processes

A number of authors have attempted to develop a double injection mechanism which can be applied to amorphous semiconductors and which would allow threshold switching to be explained in purely electronic terms. There are two principal approaches; one developed by Henisch (91) and the other by Mott (92) (93). Both arrive at the same final mechanism for switching but differ in their description of pre-switching behaviour.

The charge distribution for several bias conditions is shown in fig. 3.19. for Henisch's model. The glass is assumed to be exactly compensated so that the band shape is as shown in (a) immediately after

Fig. 3.18

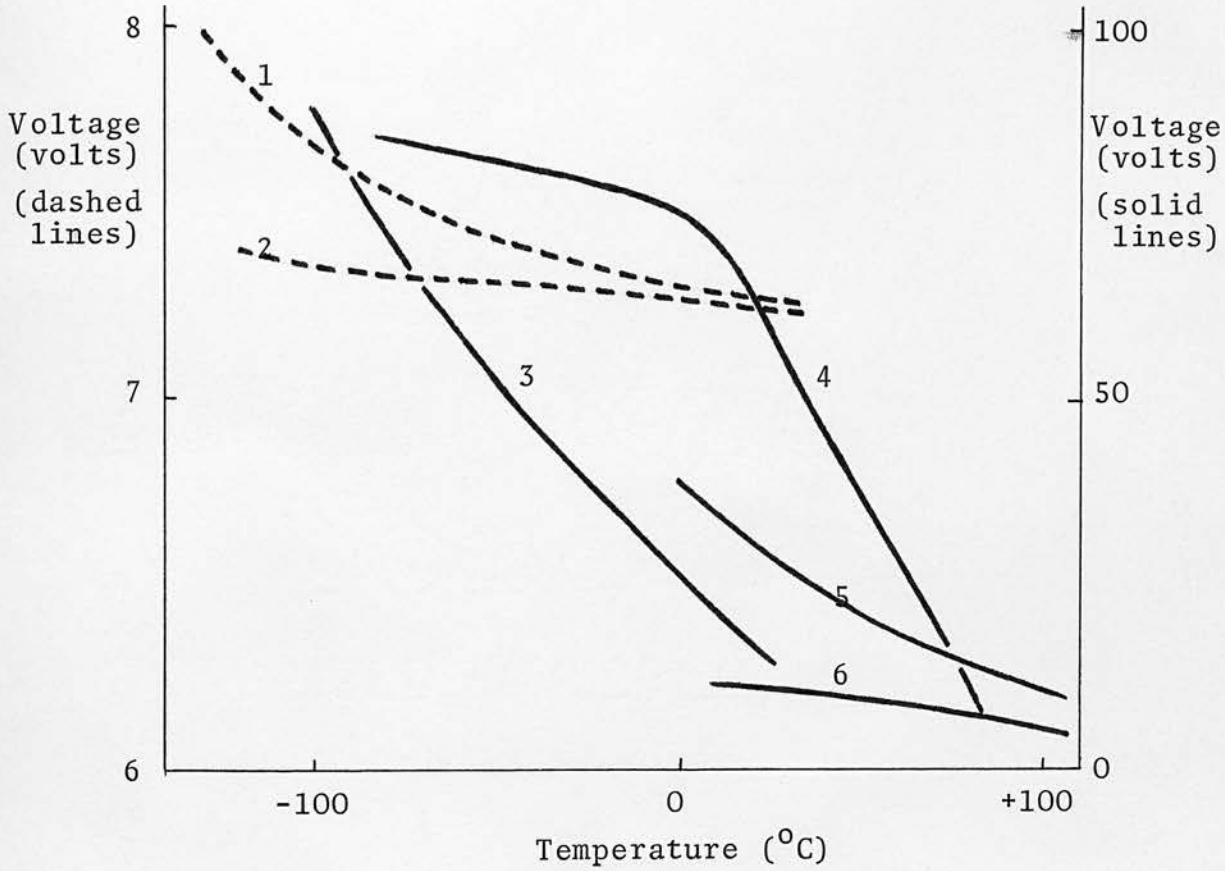

Key:
1. Iida V_{max}
2. Iida V_{min}
3. Lebedev V_{max} Zn-Si
4. Chino V_{max} irradiated Si
5. Lebedev V_{max} Pt-Si
6. Lebedev V_{min} "

Double injection: V_{max} and V_{min} as a function of temperature.

Fig. 3.19

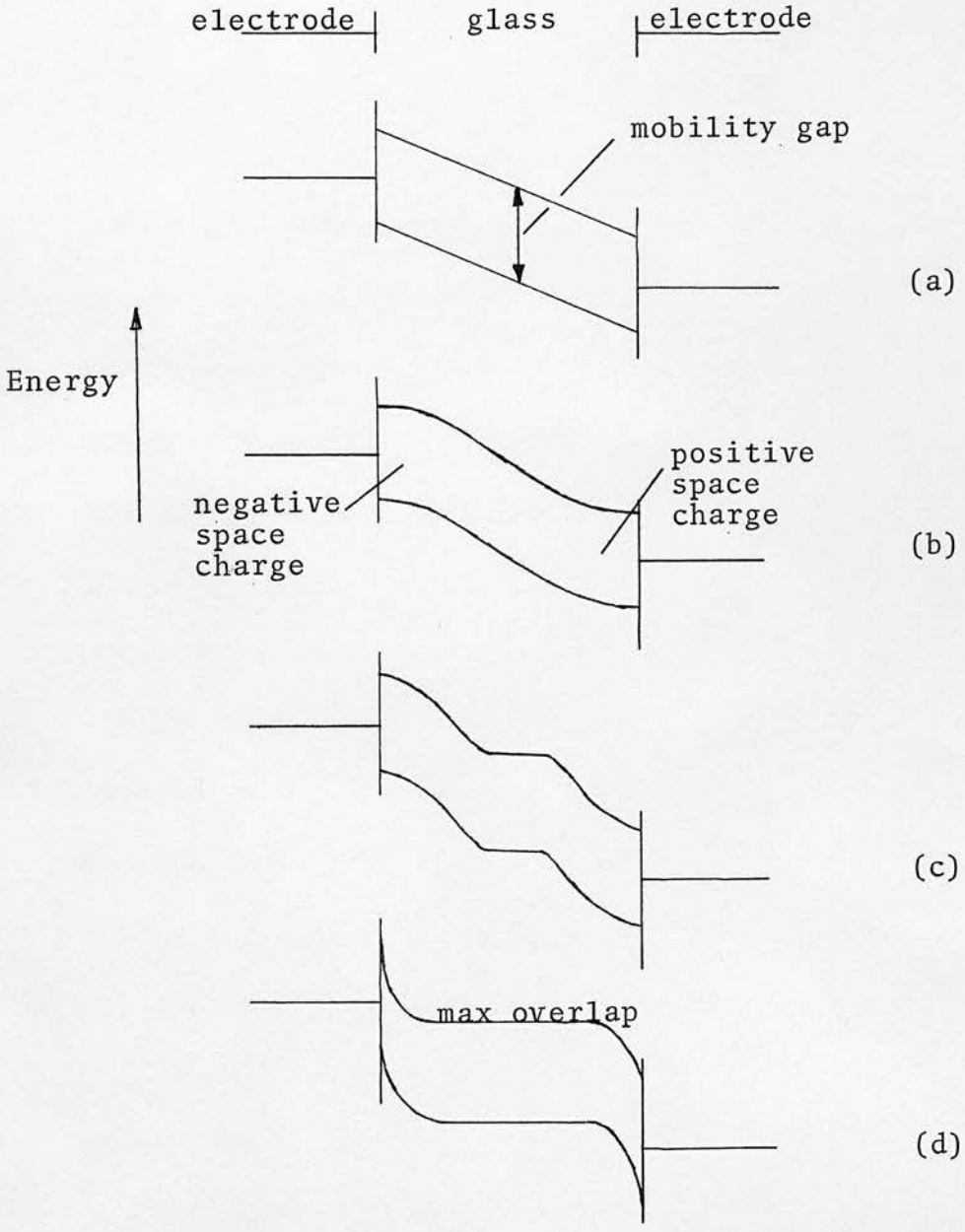

Henisch: steps involved in electronic switching.

a bias voltage has been applied. The steady-state case is shown in (b) where a space charge region has built up near each electrode. This limits the current flow and increases the effective field in the middle of the sample.

Increasing current flow results in an extension of the space charge regions until they finally overlap in the middle of the sample. The appearance of a neutral region in the middle alters the field distribution drastically to that shown in diagram (c). The low field in the centre means in turn that the field near the electrodes increases, carrier injection rises to higher levels, the neutral centre region increases in size and finally the stable configuration shown in fig. 3.19 (d) is reached. Thus, after the charge overlap condition is established, switching proceeds very quickly.

The on-state holding voltage arises from the barriers at the electrodes so V_h is of the same order as the band (or mobility) gap. For very narrow barriers the current density can be very high and relatively insensitive to temperature since tunnelling is dominant. The range of experimental values of V_h is discussed in section 6.4.9.

In the pre-switching region, an increase in ambient temperature gives a wider space-charge region through an increase in the diffusion length so overlap is accomplished at a lower voltage.

Mott's approach does not require any rapid change in field distribution. He considered a low barrier to be present initially. Electrons and holes can be trapped and recombine throughout the sample,

but near the cathode, electrons travel faster than their thermal equilibrium velocity in the bulk. This may be due either to tunnelling or to the slightly higher field near the cathode. The net effect is to give a region of uncompensated positive charge near the cathode (and negative charge near the anode). An increase in current density produces a narrower charge region and higher field near the electrodes. This result has also been obtained from the numerical solution of the charge distribution equations for a trap-free insulator (94) and a p^+nn^+ diode (95). Mott's space charge distribution is shown in fig. 3.20(a) and diagram (b) shows the variation of space charge density and its variation with normalized current density, δ , (94).

Switching occurs when all the voltage drop is concentrated at the electrodes as in Henisch's model : fig. 3.19(d). However, it is not clear from Mott's model why there should be a steady and precise voltage for switching. Also, an increase in ambient temperature would appear to demand an increase in V_{th} rather than the decrease which is observed. This may be deduced qualitatively by saying that a temperature increase would decrease the density of trapped positive charge near the cathode. This increases the width of the space charge region so a higher voltage is needed to get to the limiting on-state condition of fig. 3.19(d).

In chalcogenide glasses, the tails of localized states associated with the conduction and valence bands may overlap in the middle of the gap. As mentioned in section 2.3., this may give rise to a large density of charged states ($\sim 10^{26}\ m^{-3}.eV^{-1}$.) at the Fermi level. Consequently, the

Fig. 3.20

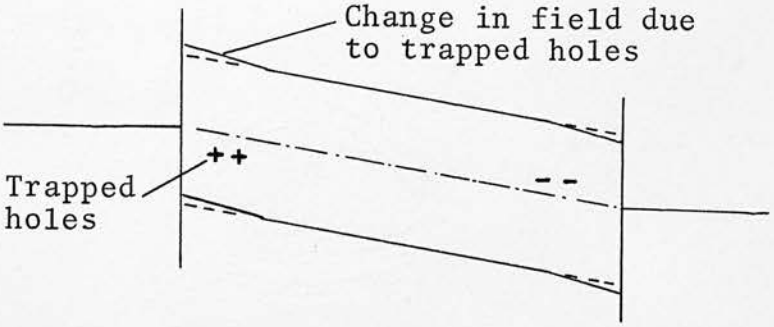

(a) Mott: low field pre-breakdown condition.

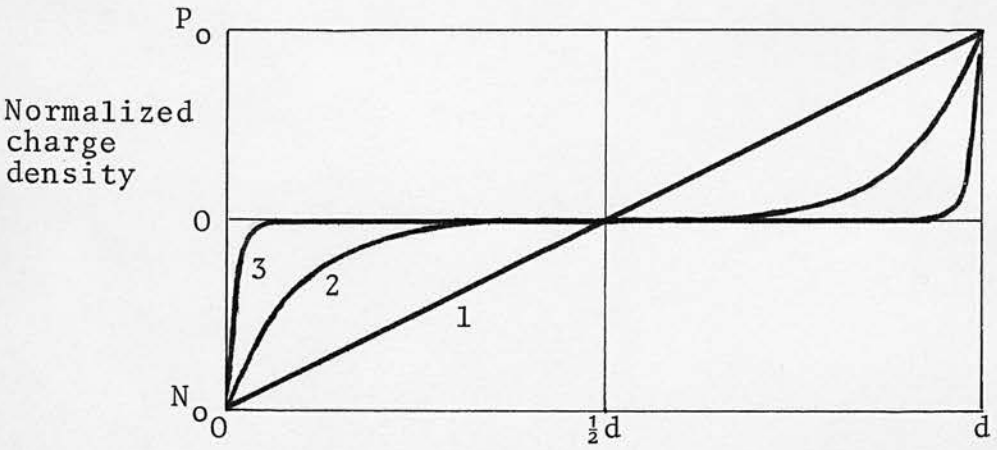

Normalized current, δ : 1 $\delta = 10^{-2}$
2 $\delta = 10^{3}$
3 $\delta = 10^{6}$

(b) Charge distribution in a $p^{+}nn^{+}$ diode.

depletion or enhancement layer depth around any source of charge imbalance is small ($\sim$ 3 nm). This could limit the extent of space charge or contact depletion layers. Thus, although the electronic switching mechanisms, particularly that of Henisch, appear to be qualitatively reasonable when applied to chalcogenide switches, their quantitative fit is less satisfactory.

3.5.5. Thermal breakdown in transistors and diodes

The operational limits of device operation may be established by electronic or thermal breakdown. Avalanche effects are likely under high field conditions but thermal limits may arise with thick or relatively high conductivity semiconductors.

In early germanium point contact rectifiers, efforts to achieve a high reverse voltage were limited by thermal processes (96) (97). A simple analysis based on the arguments used in section 3.3.3. gave a rough figure for the breakdown voltage and indicated that it should decrease with increasing ambient temperature (98). It was observed that as the ambient temperature was increased, the current level at V_{th} increased, but the $V_{th}.I_{th}$ product decreased, as shown in fig. 3.21; this cannot be explained on the basis of simple thermal breakdown.

Burgess (99) has carried out a formal analysis of the thermal breakdown of point-contact Ge diodes. He used a number of expressions for conductivity as a function of temperature. The relations are shown in table 3.1 and the resulting power-temperature relations in fig. 3.22;

Fig. 3.21

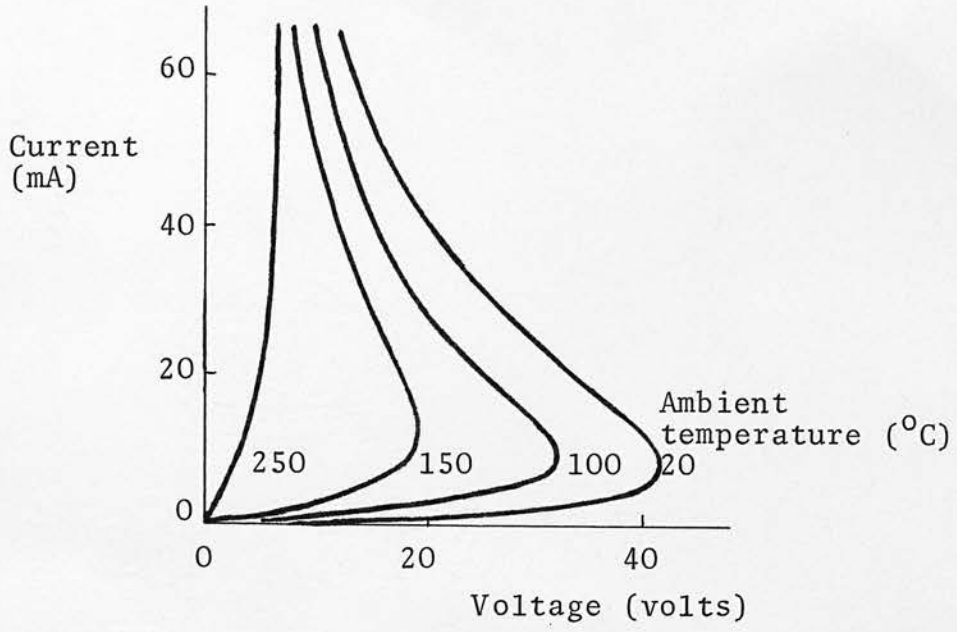

(a) I - V characteristic as a function of temperature.

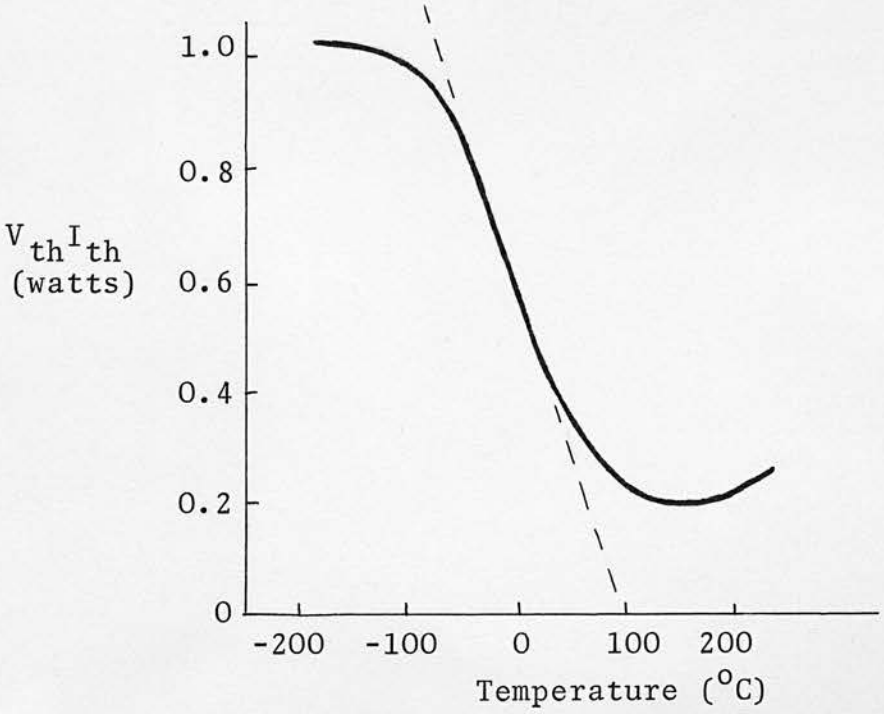

(b) Variation of threshold power with temperature.

Breakdown in Ge point contact diodes.

Form	Conductivity $\sigma(T)$ proportional to:	r	P_{th}
1	$(1 + \frac{T}{b})^n$	$\frac{n}{n - 1}$	$\Gamma(\frac{T_a + b}{n - 1})$
2	$\exp(\frac{T}{b})$	1	$b\Gamma$
3	$\exp(-\frac{b}{T})$	$(1 - \frac{2T_{th}}{b})^{-1}$	$\frac{1}{2}\Gamma\left[b - 2T_a - (b^2 - 4bT_a)^{\frac{1}{2}}\right]$
4	$(1 - \frac{T}{b})^{-n}$	$\frac{n}{n + 1}$	$\Gamma\frac{(b - T_a)}{(n + 1)}$
5	$\exp(\frac{T^2}{b^2})$	$(1 + \frac{b^2}{2T_{th}^2})^{-1}$	$\frac{1}{2}\Gamma\left[(T_a^2 + 2b^2)^{\frac{1}{2}} - T_a\right]$

Table 3.1

Burgess: expressions for P_{th} and r for five $\sigma(T)$ relationships.

Fig. 3.22

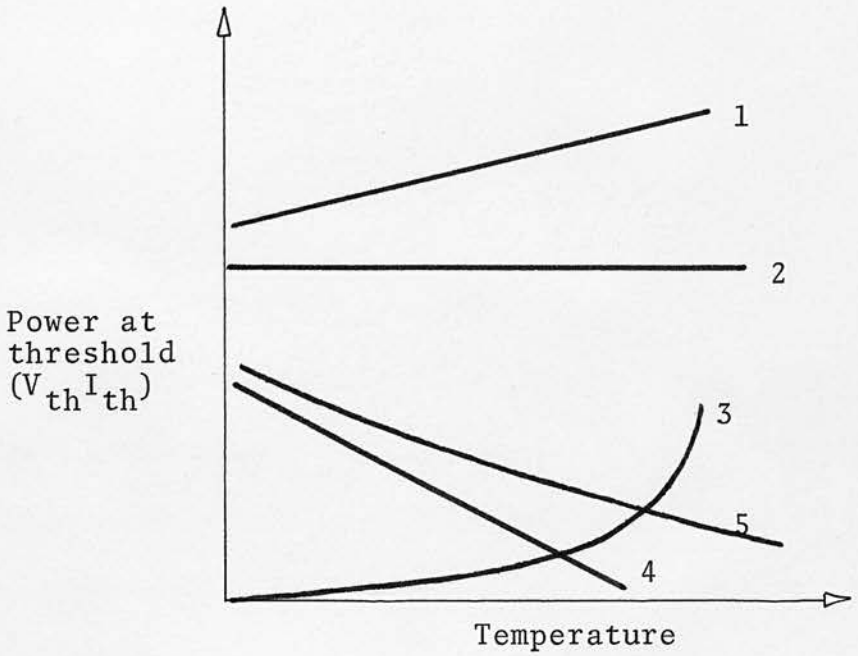

Variation of threshold power with temperature for the expressions listed in Table 3.1.

n and b are constants and r is a parameter given by:

$$r = \frac{dT_{th}}{dT_a}$$

For a germanium diode, r is required to be negative; it may also be used in the expression for threshold current:

$$\frac{dI_{th}}{dT_a} = \frac{(2r - 1)\Gamma}{2V_{th}}$$

The result of this analysis is that while relations 1, 2 and 3 in the table are typical of semiconductors, they do not yield the experimental power-temperature relation, whereas 4 and 5 are adequate for power-temperature but cannot be explained by any of the more usual conduction mechanisms.

Cutler (100) has also examined this problem but he included a term to account for the surface leakage current. If this additional current had a different temperature activation energy then the power-temperature dependence conformed to Benzer's experimental data as shown in fig. 3.21 (b).

The temperature profile in a sample was derived in section 3.3.3. This in turn gives a resistivity profile which can be integrated graphically or numerically to give the sample resistance at a specified current level. Hence, the current-voltage characteristics can be derived for a number of values of T_a (e.g. fig. 3.6.). This also results in the product $V_{th}.I_{th}$ decreasing as T_a is increased.

Thermal breakdown in Ge point-contact diodes is in many respects similar to switching in chalcogenide glasses. However in glasses $V_{th}.I_{th}$ increases slightly as T_a is increased and the Ge diodes have a well-defined negative resistance region. Turnover in Ge diodes is relatively 'soft' and with a high series resistance, a bias point on the negative I - V slope can be maintained.

Silicon diodes replaced point contact Ge diodes for high voltage applications. This change removed the importance of high-voltage thermal breakdown in Ge and is probably the main reason for an all-embracing analysis never being completed.

In transistors operated under high power conditions a failure mode known as second breakdown may occur. The general features are shown in the collector current-voltage characteristics in fig. 3.23. for forward, zero and reverse base drive. (101). In the regions marked by dashed lines the curve cannot be stabilized, i.e. the device switches from a high to a low voltage state. If the current level is increased beyond I_d permanent damage occurs.

An increase in T_a results in reductions in turnover current and voltage levels (102), (usually they are called the trigger current and voltage). Under pulsed operation there is a time lag - the trigger time - between the application of a high voltage pulse and the current runaway. This is shown in fig. 3.24. as a function of ambient temperature (103).

The mechanism responsible for second breakdown has now been established as a form of thermal runaway (104) (105). English (102) proposed

Fig. 3.23

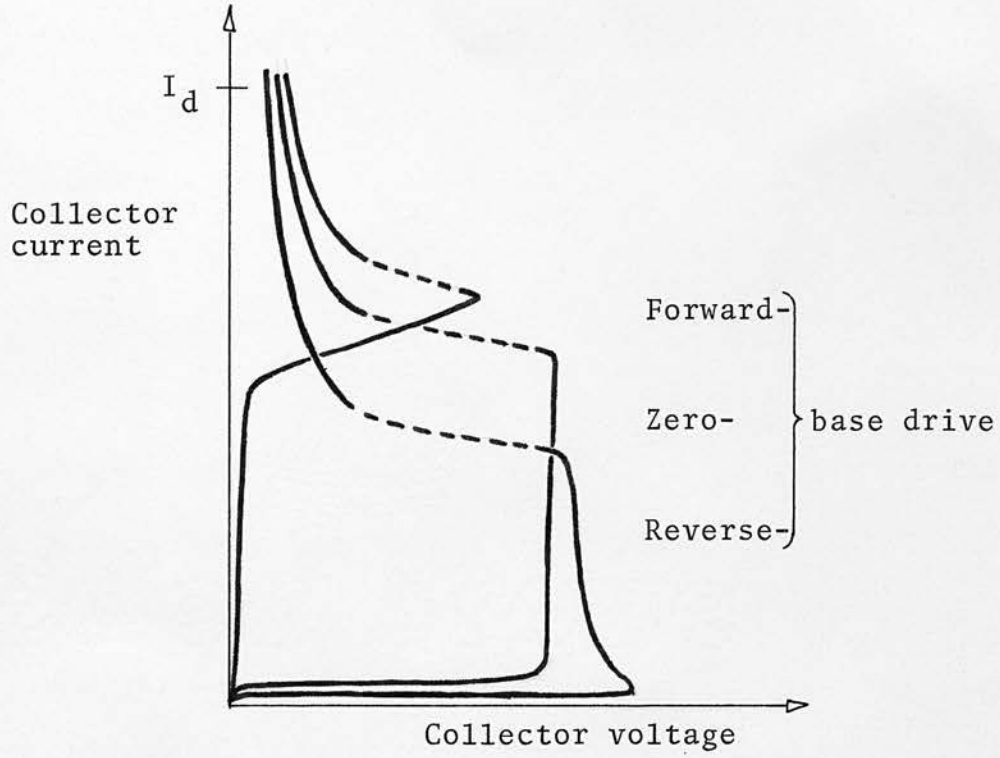

Steady state second breakdown characteristics.

Fig. 3.24

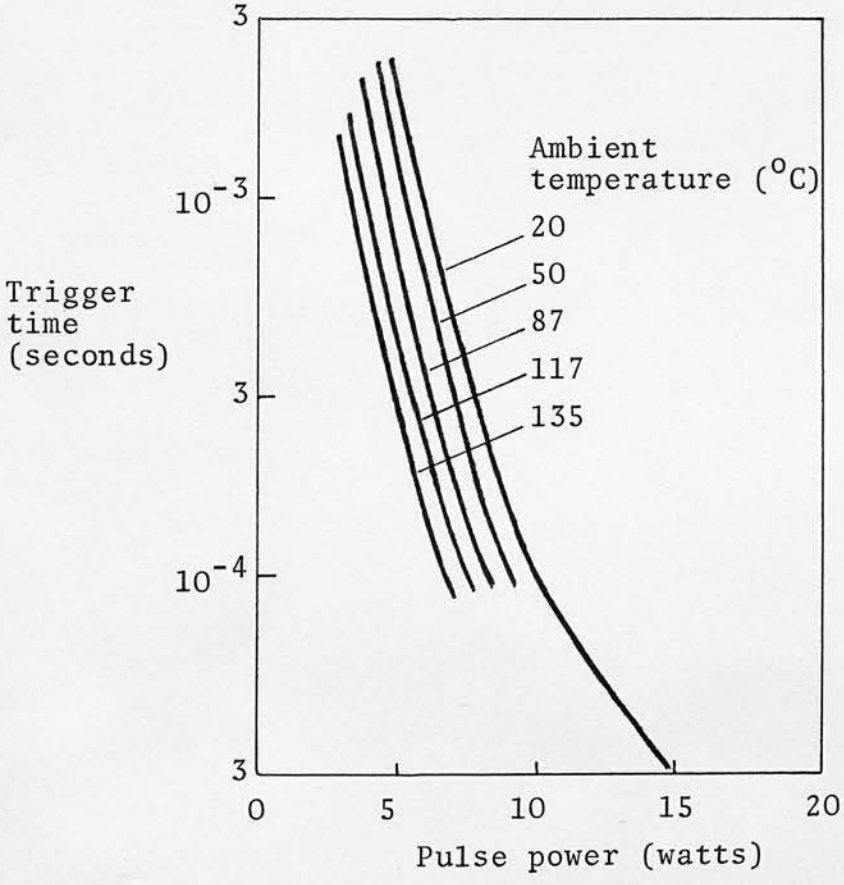

Impulse second breakdown characteristics.

that a microscopic melt is formed. This he called a 'mesoplasma' by analogy with the microplasma for avalanche breakdown. Under certain conditions, microscopic molten globules of silicon have been observed and the theoretical analysis of Weitzsch (106) has indicated that the molten zone can exist in a stable state.

There are many similarities between the experimental results for thermal breakdown in diodes and transistors and that for threshold-type switching in chalcogenide glasses. This can be taken as fairly strong circumstantial evidence that similar mechanisms may be responsible. In chapters 4 and 6 this possibility is reviewed more critically.

3.5.6. Voltage controlled negative resistance (VCNR)

The instabilities and breakdown modes discussed so far give I - V characteristics which are 'S' shaped, i.e. they have a region of current controlled negative resistance. There also exist devices which are the dual of the CCNR devices, i.e. with 'N'-shaped or voltage controlled negative resistance characteristics. Ridley (19) has shown that for VCNR high field domain formation is to be expected in the same way that current filaments occur with CCNR devices.

The most important class of devices which shows bulk VCNR is that based on the Gunn effect (107) (108). The mechanism responsible for the differential negative resistance is a field-induced transfer of conduction-band electrons from a low-energy, high mobility valley to higher-energy low-mobility satellite valleys. Materials such as GaAs, InP and Ge

conform to the special requirements for conduction band shape. Chalcogenide glasses with low carrier mobility and a non-crystalline structure, are not likely to show any Gunn-type instability.

Voltage controlled negative resistance has been observed in thin amorphous films of SiO under special experimental conditions (109). The films had at least one electrode of gold and were 0.04 - 0.3 μm thick. A forming process is necessary. The unformed device shows the typical Poole-Frenkel I - V relation observed in SiO (29). If the device is placed in a modest vacuum with a d.c. bias of about 10 volts, the conductivity shows a marked increase as the voltage is reduced. This is shown by the solid line in fig. 3.25. Any subsequent low frequency voltage sweep traces out this line. The peak : valley current ratio was typically 100 : 1 and in some devices, as high as 1000 : 1.

Under a.c. conditions (> 1 KHz) the effective sample resistance depends on the maximum voltage. The locus of the tip of lines of different V_{max} is the same as the d.c. characteristic. Two a.c. lines are shown in fig. 3.25 as dashed lines.

A memory state can be induced if the device is biased to the required resistance and the bias is quickly removed. The resistance is then maintained indefinitely for low interrogation voltages. To change the resistance level, a voltage greater than V_T (approximately corresponding to the d.c. peak) must be applied.

Simmons (109) explained the forming process as being due to injections of gold ions into the insulator. The gold atoms were assumed

Fig. 3.25

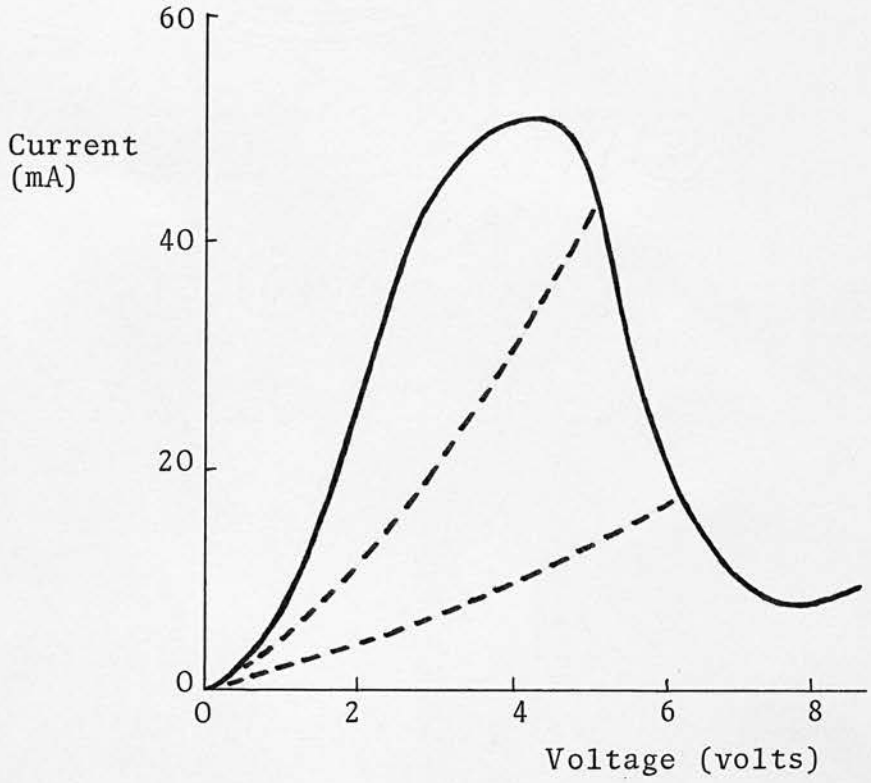

Voltage-controlled negative resistance in silicon monoxide.

to be donors and positively charged when located above the Fermi level in the insulator. Negative charge can be stored at these gold sites and the charge density is determined by the field. If the field is removed quickly, the charge may be retained within the insulator. Through Poisson's equation this reduction in space charge density implies a reduction in field at the metal-insulator interface and therefore a higher conductivity; hence the memory state.

An alternative and rather simpler mechanism has been proposed by Dearnaley (110). He considers the formation of a large number of quasi-metallic filaments through the insulator. Typcial filament diameters and densities are 1 nm and 5.10^{10} m^{-2} respectively. Memory resistance is determined by the filament density. These filaments are similar to microplasmas. Their formation, however, is not followed by the rapid radial growth which is associated with the formation of a single filament and current-controlled negative resistance.

Dearnaley's theory has some features in common with the component separation explanation for memory switching (section 3.6). No VCNR has been observed in chalcogenide glasses and this suggests that when a filament is formed, there is little to limit its radial expansion and CCNR results.

3.6. SWITCHING DUE TO BOND OR STRUCTURAL CHANGES

3.6.1. Crystallization

If a breakdown process in a semiconductor or dielectric is limited so that no permanent damage occurs, the material may return to its pre-breakdown state when the bias is removed. This forms the basis for explanations of monostable or threshold switching. For the case of memory switching, however, a physical change must occur so that the high conductivity state can be maintained without any sustaining power.

Glasses are in a state of unstable or at most metastable thermodynamic equilibrium (chapter 2). When energy is dissipated within any glass there is always the possibility that it will devitrify. The temperature at which devitrification might be expected is dependent on the glass composition but Pearson (111) and Roy (112) have shown that many of the chalcogenide glasses used for switching devices are not homogeneous (chemically or physically) and exist in the bulk in more than one phase. An evaporated film may be considered to have experienced very rapid quenching and it is possible that thin films have a more uniform phase distribution than bulk glasses of the same composition.

In chalcogenide glasses there is often a very large difference in resistivity between the amorphous and crystalline phases of the same composition. This is shown in fig. 3.26. for the system As_2Se_3 - As_2Te_3 (113). In bulk form, glasses cannot be prepared with more than 80% As_2Te_3 but thin films can be produced with up to 100% As_2Te_3 as

Fig. 3.26

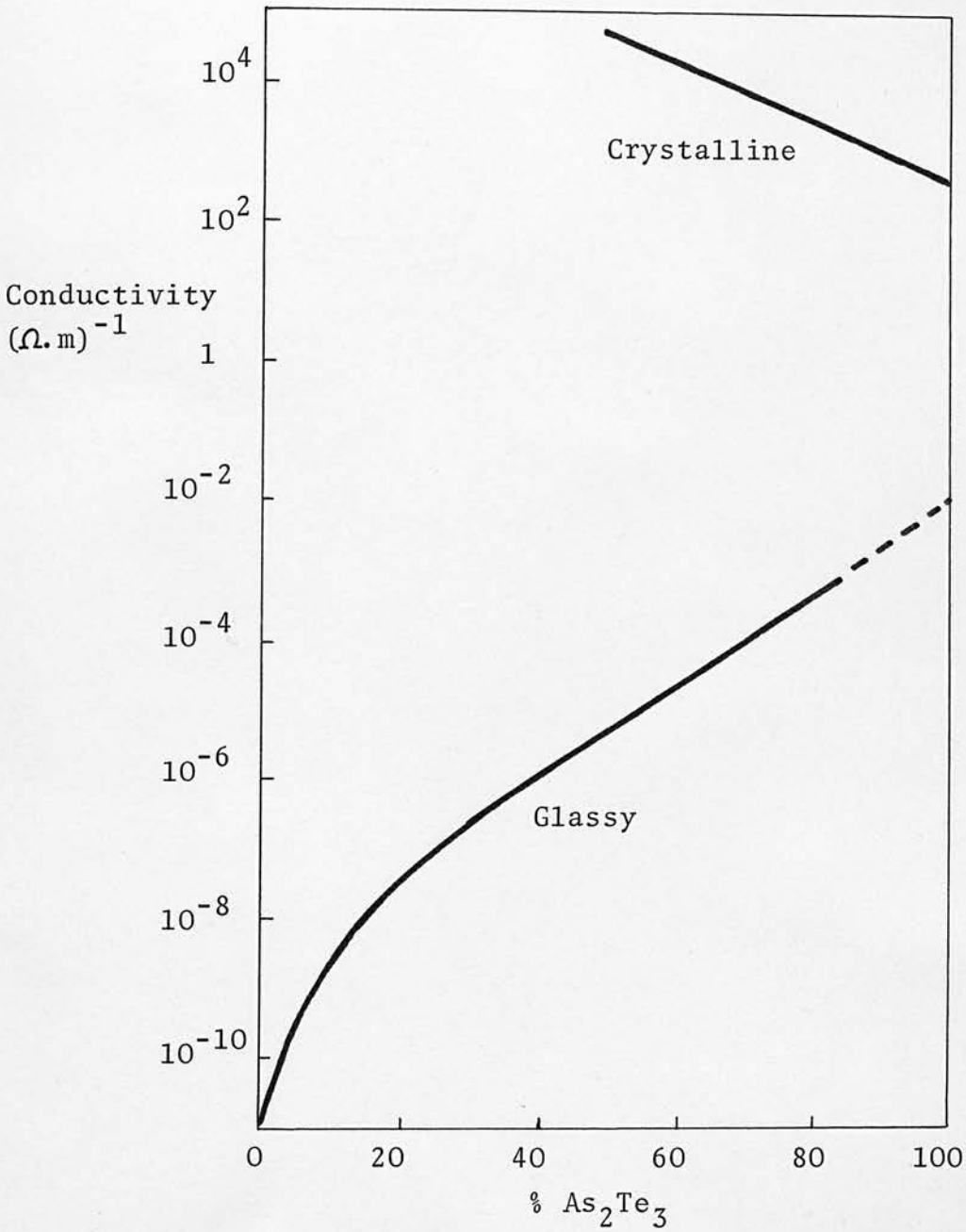

Conductivity of crystalline and glassy compositions in the system $As_2(Se,Te)_3$.

indicated by the dashed line. Switching between the glassy and crystalline states should allow resistance changes of up to 10^{10} and this can therefore be considered as the basis of a memory switch mechanism.

The calorimetric properties of the $As_2(Se,Te)_3$ system have been studied in detail by Bagley for bulk and thin film switches (114). Most were memory devices. In the high resistance state the material was amorphous and in the low resistance state it was crystalline. There was no evidence of phase separation, i.e. coexistence of the two distinct phases on a microscopic scale. Threshold switching was also observed but this was not associated with any thermally induced phase separation or crystallization.

For a glass of composition $As_4Te_{81}Ge_{15}$, Adler found evidence for phase separation (115), or possibly spinodal decomposition; the exact process was not established. Above 230°C the material consisted of two phases mixed with each other:

1. Primarily crystalline As-doped Te
2. Primarily amorphous GeTe. At 280°C this crystallizes.

Above 280°C, both of these phases show semimetallic behaviour.

An extension of the process of crystallization and phase separation is discrete component separation. This is discussed in relation to chalcogenide glasses in section 3.6.3.

3.6.2. The metal-semiconductor transition

The concept of an abrupt transition from insulator to metallic

behaviour was first developed for heavily doped materials. The theoretical development was largely due to Mott (116) and the phenomenon of metal-insulator transitions is generally described as a Mott-transition although several distinct processes have been evaluated.

The Mott transition has been observed in crystalline Sb_2Se_3 with excess Sb (117). On the Se-rich side of the stoichiometric compound, the material behaves as a wide-gap semiconductor with a resistivity in the range 10^2 Ω.m. With about 0.2% excess Sb the resistivity drops by about six orders of magnitude to a quasi-metallic state. This has been explained on the basis of Mott's theory that as the donor density is increased, the overlap of the donor ion wave functions becomes more pronounced and a sharp transition to impurity-band conduction results.

Sb_2S_3 is isomorphous with Sb_2Se_3 but only shows the transition to a conducting state when a field of the order 10^5 V.m^{-1} is applied (118). When the sample is heated to about 200^{o}C and then cooled, it regains its high resistance state. The temperature rise may be generated by interna Joule heating. A device made from Sb_2S_3 crystal doped with Sb may therefore act in a very similar fashion to a chalcogenide memory switch but it is much faster in operation : the switch-on time is $\sim$ 50 ns and switch-off time is $\sim$ 5 μs. The breakdown field decreases as the proportion of excess Sb is increased.

An extension of the Mott-transition theory has been developed by Mattis (119) (120) to explain conductivity in metal oxides. In his model

electrons are initially in an impurity band and conductivity is of the insulator-type. As electrons are excited out of their collective ground state either by field or temperature, the energy gap is reduced until at a critical temperature the material behaves as a metal. The model has been applied to Fe_3O_4 (121). It has some interesting features in common with cooperative ferroelectric-like switching which is discussed later and also with temperature controlled phase transitions of the type observed in VO_2.

A number of metal oxides show a sharp discontinuity at a critical temperature, eg. VO_2 : $68^{\circ}C$, V_2O_3 : $160^{\circ}K$, Fe_3O_4 : $119^{\circ}K$. In the case of VO_2 the change is associated with a crystallographic transformation. The resistance change can be three orders of magnitude or more and is shown in fig. 3.27 as a function of temperature (122) (123). As with the Sb_2Se_3 results, VO_2 shows semiconductor behaviour on one side and metallic behaviour on the other side of the transition. Switching can be induced in VO_2 if self-heating is great enough to raise the temperature beyond the critical value. No such temperature induced conductivity change has been observed in chalcogenide glasses below the glass transition temperature.

Switching in metal oxide glasses has been studied in considerable detail by Drake et al. (124) (125). The composition used most was copper calcium phosphate. The copper was present in both valence states (Cu^{+} and Cu^{++}) in approximately equal proportions and under low fields, carrier transport occurs by hopping between the variable valency copper

Fig. 3.27

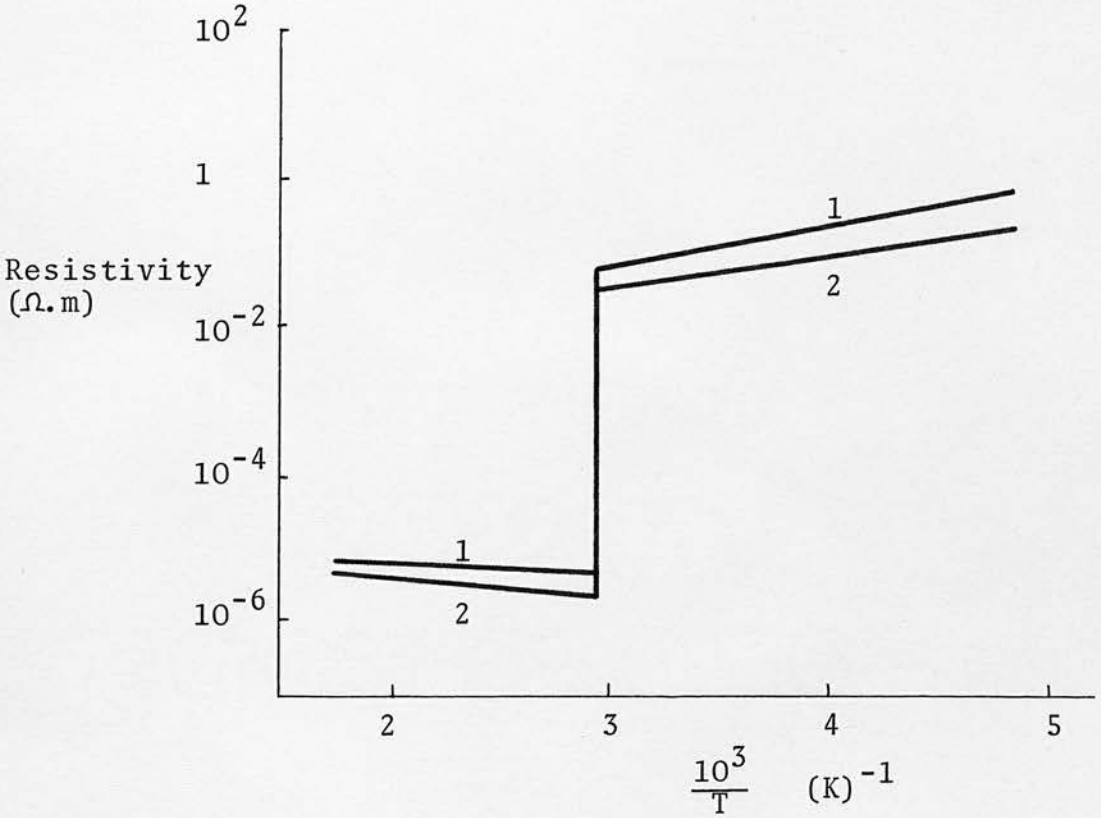

1. Measured perpendicular to the C-axis of the high temperature modification
2. Measured parallel to the C-axis of the high temperature modification.

Resistivity - temperature characteristic for VO_2.

sites. This results in a high resistance (up to $10^{10}\,\Omega$) and an activation energy which is determined largely by the energy difference between the two possible sites (Cu^{+} and Cu^{++}).

It is postulated that under high field conditions, dipole orientation and associated induced polarization occur so a ferroelectric-like ordering occurs in the field direction. Drake suggests that the different environment at the Cu sites reduces the energy difference between them. Thus the on-state has a much smaller activation energy than the off-state.

The concept of ferroelectric cooperation is attractive because switching has been observed in SbSI which is a ferroelectric compound and similar in many respects to Sb_2Se_3. Drake's theory also introduces the possibility that in high fields and with strong polarization, a form of bond interchange of the type observed in some organic polymers may occur (126). A further extension of the concept is that high fields and associated polarization could give rise to a condition which normally only exists in a glass near its transition temperature; ionic movement is enhanced and nucleation of a crystalline phase becomes likely (127).

Arguments of this nature may be able to explain the occurrence of widely differing resistance states in CS_2 (128) and Ge, Se glass at 5% Ge (129). For CS_2 the resistivity and activation energy of each state were: $10^{11}\,\Omega$ .m and 0.7 eV, 10 Ω .m and 0.02 eV. For Ge_5Se_{95}, the corresponding figures were: $10^{12}\,\Omega$ .m and 1 eV, $10^{4}\,\Omega$ .m and 0.1 eV. For both materials the occurrence of the two resistance states could not

be controlled, the same preparation technique was used for each pair. In the case of CS_2, however, the occurrence of a low resistance state could be due to the precipitation of carbon.

The occurrence of a Ge : Se glass in a relatively conducting state is particularly interesting since it represents a very simple chalcogenide system in the on-state "as-prepared". The only known difference between conducting and insulating glasses of the same composition was that the conducting samples were melted at lower temperatures (600°C rather than 950°C). In the course of the experimental work for this project, a number of Ge_5Se_{95} samples were made and melted at temperatures between 500°C and 1000°C. They were quenched at approximately two rates : $\sim 50\ Ks^{-1}$ and $5\ Ks^{-1}$. Fig. 3.28. compares the sample resistivity against the melt temperature from which it was quenched. The results of Frank are also shown in the diagram. All samples showed high resistivity and were essentially similar to other glasses of similar composition (3 - 7% Ge). Measurements of the infra-red spectra of glasses in the Ge : Se system have shown no unusual properties at 5% Ge (130) but, on the other hand, magnetic susceptibility measurements on Ge - Se glasses show an increased paramagnetic susceptibility for compositions in the range 5 - 8% Ge (131).

3.6.3. Component separation

A conducting path may be formed in an insulator by the relatively large scale movement of atoms. The electrode metal may penetrate

Fig. 3.28

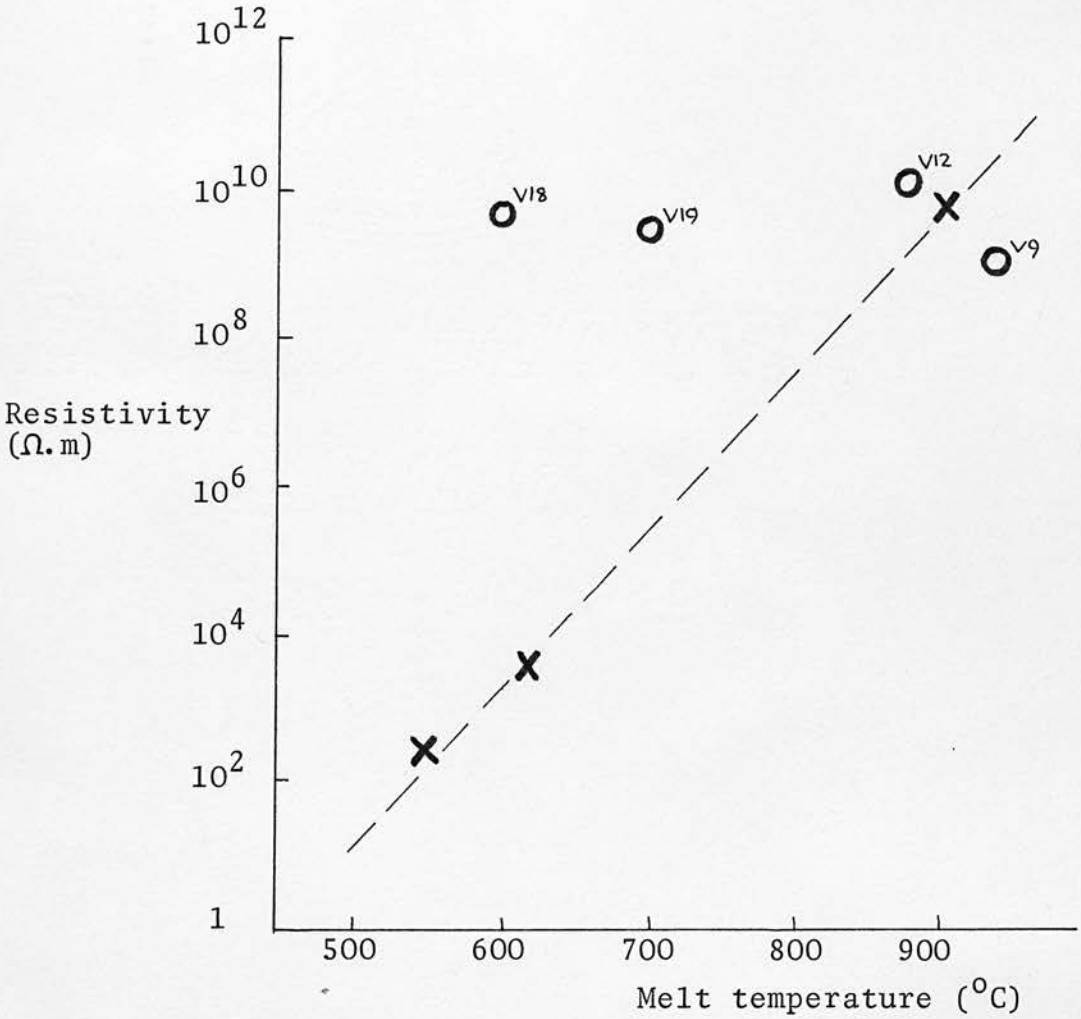

Effect of melt temperature on the resistivity of a glass of composition Ge_5Se_{95}:

✕ Results of Frank.

O Present work, sample V18, etc.

the insulator or else one of the component elements may be separated to give a conducting filament (assuming that the element itself is a reasonable conductor). This mechanism always gives a memory-type of switch and may be considered as an extension of the phase separation processes described in section 3.6.1.

The initial requirement in a metal-insulator-metal sandwich sample is that the electrode and insulator materials should be chemically and physically stable with respect to each other. Under conditions of high field and possibly also intense local heating there should ideally be no reaction or diffusion of electrode atoms into the body of the insulator. With chalcogenide glasses, many metals diffuse through them quickly at low temperatures, e.g. Ag at about 100°C and Au at about 300°C. The diffusion of metal atoms into the glass may lead to a change in sample conductivity due to:

1. Formation of an intermediate compound.
2. Behaviour as nucleating sites so that crystallization or phase separation occurs.
3. Formation of a metallic filament between the electrodes. Where the electrodes have been deposited by a process such as evaporation or electroplating, a pinhole in the insulator will also give this result.

With either processes 1 or 2, it would be difficult to produce a device which could be cycled a large number of times. For case 3, however, the conducting filament may be cleared by a high current pulse. This has

been observed in ZrO_2 (132) (but not specifically explained in this way) and also reported in some detail by Klein for SiO and SiO_2 (36) (133). The short circuit may be cleared almost as soon as it occurs by the discharge through it of the stored energy in the capacitor. If that does not clear it, a high current pulse is needed. In either case the conducting filament is vapourized and a small region of the top electrode around the filament is also removed (provided the electrode is thin enough). Klein has observed several thousand switching cycles with a single sample. After the first weak spots were cleared the switching voltage remained approximately constant, but the removal of a small area of electrode with each switch-off meant that the sample capacitance decreased steadily. Final failure occurred when the top electrode was almost completely removed.

An associated type of breakdown occurred when a steady voltage was applied to the sample and the series resistance was low. Under these conditions a self-propagating breakdown occurred where each single hole breakdown triggered another next to it. The characteristic feature of propagating breakdown is a meandering breakdown track across the top electrode.

Switching behaviour bas been observed in nickel oxide (134) (135) (136). It has been established that the conductivity change is due to a filament of nickel typically about 0.5 μm diameter. However, it is not clear whether the nickel originates from the NiO or from the Ni sheet on which the oxide was grown. The off-state resistivity is 10^6 Ω.m.

At voltages close to the breakdown point, the current increases slowly with time. Puddy has shown (135) that the magnitude of the current drift is of the order of that expected for nickel ions. Fig. 3.29 shows the effect of oxide thickness on V_{th} and on-state resistance. Films less than 3 μm thick gave poor and irreproducible results.

The most serious drawback of the NiO switch is that when switched off by a high current pulse, only a small portion of the Ni filament is ruptured. This means that the threshold voltage for the next operation is lower and when the device is cycled many times a wide spread in V_{th} occurs.

Nickel oxide switching shows a strong similarity to Dearnaley's mechanism to explain VCNR in SiO (section 3.5.6.). It is also similar to the behaviour described by Drake for copper phosphate glasses. Metallic separation or electrode diffusion must always be considered as a possible switching mechanism and it should be examined carefully before any more 'sophisticated' explanation is put forward.

For chalcogenide glass memory switches of certain compositions, component separation may occur. This may be in addition to the crystallization process described in section 3.6.1. Uttecht et al. (137) studied the glass $As_{44}Te_{48}Ge_8$ (composition in weight %) which has a bulk resistivity of $10^4 \Omega$.m. When a voltage V_1 is exceeded the sample resistance drops by about six orders of magnitude and a filament begins to grow along the surface from the positive to the negative probe. If the voltage is removed before the filament is complete the sample

Fig. 3.29

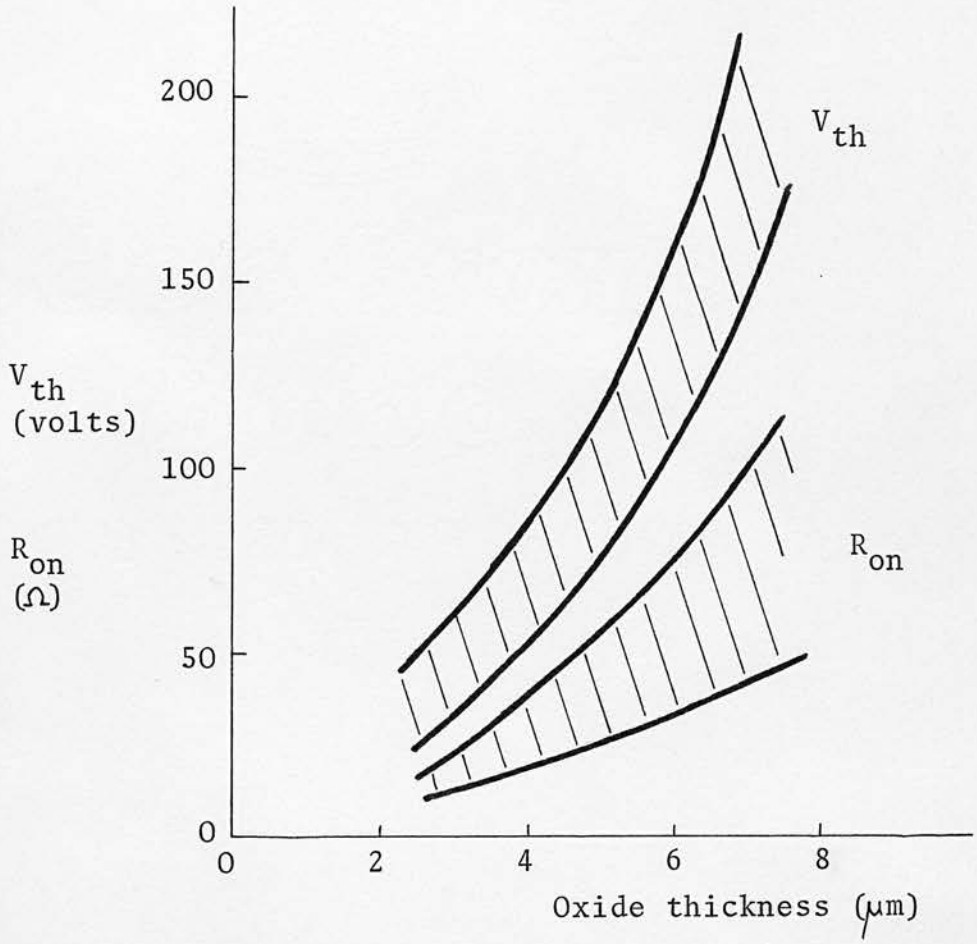

NiO switch: variation of V_{th} and R_{on} with oxide thickness.

returns to its high-resistance state. The next voltage threshold, V_2, is lower than V_1 and the filament continues to grow from the point where it stopped. Switch-off occurs when the filament is ruptured by a high current pulse.

X-ray examination of a sample with many small filaments on it revealed that a crystalline phase was present but it could not be absolutely identified. However, the most interesting result was the variation of composition across a filament. This is shown in fig. 3.30 and was obtained with an electron microprobe analyzer which had a resolution of about 2 μm. Thus, when memory switching occurs in this material, a large number of atoms must be moved through distances of 10 - 20 μm as well as change their orientation, bonding, etc. If these atoms cannot be returned to their initial positions when the device is switched off then over a large number of cycles there may be a steady change in the off-state characteristics and the voltage needed to switch on.

This emphasises a basic problem from which many of the memory device mechanisms discussed in the chapter suffer: the switch-off process must return the device to the same high resistance state after each cycle. Otherwise there may be unpredictable variations between characteristics on each cycle and/or a steady drift in the characteristics with the increase in number of operations. This is discussed later in the light of experimental data for thin films of chalcogenide glasses.

Fig. 3.30

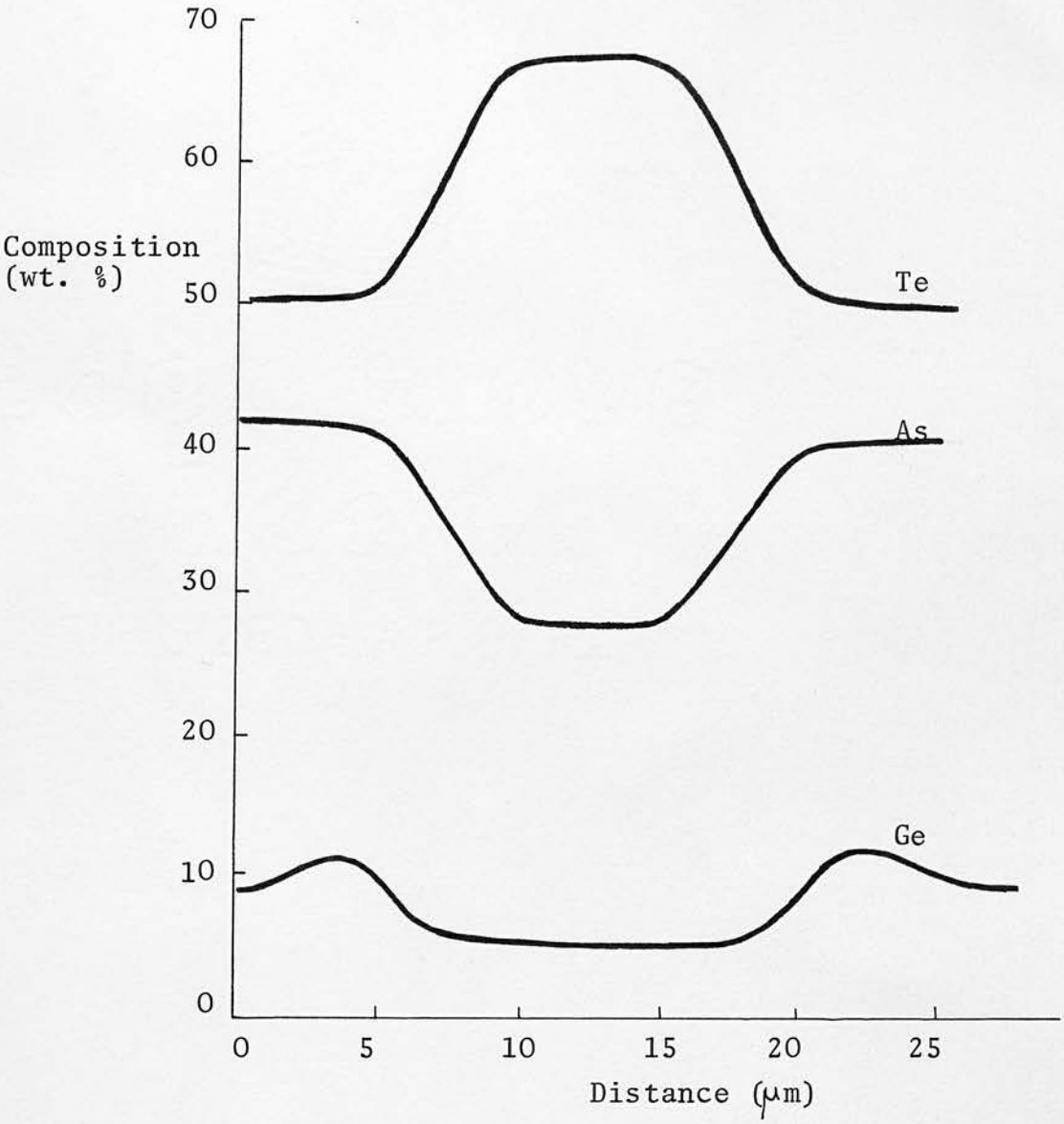

Change in composition across a conducting filament as determined by microprobe analysis.

CHAPTER 4 A REVIEW OF SWITCHING PERFORMANCE OF AMORPHOUS SEMICONDUCTORS

4.1. MEMORY SWITCHES

The memory or bistable solid state switch has been produced in a variety of forms. Several mechanisms can give rise to a change in resistance and they have been reviewed in the previous chapter. Although less controversy surrounds the mode of operation compared with a threshold or monostable switch, memory switches have only recently become commercially viable (4).

The principal features of possible memory switching mechanisms may be briefly summarised:

a) Crystallization of an amorphous chalcogenide can result in a large increase in conductivity. Bagley has shown that this occurs with glasses from the system $As_2(Se, Te)_3$ (section 3.6.1.). To change state, enough energy must be supplied to melt a small region of the glass and the final resistance state depends on the cooling rate. Problems with this type of switch have arisen from mismatch between expansion coefficients of amorphous and crystalline regions. When switch-off occurs, the whole of the crystalline region may not be converted back into the amorphous state (138). This could lead to fluctuations in switching performance.

b) Under some conditions, component separation as well as crystallization occurs within an amorphous material, so that a region of high conductivity is formed (section 3.6.3.). The production of a reliable device is very dependent on the choice of semiconductor and the conditions of switching so the composition in the on and off-states does not change throughout the device lifetime.

c) The copper phosphate switches developed by Drake et al. (section 3.6.2.) have a fast switching time - of the order of 1 μ s. However, they suffer from erratic variations in V_{th}. The switching mechanism which has been postulated for this class of devices involves a field induced ferroelectric-like ordering process.

d) The insulator - metal transition at high fields in Sb_2S_3 is one of the oldest of the solid state bistable switches. It was first described by Gildart in 1957 (139). Under the influence of a high field, donor atoms move into a different coordination environment where there is considerable overlap of valence electron orbitals and impurity band conduction occurs.

e) A metal filament either from the electrodes or from the semiconductor itself (e.g. NiO) may provide the basis for a switching process. Such devices tend to have variable switching properties and a very limited operational lifetime.

Not only are there several possible mechanisms for bistable switching,

but the effect has been observed in a large number of materials. (140) (141) The main problem with the device is a technological one; to chose a semiconductor and electrode combination which will have repeatable and predictable performance (142). Some of the experimental problems associated with this are discussed in chapter 7.

Many memory switches, in particular those made from chalcogenide glasses, show threshold switching behaviour before being locked into the memory state (143). The mechanism of threshold switching must therefore be consistent with this and provide conditions under which crystallization and/or component separation can occur.

4.2. MATERIALS IN WHICH MONOSTABLE SWITCHING HAS BEEN OBSERVED

Threshold switching has been observed in a large number of materials in addition to the chalcogenide glasses. A large class may be explained on the basis of double injection theory,(section 3.5.3.) Reversible thermal breakdown can also give a monostable switch and its application to diodes and transistors has been described in section 3.5.5.

Many of the observations of threshold switching have been published as letters or short communications with little or no attempt made to explain the mechanism which might be responsible for the effect. In most cases the results are too scanty to ascribe a mechanism to the observation, but in this section some of these results are described. The list is by no means exhaustive but it does illustrate how widespread is the phenomenon of monostable switching in solids.

In silicon and germanium, double injection has been successfully used to explain monostable switching in both bulk samples and thin films (144) (145). It may also be applicable to Au-doped SiO_2 films (146).

Negative resistance has been reported in films of Te, Se and B. In the case of Te (147), the switching process is very fast and a change in effective mass may be involved as a result of an intervalley transition by hot holes. Thermal effects are also likely to be present and the breakdown patterns for Se (148) and B (149) (150) (151) could also be due to reversible thermal breakdown. The mechanism suggested by

Feldman (150) for the case of boron films - and also for similar samples of amorphous Ge and Si - involves an avalanche process. However, all I - V characteristics for switching in elemental semiconductors show a relatively slow switching process and thermal effects must certainly be considered.

Threshold switching has been observed in a number of compound as well as elemental semiconductors. GaAs (152) (153), In_2Se (154), SnS_2 (155) and yttrium iron garnet (156) crystals have shown S-shaped I - V characteristics and similar results have also been obtained for polycrystalline CdS (157) (158) (159). The slow switching speed and stable negative resistance region of these samples suggests that thermal processes are dominant.

Impact ionization in Ge at 4K forms the basis of a negative resistance device called a 'Cryosar' (68). A similar mechanism has been used to explain switching in InSb (160) (161) and Si-Ge heterojunctions (162).

To complete the selection of threshold switching materials the transition metal oxides can be added: Nb_2O_5 (163) (164); copper-doped ferric oxide ceramic (165), copper-chromium oxide spinel and TiO_2 (167). The variety of suggested mechanisms matches the variety of the materials. One of the most clearly understood cases is switching in VO_2. When enough Joule heat is generated to raise the temperature beyond $68^{\circ}C$, an insulator - metal transition occurs. The material reverts to the high resistance state on cooling. This was discussed in section 3.6.2.

It is important to emphasise that monostable switching is not

unique to chalcogenide glasses and possible mechanisms for the effect had been proposed long before chalcogenide switches became a practical reality. From a technological point of view, however, most of the observations discussed in this section are trivial; they may require low temperature for operation, switching conditions may be incompatible with those existing in the circuitry which must be associated with the switch, the on : off ratio may be low or they may be difficult to produce reproducibly on a large scale. For one or more of these reasons, many of the devices mentioned in this section have not merited more than a single brief description in the literature. Conversely, because chalcogenide threshold switches do not have these disadvantages, they are of considerable interest.

4.3. THRESHOLD SWITCHING IN CHALCOGENIDE GLASSES

4.3.1. Historical development

The operating mechanism of amorphous monostable switches has been the subject of considerable controversy. Because of this, it is useful to put the work into perspective and review first the historical development of the devices. Subsequent sections describe the state-of-the-art and published work which is significant for the determination of the operating mechanism.

Threshold switches based on amorphous chalcogenide semiconductors were described by Pearson et al. in 1962 (168) (169). The glasses were from the system As - Te - I which form a class of low melting point glasses with resistivity in the range 10 - 10^6 Ω.m depending on the exact composition - a typical sample was $As_{53}Te_{43}I_4$ ($\sim$ 30 Ω.m). Glasses of similar composition were examined by Eaton (170) and he explained the whole switching process in terms of reversible thermal breakdown. Physically the samples were large ($\sim$ 1 mm between electrodes) and on the basis of the simple theory developed in section 3.3.3., thermal breakdown could be expected at low fields: $\sim 10^6$ $V.m^{-1}$. Switching in bulk samples of chalcogenide glass was also reported by Kolomiets and Lebedev (171). The glasses were of low resistivity and belonged to the $TlAs(Se, Te)_2$ system. The results of Kolomiets were consistent with thermal breakdown and experimental results for materials of similar composition are described in section 6.2; they are also examples of thermal breakdown. Switching has been observed in melts of

Te with S or Se (172). The characteristics are similar to those described for solid chalcogenides of the same geometry and resistivity.

Studies of switching in chalcogenide glasses were also being pursued independently by Ovshinsky from about 1960. Although the first account of his work was not published in the scientific press until 1968 (173), several descriptions had appeared earlier in the technical press (for a full list, see reference (174)). Ovshinsky claimed that his devices were based on an electronic process and his 1968 paper (173) aroused a great deal of publicity. There were statements that Ovonic switches (as they were described) would replace transistors; that a fundamentally new class of electronic device had been discovered. There were equally strong reactions that there was nothing new and it had all been described before. Out of this controversy grew another - whether the basic operating mechanism was thermal or electronic. A great deal of work has been done over the past two years to try to elucidate the mechanism. The next two sections describe typical properties of an amorphous threshold switch (over which there is little controversy) and then the significant results which have been published and which bring some understanding to the underlying physical process.

4.3.2. Experimental characteristics of amorphous threshold switches

In the off-state, all chalcogenide switches show a region of non-ohmic behaviour before switching occurs. The exact shape of the off-state characteristics depends on device geometry, glass composition and

environment. D.C. characteristics published by Fagen (18) are shown in fig. 4.1. for temperatures in the range 77 K - 333 K. The film composition was determined by microprobe analysis to be $As_{35}Te_{28}Ge_{16}S_{21}$. The curves are ohmic at low voltages followed by an exponential region. At low temperatures and with V > 15 volts another mechanism appears to occur and this gives a very rapid rise in current with voltage until switching occurs.

Fagen does not offer a physical explanation for the data in fig. 4.1., but two comments can be made:

1. The characteristics were measured under d.c. conditions. A 1 μs pulsed voltage source gave a very similar room temperature curve, but the possibility of Joule-heating at low temperature and high voltage was not considered. This work is discussed more fully in section 6.4.5.
2. When the data in fig. 4.1. are plotted as Log I - $(V)^{\frac{1}{2}}$, the curves have the same general shape as in fig. 4.1. : an ohmic region then a linear region and finally at low temperatures and high voltages, a region where I varies very rapidly with $V^{\frac{1}{2}}$. A similar group of curves has been published by Servini and Jonscher for SiO (175). This is also discussed later in the light of the experimental evidence presented in chapter 6.

The most detailed study of the variation of V_{th} with sample thickness has been made by Kolomiets (176). The results are shown in fig. 4.2. For samples greater than 50 μm thick, $V_{th} \propto d^{\frac{1}{2}}$; the relation

Fig. 4.1

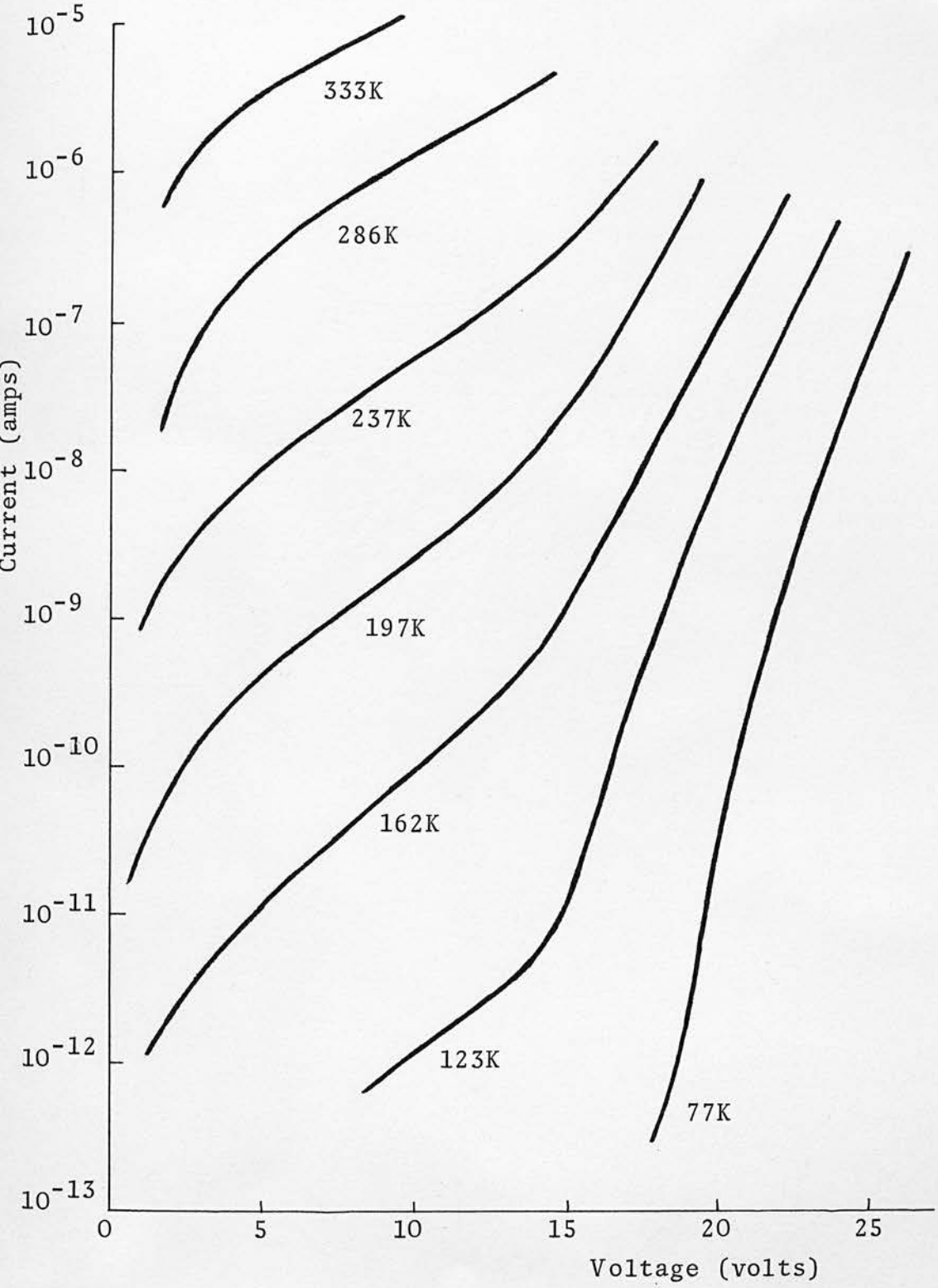

Current - voltage characteristics as a function of temperature for the glass $As_{35}Te_{28}Ge_{16}S_{21}$.

Fig. 4.2

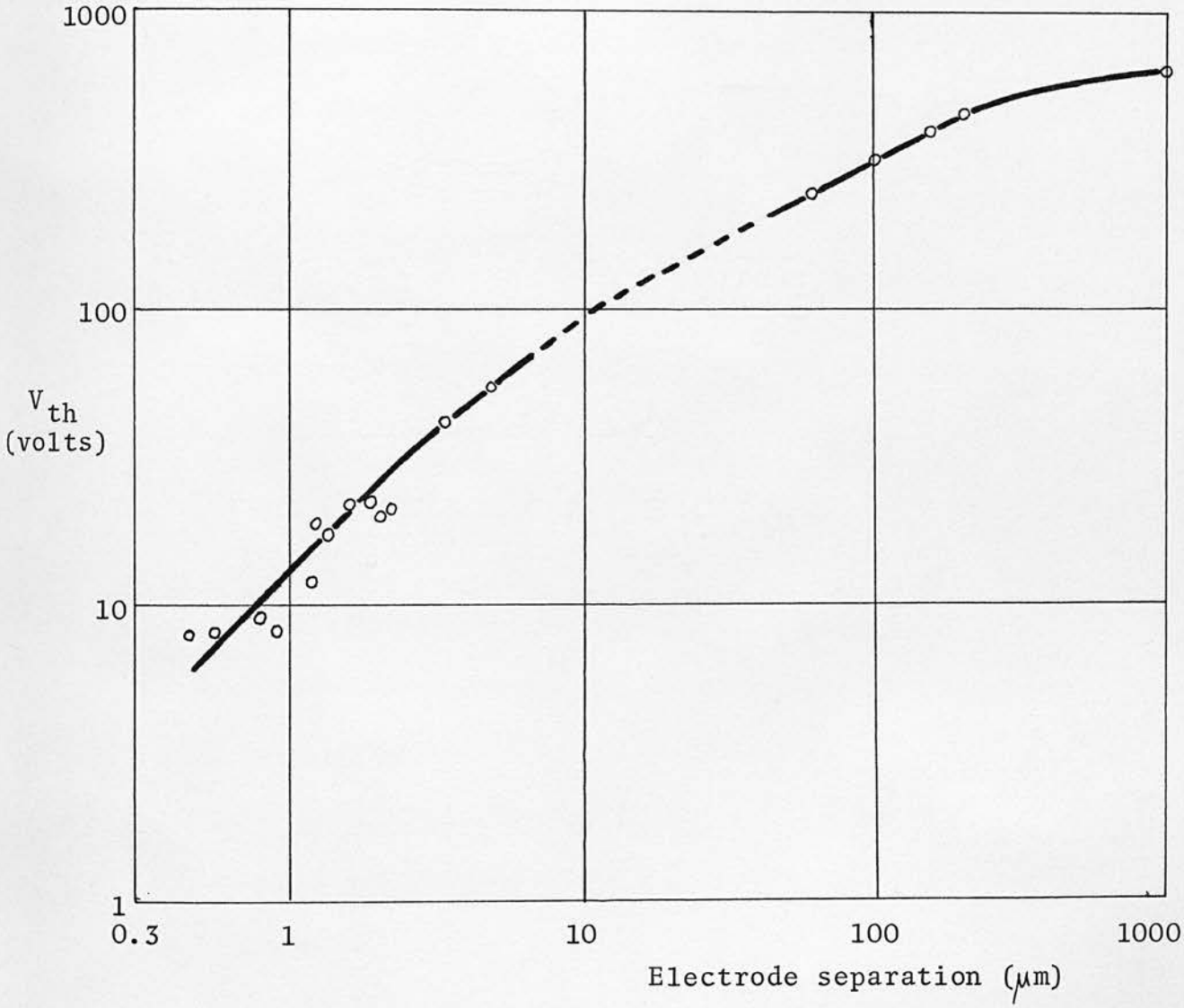

Variation of threshold voltage with electrode separation: Kolomiets' data.

expected for simple thermal breakdown. However, for films less than $\sim 5\ \mu m$ thick, $V_{th} \propto d$. It is difficult to produce thin films thicker than $5\ \mu m$ and it is also difficult to work with bulk samples less than $50\ \mu m$ thick so no published data is available to show whether the changeover from $V_{th} \propto d$ to $V_{th} \propto d^{\frac{1}{2}}$ is abrupt or smooth.

A summary of the variation of V_{th} with ambient temperature is shown in fig. 4.3. (18) (177) (178). The samples are all about $1\ \mu m$ thick. Above room temperature, V_{th} decreases uniformly as the temperature is raised. This is quite different from a relationship which involves an activation energy; the latter has a distinct curvature and the dashed line in fig. 4.3. relates to the equation:

$$V_{th} = V_{tho} \exp\left(\frac{\Delta E}{kT}\right)$$

$$\Delta E = 0.2 \text{ eV}.$$

The curves in figs. 4.1., 4.2. and 4.3. refer to steady-state measurements made either at d.c. or with low frequency a.c. However, when a voltage pulse, V, is applied to a chalcogenide threshold switch and $V > V_{th}$, there is a finite delay time, t_d, before switching occurs. The experimental relation between t_d and V is given by an equation of the form:

$$t_d = t_o \exp\left(-\frac{V}{V_2}\right) \qquad \ldots\ldots 4.1$$

For the data of Shanks (178), the constants are: $t_o = 7\text{ms}$ and $V_2 = 2$ volts at room temperature. Delay time as a function of voltage and temperature are shown in fig. 4.4. (179). In the region described by equation 4.1, t_d has an activation energy: $\Delta E = 0.37$ eV.

Fig. 4.3

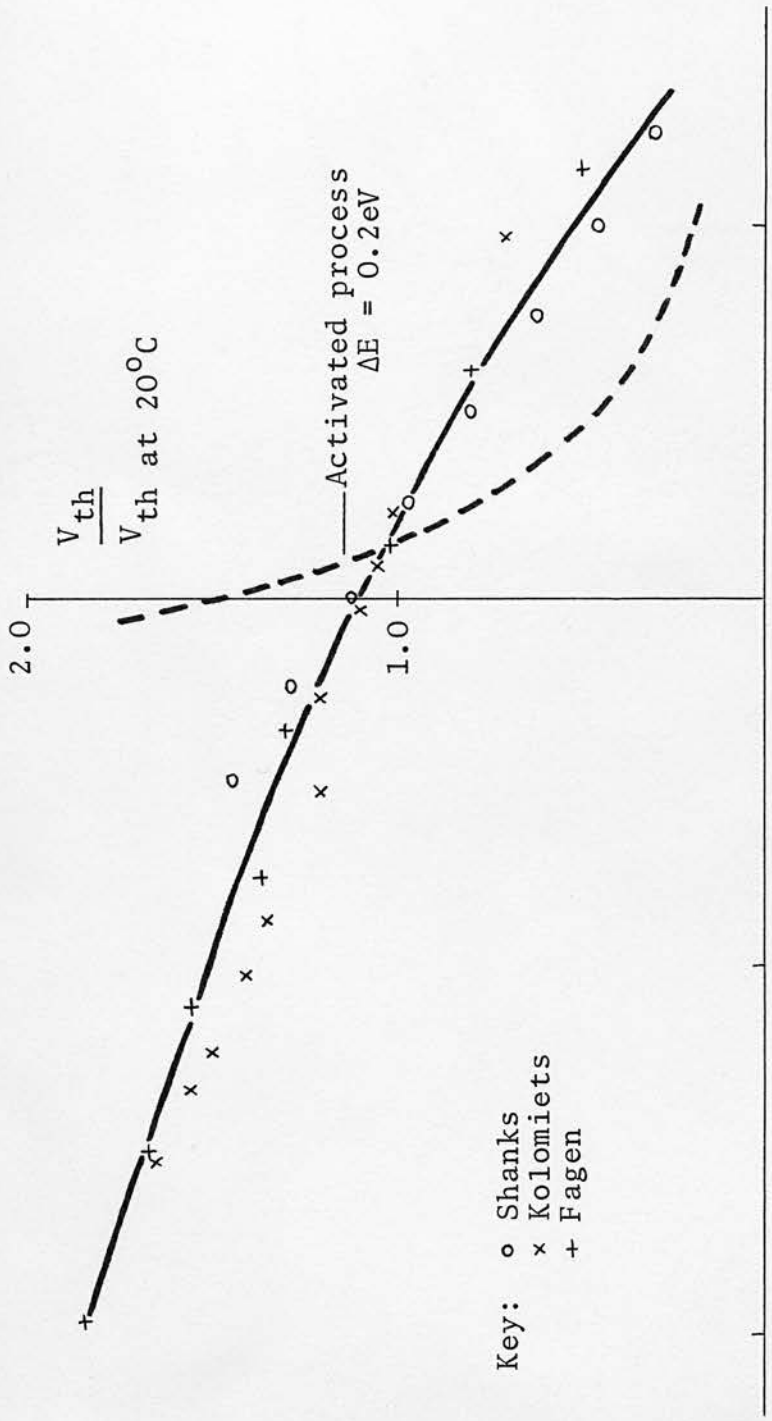

Variation of threshold voltage with temperature.

Fig. 4.4

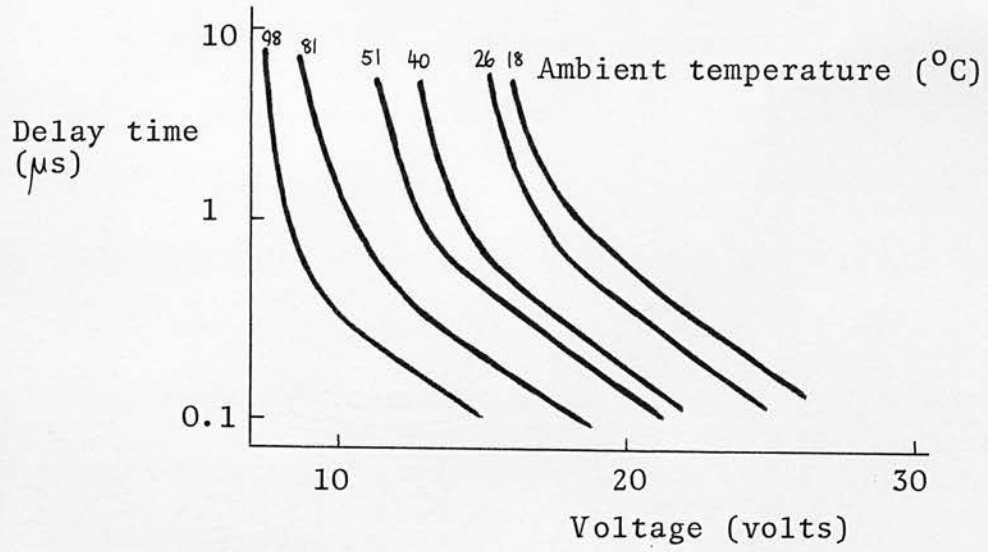

Variation of delay time with pulse voltage and ambient temperature.

Fig. 4.5

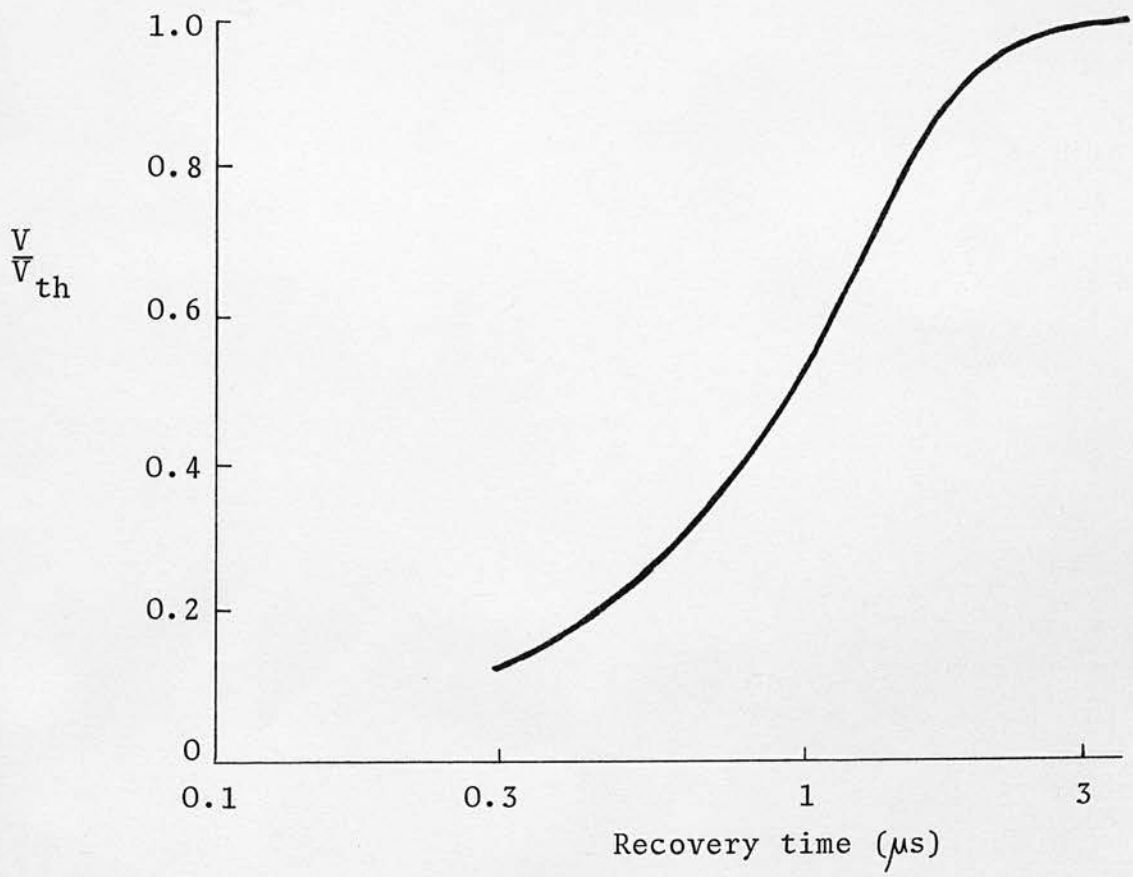

Recovery from a switching operation.

After a switching cycle, there is a recovery period during which the device has a reduced value of V_{th} i.e. if a voltage pulse is applied during the recovery period, switching occurs at a lower voltage than it would if the recovery process were complete. This is shown in fig. 4.5. (178). For this sample, recovery is complete after 3 μs. Thus, the device would show no variation in switching properties with frequency up to about 200 KHz (2 μs pulse, 3 μs separation). At higher repetition rates, the effective threshold voltage would fall. The delay time also has a recovery characteristic which is related to that for V_{th} through equation 4.1.

In the 'on' portion of the I - V characteristic, the dynamic resistance is close to zero and the holding voltage is approximately constant and often in the range 1 - 3 volts. The on-state current is not a function of device area or of temperature and this suggests that a small quasi-metallic filament forms the current path. The experimental data for the on-state are reviewed in more detail in section 6.4.9.

Because threshold switches are made from amorphous semiconductors, they are not sensitive to structural defects in the same way that transistors are. They can therefore be operated in an environment with a high radiation flux (180).

Threshold switching devices have been independently made and studied by a number of different groups. The results described in this section are typical of those published. There is general agreement on the observations; the controversy is over their interpretation.

4.3.3. Assessment of comments on threshold switching mechanisms

The mechanisms which can lead to breakdown in dielectrics have been reviewed in chapter 3. Most are only significant when field strengths of the order of 10^8 $V.m^{-1}$ or more are attained; threshold switching in thin films occurs at about 10^7 $V.m^{-1}$. The two processes which are viable - thermal breakdown and space charge inversion - have been reviewed in sections 3.3. and 3.5.4. respectively. The description of the electronic mechanism, however, has not progressed beyond the qualitative stage and the arguments in its favour have mainly been based on the inadequacies of the alternative - thermal breakdown.

Thermal effects are inevitably present in any device and there is general agreement that they are significant in the on-state of a threshold switch (181). Stocker (182) has measured a small hot region on the surface of a switched thin film and Pearson found that the temperature could be high enough to melt a Pb 'top' electrode (183). The recovery of a device from a switching event, shown in fig.4.5. represents, therefore, the cooling of the device to ambient temperature.

The questions to be answered are: what mechanism initiates the switching process? Will it give the observed off and on-state characteristics? Is it primarily thermal or electric?

The arguments in favour of an electronic process rest mainly on the very short switching time. After the delay time (0.1 - 10 μs) switching occurs in about 100 ps. There is no region of stable negative resistance between the off and the on-states. This suggests that there

may be a discontinuous change from a current-limiting mechanism characteristic of the off-state to a different mechanism which is characteristic of the on-state. This forms the basis for the theories of Henisch and Mott discussed in section 3.5.4. They envisage the on-state being determined by tunnelling through barriers at the electrodes - hence its insensitivity to temperature and a holding voltage that is close to the value of the band gap.

Vogel and Walsh measured the admittance of chalcogenide threshold switches as a function of d.c. bias (184). They found that close to V_{th} the behaviour of the admittance changed from capacitive to inductive. From this they deduced that "a dielectric phase transition was implicated in the switching process". However, negative capacitance in itself is not necessarily evidence for an electronic process and the effect is considered from the viewpoint of thermal inertia in section 6.4.7.

Several interpretations of threshold switching based on thermal breakdown have been published. (26) (185) (186). They represent different approaches to the problem of solving the thermal energy dissipation equation and the conductivity equation. The solution is discussed in detail in section 3.3., but in the published work only the simple case has been considered where conductivity is a function of temperature, $\sigma = \sigma(T)$. The extension to include field, $\sigma = \sigma(T,E)$ has been treated theoretically in 3.3. and experimentally in 6.4. A brief theoretical paper on similar lines has recently been published by Warren (187).

When the simple relation $\sigma = \sigma(T)$ is used, the basic features of threshold switching result: the pre-breakdown characteristic is non-ohmic, after a voltage pulse has been applied; there is a delay time before rapid thermal runaway occurs, but the functional dependence of the principal parameters is different from that observed experimentally. This is summarised in table 4.1.

In addition to the poor correlation of functional dependence, numerical correlation is poor; the simple thermal theory requires a breakdown voltage of about 100 volts for a 1 μm thick film whereas switching occurs at 10 volts. The temperature rise within the period of the delay time is insufficient to produce thermal runaway. Collins (26) overcame both of these problems by assuming quite arbitrarily that only a small volume of glass was heated. However convenient the assumption may be, there is no physical justification for it. Warren considered a change in activation energy of conductivity with temperature (185) and this could certainly contribute to the very short switching time, but it does not explain the mechanism for initiation of switching.

Two other groups of experimental results indicate that switching is an energy-controlled process (but not necessarily thermal).

1. Shanks observed that the polarity of the voltage pulse could be changed during the delay time without affecting the magnitude of t_d (178).
2. Csillag found that switching occurred when a specified amount of energy had been accumulated with the device (188). Shanks

Relation	Experimental result	Simple thermal theory
$I - V \ (V < V_{th})$	$\frac{I}{I_o} = \exp \frac{V}{V_o}$	$\frac{I}{I_o} = \exp \frac{V}{V_o}$
$V_{th} - V_o$	$V_{th} \doteqdot 3V_o$	$V_{th} \doteqdot 3V_o$
$V_{th} - d$	$V_{th} \propto d$	$V_{th} \propto d^{\frac{1}{2}}$ or constant V_{th}
$V_{th} - T$	$V_{th} \propto -T$	$V_{th} = V_{tho} \exp \frac{\Delta E}{2kT}$ $(\rho = \rho_o \exp \frac{\Delta E}{kT})$
$t_d - T$	$t_d = t_{do} \exp \frac{0.8\Delta E}{kT}$	$t_d = t_{do} \exp \frac{\Delta E}{kT}$
$t_d - V$	$t_d = t_o \exp - \frac{V}{V_2}$	$t_d \propto V^{-2}$
Stable negative resistance region?	No	Yes

Table 4.1

Comparison of simple thermal breakdown expressions with experimental results.

made a similar observation (178) by applying a conditioning pulse ($< V_{th}$) immediately before the switching pulse ($V > V_{th}$). The delay time was shorter than that for the switching pulse alone. Both effects are shown in fig. 4.6.

Most of the work aimed at elucidating the mechanism responsible for monostable switching in chalcogenide thin films has been carried out over the past 2 - 3 years. Accordingly there have been several parallel but independent assessments. Although an electronic mechanism has been strongly advocated, no model has progressed beyond the qualitative stage. Thermal breakdown theories are better established but although they predict the general features of switching behaviour, the detailed correlation with experimental results has been poor.

Fig. 4.6

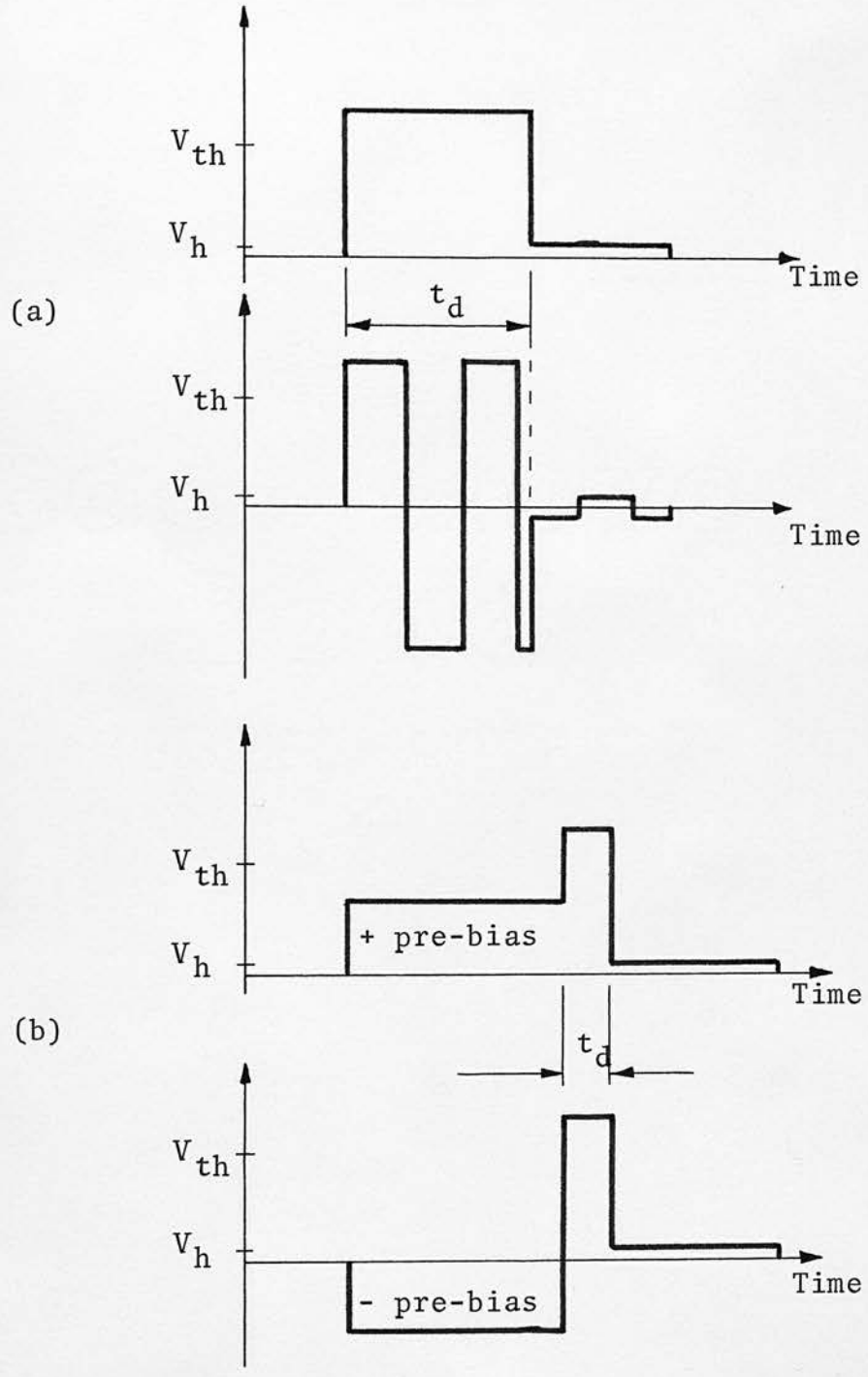

Voltage across threshold switch for different input pulse shapes.

CHAPTER 5 SAMPLE PREPARATION AND EVALUATION

5.1. BULK GLASSES

5.1.1. Bulk glass selection

Many elements from groups 3A - 7A of the periodic table can be mixed together, melted and then quenched to give glasses. A brief summary of resistivity and composition ranges was given in chapter 2. Glasses which form the basis of switching devices have to meet several specifications and this limits the range of suitable compositions.

Memory switches operate by crystallization and/or component separation which occurs as a result of internal Joule heating, so the glass must readily show this change when heated. The resistance change between the on- and off-states of a switch should be large. To fulfil these conditions, the glass should have a resistivity greater than 10^3 Ω.m, $\Delta E \geqslant 0.3$ eV and a relatively low glass transition temperature (100 - 300°C). For easy devitrification, a composition close to the edge of the glass-forming region is usually chosen, e.g. $As_4Ge_{15}Te_{81}$ (115) or $As_{55}Te_{35}Ge_{10}$ (137). Unless proportions by weight are specifically indicated, all compositions refer to atomic proportions.

The glass for a threshold switch must fulfil the same electrical requirements as a memory glass, but it should <u>not</u> be prone to

devitrification. To anticipate the results of the next chapter, threshold switching depends on a thermal runaway process. When the voltage supply is removed, the material must return to the glassy state even if it is cooled slowly. Therefore a glass is needed which shows little tendency to devitrify and has a high transition temperature.

Since both memory and threshold switches involve high local temperatures within the glass, the electrodes must provide stable contacts under these conditions.

The range of possible glass combinations is so large that a deliberate decision had to be made at the beginning of this work to concentrate on a few simple glasses. The composition $As_{30}Te_{48}Si_{12}Ge_{10}$ can provide the basis for good threshold switches (173) and it has been widely studied. It therefore represents a good material to use as a standard for comparison of results with published data.

Most effort was concentrated on simpler glasses from the ternary system As_2Te_3:Si. The AsTeSi glass-forming region is indicated on the diagram in fig. 5.1. (189). The figures on the diagram are temperatures at which bulk specimens of the glass would bend. This is not exactly the same as the glass transition temperature but the two values do bear a constant relation to each other. The AsTeSi system provides glasses with a wide range of softening temperatures. The resistivity range is also wide; from about 10^2 Ω.m for As_2Te_3 to 10^8 Ω.m for $(As_2Te_3)_{55}Si_{45}$ at the limit of the glass-forming region. Thin film samples were prepared from six compositions. They are marked in

fig. 5.1. and the silicon compositions were (Atomic %): 40, 35, 30, 20, 10, 0.

To examine low resistivity glasses which could be used in memory switches, two compositions from the AsTeGe system were chosen; $As_{20}Te_{70}Ge_{10}$ and $As_{55}Te_{35}Ge_{10}$. There are two glass-forming regions in this system and these compositions are representative of each (fig. 5.2.)

The description 'glass' as used in relation to figs. 5.1. and 5.2. applies to relatively large quantities of material (> 1 g) which have been quenched from the melt and which show no evidence of crystallization when examined with X-ray diffraction techniques. For very small samples which can be very rapidly quenched or films deposited from the vapourphase, an amorphous structure can be produced for a much wider range of compositions than is shown in figs. 5.1. and 5.2.

5.1.2. Glass preparation

Most chalcogenide glasses are easily prepared by rapidly quenching the melt. The rate of cooling which is necessary depends on the composition. In this work, the slowest average quench rate was approximately 30 $K.s^{-1}$ which was adequate to produce glasses for the compositions used.

Glasses were prepared from the elements or from simple compounds (As_2Te_3, As_2Se_3 etc.). The purity level was 5N and where necessary, the material was crushed into small lumps just before weighing. The weight of each component required was calculated to give the desired

Fig. 5.1

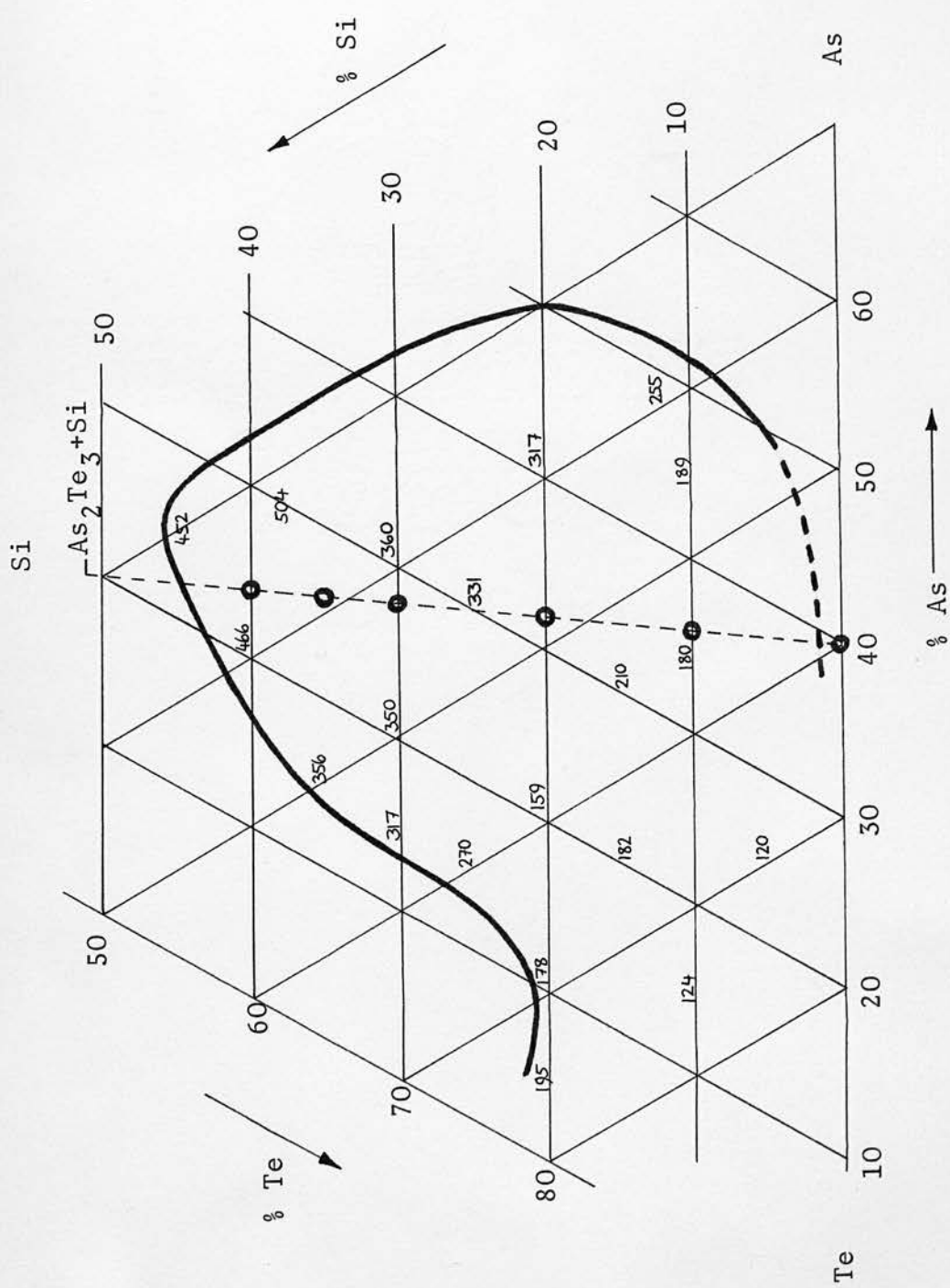

Glass-forming regions in the ternary system: As-Te-Si.

Fig. 5.2

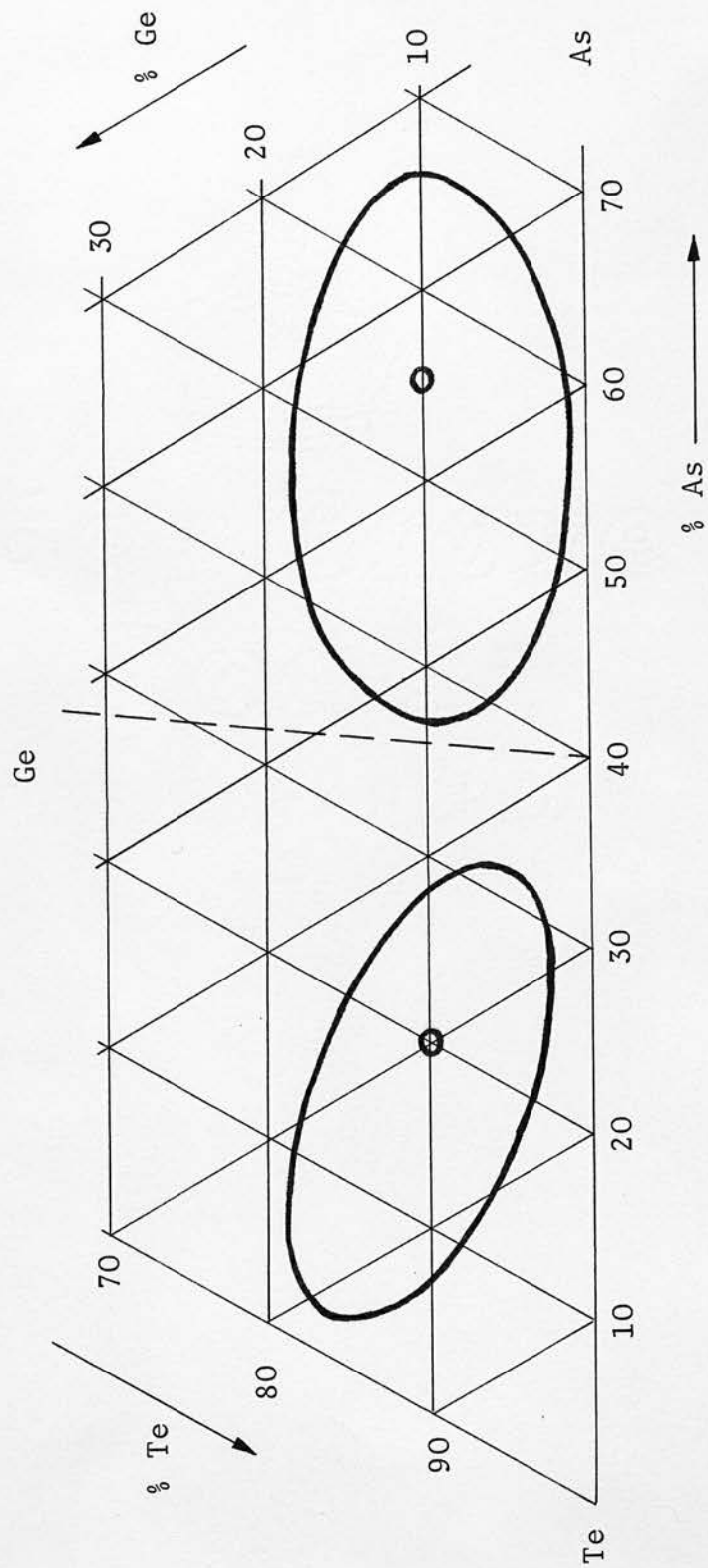

Glass-forming regions in the ternary system: As-Te-Ge.

final glass composition. Weighing was done to ± 1 mg with a total sample weight of 1 - 10 g.

The weighed materials were placed in a quartz tube which was sealed at one end and had a slight indentation about half-way along its length. The materials to be melted filled about one-third of the bottom half of the tube. A small quartz rod was dropped into the tube and rested on the neck in the tube. When the quartz tube was connected to a vacuum system, the small rod throttled the pump speed so there was minimum disturbance to the material in the bottom of the tube. If any particles did jump up they could not get past the quartz rod. The capsule was sealed off at about 10^{-4} torr. The wall of the quartz tube was heated until it collapsed on to the inner quartz rod. Further heating then sealed the two together.

The melting sequence was similar for all glasses. The capsule was put into a cold furnace which took about 2 hours to heat to 1000°C. The capsule was left at 1000°C for two hours and then the furnace was rocked for 20 hours to allow thorough mixing of the components in the melt. A schematic diagram of the capsule in the furnace is shown in fig. 5.3.

Two sizes of capsule were used; 6 mm bore for small quantities (2 - 5 g) and 10 mm bore for larger quantities (10 - 20 g). The wall thickness was 1 mm in each case. This wall thickness was not sufficient to contain the vapour pressure of the composition $As_{55}Te_{35}Ge_{10}$, so 2 mm thick quartz tube was used.

Fig. 5.3

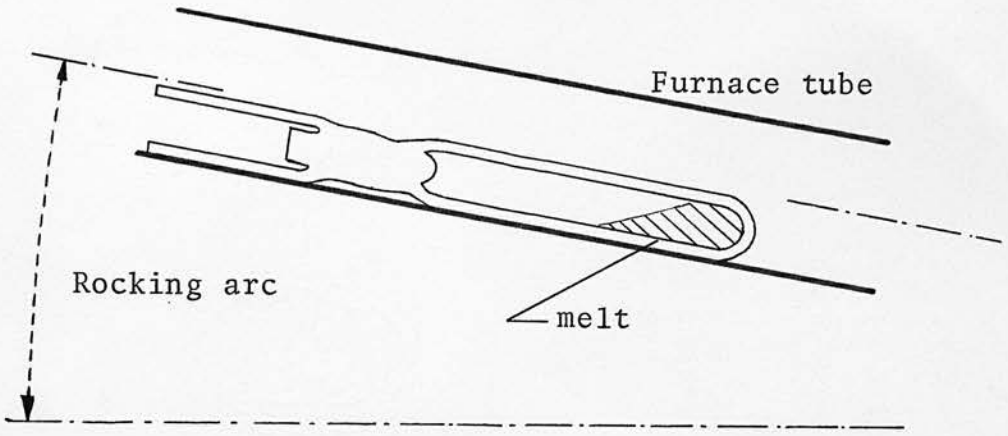

Schematic diagram of capsule in furnace.

Fig. 5.4

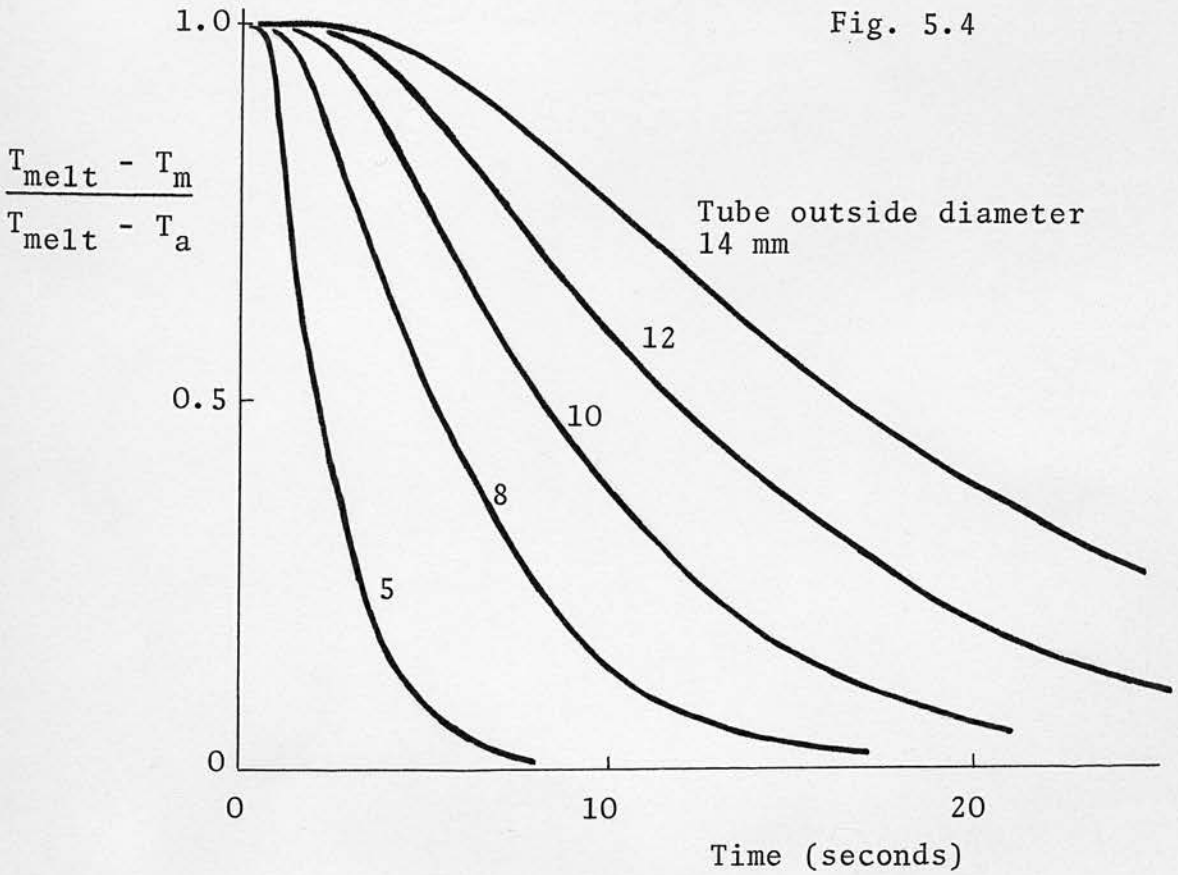

Quenching: variation of capsule mid-point temperature (T_m) with time.

Small capsules were quenched in air. Larger capsules were cooled in air for about 10 s then dropped into a water bath. The rate of cooling depends on the tube diameter. Fig. 5.4. shows how the temperature in the middle of the tube (T_m) falls if the walls are suddenly cooled at time t = 0 from a temperature T_{melt} to T_a (33). It has been assumed that the thermal conductivities of quartz and the chalcogenide glass are equal and not temperature dependent.

5.2. THIN FILM SAMPLE PREPARATION

5.2.1. Deposition of thin films of chalcogenide glass

During the evaporation of compounds, dissociation frequently occurs and the component elements evaporate at a rate appropriate to the source temperature. The simple chalcogenide glasses such as As_2Se_3, in which the elements are about equally volatile and which do not dissociate appreciably in the vapour phase, are easily evaporated. A thin-walled quartz boat was used with a molybdenum wire heater wrapped around it. The boat was made from 1 cm bore tube sealed at one end and about 2 cm long. The material in the boat melted and evaporated steadily. This technique was used for As_2S_3, As_2Se_3, As_2Te_3, Te, Se, As, $Tl_2Te.As_2Te_3$ and $Tl_2Se.As_2Te_3$.

Chalcogenide glasses which contained Si or Ge were more difficult to evaporate - they had to be heated to 400°C or more and other techniques were necessary.

1. A resistance-heated Mo boat gave good reproducible films. The boat was made from 0.003" thick Mo sheet. It was bent so that it enclosed an ingot (¼ - 1 g) of glass with only a small hole in the top of the boat for the vapour to escape. A new boat was used for each evaporation and it was heated slowly until evaporation started. This was an easily repeated technique. However, there were large differences in resistivity between bulk and thin film samples (section 5.3.) and a grey residue was left in the boat after

evaporation. Analysis confirmed that the films were deficient in Si (or Ge) relative to the starting material so this evaporation technique has only limited application.

2. An electron-beam gun provides a localised high temperature source. Several films were evaporated with a Bir-Vac RG2 electron-beam evaporation system. The glass in a carbon crucible melted and evaporated very quickly. However, under these conditions it was difficult to maintain a steady power input to the glass and the whole evaporation process was not easily controllable. The electron beam gun did provide a good source for the evaporation of Ge. It could therefore be used in conjunction with a heated quartz boat containing As_2Te_3 for coevaporation to provide thin films of As, Te and Ge.

3. Flash evaporation is a technique which has been widely used for evaporation of compounds which are easily dissociated. The experimental arrangement used in this work is shown in fig.5.5. The bulk glass was finely ground and fed from a hopper on to a rotating disk. A thin stainless steel wiper pushed the powder off the disk so that it fell down the chute and on to the hot source. An alternative delivery system which used a drill to feed powder on to the chute is also shown in fig. 5.5. This was not as successful as the disk and wiper combination. The source was a V-shaped boat made from Mo sheet. The difficulty encountered with all flash evaporation systems is that when a

Fig. 5.5

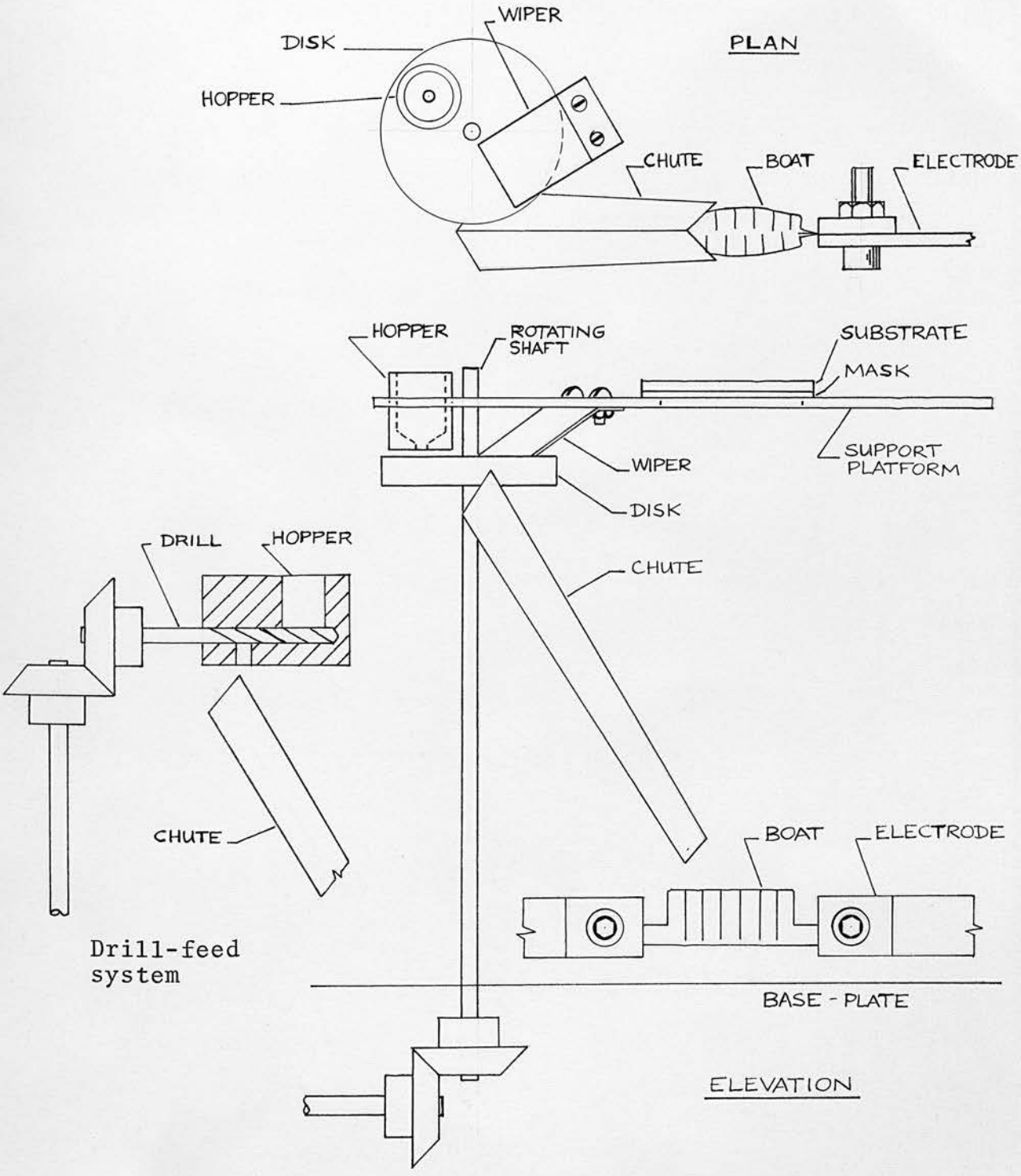

Schematic diagram of flash evaporation system.

particle lands on the hot source, it vapourises at the point of contact and this tends to throw the particle out of the boat. This effect was minimised by using finely crushed glass and by having high sides to the source. The sides were slotted so that the current needed to heat the source would not be greater than 20 amps.

Film thicknesses were between 0.2 and 3 μm. In general, it was more difficult to produce thick flash evaporated films. In all cases, substrates of Corning 7059 glass were used. Adhesion was good throughout the range of film thicknesses.

Electron beam evaporation was done at 2.10^{-5} torr in a Bir-Vac T300 plant. The other glass evaporations were carried out in a 'home-made' vacuum system at pressures between 5.10^{-5} and 10^{-4} torr. A cold trap was not used with either plant. The electrodes and glass films were deposited in separate pump-downs.

When a glass dissociates and its component elements or simple molecular groups evaporate at different rates, good quality thin films may result, but there is likely to be a difference in composition between film and bulk and this could pose serious problems, e.g. in the comparison of bulk and thin film optical properties. It also means that each film is likely to be slightly different from all others and this could limit the large-scale application of the thin films.

Apart from simply improving the evaporation technique, other deposition methods may be used to overcome the composition problem.

R.f. sputtering has been widely used where film stoichiometry is important. It requires specialised and expensive equipment but the technique is well established.

Many glasses can be blown into thin bubbles or hot-pressed to give thin bulk samples. These techniques are not likely to be used on a large scale so they have not been investigated in this work. Silk screen printing is an attractive technique but the minimum film thickness is around 25 μm. Another deposition method which was investigated briefly was to suspend finely powdered glass in a suitable liquid and centrifuge the powder down on to a substrate (190). The film was then fired to remove any of the suspension liquid and to produce a smooth glass film. It appears to be an attractive technique for producing films in the thickness range 1 - 20 μm.

5.2.2. Thin-film sample geometry

In most thin film evaporations, standard samples were produced for resistivity evaluation. Two electrode arrangements were used: coplanar and sandwich. The layout and dimensions are shown in fig. 5.6. The area of each film was defined by an out-of-contact mask. With coplanar electrodes, the gap was formed by a wire stretched across the mask and in contact with the substrate. The usual gap width was 120 μm. In all coplanar samples,the electrode separation was much greater than the film thickness. The electrodes could therefore be considered as being effectively normal to the direction of current flow and the current density

Fig. 5.6

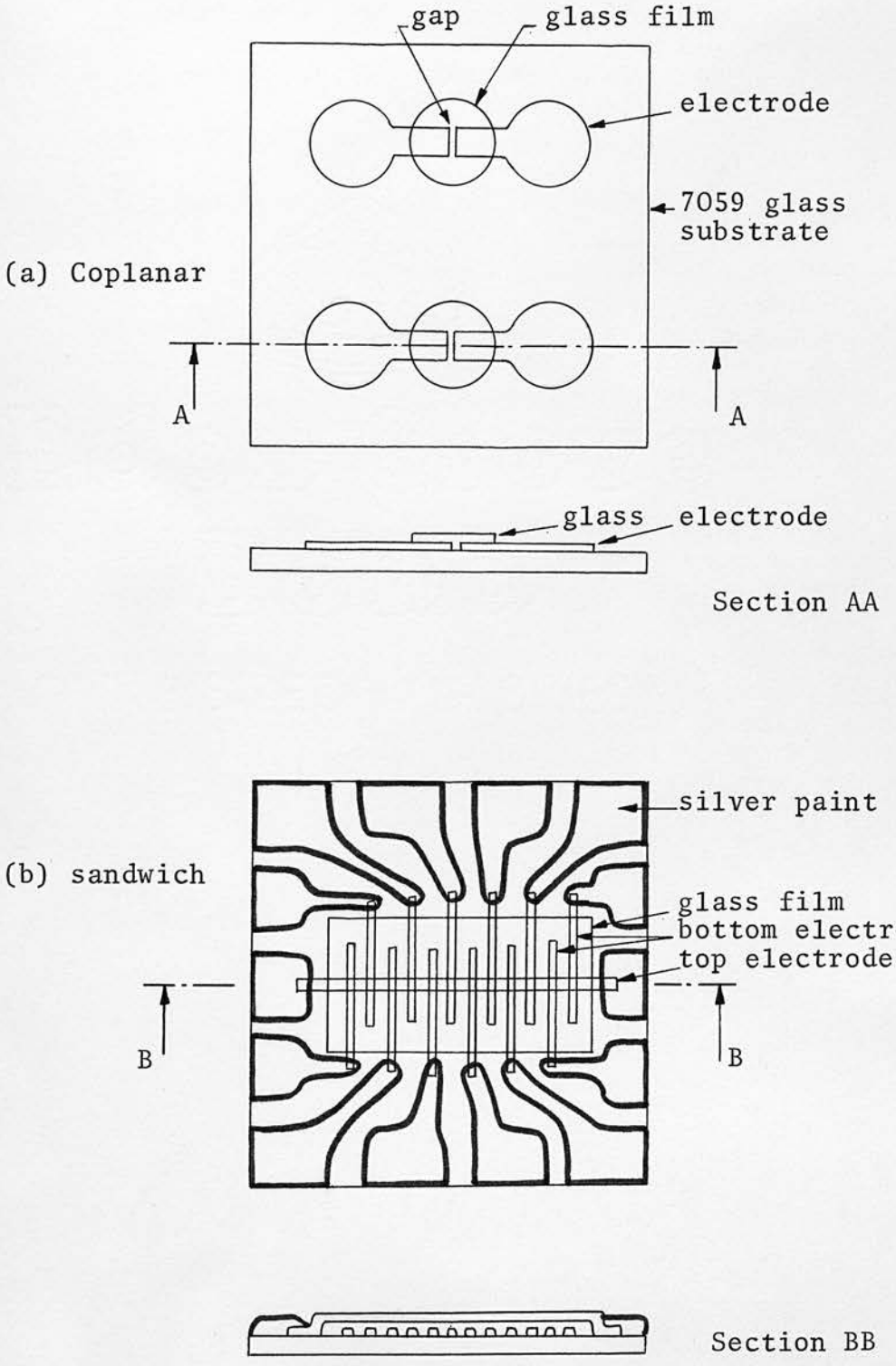

Thin film patterns for sandwich and coplanar electrode arrangements.

uniform throughout the volume of the film between the electrodes (191).

The coplanar and sandwich structures allowed the film resistivity to be measured in two different directions. This was a useful check on the uniformity of film composition and is discussed in more detail in section 5.3. The resistance values with the two electrode arrangements are very different, e.g. for a uniform glass film 1 μm thick and with $\rho = 10^4\ \Omega$.m, the sandwich resistance for an electrode area $2.10^{-7}\ m^2$ is 50 KΩ . For coplanar electrodes 1.2 mm wide and separated by a 120 μm gap, the resistance is $10^9\ \Omega$.

It was not necessary to connect the electrodes to the measuring circuit with a strong or noise-free contact, so silver paint was used and clips fastened to that. If a more reliable or rugged contact were required it could be made by soldering a wire to a gold film which had an underlayer of nichrome. Gold itself does not adhere well to 7059 glass, but this did not pose serious problems in this work since no mechanical strain was put on the contact.

5.3. RESISTIVITY AND COMPOSITION

5.3.1. Measurement methods

The resistivity of chalcogenide glasses is strongly dependent on composition. The range of resistivity and composition variations was outlined in chapter 2. As changes in composition are introduced, there are corresponding changes in most of the glass properties, e.g. glass transition temperature, activation energy for resistance and resistivity itself. The latter, however, is the most sensitive to composition changes. The off-state properties of a switch are determined by those of the bulk or thin film chalcogenide used. It is therefore important to know the relationship between composition, resistivity and the method of film deposition so that device performance can be predicted and controlled.

At 10^{-4} torr, the evaporation temperatures for the typical elements contained in chalcogenideglasses are: (192)

Element	Temperature at which its vapour pressure = 10^{-4} torr. (^{o}C)
Se	170
As	200
Te	270
Ge	1120
Si	1340

There is almost no useful information in the literature about the fractionation of chalcogenide glasses and in the course of this work, it was not possible to measure directly the atomic groups which were present in the evaporant stream. However, it was possible to measure the final film composition and then check it with resistivity data. From this and the evaporation technique used, it is possible to infer how much fractionation occurs. The table of evaporation temperatures shows that Ge and Si are much less volatile than the other elements which may be in the glass, so if any fractionation does occur the thin film is likely to be deficient in Si and/or Ge.

Thin film composition was determined with a Philips X-ray fluorescence analysis (XRF) instrument. A thin film of chalcogenide glass was deposited on a substrate disk 1.35" diameter. The substrate was usually of soda-glass and it was placed alongside the other substrates inside the vacuum system. Thus the deposition conditions for the analysed thin film were as close as possible to those for films used for resistivity and switching measurements.

The XRF technique involved irradiation of the thin film disk with X-rays and then identification of the secondary X-rays emitted from the film. The X-ray wavelength identifies the element and the intensity depends on the amount of that element present. For films up to about 6 μm thick, the intensity was proportional to film thickness. The incident X-ray intensity was constant over a series of analyses. To calibrate the instrument, disks coated with Ge, Se and Te were irradiated.

The detector output for each was divided by film thickness to give a figure which represented 100% of the particular element in the form of a 1 μm film. When a chalcogenide alloy was irradiated in the same way the detector output, e.g. for Te, was first normalised to represent a 1μmthick film and then divided by the Te calibration figure to give the proportion of Te in the film.

The biggest source of error arose in the measurement of film thickness. Talysurf measurements at 1 μm were subject to about $\pm$ 10% variation over the surface of the XRF disk. The surface of the Te calibration disks were slightly bloomed, indicating that some oxidation at the surface may have occurred and this introduces another error in the calibration measurement. In general, the composition of any chalcogenide film could only be specified to within about $\pm$10%.

The XRF calibration sensitivities for Ge, As and Se are expected to be similar since they are adjacent in the periodic table. Arsenic oxidised too readily to provide a reliable speciment for XRF calibration but the figures for Ge and Se agreed. The high silicon content of the soda glass substrate dominated the measurement of Si concentration, so the Si content of the chalcogenide films could only be determined by subtracting the total of the other components from 100%.

5.3.2. Films of As_2Se_3 and As_2Te_3

The simple chalcogenides, As_2Se_3 and As_2Te_3, evaporate readily from a heated quartz boat at about 200 - 300^{o}C. Films were also

produced by flash evaporation but there was no systematic difference in films produced by these two techniques.

Films of As_2Se_3 were dark red in colour. They were strongly photosensitive and the dark resistivity was about 10^9 Ω.m. The resistivity values derived from coplanar and sandwich measurements were similar, indicating that the composition throughout the film was uniform. XRF results indicated that the film composition was within 3% of stoichiometric As_2Se_3.

As_2Te_3, like all the complex alloys for which it provides a base, was deposited as a black shiny film. The current was not light-sensitive and the coplanar and sandwich resistivities were both 60 Ω.m. The film composition derived by XRF analysis was As_2Te_3 to within 3%. It is not possible to produce amorphous As_2Te_3 in bulk form, but an estimate of its resistivity can be made from two sets of data:

1. The system $As_2Te_3 + As_2Se_3$ can be produced in bulk glassy form up to 80% As_2Te_3. The variation of resistivity with composition was discussed in section 3.6.1. The $\log \rho$ - composition line may be extrapolated to obtain a value for the resistivity of amorphous As_2Te_3.
2. The system As_2Te_3 + Si which is discussed in the following section shows a steady change in resistivity as more Si is incorporated into the glass. Again the $\log \rho$ - composition line may be extrapolated to zero silicon content (fig. 5.7.).

Both extrapolation techniques give a resistivity figure for bulk

amorphous As_2Te_3 which agrees with the thin film value.

5.3.3. Films of As_2Te_3 + Si

The AsTeSi system has a large glass-forming region (fig. 5.1.). In particular, mixtures of As_2Te_3 + Si can be produced in glassy form, by quenching from the melt, with up to 45% Si. Such a wide composition range provides a correspondingly wide range of physical and electrical characteristics and the system therefore provides a very flexible basis for experimental work on the more complex chalcogenide alloys.

The variation of resistivity with silicon content is shown in fig. 5.7. for bulk glasses. There is a uniform logarithmic increase in resistivity as silicon is added, from 2.10^3 Ω .m for $(As_2Te_3)_{90}Si_{10}$ to 2.10^8 Ω .m for $(As_2Te_3)_{60}Si_{40}$. When the line is extrapolated to zero silicon content, the resistivity value corresponds to that mentioned in the previous section for thin film As_2Te_3.

When a glass composed of As_2Te_3 + Si is evaporated, the film resistivity depends on the evaporation method used but in all cases it was lower than the resistivity of the bulk glass. This is also shown in fig. 5.7. The flash evaporated films (denoted by the film number followed by the letter 'F') follow the same general trend as the bulk samples : high silicon content in the bulk glass gives a film with high resistivity. However there is a greater spread in the film resistivity at any single composition. This is due almost entirely to the differences in the temperature of the evaporation boat, e.g. the boat temperature for film

Fig. 5.7

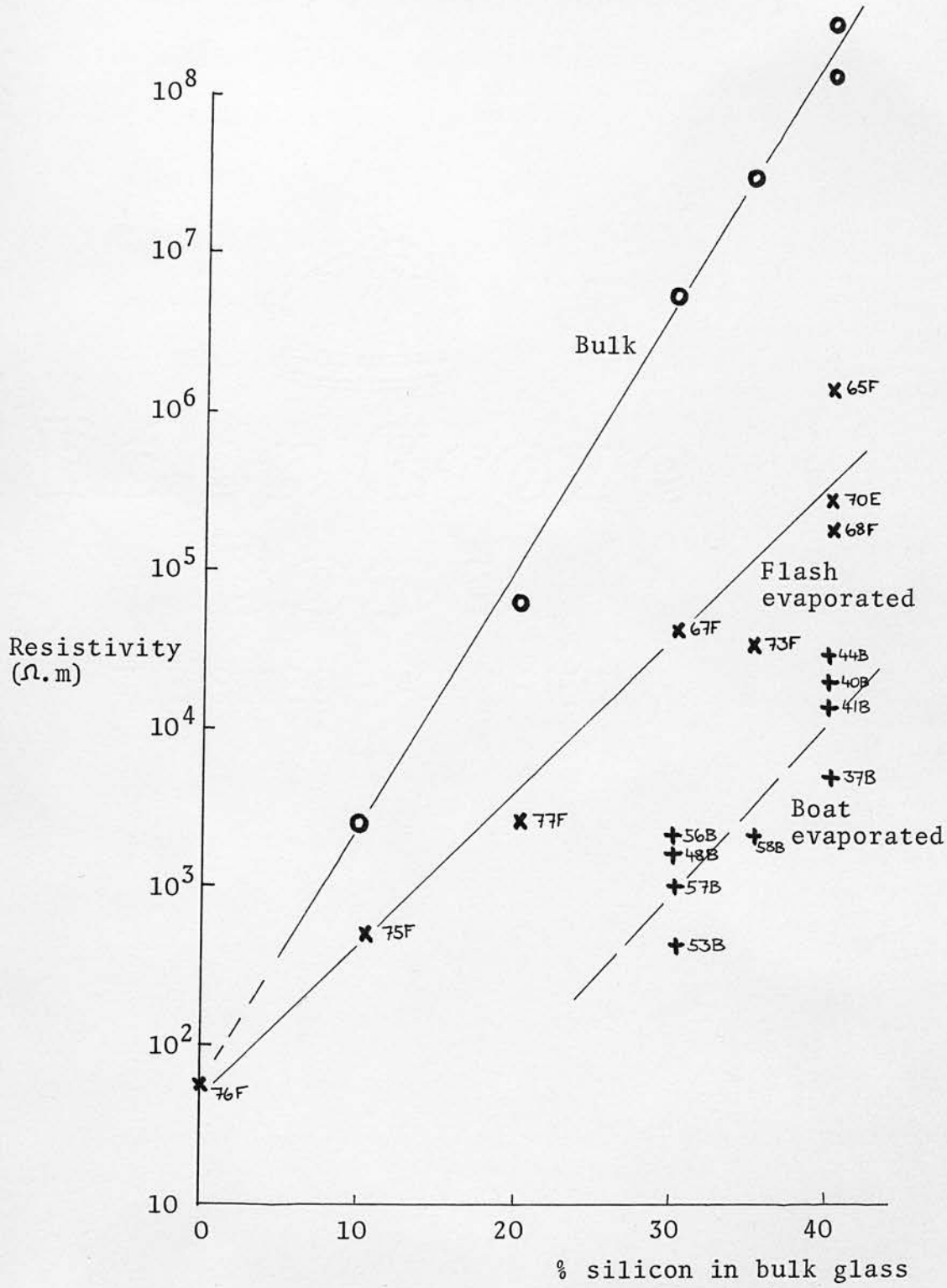

Variation of resistivity with silicon content (for thin films the % Si is that of the bulk starting material).

65 was visibly hotter than that for film 68. A more detailed study of the effect of boat temperature on film resistivity was not made.

One film was evaporated by an electron beam source. It is marked '70E' in fig. 5.7. and had a resistivity similar to the flash-evaporated samples. The ingot which was evaporated had the composition $(As_2Te_3)_{60}Si_{40}$.

Films evaporated from a hot molybdenum boat had lower resistivities than the corresponding flash-evaporated films. In fig. 5.7. the boat-evaporated films are described by the film number followed by the letter 'B'. There is a wide spread in resistivity which can be mostly associated with differences in boat temperature from run to run.

Films evaporated on to glass disks were analysed with the X-ray flourescence instrument. Figures for As and Te percentage concentrations were obtained and the silicon figure was deduced by subtracting their total from 100. The results are summarised in table 5.1.

The errors in the XRF analysis are large (approximately ± 10%) but the data serves to provide a first-order treatment. The As : Te ratio in the bulk starting material for each film was 0.67. This is approximately preserved in the thin film. There may be some significance in the correlation of low As : Te ratios (0.5) with the lower temperature evaporation sources E44, 68 and 49.

The description of the evaporation process therefore appears to be

Film number	% Si in bulk	Evaporation source	% from XRF As	Te	Si	% Si from resistivity	As:Te ratio
44	40	boat	28	52	20	17	0.5
65	40	flash	28	42	30	27	0.7
68	40	flash	23	44	33	23	0.5
73	35	flash	34	48	18	13	0.7
49	30	boat	32	60	8	6	0.5
67	30	flash	40	53	7	18	0.7

Table 5.1

Composition of thin films evaporated from As_2Te_3:Si glasses.

that As and Te in the proportions of As_2Te_3 evaporate easily. Silicon, however, is less volatile and the thin films are deficient in silicon relative to the bulk starting material. If this is so, then it should be possible to determine the silicon concentration of a film from its resistivity, e.g. in fig. 5.7., film E65 was produced by flash evaporation of a glass containing 40% Si. However, the resistivity of E65 corresponds to a bulk sample with only 27% Si. Silicon concentrations determined in this way are shown in the table and compare favourably with the concentrations derived from XRF analysis.

A routine measurement was made on each film of the variation of resistance with temperature. The range was room-temperature to $100^{o}C$. In all cases the behaviour conformed to the equation:

$$R = R_o \exp(\frac{\Delta E}{kT})$$

This is a common feature of all chalcogenide glasses and was discussed in chapter 2. The activation energy, ΔE, varied between 0.40 and 0.50 eV. It did not depend on bulk composition, but did tend to increase with film resistivity, i.e. 0.40 eV for 100 Ω.m and 0.50 eV for 10^3 Ω.m. For all cases, however, there was a spread of $\pm$ one order of magnitude in resistivity so the activation energy cannot be used for any precise description of glass composition in the same way that film resistivity can be used.

5.3.4. Films of AsTeGe

The system AsTeGe has two glass-forming regions (fig. 5.2.) and one

bulk composition from each region was examined: $As_{20}Te_{70}Ge_{10}$ (V31) and $As_{55}Te_{35}Ge_{10}$ (V38).

The bulk V31 glass had a resistivity of 250 Ω.m. There was no difference between flash-evaporated and boat-evaporated film resistivities, both were 150 Ω.m for sandwich samples. XRF analysis of a flash evaporated film indicated that the composition was $As_{30}Te_{70}$ with the Ge concentration below 1%. There appears to be no simple reason for the low Ge content. The flash evaporation technique was the same as that used for the As_2Te_3 + Si samples described in the previous section and on the basis of the silicon concentrations reported there, a Ge content of about 5% would have been expected in films produced from V31 glass.

The high As-content glass (V38) was studied in more detail than V31. The bulk resistivity was 1.5 KΩ.m. Flash-evaporation gave films of approximate composition: $As_{56}Te_{40}Ge_4$. This is close to the bulk composition and the loss of Ge is similar to the loss of Si described in the previous section.

Evaporation of V38 glass from a molybdenum boat gave films which had very different sandwich and coplanar resistivity values. Most films showed some difference between the two resistivities, perhaps up to an order of magnitude, but for the case of V38 glass, it was two orders: 10 KΩ.m for sandwich resistivity and 100 Ω.m for coplanar resistivity.

To investigate composition as a function of deposition conditions, a set of resistivity and XRF substrates were exposed during one half of

an evaporation. They were then masked off and a second set exposed for the second half. There was little difference in the sandwich resistivities for each half, but the coplanar resistivity was higher for the first half of the evaporation than the second. The As : Te ratio in the bulk glass is 1.6. In the first half of the evaporation it was about 5; in the second it was about 1.8. The Ge concentration increased from about 0.4% in the first half to about 4% in the second half.

The picture which this gives of the evaporation process is of a film which is initially rich in As. This has a higher resistivity than the bulk glass. In the later stages of the evaporation, the Ge and Te concentrations are closer to those of the bulk glass. The boat temperature was about 400°C. This is much lower than the temperature needed to evaporate Ge itself (1120°C) so it appears likely that Ge is evaporated as part of a compound, perhaps GeTe. There is clearly scope for more detailed study of evaporation kinetics if the technique is to be used to give uniform and reproducible films for electronic devices.

5.3.5. Films of AsTeGeSi

Glass of composition $As_{30}Te_{48}Ge_{10}Si_{12}$ has been widely studied following its successful use in switching devices (173). The bulk glass resistivity is 12 KΩ.m and measurements made on thin films produced by evaporation of this glass conform to the general properties described

in the literature and the features already described for the AsTeGe and AsTeSi systems.

Electron beam and boat-evaporation both gave films with resistivities in the range 200 Ω .m - 2 KΩ.m. Flash evaporation gave higher resistivity values: 10-20 KΩ.m. XRF analysis of a flash-evaporated film indicated that the film composition was close to that of the bulk glass with only slight deficiencies in Ge and Si.

5.4. CONTACTS TO THIN CHALCOGENIDE FILMS

In any electronic device it is important that the semiconductor be provided with stable and reliable contacts. It was mentioned in chapter 2 that most metals make good ohmic contacts to bulk chalcogenide glasses. The high density of trapping sites in the middle of the forbidden gap gives a very short screening length. Thus, the width of any barrier layers at the contacts is small (2 - 3 nm) and high injection current densities can be achieved by tunnelling. A similar process appears to apply also to thin film chalcogenide glasses.

Most contacts were made by evaporating thin metal films on to the glass film. To provide a good contact, there must be good physical adhesion. This did not present a problem for any metal-glass combination. During switching cycles, high local temperatures can exist in chalcogenide films. Under these conditions the electrode metal must

1) not react with the film
2) not diffuse into the glass
3) not induce crystallization in the glass
4) continue to act as as efficient source of carriers
5) not be liable to oxidation

As well as being important when heating may occur within the glass film, the last point must also be considered when electrodes and glass are not deposited in a single pumpdown. Exposure to air after the deposition of the bottom contact of a sandwich can result in a thin oxide

barrier between the metal and the glass and the carrier injection efficiency may be reduced.

An ideal ohmic contact should act as an infinite reservoir of carriers for the semiconductor film. Conversely, the absence of ohmic contacts is indicated by anomalously high film resistivities. The comparison of sandwich and coplanar resistivity values provided a useful additional method of checking the ohmic nature of contacts. For the typical dimensions discussed in section 5.2.2., coplanar resistance is greater than the sandwich value by a factor of 2.10^4. With a barrier at either contact, the low-field ratio of coplanar : sandwich resistances would be determined only by the effective area ratio - about 200. Since the effect of non-uniform composition throughout the film thickness is to produce a similar result, film composition homogeneity must be checked before any resistivity anomalies are ascribed to non-ohmic contacts.

Gold was most widely used as an electrode material in this work. In most cases, it was deposited by an electron-beam evaporation process. For field strengths below 10^6 $V.m^{-1}$ (i.e. low-field off-state characteristics of chalcogenide switches), gold behaved as a good reproducible ohmic contact. Switches with gold contacts had limited lifetimes; this is treated in chapter 7.

Molybdenum behaved very much like gold as a contact metal and it was also evaporated by an electron-beam source. Molybdenum, however, was much more difficult to evaporate - it requires a source temperature of 2200 K at 10^{-5} torr. Excessive heating of glass films had to be

avoided in case it induced devitrification, so molybdenum films were always thin and had to be used with another metal to provide a low electrode resistance. There are indications that Mo is much better than Au as a reliable electrode for devices (193).

Tellurium was evaporated from an indirectly heated quartz boat and provided a good ohmic contact to chalcogenide films, but it had a resistivity of $\sim 10^{-3}$ Ω.m and tended to oxidise so it was used infrequently. Tin, evaporated from an electron-beam heated source, behaved as an ohmic contact but it too tended to oxidise and therefore could not be regarded as a stable contact in the long term.

Silicon is a particularly interesting contact material. When a glass switch is used in an array, it also requires an isolating element at each crosspoint. The most obvious device for this is a silicon diode. With a diode in series with the glass switch, an ohmic glass-silicon contact means that there is no need for an intervening metal layer to provide an ohmic contact for both glass and silicon.

The I - V characteristics of a gold-pSi diode are shown in fig. 5.8. The back contact to the silicon was silver paint. When a film of glass was interposed between the gold and the silicon, the resulting characteristics were of the same shape as for Au-Si but shifted as if by the addition of a high, non-linear series resistance. Over most of the voltage range, the glass characteristic is non-ohmic. However at low currents ($< 1\ \mu$A) the Au-Si curves coincide and the glass provides a series resistance of 0.3 MΩ. This is approximately the resistance

Fig. 5.8

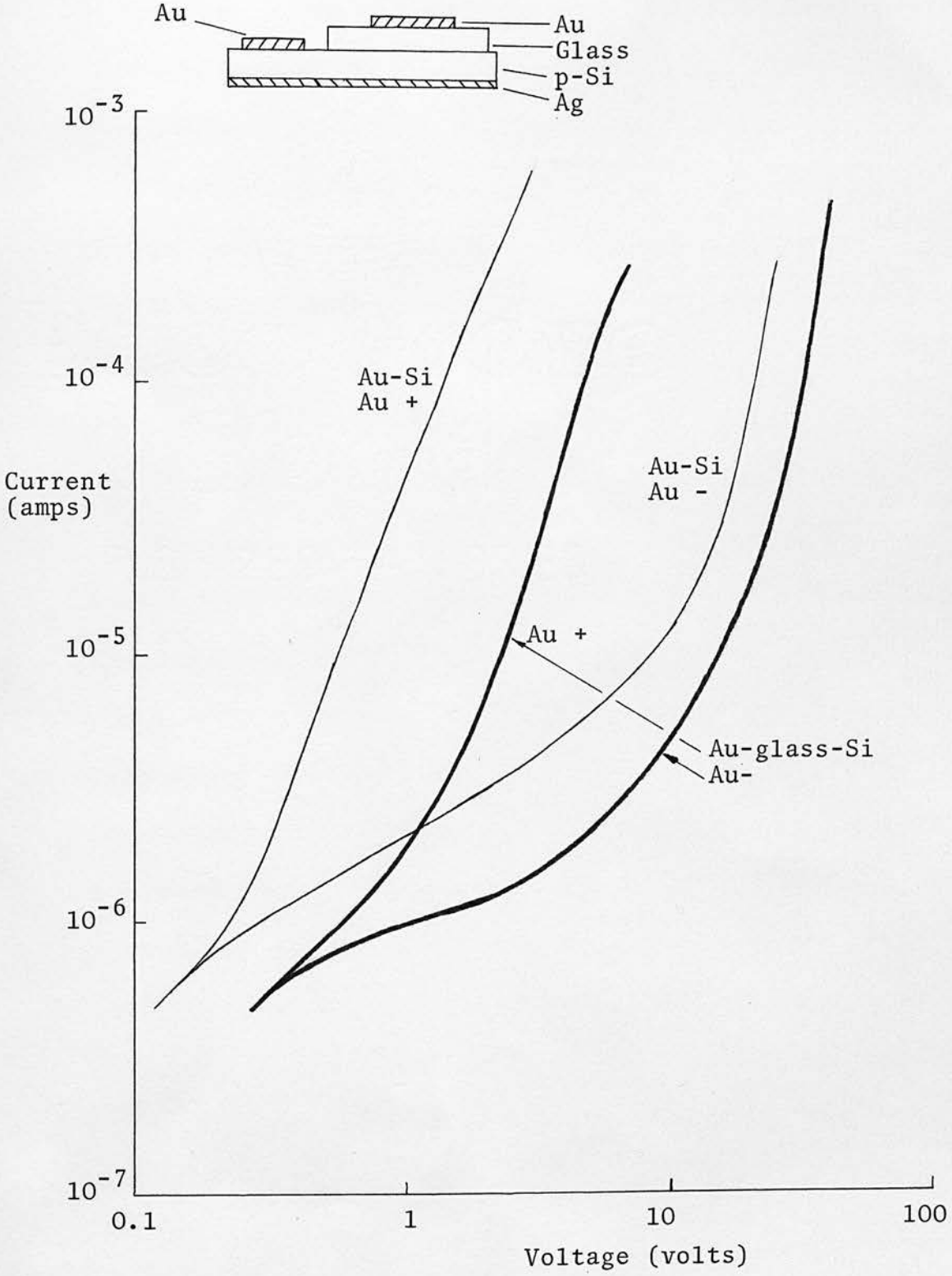

Characteristics for Au-Si and Au-glass-Si contacts.

value expected from the geometry and resistivity. Thus, silicon would appear to act as an ohmic contact.

Arsenic, evaporated from a quartz boat, was briefly examined. It oxidised readily in air and it had a very high contact resistance. It therefore appears to be unsuitable as an ohmic contact.

Silver paint is a very convenient electrode material but there is evidence that silver diffuses quickly in chalcogenide glasses. The biggest disadvantage of silver paint, however, was that it did not make a uniform area contact. The characteristics were those of a good ohmic contact but the resistivity indicated that the area was smaller than the geometrical value and varied from contact to contact.

Aluminium is readily evaporated and was used frequently as a contact. It gave a resistance value which corresponded to that of a gold electrode at high fields as shown in fig. 5.9. This and other results with Al contacts conform to those expected for a Schottky barrier about 10 nm thick. When the voltage is sufficiently high to allow a high injection rate over the barrier, the bulk may have switched as in the case of E74 in fig. 5.9.

The overall conclusion regarding contacts is that gold is the most convenient and reliable metal to use for examination of off-state characteristics and occasional switching events. For a more reliable contact, e.g. to be used in a commercial switching device, materials such as Ta, Mo, W or Si appear more suitable than gold.

Fig. 5.9

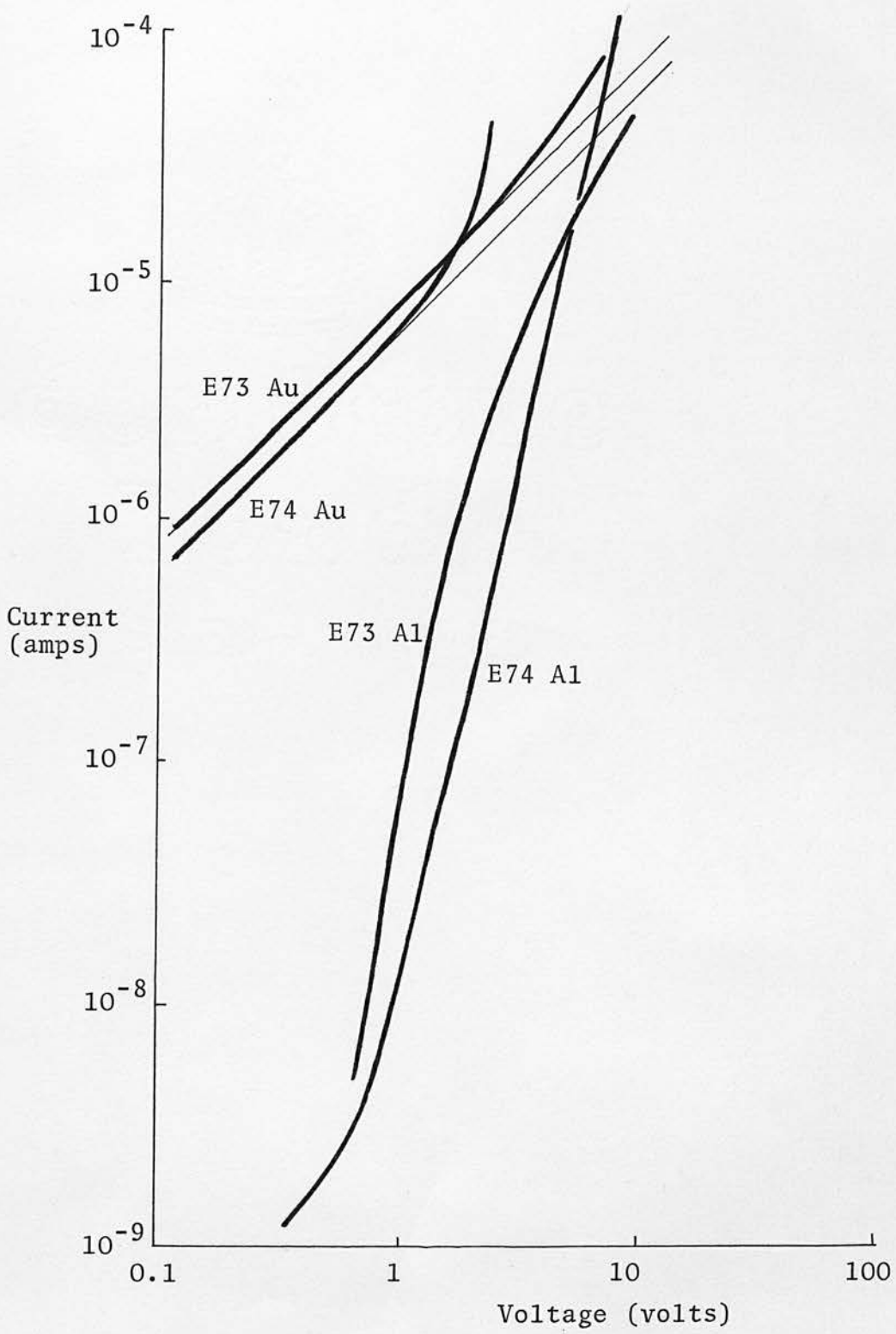

Chalcogenide glass I - V characteristics with gold and aluminium electrodes.

CHAPTER 6 EXPERIMENTAL RESULTS: THRESHOLD SWITCHING AND PRE-BREAKDOWN CONDUCTIVITY

6.1. INTRODUCTION

For field strengths above approximately 10^6 V.m^{-1}, chalcogenide glasses of the type used in switching devices show non-ohmic behaviour. When switching occurs a drastic change also occurs in the current-limiting mechanism so an understanding of the factors which influence conduction at fields just below breakdown is important.

Film composition and deposition conditions have important effects on resistivity and in this way have a bearing on switching performance. This, however, is a quantitative effect; it determines the current and voltage levels at which switching occurs. All chalcogenides of the type discussed in chapter 5 can show threshold switching behaviour and for those in the resistivity range 10 Ω.m - 10^7 Ω.m the general features of threshold switching are very similar over a wide range of compositions.

In this chapter, pre-switching behaviour is examined for three very different geometrical arrangements:

1. A bulk sample with a probe contact on one side.
2. A coplanar layout on an evaporated glass film. The electrodes were usually under the chalcogenide film.
3. Sandwich electrodes on either side of an evaporated glass film.

The thin film samples are those described in chapter 5 and in most

cases are the same units as those used for the low field conductivity measurements. The results for sandwich samples are more extensive than for the other two arrangements.

6.2 BULK SAMPLES

6.2.1. General approach

For each glass composition used in this work, a bulk sample was prepared for conductivity measurement. Data on low field conductivity and activation energy are given in chapter 5, but many samples also showed threshold switching. The threshold voltage was determined mainly by the glass resistivity, e.g. 10^4 Ω.m gave $V_{th} \doteqdot$ 300 volts; 10^6 Ω.m gave $V_{th} \doteqdot$ 2 KV. Since the more conducting samples were easier to study experimentally, the measurements in this section refer to them.

The compositions examined were: $As_2Te_3.Tl_2Se$; $As_2Se_3.Tl_2Se$; $(As_2Te_3)_{80}Si_{20}$; $As_{55}Te_{35}Ge_{10}$; $As_{20}Te_{70}Ge_{10}$ and $(As_2Te_3)_{78}.Si_{12}Ge_{10}$. The last composition (V20) is similar to that described by Ovshinsky (173) as a basic threshold switch material. Most of the measurements of bulk switching were done with V20 samples. However, all the other compositions gave qualitatively similar results.

Slices were cut from an ingot of V20 glass to give samples typically 3 mm diameter and 0.3 mm thick. Top and bottom faces were polished with 3 μm alumina powder and the sample was bonded to a metal backing plate with conducting silver paint. The top contact was made with a probe so that the effective contact area was $\sim 10^{-7}$ m^2. The bulk resistivity of V20 glass was 10^4 Ω.m.

Most measurements were made with a 50 Hz a.c. supply. The mains voltage was fed to the sample via a variac and a step-up isolating

transformer. The current was measured with a small sampling resistor - usually 10^3 - $10^4 \Omega$ in series with the sample.

Fig. 6.1. shows typical threshold switching characteristics. The curves are completely symmetrical and show no dependence on bias polarity. Photograph (a) is of a single scan, with an exposure of 20 ms. For (b) the exposure was 1 s and this shows a variation of about $\pm$ 5% on the threshold voltage. Three other features of these characteristics are important:

1. When the supply voltage is increased from zero (on the variac) the threshold voltage is much higher than the value measured for continuous 50 Hz operation (and shown in fig. 6.1.).
2. The time taken to switch along the load line from the high to the low resistance state is of the order of 1 ms. This is much slower than any switching speeds reported in the literature for thin films.
3. The holding voltage, V_h, is in the range 6 - 9 volts; again much greater than the values reported for thin films.

Samples could be run for several hours at 50 Hz. The first indication of failure was a slow decrease in V_{th} and finally the device remained in the on-state. Physically it appeared that local heating had occurred since the probe had sunk into the surface and was stuck to it. In one sample the glass around the probe had melted and bubbled. When these results are considered together it is reasonable to consider thermal breakdown as a possible mechanism.

Fig. 6.1

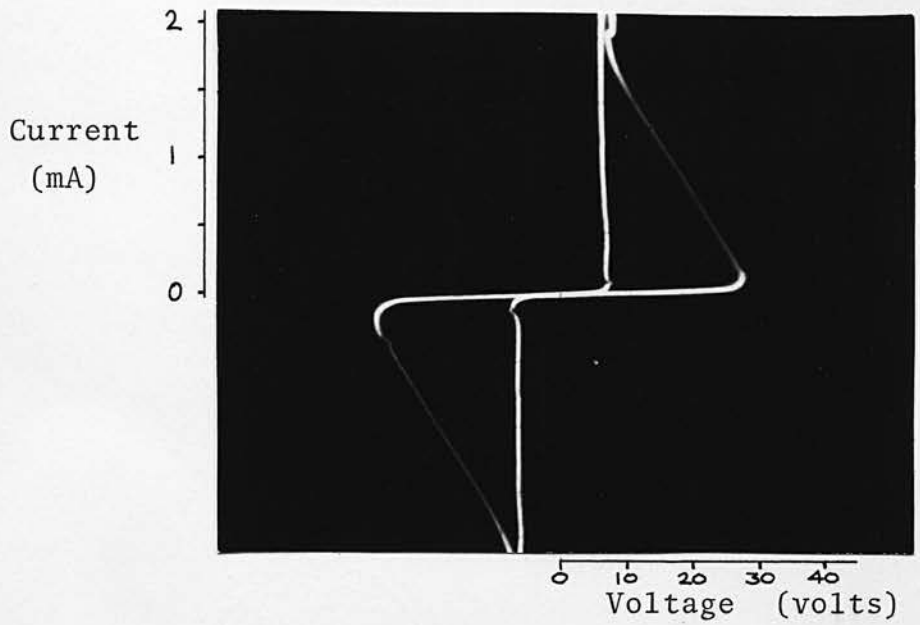

(a) 20 ms exposure.

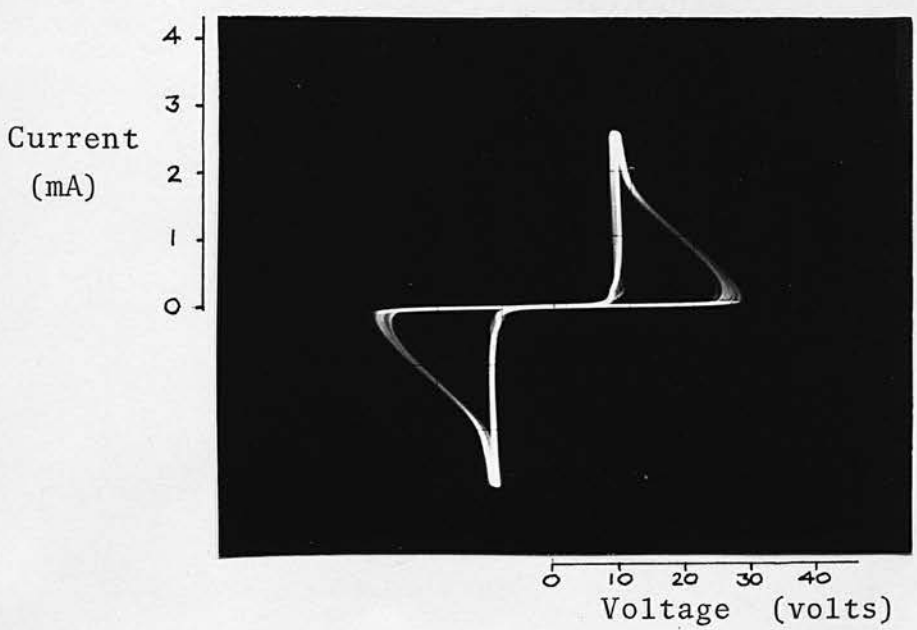

(b) 1 s exposure.

Threshold switching characteristics of a bulk sample (V20 glass).

The steady-state thermal breakdown analysis in section 3.3. indicated that at V_{th} the internal sample temperature is about 25 K above ambient. A chalcogenide glass such as V20 has an activation energy of 0.43 eV (or a = 0.04). Thus if the off-state resistance is 12 MΩ at T_a, at (T_a + 25) the resistance has dropped to about 4 MΩ. In thick samples, the field-dependence of conductivity is not important since $E_{th} \ll E_0$. Thermal conductance depends on geometry as given by equation 3.26:

$$\Gamma \doteq \frac{3\kappa A}{2d} \qquad \ldots\ldots 6.1$$

where thermal conductivity $\kappa = 1\ W.m^{-1}.K^{-1}$., $A = 10^{-7}\ m^2$ and d = 0.3 mm. This gives $\Gamma = 0.45 mW.K^{-1}$. For a sine wave with <u>peak</u> voltage and current values V and I respectively,

$$0.4\ VI = \Gamma \Delta T = 11\ mW$$

for ΔT = 25 K. The factor 0.4 converts peak power to r.m.s. power.

When taken with the resistance value at T_a + 25, this gives the conditions at turnover as : V_{th} = 330 volts, I_{th} = 85 μA. The experimental values for single-shot breakdown are 300 V and 60 μA for V20 so the simple thermal analysis appears to be adequate in this case. The single-shot breakdown voltage is always greater than the value measured under continuous switching conditions as in fig. 6.1. In this case the single and continuous values are 300 volts and 30 volts respectively. The difference can be explained on the basis of a high mean temperature in the a.c. case (fig. 6.1.). It is treated

quantitatively in section 6.2.3.

6.2.2. Pre-breakdown conduction

The high-field off-state characteristics were measured with an a.c. supply (50 Hz) and displayed on an HP 140 oscilloscope as current against voltage. For any value of peak voltage the trace was linear but the locus of the peak values gave a non-ohmic curve. This is also evidence of internal heating with a time constant greater than the supply repetition period, i.e. isothermal resistance lines are displayed (cf. fig. 3.12). Only close to V_{th} was the trace curved and hysteresis present.

Geometry did not affect the characteristics in a significant way. Current increased uniformly with area and the threshold voltage was not thickness dependent over a range 0.3 - 1 mm. Again this conforms to the 'thick sample' thermal analysis of section 3.3.5.

The current-voltage curve was strongly temperature dependent. Typical results (for V20) are shown in fig. 6.2. In the non-ohmic region, each line is described by an equation of the form:

$$I = I_0 \exp\left(\frac{V}{V_0}\right) \qquad \ldots\ldots 6.2$$

where I_0 and V_0 are constants at any specified temperature. The shape of the curves in fig. 6.2. is very similar to those derived for thermal breakdown and shown in fig. 3.6. The fact that I_0 and V_0 contain all the temperature-dependent terms is shown in the

Fig. 6.2

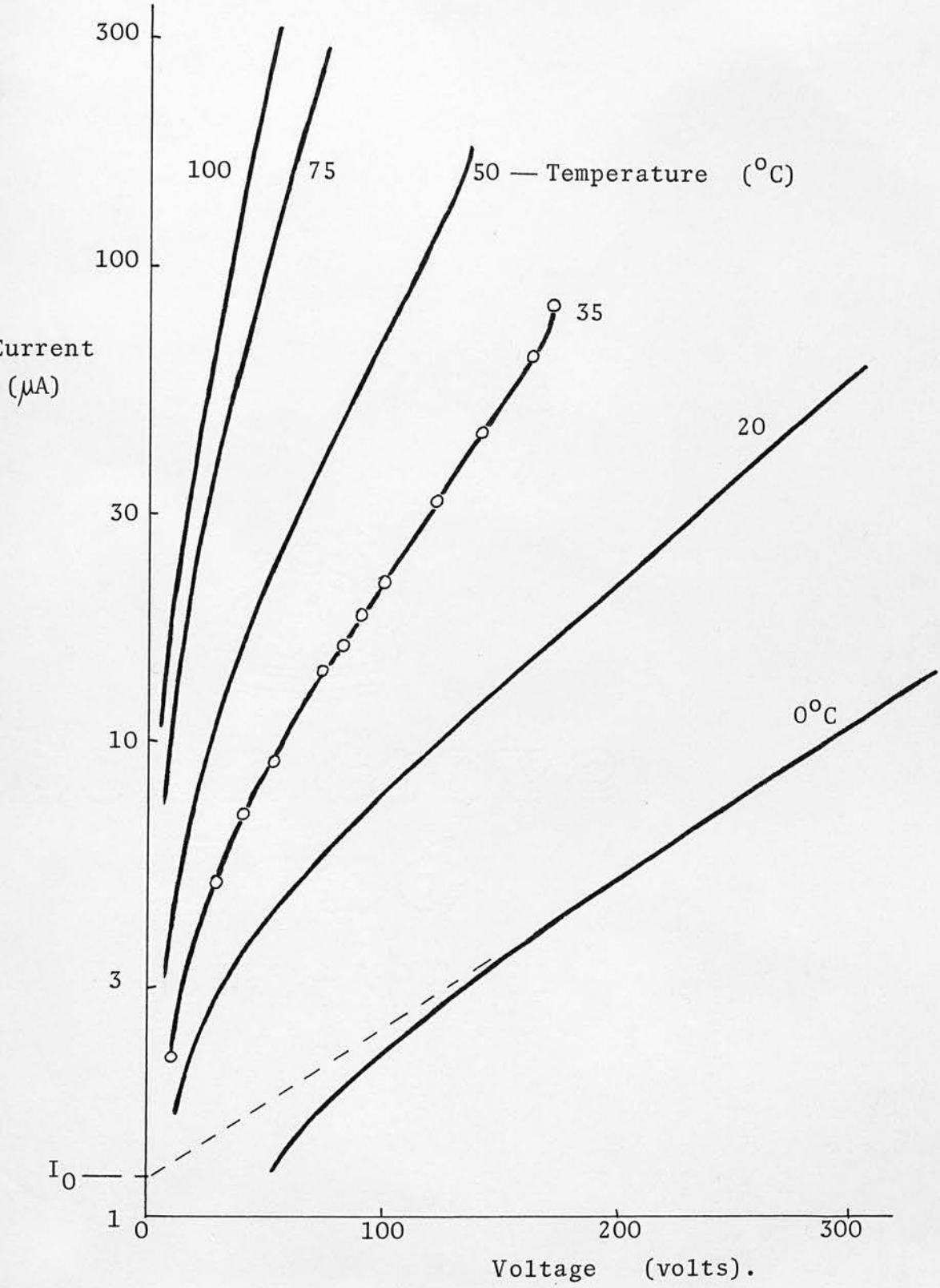

Bulk current - voltage characteristics as a function of temperature.

reduced curve in fig. 6.3. for Log I/I_0 against V/V_0. All points lie on the same curve. For comparison, the data of Walsh (194) for thin films are also shown. The coincidence of these data points indicates that the same mechanism may be responsible for both sets of results.

The temperature dependence of R_Ω, V_0, V_{th}, I_0 and P_{th} is shown in fig. 6.4. R_Ω is the low-field ohmic resistance and $P_{th} = V_{th} I_{th}$. The terms all have activation energies (over the temperature range 0 - 100°C). The values are:

R_Ω	0.38 eV
V_{th}	0.18 eV
P_{th}	- 0.07 eV
I_0	- 0.24 eV
V_0	0.19 eV

Since $P_{th} = V_{th} I_{th}$, the activation energy for I_{th} is - 0.25 eV. Each activation energy can be determined to within $\pm$ 0.02 eV from the graphs in fig. 6.4. The activation energies for V_{th} and V_0, I_{th} and I_0 are approximately equal. This was also the result obtained from the theoretical thermal breakdown characteristics shown in fig. 3.6. The activation energy for V_{th} is about half that for R_Ω. This is in accord with the thermal breakdown condition for thick samples given by equation 3.35. For all the terms in fig. 6.4., an activated process accurately describes their temperature dependence. Other relationships such as $V_{th} \propto T$ and $V_0/T \propto T$ suggested by

Fig. 6.3

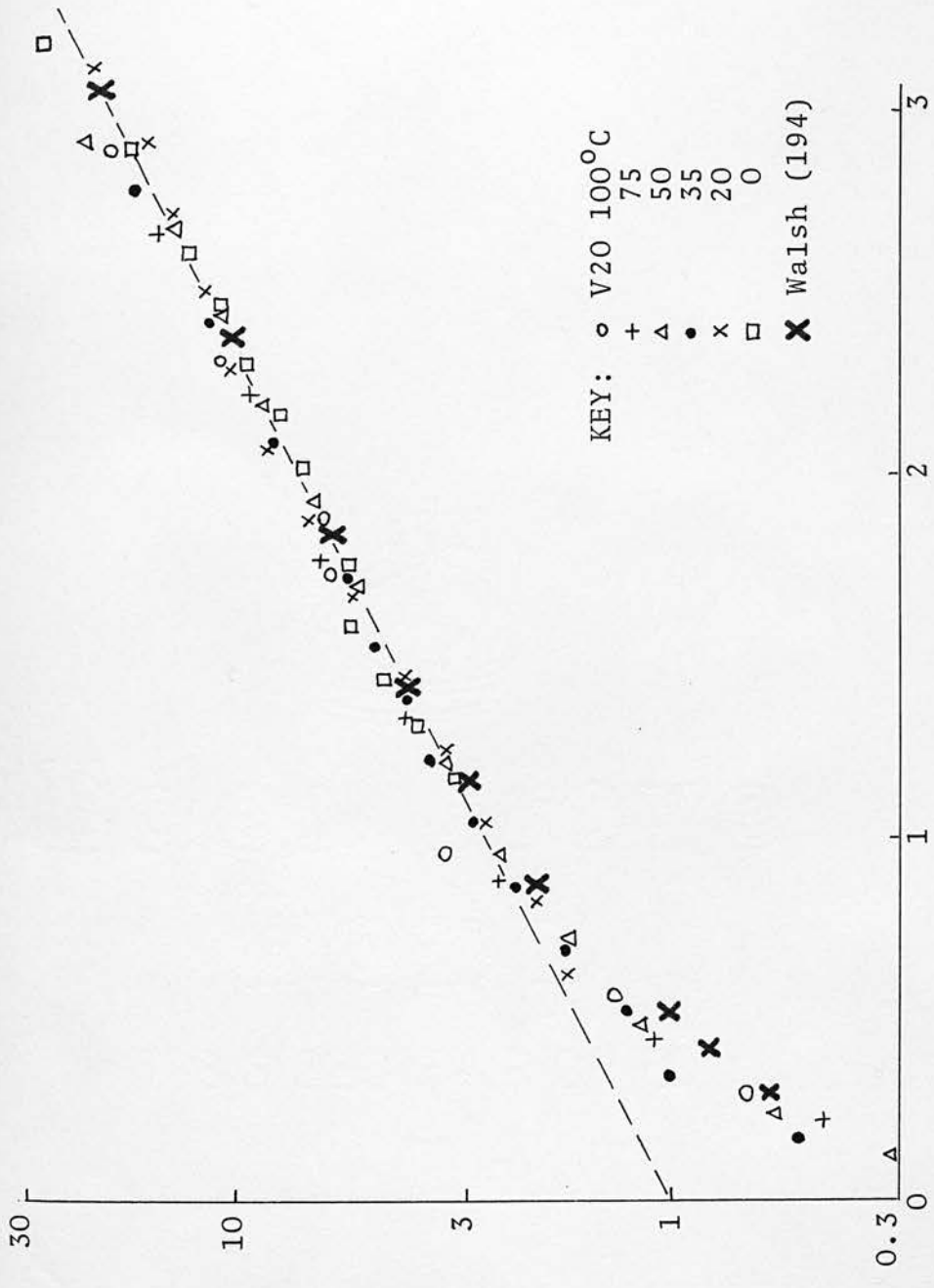

Reduced characteristics derived from fig. 6.2.

Fig. 6.4

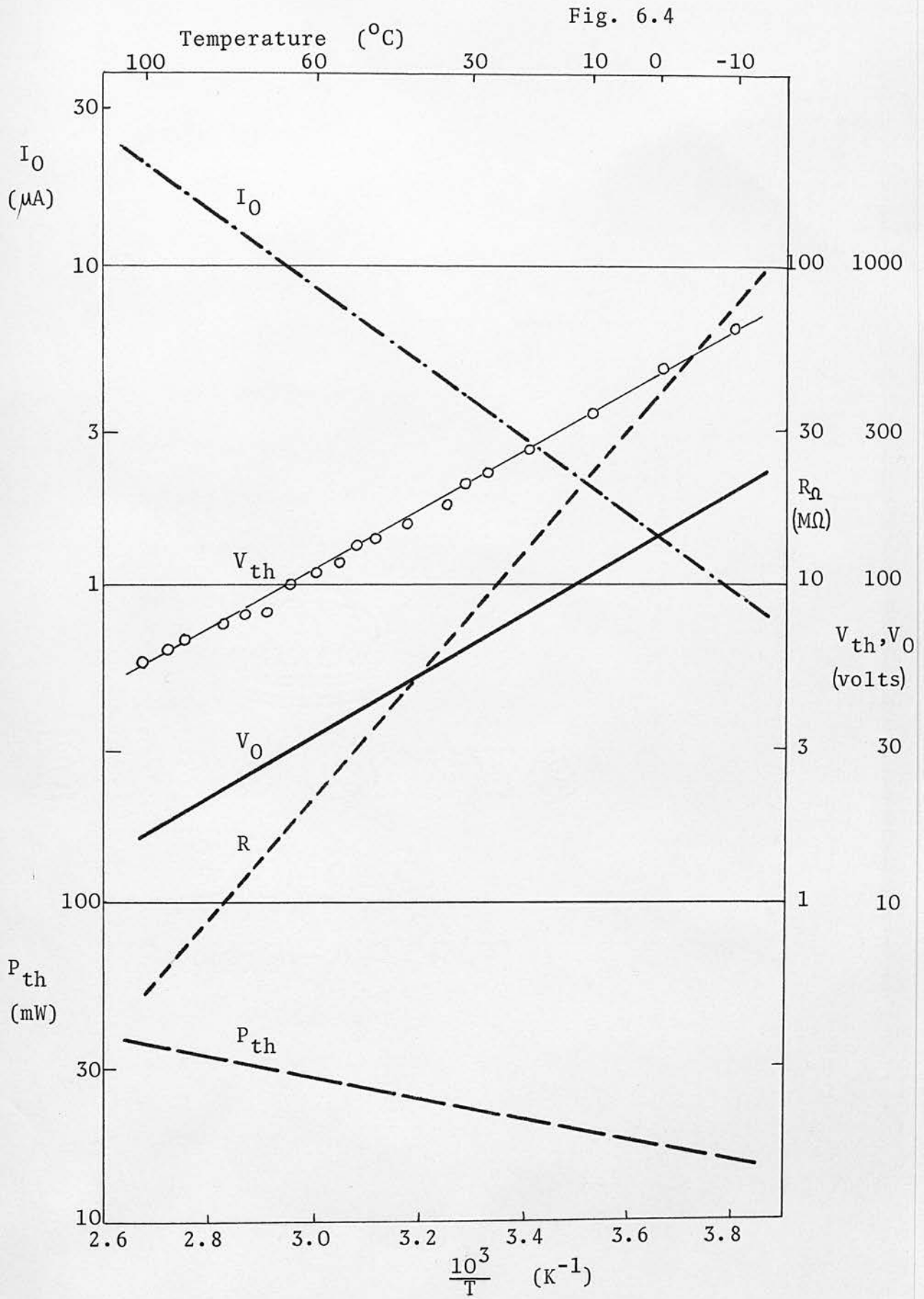

Temperature dependence of bulk properties:
V_{th}, V_0, I_{th}, I_0, R_Ω and P_{th}.

Walsh (194) for thin film results do not give linear characteristics with the data on V20.

The experimental results of fig. 6.3. may be described by two very similar I - V relations.

1. For $V < V_0$, $V = IR_\Omega$.

   For $V > V_0$, $I = I_0 \exp(V/V_0)$.

2. A single expression: $I = 2I_0 \sinh(V/V_0)$.

The two relations are shown in fig. 6.5. on logarithmic scales. Current and voltage scales have been expressed in terms of I_0 and V_0 respectively. For $V \gg V_0$, the sinh term reduces to $\frac{1}{2}\exp(V/V_0)$, so both relations coincide.

An expression of the type $I = I_0 \exp(V/V_0)$ has a slope which is ohmic at $V = V_0$. At V_0 the resistance value is:

$$R_\Omega = \frac{V_0}{eI_0} \qquad \ldots\ldots 6.3$$

With this constant resistance below V_0 there can be a smooth transition from an ohmic to an exponential characteristic at V_0.

The second possible relation, $I = 2I_0 \sinh(V/V_0)$ is almost identical to the exponential expression for $V \gg V_0$. At low voltages, however, the resistance is given by:

$$\frac{1}{R_\Omega} = \frac{2I_0}{V_0} \cosh \frac{V}{V_0}$$

Fig. 6.5

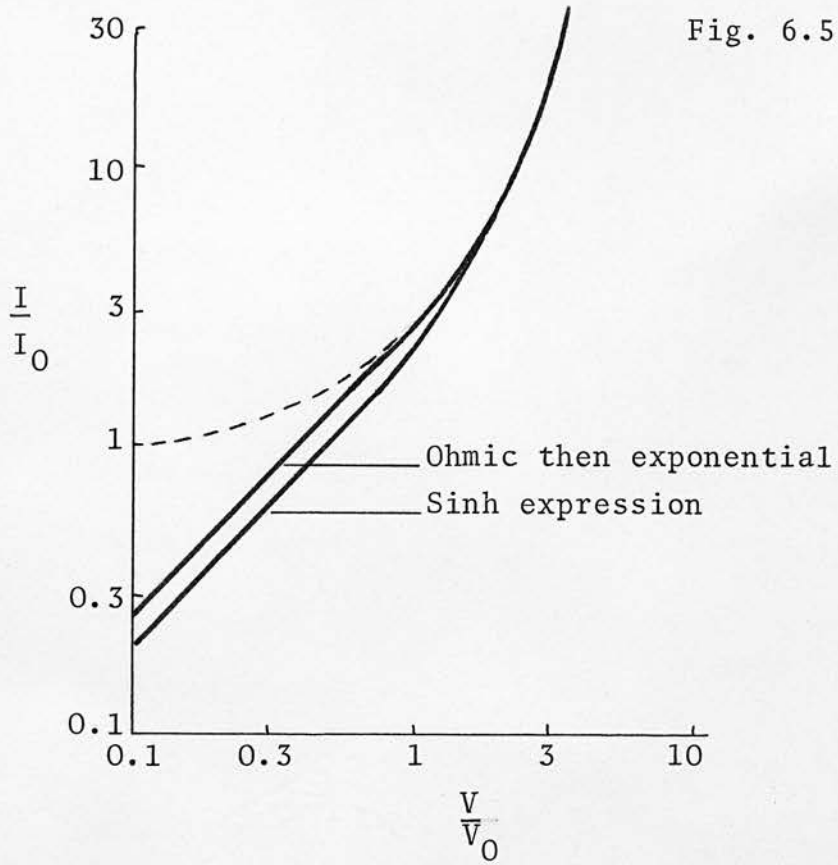

Comparison of ohmic / exponential and sinh expressions.

Fig. 6.6

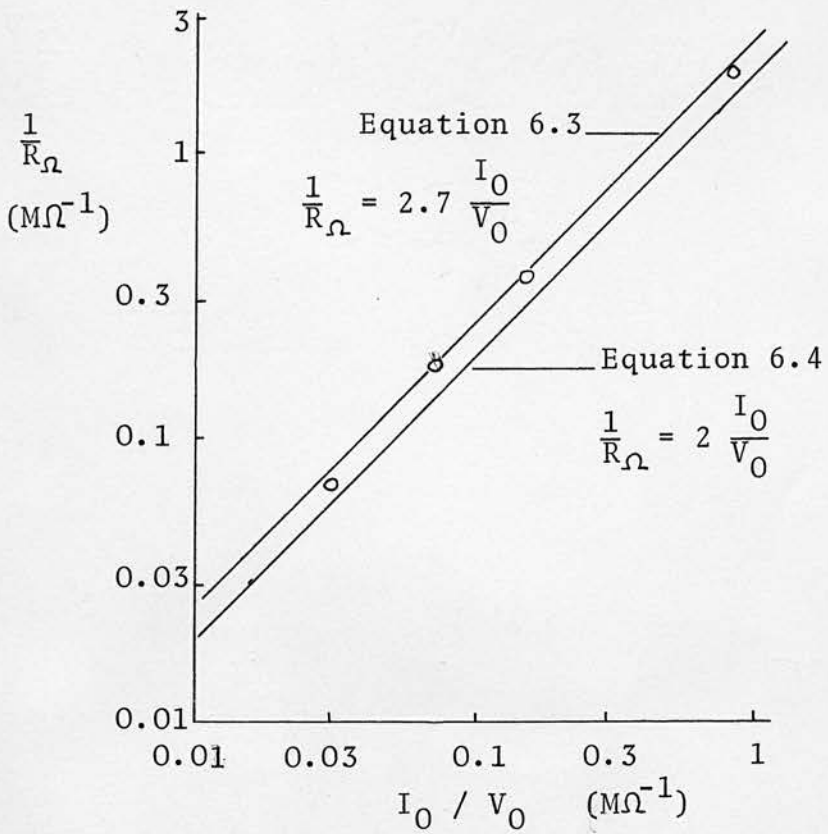

Evaluation of an expression to relate R_Ω^{-1} and I_0 / V_0.

i.e. $$\frac{1}{R_{\Omega}} = \frac{2I_0}{V_0} \quad \text{when } V = 0. \qquad \ldots\ldots 6.4$$

The difference in the low voltage resistance values as expressed by equation 6.3 and 6.4 is also shown in fig. 6.5.

In order to assess whether equation 6.3 or 6.4 is more applicable to the experimental data of V20, the results are plotted in fig. 6.6. as $\log R^{-1}$ against $\log (I_0/V_0)$. This indicates that equation 6.3 is more accurate, so the I - V relation is ohmic then exponential at high voltages ($V > V_0$).

The general consequence of this I - V relation is that reduced characteristics (i.e. I/I_0 against V/V_0) will always have the form shown by the curve in fig. 6.3. The activation energy for R_{Ω} should be given by the difference between the values for V_0 and I_0. This is approximately true for the activation energies derived from fig. 6.4.

Walsh et al. (194) obtained a relation:

$$\frac{V_0}{I_0} = 1.7\, R_{\Omega}$$

and suggested that because the constant was close to unity, a single process was operative in both ohmic and exponential regions. The single process concept may well be true but the constant relation between R_{Ω} and V_0/I_0 (actually 2.7) follows automatically from the shape of the I - V characteristic.

As well as their relationship to R_{Ω}, V_0 and I_0 are related to

the threshold values of voltage and current, V_{th} and I_{th}. For V20 over the temperature range $0^{o}C$ - $100^{o}C$, $V_{th} = 3.1\ V_0$ and $I_{th} = 32 I_0$. These empirical relationships and the similarities in activation energy for V_0 and V_{th}, I_0 and I_{th} are very consistent from sample to sample. They also correspond closely to the relations derived in section 3.3. for the case of thermal breakdown in thick samples.

6.2.3. Switching in bulk samples

When a d.c. voltage, V, is applied to a thick glass sample, the current increases with time as shown in fig. 6.7. This behaviour is representative of that for glasses whose pre-breakdown conduction pattern was described in the previous section. In fig. 6.7. there is a delay time, t_d, before the runaway condition occurs. For thermal breakdown in thick samples, t_d was given by equation 3.50 in section 3.3.8. :

$$V^2 t_d = \frac{C \rho_a d^2}{a} \qquad \ldots\ldots 6.5$$

where C is the specific heat per unit volume

a is a constant which is related to the activation energy for ρ_a, the sample resistivity at ambient temperature, T_a.

The current-time curves for a slice of V20 glass were drawn on an X - Y recorder. The results are shown in fig. 6.8. plotted as V^2 against t_d^{-1}. The linear dependence is as expected from equation 6.5. The slope of the experimental line in fig. 6.8. is $1.5.10^{-3}\ V^{-2}.s^{-1}$.

Fig. 6.7

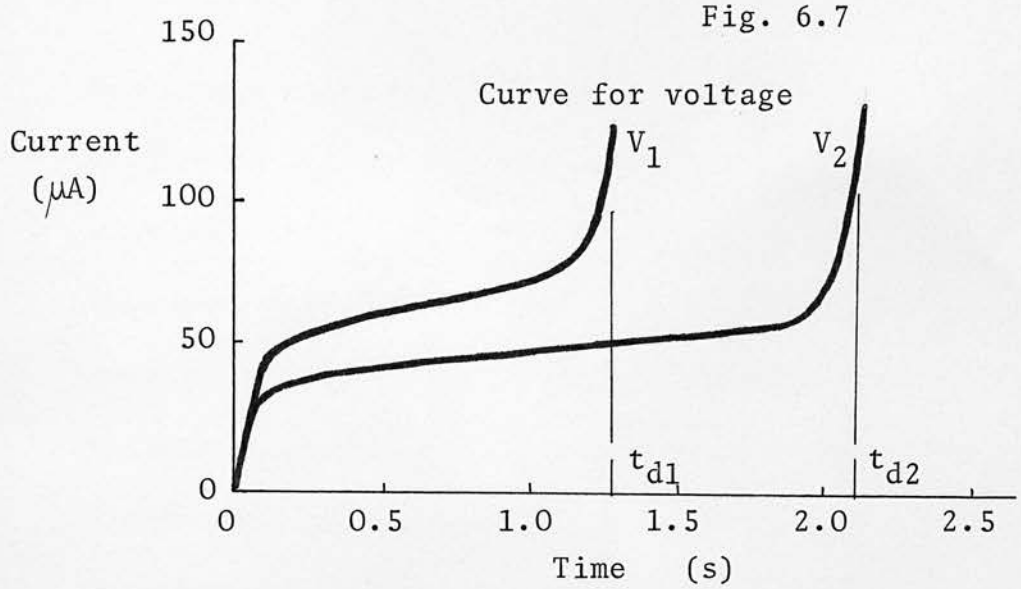

Impulse breakdown for bulk samples. ($V_1 > V_2$)

Fig. 6.8

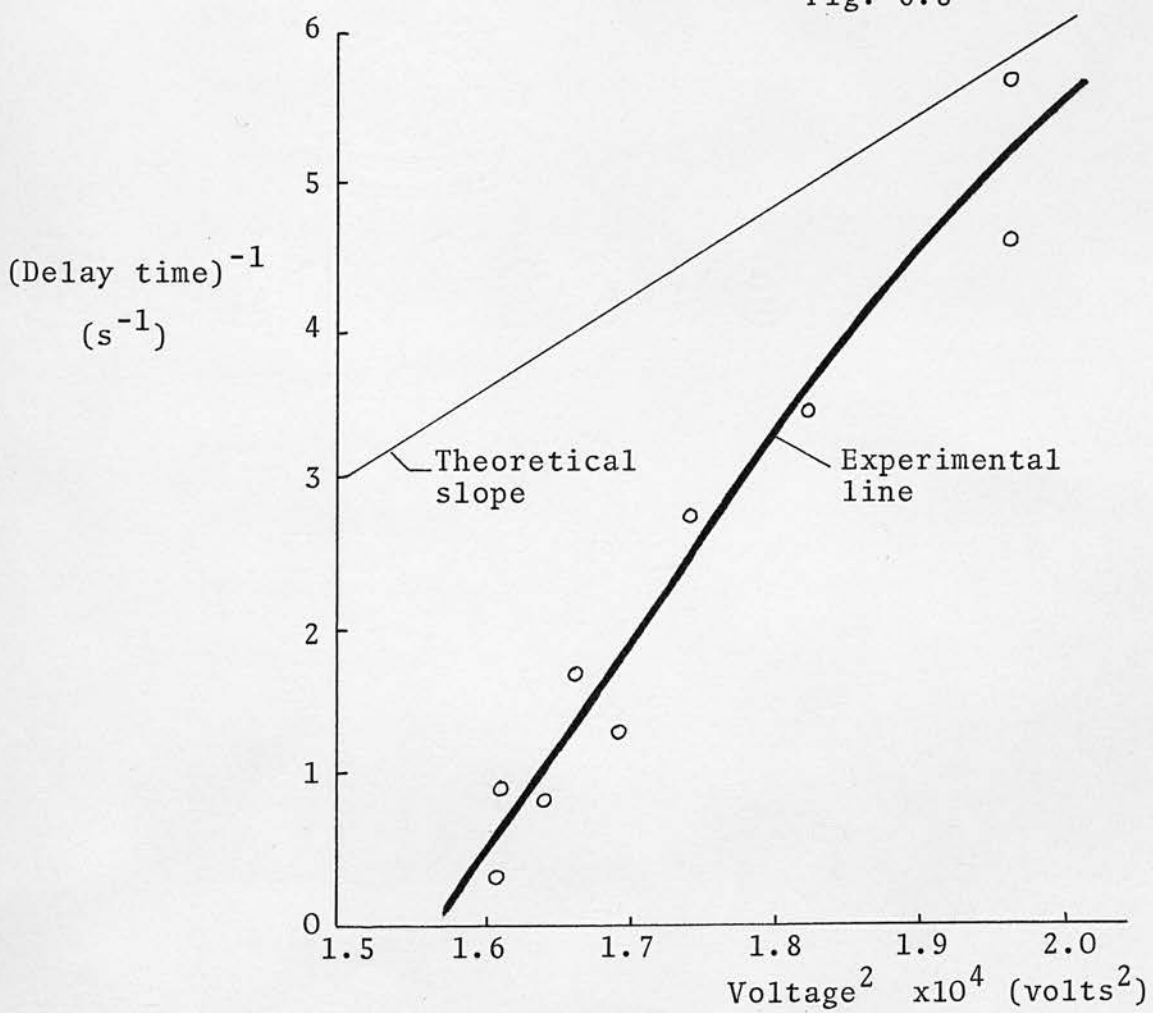

Variation of delay time with voltage for bulk samples.

From equation 6.5 the slope should be $a / C \rho_a d^2$. For this sample, d = 0.1 mm, $\rho_a = 10^4 \Omega$.m and $C = 2.10^6 J.m^{-3}.K^{-1}$., i.e. the slope should be $2.10^{-4} V^{-2}.s^{-1}$. This is also shown in fig. 6.8. The theoretical and experimental lines only coincide at high voltages. However, the derivation of equation 3.50 in section 3.3.8. was made on the basis that there was no heat loss via the electrodes, etc. Thus equation 6.5 is only valid for voltages which are much greater than V_{th} and where the delay time is short compared with the thermal time constant. For voltages only slightly greater than V_{th}, considerable heat loss may occur and the measured delay time would be expected to be greater than the theoretical value derived from equation 6.5. This is the situation shown in fig. 6.8.

With square voltage pulses 7 ms long and 6 ms apart, switching occurs for each pulse if the pulse amplitude is great enough. As in the d.c. case, $V^2 \propto t_d^{-1}$. However, the value of t_d for each pulse is very much smaller than for the d.c. case and V_{th} (the voltage which makes $t_d = \infty$) is approximately 70 volts. The measurements of pre-switching behaviour in section 6.2.2. indicate that for V_{th} = 70 volts, the effective sample temperature is 330 K. Under pulsed conditions the mean sample temperature therefore appears to be above T_a.

This result is similar to that shown in the photographs in fig. 6.1. The dynamic threshold voltage, i.e. V_{th} under continuous switching conditions (100 Hz), is much lower than the initial value for the first switching cycle (as in fig. 6.2.). When the load resistor is decreased

or the maximum on-state a.c. current level is increased, V_{th} and V_h decrease, I_{th} increases and the whole switching process is slower and less well-defined. All of these effects can be explained by a rise in the internal temperature of the sample.

The thermal time constant for cooling, τ, was given by equation 3.53 in section 3.3.9. :

$$\tau = \frac{CAd}{\Gamma} \qquad \ldots\ldots 6.6$$

For typical bulk samples, $C = 2.10^6$ J.m^{-3}K^{-1}, $A = 10^{-7}$ m^2, $d = 0.3$ mm and $\Gamma = 0.45$ mW.K^{-1} (equation 6.1). This gives $\tau = 0.13$s. It was shown in section 3.3.9. that under a.c. conditions when the period of the signal is much shorter than τ, an isothermal characteristic is measured where the mean temperature is greater than the ambient value, T_a. This is the condition which applies for 100 Hz sine wave and pulsed operation.

In order to estimate the magnitude of the temperature rise within the sample, the rate of power dissipation throughout each cycle must be known. Fig. 6.9. shows the experimental variation of current and voltage with time. The line marked 'power' was derived by multiplication of current and voltage values. Most power dissipation occurs during the on-state so I_{max} is the dominant factor controlling the power level since V_h is approximately constant throughout the on-state. The mean internal temperature can be derived from the position of V_{th} on the V_{th}-temperature line in fig. 6.4. Fig. 6.10. shows how the internal temperature increases

Fig. 6.9

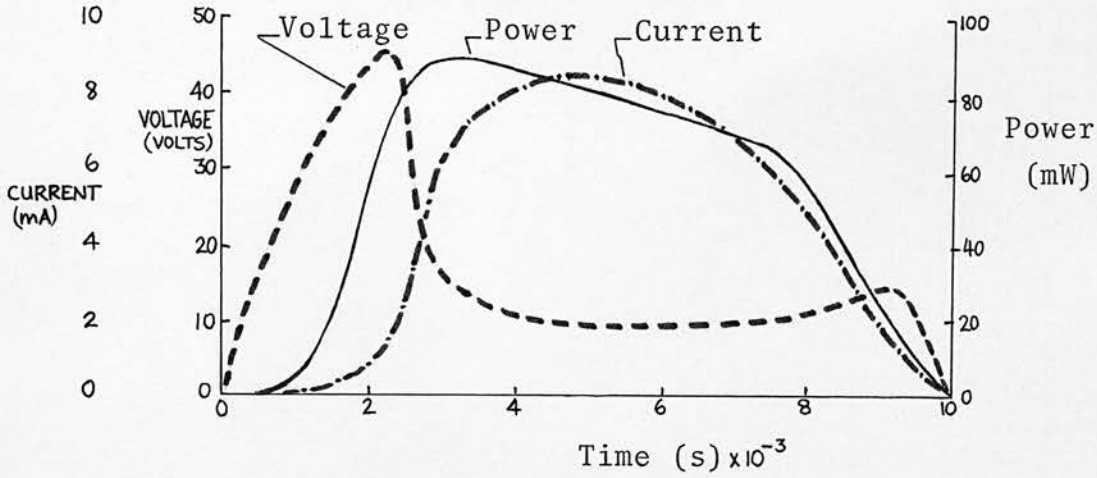

Variation of voltage, current and power throughout a switching cycle.

Fig. 6.10

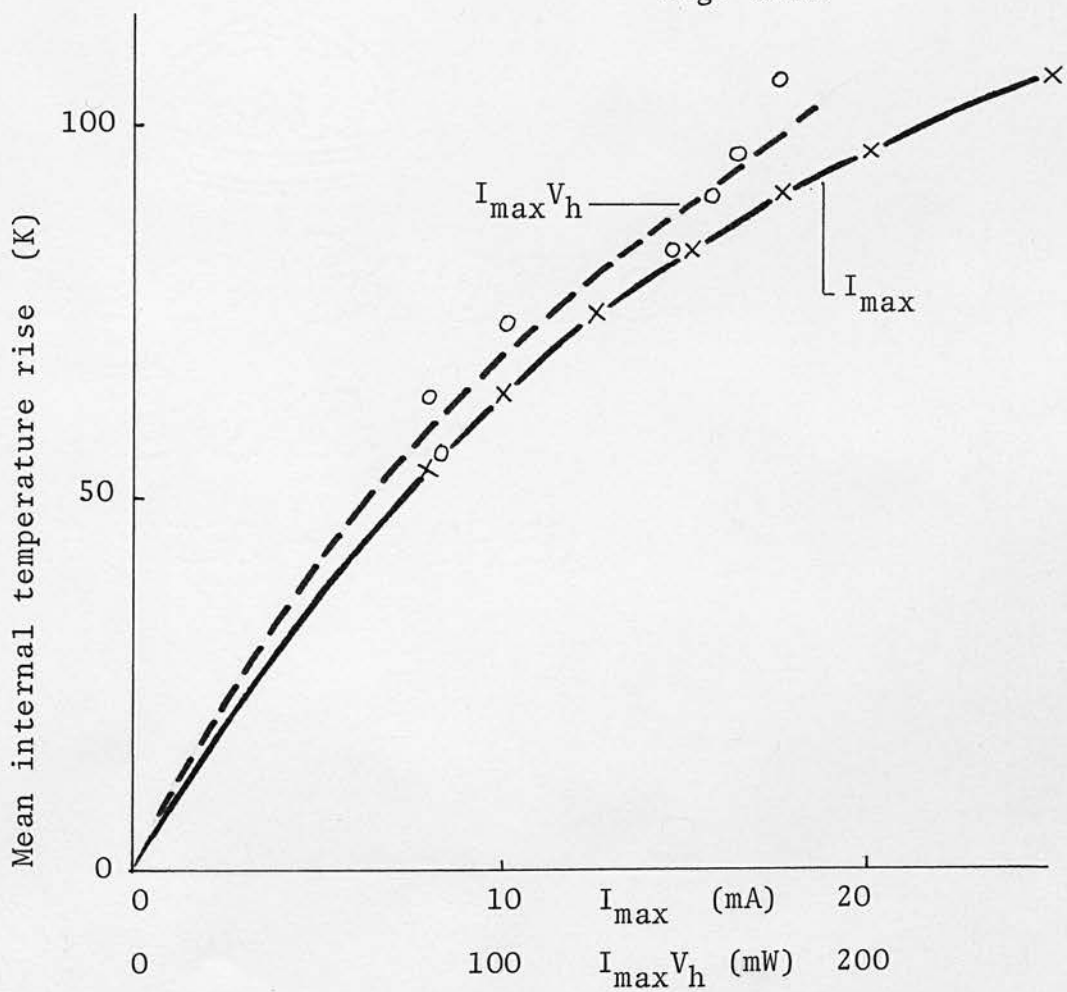

Effect of I_{max} and $I_{max}V_h$ on the mean internal temperature rise during a.c. switching.

with I_{max} and $(I_{max}.V_h)$.

Switching in bulk samples of chalcogenide glass shows good agreement with thermal breakdown theory provided the effects of heat loss and 'high' frequency signals are considered.

6.3. COPLANAR SAMPLES

6.3.1. General treatment

Thin film samples with coplanar electrodes were fabricated mainly to provide low-field resistivity data. The area and electrode separation are radically different to the corresponding values for a sandwich electrode arrangement. Coplanar and sandwich resistivity values when measured for the same film can give useful information about the uniformity of resistivity throughout the thin film; this has been treated in chapter 5. Many coplanar samples were also tested at high fields and their breakdown behaviour has much in common with that for bulk samples.

In a typical coplanar sample, the electrodes were of gold, about 0.3 μm thick, deposited on a substrate of 7059 glass. The electrode width, W, was 1 mm and the electrode separation, d, about 0.1 mm. The film of chalcogenide glass was deposited on top of the electrodes and was in the range 0.2 - 3 μm thick. These are typical figures and the exact dimensions were measured for each sample.

In order to calculate the current and voltage levels which are necessary for thermal breakdown, some estimate must first be made of the sample thermal conductance.

Heat is generated in the thin film of chalcogenide glass and its dissipation is determined by the rate of conduction through the chalcogenide glass, through the 7059 glass substrate and along the electrodes. Conduction and convection into the air above the

chalcogenide film is relatively small and may be neglected.

When the surface temperature of a thick slab is changed suddenly, the temperature within the slab varies with time and distance from the surface. For an initial temperature T_a and surface temperature T_s, the temperature T_x at a point x below the surface and time t is given by:

$$\frac{T_s - T}{T_s - T_a} = f\left[\frac{x}{2(\alpha t)^{\frac{1}{2}}}\right] \qquad \ldots\ldots 6.7$$

where $\alpha = K/C$ and the function $f[\ ]$ is the error function (33).

A similar situation applies to coplanar samples where all heat is generated in a thin surface film. With an a.c. supply at 100 Hz, it can be specified that the heat generated in the chalcogenide film must be dissipated within 1 ms or less (i.e. 10% of the supply period). This is a basic requirement for steady state operation.

If the temperature at point x is mid-way between T_a and T_s, the left side of equation 6.7 reduces to 0.5. For this value, the error integral is approximately equal to the integrand, so:

$$f\left[\frac{x}{2(\alpha t)^{\frac{1}{2}}}\right] \doteqdot \frac{x}{2(\alpha t)^{\frac{1}{2}}}$$

The thermal properties of 7059 glass are very similar to those for chalcogenide glasses : $C = 2.10^6$ J.m^{-3}.K^{-1} and $K = 1.0$ W.m^{-1}.K^{-1}. When these values are substituted in equation 6.7, x = 25 μm, i.e. 1 ms after the surface temperature was

changed, the temperature at a point 25 μm below the surface has increased by half the surface temperature increment. For the calculation of thermal conductance, the substrate may be taken to have an effective thickness of 2x : i.e. $\sim$ 50 μm. The surface area of chalcogenide glass in contact with the substrate is A = Wd. so the thermal conductance is given by:

$$\Gamma_{7059} = \frac{K W d}{2x} \doteq 2 \text{ mW.K}^{-1}. \qquad \ldots\ldots 6.8$$

The large effective substrate thickness means that the temperature within the chalcogenide glass film can be considered to be uniform, so the limit to heat conduction associated with the glass film is not serious.

Heat conduction along the gold electrodes may be calculated in a similar fashion. For gold, K = 300 W.m^{-1}.K^{-1}. and $C = 2.10^6$ J.m^{-3}.K^{-1}. The 'half-thickness' for this case is x = 0.4 mm and the effective thermal conductance of a gold electrode is 0.2 mW.K^{-1}. With two electrodes, the overall thermal conductance of the electrodes is therefore 0.4 mW.K^{-1}. and with the conductance of the substrate, Γ_{total} = 2.4 mW.K^{-1}.

The thermal breakdown conditions can be calculated in the same way as for bulk samples; by assuming that thermal runaway occurs when the sample temperature is 25 K above ambient. The product of peak current and voltage at threshold is:

$$V_{th} I_{th} = 2.5 \, \Gamma \, \Delta T = 150 \text{ mW}.$$

where the factor 2.5 takes account of the fact that heating depends on r.m.s. power rather than peak power. If the low-field resistance at T_a is 7 MΩ , at a temperature (T_a + 25), it is approximately 2 MΩ for ΔE = 0.45 eV or a = 0.04 K^{-1}. When the resistance equation at threshold is solved with that for $V_{th} I_{th}$, then V_{th} = 540 volts and I_{th} = 270 μA. The experimental values (shown later in fig. 6.12) are V_{th} = 350 volts and I_{th} = 150 μA. For the approximations used to derive Γ this correlation is good enough to show that thermal breakdown is a viable mechanism.

At voltages close to V_{th}, hysteresis appears in the current-voltage characteristic. This indicates that the time taken for the sample temperature to rise to its steady state value is a significant proportion of the supply cycle time.

Switching is accompanied by catastrophic breakdown. The thin film cannot sustain a high current, high temperature on-state so destruction occurs. The film between the electrodes is often completely evaporated and physical damage extends up to 1 mm from the gap. For stable coplanar threshold switching, the chalcogenide films would have to be much thicker than those used in this work, probably in the range 20 - 50 μm.

6.3.2. Pre-switching behaviour

Conduction in thin film samples with coplanar electrodes is influenced by a number of controllable factors. The effect of ambient

temperature may be examined in the same way as for bulk samples. Chalcogenide glasses composed of As, Te, Ge and/or Si all have certain similarities in their physical and thermal properties. However some properties, especially resistivity, are very dependent on composition. With thin film samples, geometry is also easily controlled. Since a coplanar sample was produced in almost every glass evaporation run, a large number of samples have been examined to determine the effects of temperature, resistivity and geometry on conduction and breakdown conditions. All measurements were made with an a.c. supply (100 Hz).

Current-voltage characteristics as a function of temperature are shown in fig. 6.11. They are very similar to the bulk characteristics of fig. 6.2. and the theoretical thermal characteristics of fig. 3.6. The sample number was E84A.2 and it was produced by evaporation of an ingot (composition $As_{55}Te_{35}Ge_{10}$) from a resistance-heated boat. As with bulk samples, each characteristic may be described by an ohmic region, resistance R_Ω , and then an exponential region where

$$I = I_0 \exp V/V_0 \qquad \ldots\ldots 6.9$$

and the terms I_0 and V_0 are temperature-dependent. For any value of T_a, V_0, I_0 and R_Ω conform to the relation $V_0/I_0 = 2.7\, R_\Omega$. This was discussed in section 6.2.2. and indicates that the function is ohmic then exponential rather than a sinh function.

The temperature dependence of R_Ω , V_0, V_{th}, I_0 and I_{th} are

Fig. 6.11

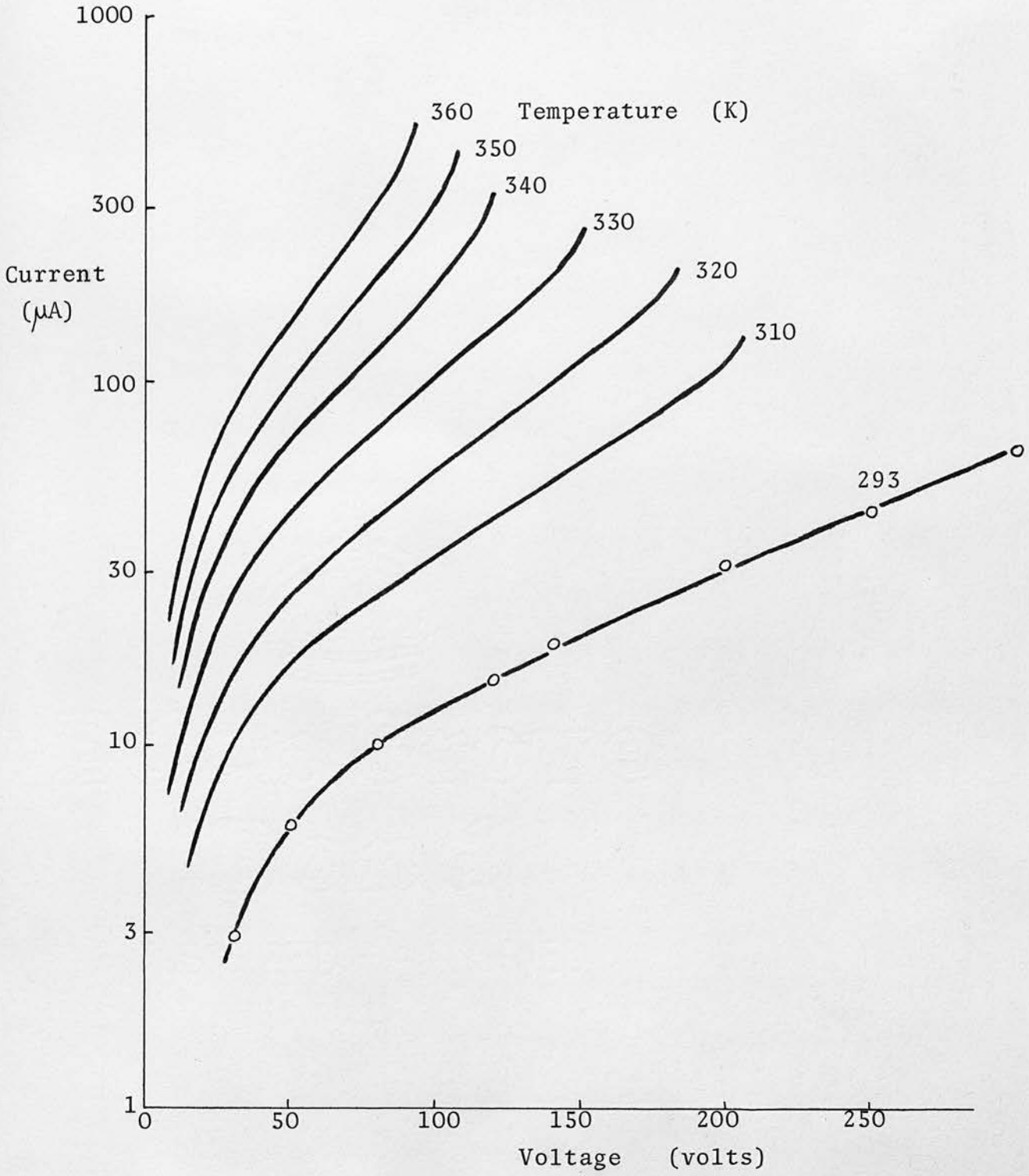

Coplanar current - voltage characteristics as a function of temperature.

shown in fig. 6.12. Each of the terms has an activation energy and the values are:

R_{Ω}	0.41 eV	(0.38)
V_{th}	0.16 eV	(0.18)
V_0	0.16 eV	(0.19)
I_{th}	- 0.28 eV	(-0.25)
I_0	- 0.28 eV	(-0.24)

For comparison, the corresponding activation energies given in section 6.2.2. for bulk samples, are shown in brackets. The numerical similarity and the relationships between the terms confirm that the coplanar breakdown process is fundamentally similar to that for bulk samples.

Coplanar films of different composition to E84A.2 have different resistivities. However, the current-voltage relations are of the same form as those in fig. 6.11; an ohmic then an exponential region. The constants V_0 and I_0 differ from film to film but a normalized characteristic as given by equation 6.9 is shown in fig. 6.13. For comparison, data for E84A.2 is also plotted in fig. 6.13.

The chalcogenide films all have similar activation energies for resistance and in the coplanar layout they all have similar values of thermal conductance since Γ is determined mainly by the glass substrate and electrode arrangement. Thus, from the viewpoint of thermal breakdown they may all be considered as a single composition where resistivity changes occur due to a change in ambient temperature.

Fig. 6.12

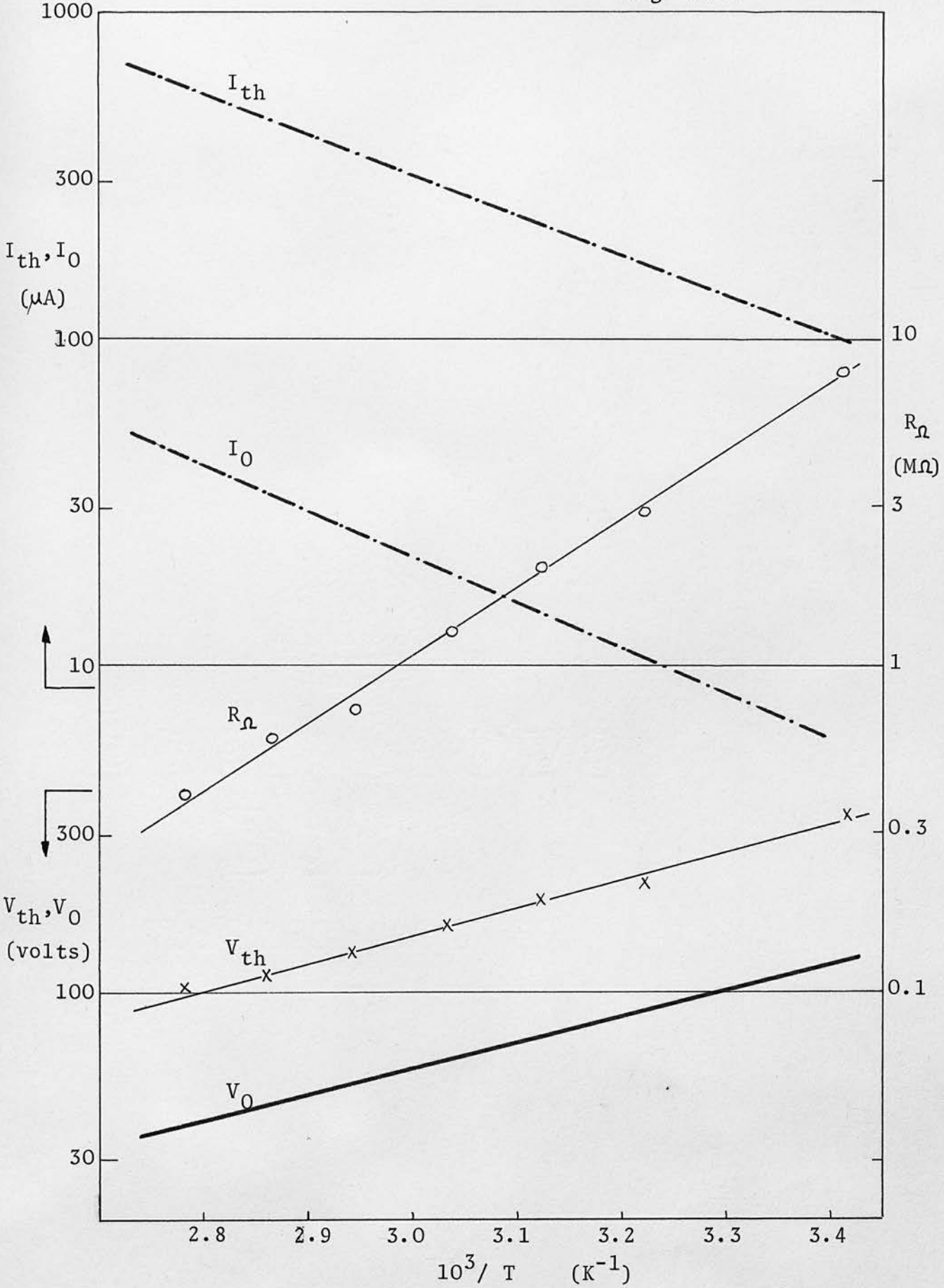

Variation of coplanar V_0, V_{th}, I_0, I_{th}, R_Ω with temperature.

Fig. 6.13

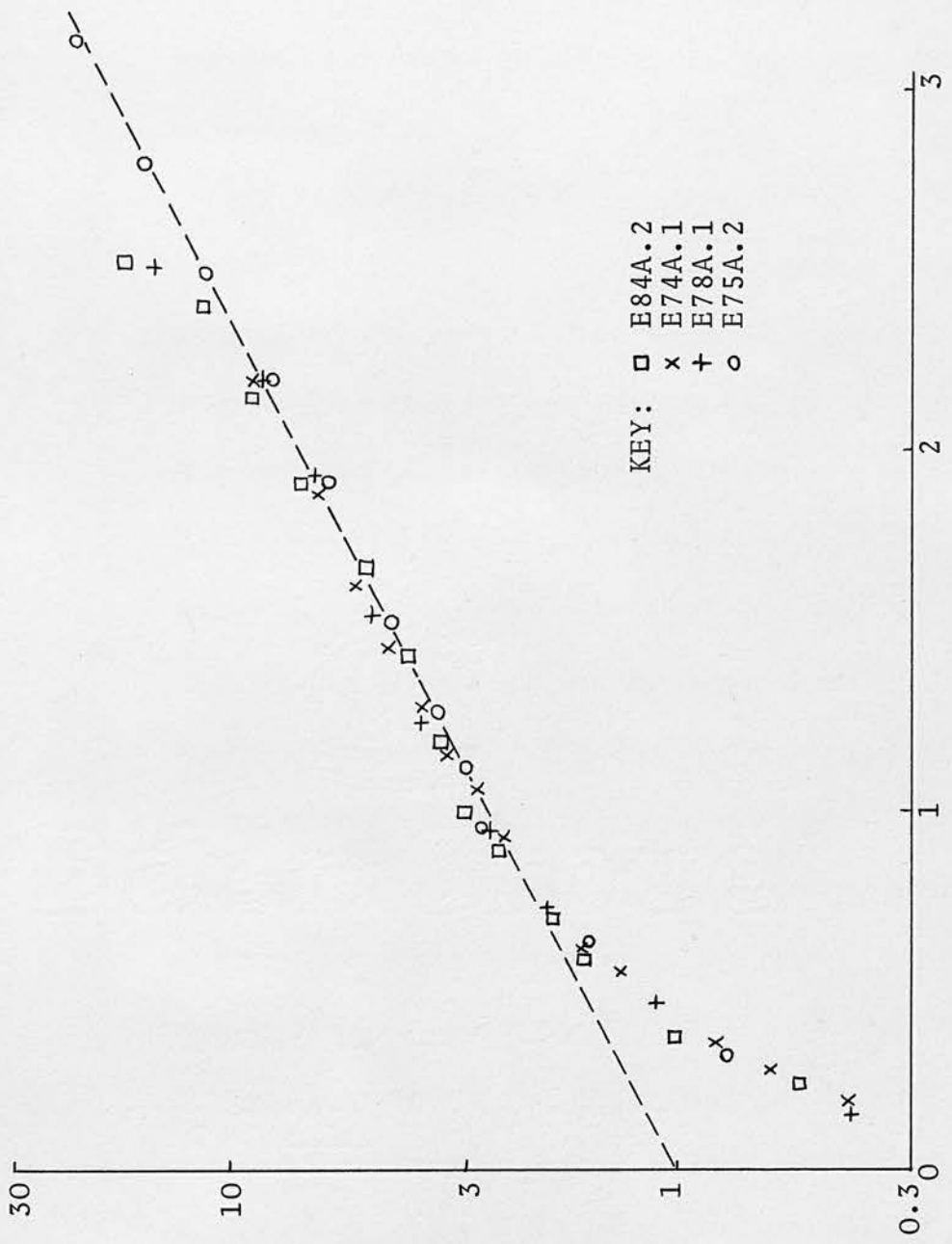

Reduced characteristics for coplanar films.

In table 6.1, the resistivities of four other films are made equal to that of E84A.2 by a change in effective ambient temperature. It has been assumed that the resistance activation energy for all the samples is 0.45 eV.

The compositions of V38 and V41 are $As_{55}Te_{35}Ge_{10}$ and $As_{36}Te_{54}Si_{10}$ respectively. Log V_{th} is plotted against $10^3/T_{effective}$ in fig. 6.14. Errors due to small differences in sample geometry mean that the spread in data points is greater than for a single sample. However, the line corresponding to an activation energy of 0.18 eV fits the data and is approximately the same as the V_{th} activation energy for a single sample (derived from fig. 6.12).

The gap between coplanar electrodes is defined by a wire which acts as a shadow-mask during the metal evaporation. To measure breakdown as a function of gap width, wires of different diameter were used. In fig. 6.15. the breakdown field has been plotted against gap width for four units produced in experiment E83. The bulk material was $As_{20}Te_{70}Ge_{10}$ and it was flash evaporated. The pre-breakdown I - V relations were of the usual ohmic then exponential shape and the normalized curve for each gap width fitted the curve in fig. 6.13.

From fig. 6.15., $E_{th} \propto d^{-\frac{1}{2}}$. This is the relation expected from thermal breakdown theory for samples where the thermal conductance is not geometry-dependent (cf. section 3.3.5.). Kolomiets (177) has measured the variation of E_{th} with d in sandwich samples. He found $E_{th} \propto d^{-\frac{1}{2}}$ but his thinnest bulk sample was 60 μm. He also produced

	E84A.2	E74A.1	E75A.2	E78A.1	E76A.1
Bulk glass	V38	V38	V41	V38	As_2Te_3
Evaporation source	Boat	Flash (hot)	Flash	Flash (cool)	Flash
Coplanar ρ (Ω.m)	100	2000	50	630	50
ρ / ρ_{E84}	1.0	20	0.5	6.3	0.5
Effective T_a (K)	293	251	305	265	305
$\frac{10^3}{T_{effective}}$	3.41	4.0	3.28	3.77	3.28
V_{th} (volts)	350	1300	500	950	400

Table 6.1

Representation of coplanar resistivities in terms of changes in ambient temperature: correlation with threshold voltage.

Fig. 6.14

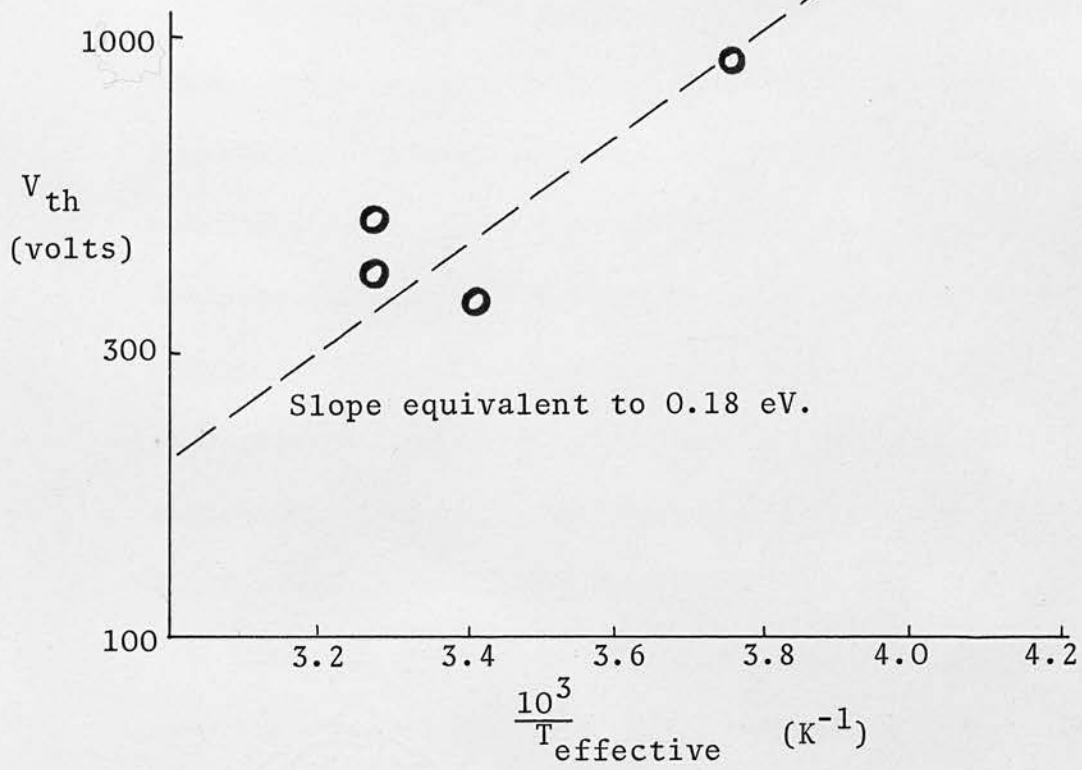

Interpretation of resistivity changes in terms of an effective temperature and its influence on V_{th}.

Fig. 6.15

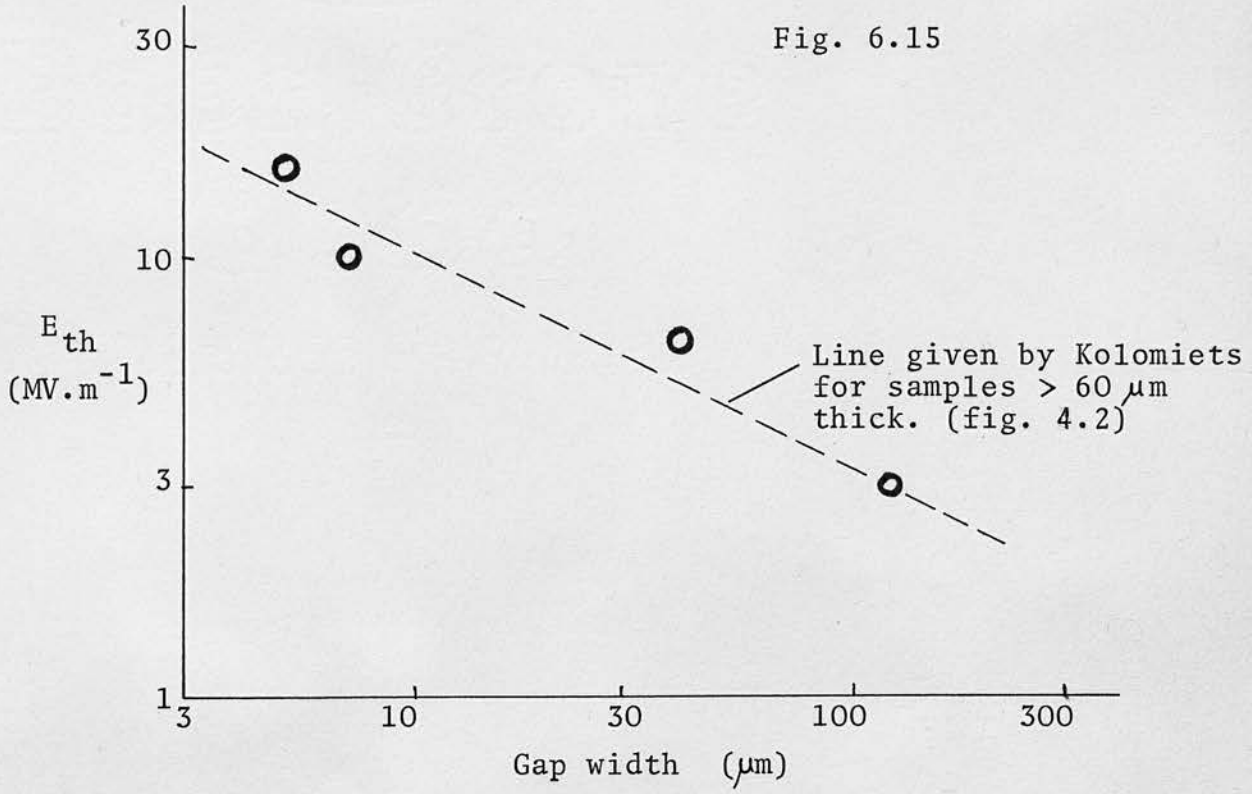

Variation of breakdown field with gap width for coplanar samples.

data for films $< 5\ \mu m$ thick and his results have been reproduced in fig. 4.2. It is significant that the coplanar data of this section fits into the thickness range not covered by Kolomiets. The dashed line in fig. 6.15. is in fact an extension of that obtained by Kolomiets for thicker samples. Thus in coplanar samples thermal breakdown is responsible for switching down to gap widths of $5\ \mu m$ at least. It is not possible to produce reliable gaps less than $5\ \mu m$ wide but the sandwich electrode arrangement provides electrode separations of $3\ \mu m$ or less; that is discussed in the next section.

No results are available for the performance of coplanar switches in the on-state since the power dissipation proved excessive in all cases and the samples were destroyed. However, the pre-breakdown characteristics as a function of temperature, resistivity and geometry all conform to the expected behaviour for thermal breakdown.

6.4. SANDWICH SAMPLES

6.4.1. Introduction: the significance of self-heating

Thin films of chalcogenide glass sandwiched between metal film electrodes were produced from a wide range of bulk glasses. The relationship between film composition and resistivity and the influence of electrodes were treated in chapter 5. Nearly all films, however, were also tested under high field conditions to see whether threshold switching occurred and if it did, to establish which experimental factors influenced it.

The standard sample layout comprised a substrate of 7059 glass with twelve gold electrodes deposited on it (fig. 5.6.). These electrodes were 0.3 mm wide and 0.3 μm thick. The evaporated chalcogenide film covered the centre portion of the electrodes leaving the ends exposed. The top contact, also of gold 0.3 μm thick, was 0.7 mm wide. The chalcogenide glass film was in the thickness range 0.2 - 2 μm and in some samples, variations in electrode thickness and/or width were introduced. Off-state resistance values were in the range 100 Ω to 10 MΩ.

Steady state current-voltage characteristics were measured by a number of techniques and the results are compared in fig. 6.16(a) All gave the same resistance value at low voltages (500 Ω). The d.c. threshold voltage was less than that measured with a 100 Hz a.c. supply (PM 6507 curve-tracer). For the pulse measurements, square voltage pulses were used with a low repetition rate (100 Hz). The

Fig. 6.16(a)

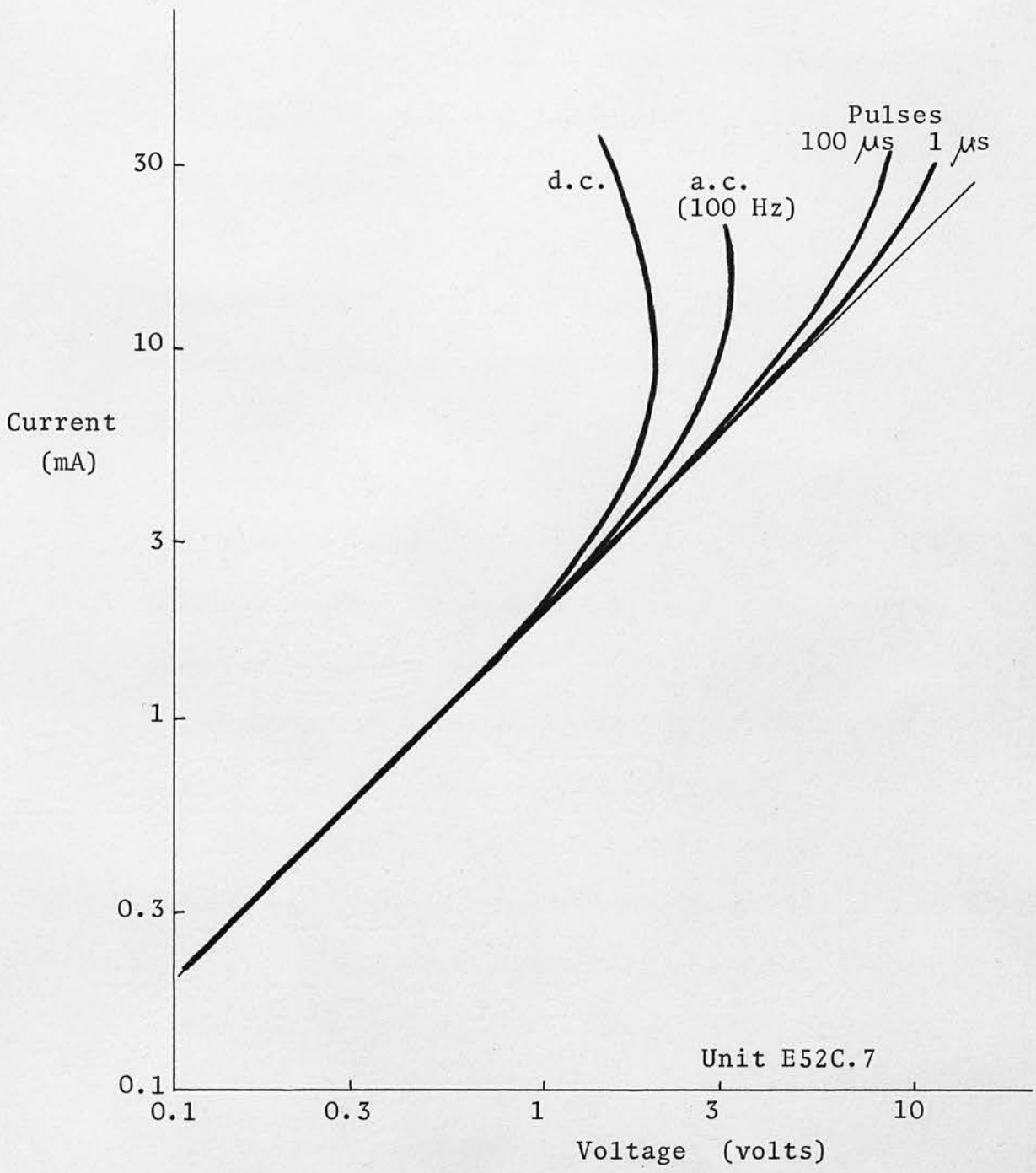

Sandwich current - voltage characteristics: influence of measurement technique.

current recorded was the value at the end of the pulse. In the d.c. case and to a lesser extent in the 100 Hz measurements, a region of negative resistance occurred before the device switched. Curves such as those in fig. 6.16(a) would be expected if self-heating occurred within the sample.

In order to establish the conduction mechanism at high fields, it is necessary to measure the current-voltage characteristic without the complication of self-heating. This may be done by applying a short voltage pulse and measuring the current at t = 0. For most of the samples used in this work the capacitive current spike which occurs when a pulse is applied was very short; where the initial current level was masked by the spike, the current pulse shape was extrapolated back to t = 0 to give the initial current value. Fig. 6.16(b) shows the current at the beginning and end of a 70 μs pulse and its variation with the voltage pulse height.

The current rise during a pulse cannot be uniquely attributed to Joule heating. It was not possible to measure any consequence of heating (other than current rise) which would give an alternative measurement of the temperature increase. There are, however, three calculations which show that Joule heating should be significant.

1. The power dissipated during one pulse is enough to give a temperature rise of several K.
2. The increase in current during a pulse is large enough to be due to a temperature rise of several K.

Fig. 6.16(b)

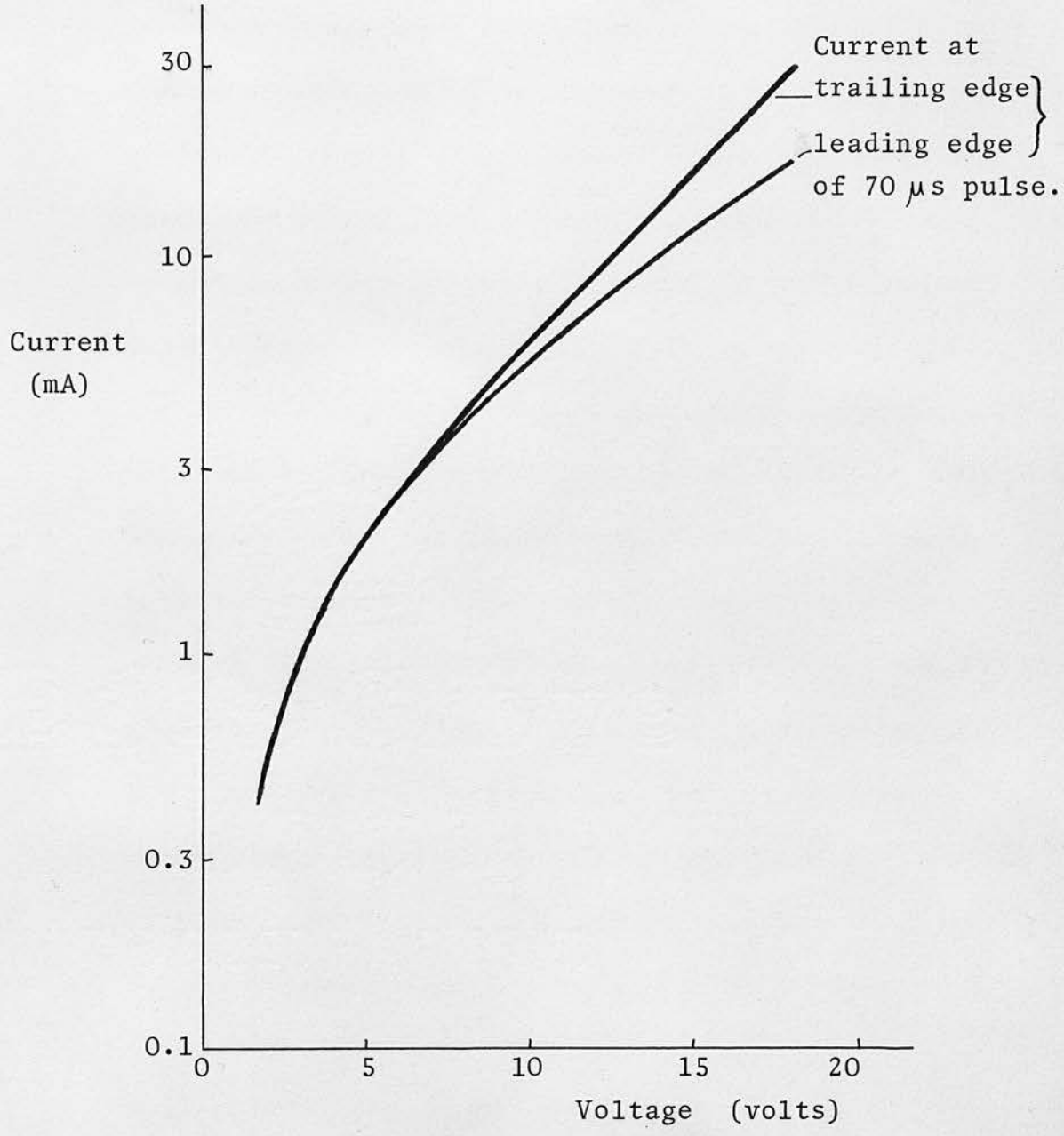

Current - voltage characteristics taken at the beginning and end of a 70 μs pulse.

3. The time taken for the current to reach a steady value is of the same order as the expected thermal time constant for a thin film sandwich sample.

Each of these cases is considered quantitatively in later sections but they do indicate a temperature rise of 2 - 20 K in the pre-breakdown region. Thus, although it is not possible to prove conclusively that the increase in current is entirely due to Joule heating, the effect is present and is probably the most significant factor in determining the current rise during a single pulse.

On the basis of fig. 6.16(b) there are therefore two characteristics to be studied: the first excludes and the second includes the self-heating effect. The relative importance of each effect is determined by the sample resistivity; hence the importance of a wide range of ρ values. This work forms the basis of the next five sections and establishes the conditions which prevail in the pre-switching region.

As with bulk and coplanar samples, the current-voltage characteristics with and without the Joule-heating component show an ohmic region up to a voltage V_0 and then a non-linear region for $V > V_0$. However, switching occurs when $V \doteqdot 3V_0$ so there is only a relatively small voltage range over which the non-linear characteristics can be measured. This introduces the complication that the results can be fitted to several conduction mechanisms. This has been done in the following three sections for the I - V curve without the Joule heating term. There is a reasonable fit for

each of three models so an assessment has been made in terms of how realistic it is to expect each model to be valid.

Experimentally, flat-topped voltage pulses were applied. The pulse length was 1 - 10 μs with a repetition rate of 100 - 300 Hz. The associated current pulse was measured as the voltage across a resistor in series with the sample. This voltage was subtracted from that supplied by the pulse generator to give the voltage across the sample. In most cases this was only a small correction. All thin film sandwich samples gave results which had the same general form so the analysis has been concentrated on those for which I - V characteristics have been measured as a function of temperature and electrode separation - the two most accessible experimental variables.

6.4.2. Space-charge-limited current flow

If switching is assumed to be controlled by some electronic process such as double injection (section 3.5.3.) or Henisch's field inversion concept (section 3.5.4.), then the current flow in the pre-switching region is likely to be space-charge limited. The expressions which describe space-charge-limited currents (SCLC) are dependent on the distribution of traps between the Fermi level and the conduction band (for electron flow) and these equations have been outlined in section 3.5.3.

Experimental current-voltage characteristics do not fit the

power law relationship which would be expected for either a single trap level or for traps with an exponential density distribution throughout the forbidden gap. However, the uniform trap distribution gives an equation:

$$J = \frac{9}{8} \sigma_a E \exp(t_1 E) \qquad \ldots\ldots 6.10$$

where $$t_1 = \frac{C}{A e N_t kT}$$

and σ_a is the ohmic conductivity

C is the sample capacitance for area A and thickness d

N_t is the trap density expressed in $m^{-3} eV^{-1}$.

Equation 6.10 indicates that the relation between log R and V should be linear with slope t_1/d. Results for three films of different thickness are shown in fig. 6.17. If the dimensions for unit E57A.10 are substituted in equation 6.10 and it is assumed that the dielectric constant is $K_i = 11$, the slope of the log R - V line gives $N_t = 5.10^{23}\ m^{-2} eV^{-1}$. This calculation has also been done for a number of other films and in all cases N_t was in the range $2.10^{23} - 2.10^{24}\ m^{-3} eV^{-1}$. Composition and resistivity do not appear to have any consistent effect on the value of N_t; they do of course determine the resistance value at V = 0.

From equation 6.10 the slope of the log R - V graph should be proportional to T^{-1} and d^{-2} (since capacitance $C \propto d^{-1}$). The experimental values have been plotted to show these relationships in

Fig. 6.17

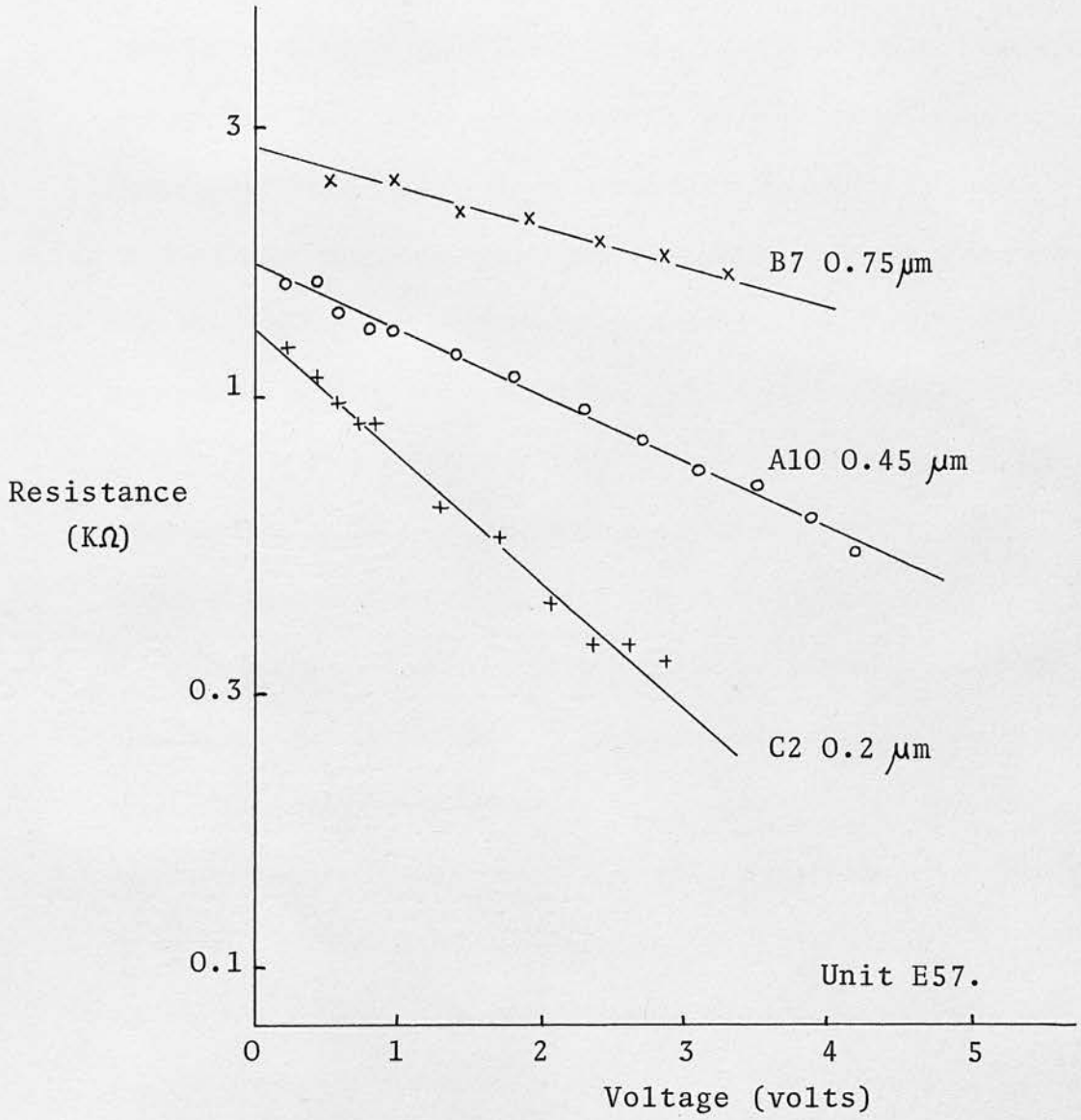

Current - voltage data without Joule heating represented as Log R against V for films of different thickness.

fig. 6.18. and 6.19. Units E56C and E57A have the same thickness and fit the same line in fig. 6.18. Similarly in fig. 6.19. all measurements refer to room temperature so the only variable is thickness. Although the data shows the expected functional dependence on temperature and thickness, none of the lines in fig. 6.18. or 6.19. pass through the origin. This is confirmed by the results of Fagen (18). His I - V curves are shown in fig. 4.1. and they cover a much wider temperature range than those in fig. 6.18. Fagen's results have been replotted as log R against V and the slope of each line has been plotted against 1/T in fig. 6.20. For comparison the two lines from fig. 6.18 have also been included. Fagen's data refer to a film composition $As_{45}Te_{35}Ge_{20}$ and different geometry, so the numerical values of slope cannot be correlated with those for E56 or E57.

Space-charge-limited current flow with a uniform trap density distribution throughout the band gap seems at first sight to be a reasonable conduction mechanism for chalcogenide films. The numerical value for the trap density and the functional dependence of current on voltage, geometry and temperature appear to confirm the application. However, the non-zero intercepts in figs. 6.18, 6.19. and 6.20. cast serious doubts on the applicability of SCLC and probably mean that the features which support the mechanism are no more than a coincidence.

Fig. 6.18

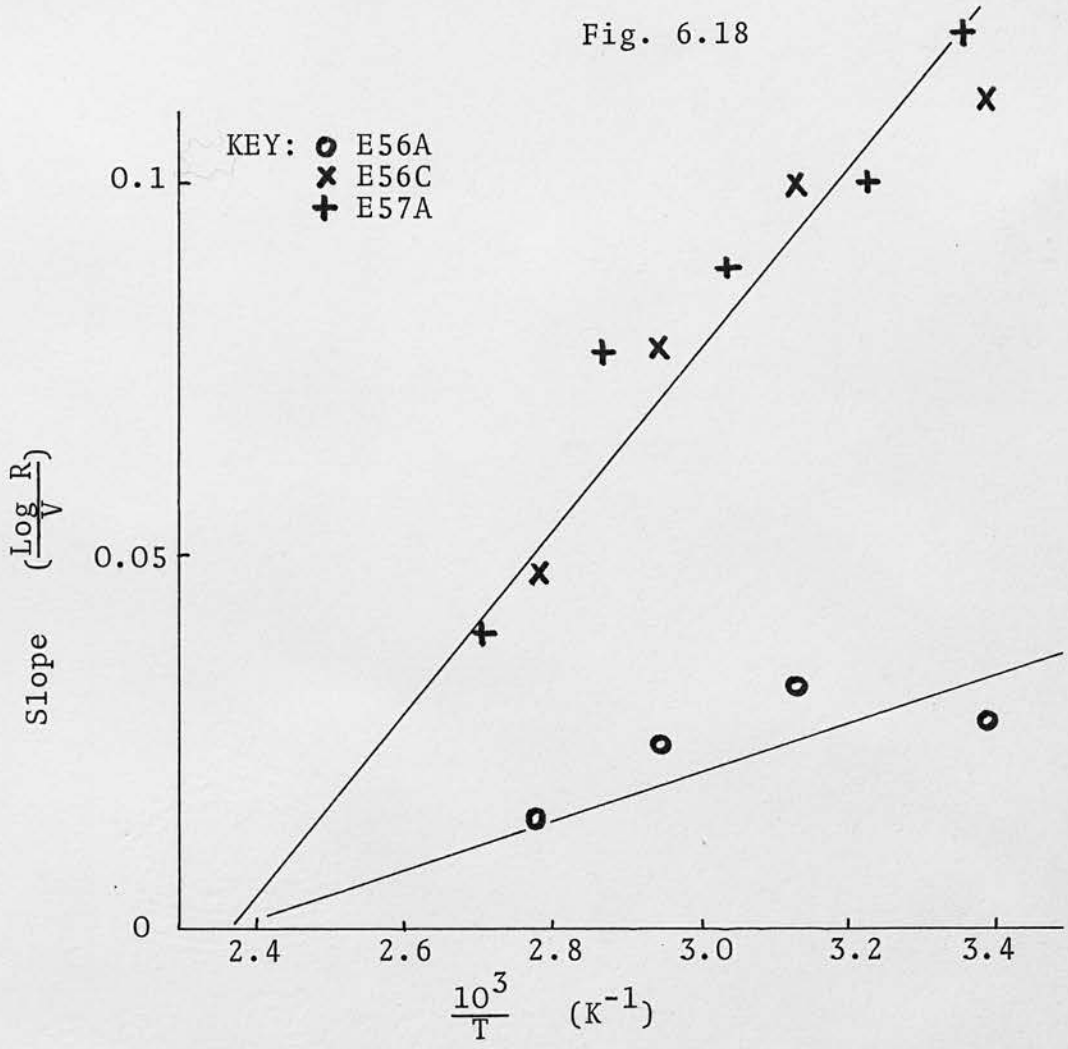

Influence of temperature on the slope of the lines on a Log R - V graph, e.g. fig. 6.17.

Fig. 6.19

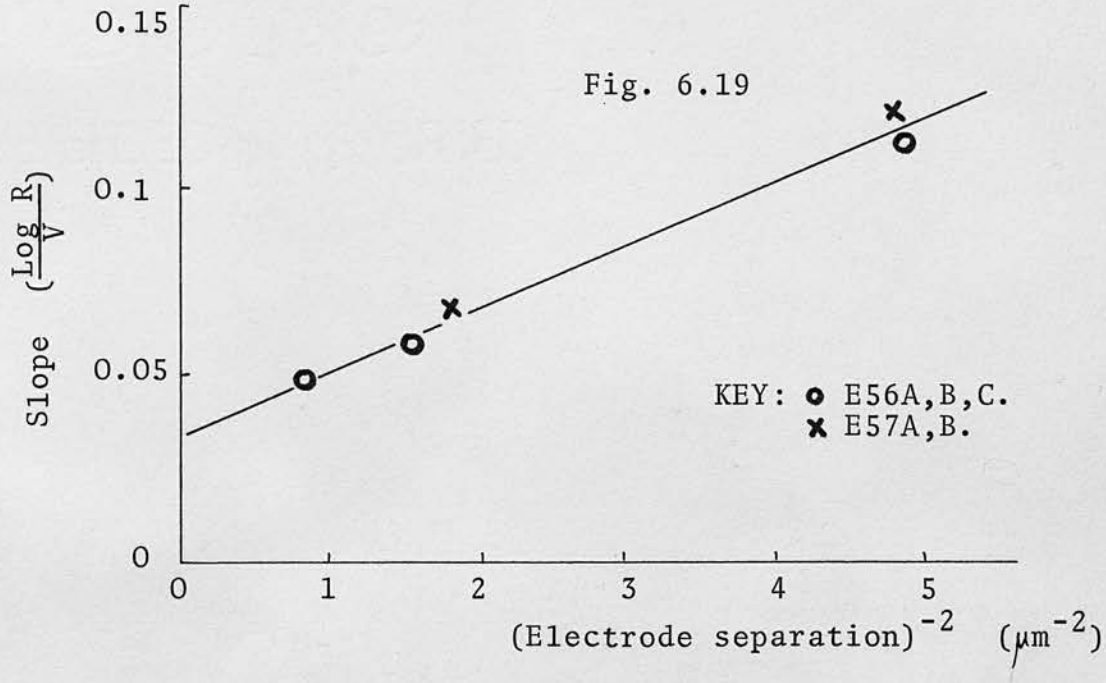

Influence of electrode separation on the slope of the lines on a Log R - V graph, e.g. fig.6.17.

Fig. 6.20

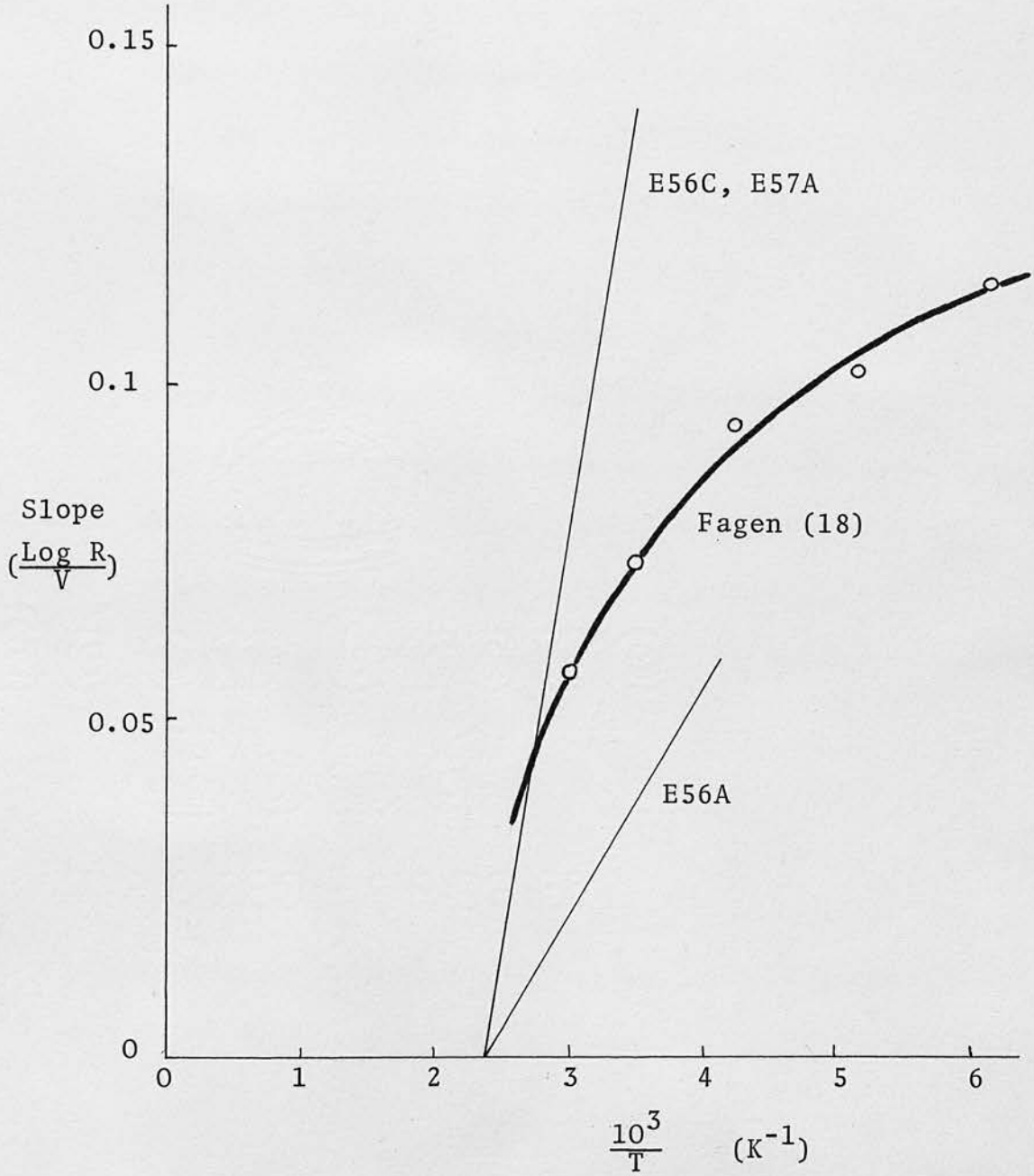

Influence of temperature on the slope of lines on a Log R - V graph: comparison of Fagen's data with that from Fig. 6.18.

6.4.3. Hopping conduction

In an amorphous semiconductor with a high density of localized states a large fraction of the carriers are likely to be trapped at any instant. One mechanism of transport is by direct hopping of carriers between traps. If a carrier is considered to exist in a potential well, depth ϕ, and separated from the adjacent trapping site by a distance a, then the probability that the carrier will move out of its trap is given by

$$p = \nu_0 \exp(-\phi/kT)$$

where ν_0 is the frequency of vibration of the carrier in the potential well, i.e. an escape attempt frequency. This equation assumes a Boltzmann energy distribution. The effect of an applied field is to reduce the well depth slightly in one direction and increase it correspondingly in the opposite direction. The probability of motion in the direction of the field is p_+ :

$$p_+ = \tfrac{1}{2} \nu_0 \exp -(\phi - \tfrac{1}{2} eEa)/kT$$

and against the field:

$$p_- = \tfrac{1}{2} \nu_0 \exp -(\phi + \tfrac{1}{2} eEa)/kT$$

assuming one dimensional movement only. Thus, the mean velocity of drift $\bar{v}$ will be in the direction of the field:

$$\bar{v} = a(p_+ - p_-)$$

i.e.
$$\bar{v} = a \nu_0 \sinh\left(\frac{eaE}{2kT}\right) \qquad \ldots\ldots 6.11$$

Thus, the current-voltage relation is of the form:

$$I = I_0 \sinh V/V_0 \qquad \ldots\ldots 6.12$$

where

$$I_0 = \text{Anea}\ \nu_0 \exp(-\phi/kT) \qquad \ldots\ldots 6.13$$

$$V_0 = \frac{2kT\,d}{ea} \qquad \ldots\ldots 6.14$$

n is the carrier concentration.

The experimental data for conduction in thin chalcogenide glass films may be examined for conformity to these equations.

The general form of equation 6.12 is almost the same as that used to describe bulk and coplanar samples in the pre-switching region. At low voltages $V \propto I$ with resistance R_Ω and at voltages greater than V_0, the characteristic is approximately exponential. However, as pointed out in section 6.2.2., the distinguishing feature of a sinh expression is the relation

$$V_0/I_0 = 2R_\Omega \qquad \ldots\ldots 6.15$$

The constant is 2.0 rather than 2.7 which occurs if the characteristic is simply ohmic then exponential.

Current-voltage characteristics (without any Joule heating) are shown in fig. 6.21. for samples produced in experiment E53. By suitable masking during the glass evaporation, three thicknesses were produced. An increase in ambient temperature results in an increase in I_0 and a decrease in V_0. Increased thickness has the opposite effect on I_0 and V_0. At first sight, this would appear to be contradictory to equations 6.13 and 6.14 which indicate that V_0 should increase with

Fig. 6.21

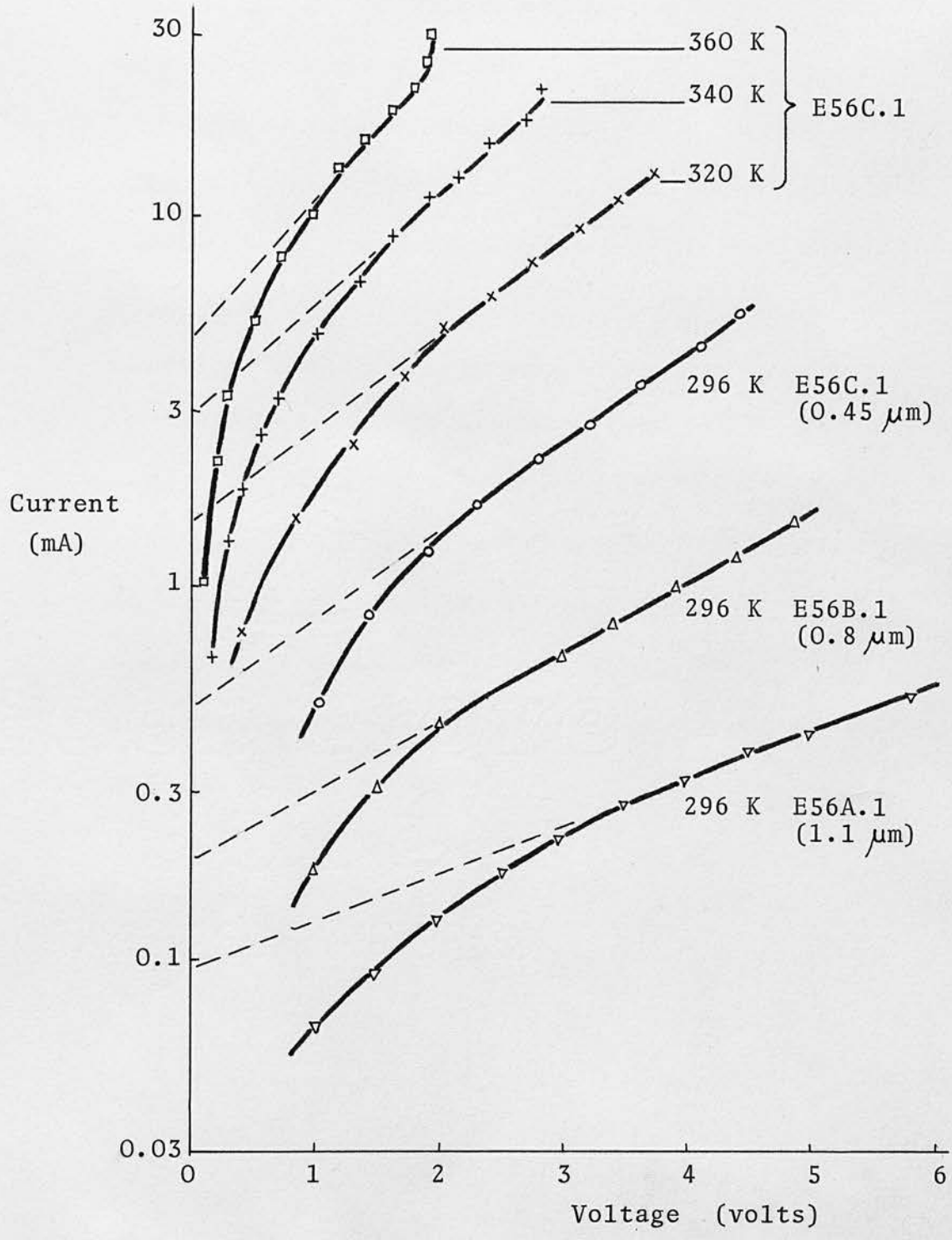

Sandwich I - V characteristics without Joule heating: influence of temperature and electrode separation.

T and I_0 should be independent of film thickness. The experimental data from fig. 6.21. and other similar films may be used to establish the functional dependence of I and V on T and d.

Fig. 6.22. shows the variation of V_0 with d. The straight line indicates a constant field: $E_0 = 3.3.10^6 \text{ V.m}^{-1}$. This conforms to equation 6.14 and from that equation, a value for the jump distance, a, may be derived. At room temperature a is of the order of 15 mm; values for a number of films are summarised later.

The temperature dependence of V_0 represents a more interesting problem. V_0 does not vary directly with temperature, nor with 1/T. However, in fig. 6.23 log V_0 has been plotted against 1/T for four films. The corresponding lines for log I_0 against 1/T are also shown. The activation energies derived from fig. 6.23 are summarised in table 6.2 along with the corresponding low field activation energies for resistance.

Table 6.2

Unit	Activation energies (eV)			
	for V_0	for I_0	difference	for R_Ω
E56A	0.06	- 0.40	0.46	0.48
E56B	0.12	- 0.40	0.52	0.49
E56C	0.07	- 0.33	0.40	0.44
E57A	0.14	- 0.30	0.44	0.48

Fig. 6.22

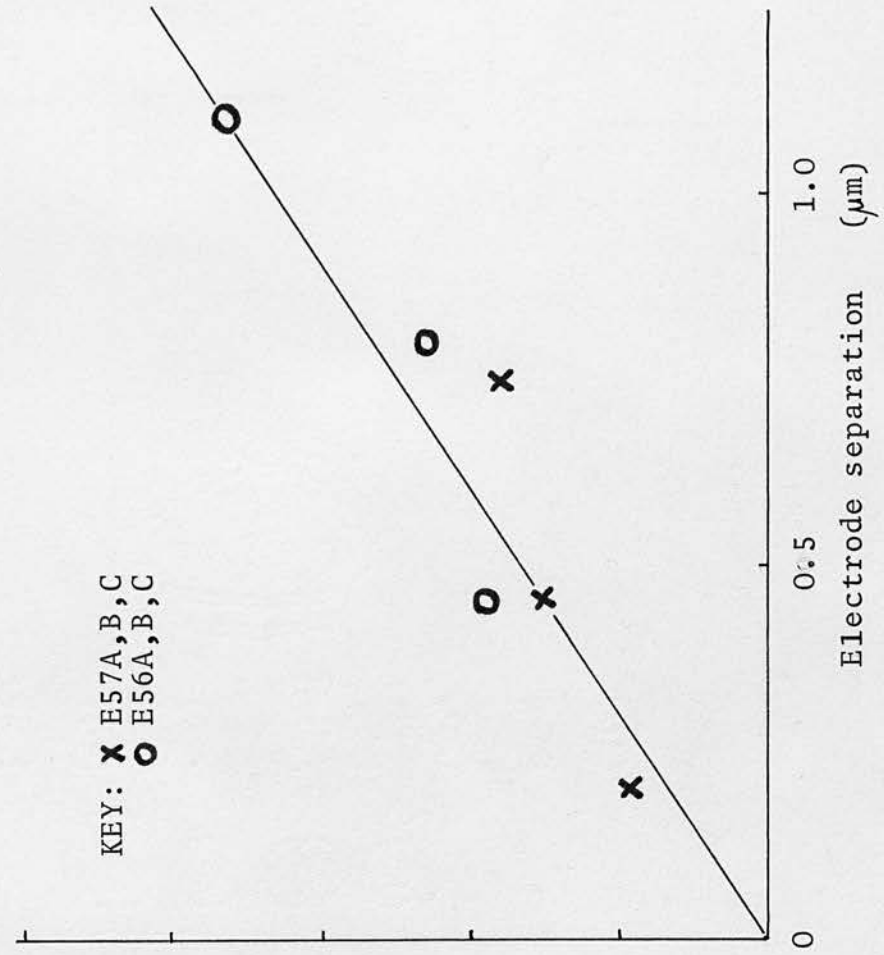

Variation of V_O with electrode separation (i.e. film thickness)

Fig. 6.23

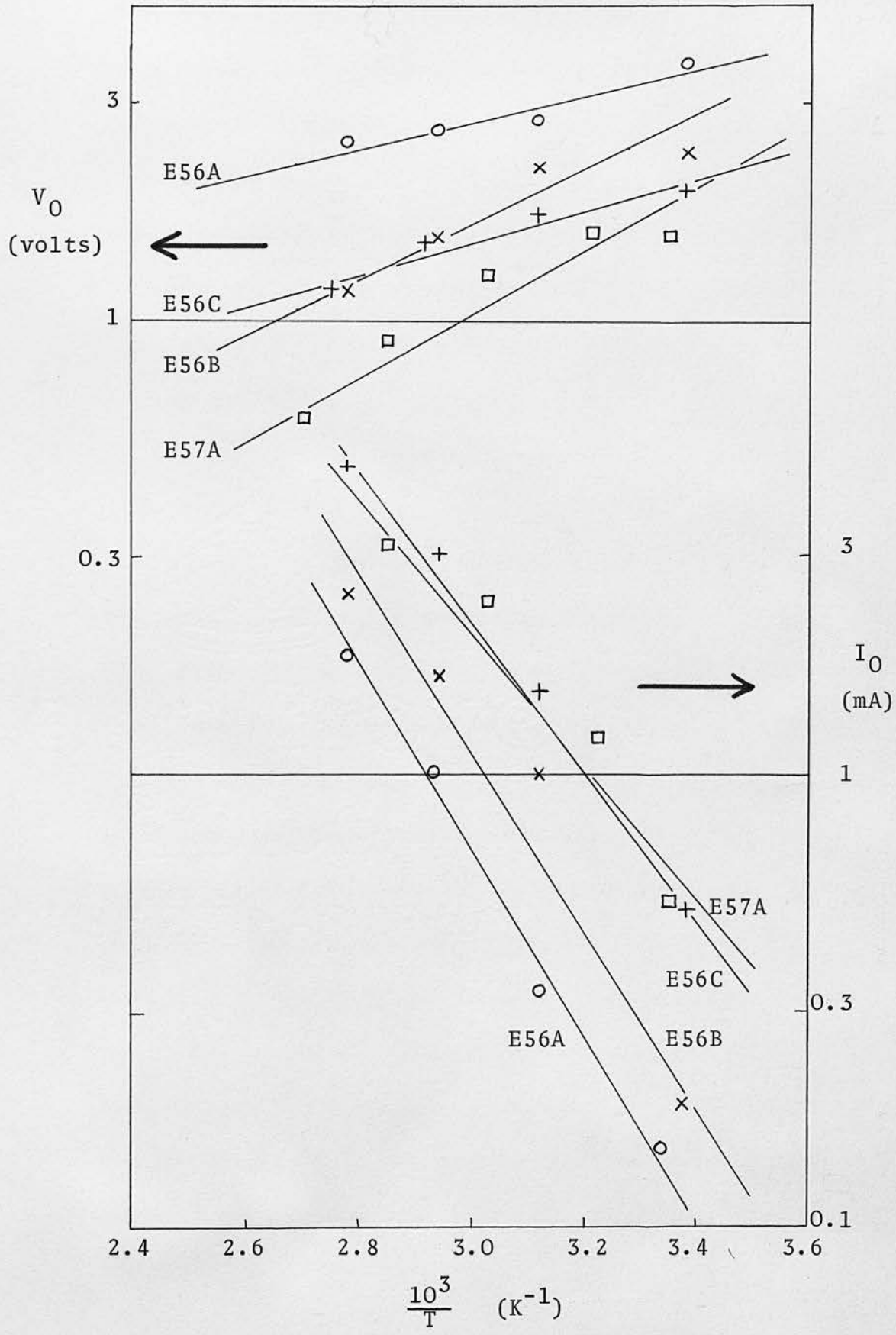

Variation of V_O and I_O with temperature.

There are two important features of these results:

1. The activation energy for R_{Ω} corresponds to the difference between the values for V_0 and I_0. This is in accord with equation 6.15.

2. The equation for V_0 (6.14) contains a term with an activation energy. The only suitable term which could be temperature-activated is a, the jump distance. Therefore a can be expressed as

$$a = a_0 \exp\left(-\frac{\psi}{kT}\right)$$

where

$$\psi = 0.06 - 0.14 \text{ eV}$$

and a_0 is in the range 0.2 - 4 μm.

In fig. 6.23. log V_0 rather than log V_0/T was plotted but the error this introduced was neglegible.

The cause of the variations in activation energies between films is not known, but there are small differences in composition and resistivity which could be responsible. This could also cause the slight dependence of I_0 on film thickness. The average activation energy for I_0 is about 0.36 eV. This is ϕ in equation 6.13. If the value of jump distance, a, is substituted into equation 6.13, an estimate of the carrier density, n, may be made. The spread in possible values of ϕ introduces an error of about one order of magnitude into the value of n. The term ν_0 is a phonon frequency, taken as 10^{13} s^{-1}. This gives $n \doteqdot 10^{23}$ m^{-3}.

The carrier mobility may be derived from the low field conductivity and n. However it is also given by the equation:

$$\mu = \frac{e a_0^2 \nu_0}{kT} \exp - \left(\frac{\phi}{kT} + \frac{2\psi}{kT} \right) \quad \ldots\ldots 6.16$$

i.e. the mobility has a slightly stronger temperature dependence than the conductivity due to the term ψ which arises from the activation energy for the jump distance.

A summary of the values of resistivity, carrier density, jump distance and mobility for six films is given in table 6.3.

The experimental results fit the required characteristics for carrier hopping if the jump distance, a, is temperature dependent. By analogy with the data for thick and coplanar samples, one of the effects of Joule heating is to make V_0 temperature dependent: cf. figs. 6.4 and 6.12. However, in the case of sandwich samples, Joule heating effects can be excluded by the technique described in section 6.4.1. Although current is described by an equation which is similar to that used where Joule heating is present, the origin of the V_0 term and therefore its temperature dependence arise from a completely different mechanism.

Hopping conduction in chalcogenide glasses was discussed briefly in chapter 2. However, when hopping occurs between localized states in the forbidden gap, the jump distance is small - of the order of one atomic spacing, 0.3 nm. This occurs because of the high density of

Table 6.3

Film	Thickness (μm)	Area ($\times 10^{-7}$ m^2)	ρ (KΩ.m)	V_0 (VOLTS)	I_0 (mA)	a (nm)	n ($\times 10^{22}$ m^{-3})	μ ($\times 10^{-8}$ m^2.V^{-1}.s^{-1})
E56A.1	1.1	3.6	5.6	3.7	0.1	15	1.4	8
E56B.1	0.8	3.4	3.0	2.3	0.18	17	2.4	9
E56C.1	0.45	4.8	2.8	1.9	0.5	12	6.7	3
E57A.10	0.45	2.2	0.83	1.5	0.52	15	12	6
E57B.7	0.75	3.0	1.1	1.7	0.3	22	3.5	16
E57C.2	0.2	2.6	1.7	0.9	0.45	11	12	3

Summary of results for hopping conduction.

Fig. 6.24

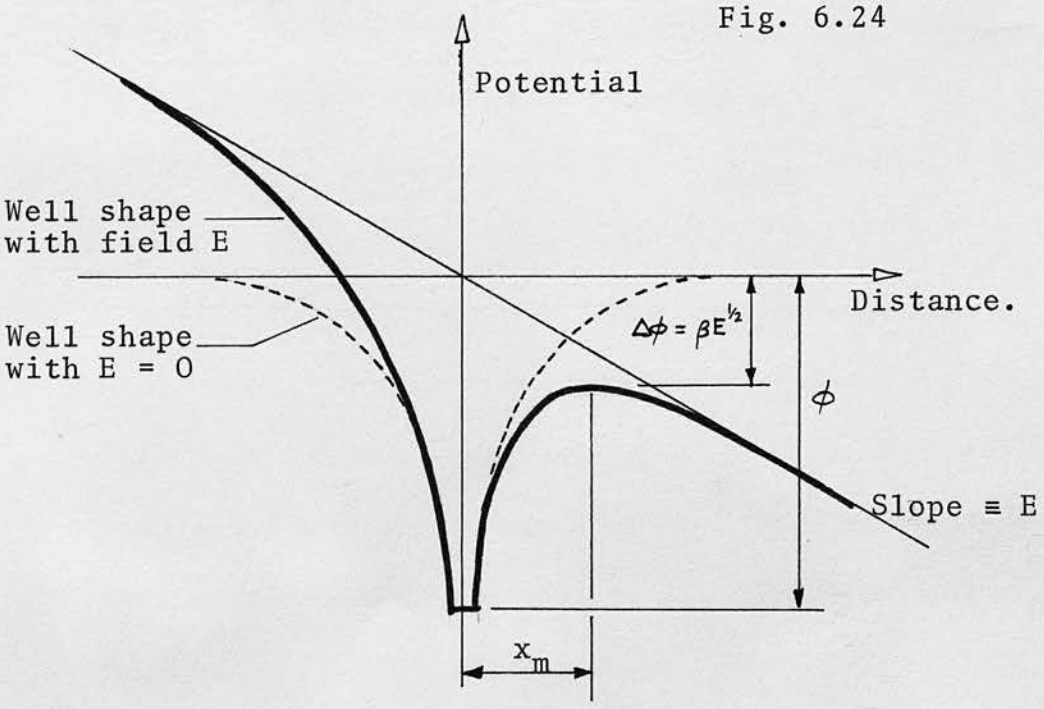

Poole-Frenkel effect: influence of field on the shape of a Coulombic well.

states. Their energy separation is also small so it would be expected that the hopping conductivity would not be strongly temperature dependent.

On the basis of the hopping model derived in this section, the jump distance at room temperature is much greater than the interatomic spacing : a $\doteqdot$ 15 nm. The activation energy measured for conductivity and the trap depth (ϕ = 0.35 eV) imply that hopping occurs by excitation of a carrier into the conduction band where conduction is scattering or diffusion limited until the carrier is retrapped. As temperature is reduced, the jump distance a decreases and for values of a below about 5 nm, tunnelling between sites becomes significant. It would be expected therefore that the conductivity activation energy would be reduced at low temperatures. It was not possible to extend the characteristics of thin sandwich samples to low temperatures. However, low temperature results for similar materials are treated in section 6.4.5.

6.4.4. Poole-Frenkel hopping

For semiconductors with trapping sites which are many atomic distances apart, the potential barrier surrounding each trap can be considerably reduced by a high field. The process of field-assisted emission of carriers from traps is known as the Poole-Frenkel effect. For the case of conduction by electrons, the traps are donors, i.e. they lie between the Fermi level and the conduction band and are

neutral when occupied.

The influence of field on the shape of a one-dimensional potential well of depth ϕ , is shown in fig. 6.24. The field reduces the effective barrier height by

$$\Delta\phi = \beta E^{\frac{1}{2}}$$

so the low field conductivity σ_a is increased at high fields to:

$$\sigma = \sigma_a \exp\left(\frac{\beta E^{\frac{1}{2}}}{kT}\right) \qquad \ldots\ldots 6.17$$

where σ_a is of the form:

$$\sigma_a = N_d e \mu \exp\left(-\frac{\phi}{kT}\right) \qquad \ldots\ldots 6.18$$

N_d is the density of donors and the constant β is:

$$\beta^2 = \frac{e^3}{\pi K_i \epsilon_0} \qquad \ldots\ldots 6.19$$

K_i is the dielectric constant for the semiconductor.

The distance from the trap centre to the minimum in the potential barrier is x_m :

$$x_m = \frac{\Delta\phi}{eE} = \left(\frac{e}{\pi K_i \epsilon_0 E}\right)^{\frac{1}{2}} \qquad \ldots\ldots 6.20$$

With this model the maximum density of traps is limited by their minimum separation of $2x_m$.

Three dimensional models for field-assisted emission have been considered by Hartke (195) and Jonscher (196). In this work the field range for non-ohmic conduction is small and the magnitude of the field itself is also relatively low so the simple one-dimensional treatment is adequate.

In order to see how experimental data fits equation 6.17, log R has been plotted against $V^{\frac{1}{2}}$ in fig. 6.25. for different values of temperature and film thickness. The same data was used in section 6.4.2., fig. 6.17., to examine the applicability of space-charge-limited current flow with a uniform distribution of traps. The data fits log R - V and log R - $V^{\frac{1}{2}}$ equally well and this emphasises one of the biggest experimental difficulties: only a small non-ohmic voltage range can be studied before switching occurs.

The general shape of the lines in fig. 6.25. agrees with that expected for a Poole-Frenkel process. At constant temperature, lines representing films of different thickness extrapolate to a constant value at V = 0 (allowing for small errors due to slightly different areas). Slope decreases as thickness and temperature increase. The detailed variation of slope with temperature and thickness is shown in fig. 6.26. and fig. 6.27. and is less satisfactory. Neither line passes through the origin and this cannot be accounted for by the errors which arise from the experimental readings.

There are two important factors, one experimental and one theoretical, which limit further analysis of the data in fig. 6.25.

Fig. 6.25

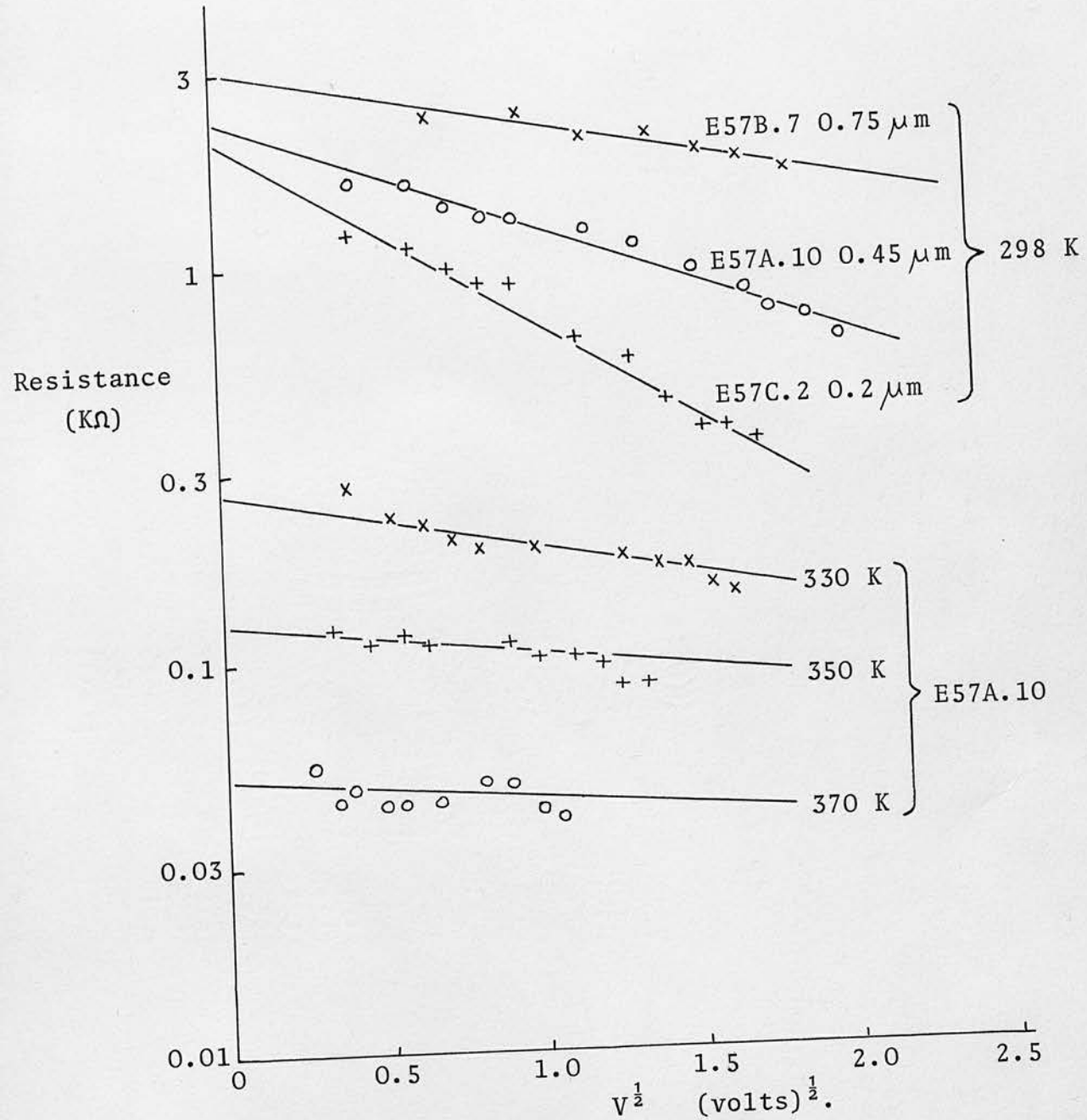

Variation of Log R with $V^{\frac{1}{2}}$ as a function of temperature and film thickness.

Fig. 6.26

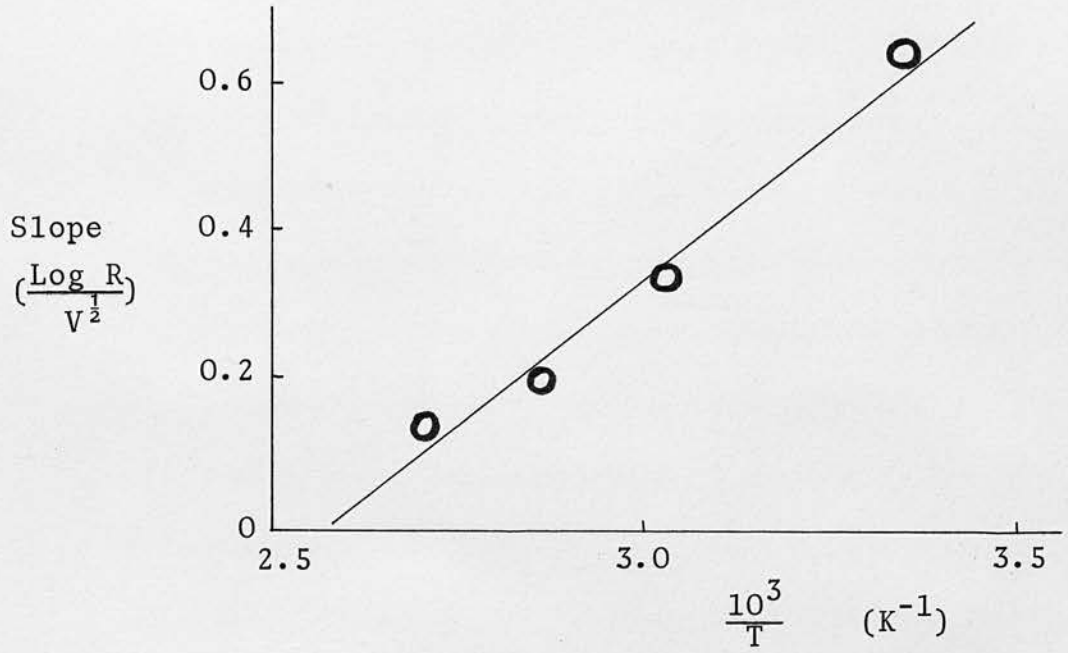

Effect of temperature on the slope of the lines in fig. 6.25.

Fig. 6.27

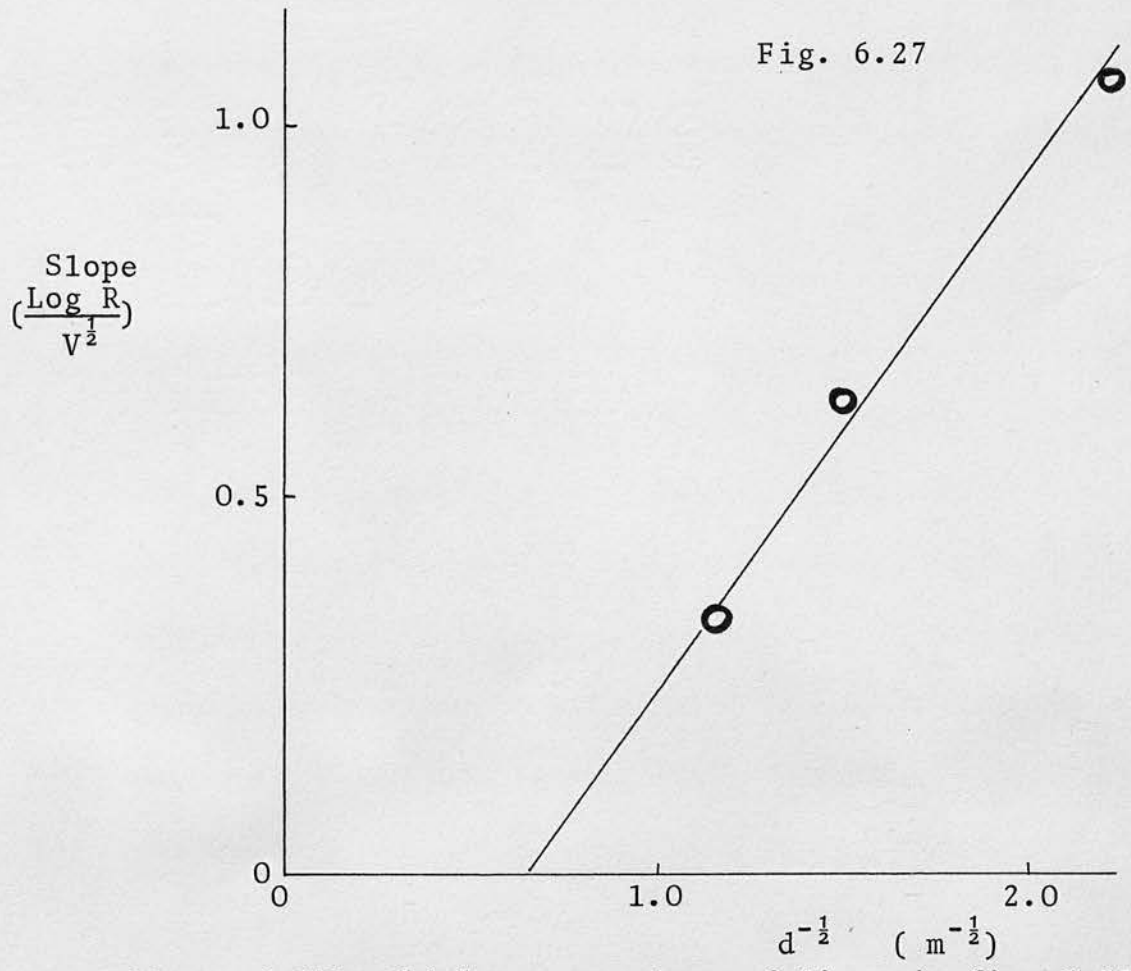

Effect of film thickness on slope of lines in fig. 6.25

1. Film composition and hence resistivity vary throughout the thickness of the film. It is therefore difficult to estimate the field distribution and hence the Poole-Frenkel contribution to current.
2. The model used has only required donor levels. In an amorphous chalcogenide film considerable compensation may occur. The degree of compensation affects β (equation 6.19) (197) (198) which in turn determines the slope of the $\log R - V^{\frac{1}{2}}$ plot.

For a field of 4 $MV.m^{-1}$, the minimum trap separation is $2x_m$ and is given by equation 6.20, i.e. approximately 20 nm. This is of the same order as the mean jump distance derived in the previous section. It implies a maximum donor density of 10^{23} m^{-3}. This is also the approximate carrier density if the time spent by a carrier at a trapping site is much larger than the time spent in transit between traps.

6.4.5. Comments on off-state conduction

The off-state characteristics of thin film sandwich samples have been analysed on the basis of three possible conduction mechanisms. The influence of Joule heating has been eliminated by the use of low repetition rate short pulses applied to low resistivity chalcogenide glasses. The component of current due to Joule heating under these conditions may be identified and excluded. This technique gives less accurate results but has the merit of providing unambiguous data

(as far as self-heating is concerned).

Conductivity shows field-dependence but the range of field values over which this occurs is small. This means that each of the models in the previous three sections shows reasonable agreement with the results; there is not a wide enough range in the experimental variables to provide a unique description of the conduction mechanism.

The space-charge-limited current model of section 6.4.2. gives a uniform distribution of traps throughout the forbidden gap of density 10^{23} $m^{-3}.eV^{-1}$. For a band gap (or perhaps more accurately, a mobility gap), of 0.9 eV, this trap density is of the order expected for chalcogenide glasses. However, a uniform distribution does not conform to the general picture of the type of trap distribution which is usually associated with tail states in the forbidden gap, so it can only represent an approximation. The detailed correspondence of SCLC behaviour with changes in temperature and electrode separation do not correspond to the experimental results. The SCLC model is not therefore the most accurate to use.

The models based on hopping and on the Poole-Frenkel effect have many similarities. With the range of experimental data available it is not possible to distinguish between graphs of log I against V and log R against $V^{\frac{1}{2}}$. Both models indicate that there is a set of dominant donor levels about 0.35 eV below the conduction band. Both models give a trap separation at room temperature of about 20 nm. The trap density and carrier concentration have similar values if a

carrier spends much more time trapped than free. Both models give $n \doteqdot 10^{23}\ m^{-3}$.

There are, however, important differences. In general, the Poole-Frenkel equation provides the more accurate description of room temperature I - V characteristics. This is difficult to justify for a single film, but when results for a large number of films are examined, there are small but consistent deviations from linearity in the graphs of $I \propto \sinh V$ and good linearity for $I \propto \exp V^{\frac{1}{2}}$.

In the Poole-Frenkel process, the minimum donor separation is determined by equation 6.20. This is not temperature dependent. In the hopping model of section 6.4.3., the jump distance has a small activation energy : 'a' decreases with a decrease in temperature. At low temperatures, transfer of carriers between trapping sites can occur by tunnelling and the temperature dependence of conductivity should be much reduced relative to room temperature values.

Fig. 6.28(a) shows conductivity data for silicon monoxide (175) expressed as log I against log V and also log I against $V^{\frac{1}{2}}$. At temperatures below 77 K the I - V characteristics are almost temperature-independent. These curves have been interpreted on the basis of a Poole-Frenkel effect. Fig. 6.28 (b) shows corresponding curves for a thin film of composition $As_{35}Te_{28}S_{21}Ge_{16}$ (18). No clear conduction mechanism was suggested for these curves, but they do bear a strong resemblance to those in fig. 6.28 (a).

The experimental variation of jump distance with temperature

Fig. 6.28

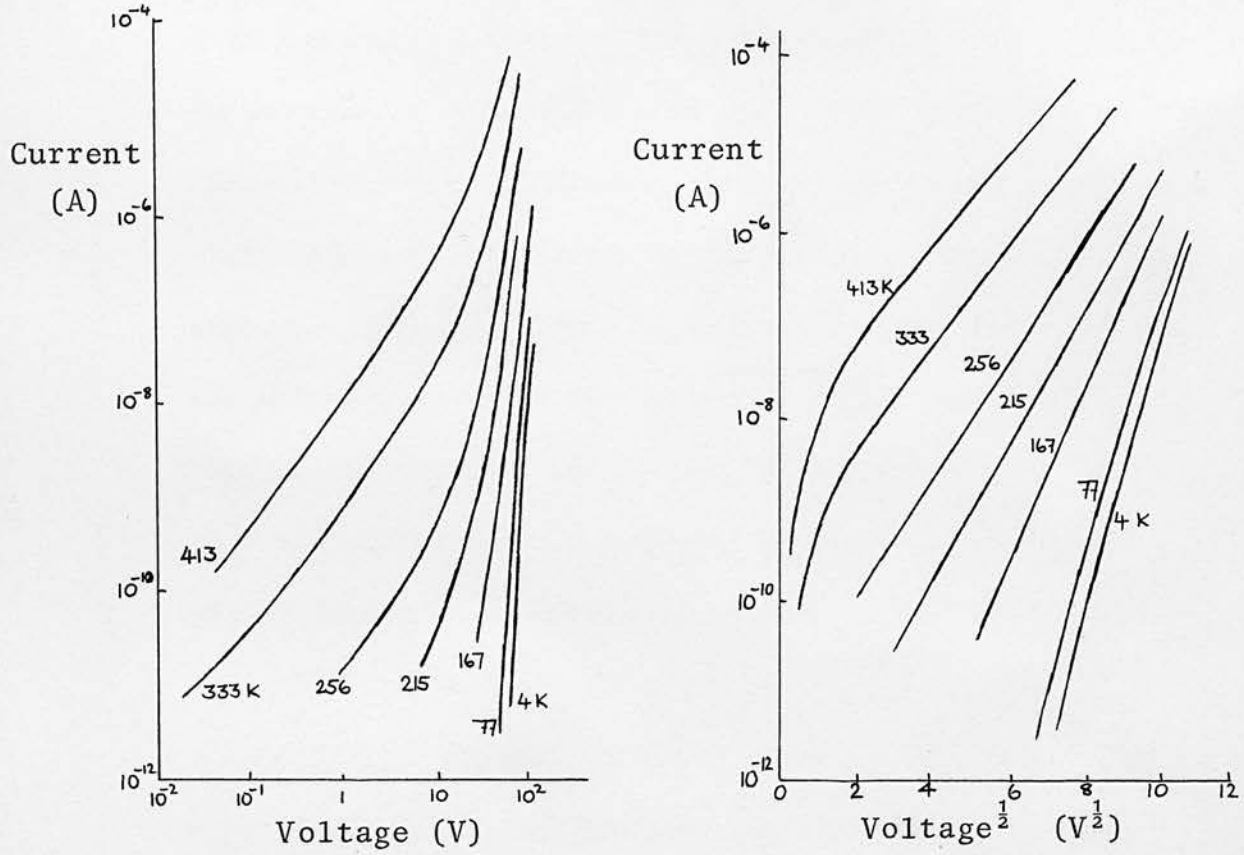

(a). Characteristics for silicon monoxide, for temperatures between 4 K and 413 K.

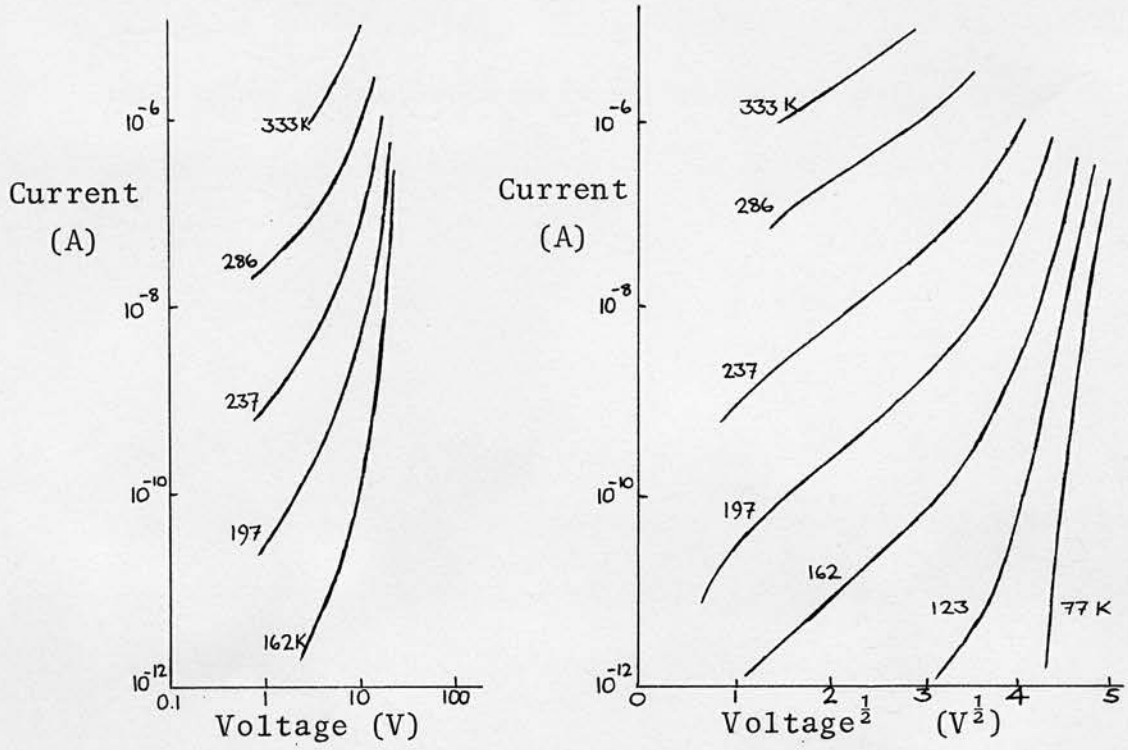

(b) Characteristics for $As_{35}Te_{28}S_{21}Ge_{16}$ for temperatures between 77 K and 333 K.

given in section 6.4.3. implies that a = 5 nm when T = 120 K, i.e. for temperatures below 120 K, tunnelling between centres should be the most important transport mechanism. The I - V relation should conform to a high power law or sensitive exponential function (e.g. as in fig. 3.14.) and be almost temperature independent. These requirements are met by the curves in fig. 6.28. It is possible, therefore, that the most accurate model to describe conduction in thin chalcogenide films is a modified Poole-Frenkel process which involves hopping and where the jump distance is thermally activated.

6.4.6. Thermal effects

In thin chalcogenide films it has been shown that conductivity is a function of field as well as temperature. When a constant voltage pulse is applied to a sample and internal Joule heating occurs, temperature and hence current increase with time. The temperature-time relation can be derived from the thermal energy-balance equation which was introduced in section 3.3. :

$$\sigma E^2 = C\frac{dT}{dt} + \frac{\Gamma}{Ad}(T - T_a) \qquad \ldots\ldots 6.21$$

The left hand term represents the Joule heat generated per unit volume and it is assumed that the field E is constant. The extreme right hand term is the heat lost via electrodes, substrate, etc. in terms of geometry (area A and electrode separation d) and thermal

conductance, Γ .

The graphical representation of each of the terms in equation 6.21 is shown in fig. 6.29. as functions of temperature increase above ambient, $\Delta T = T - T_a$. The lines P_1 and P_2 represent two different values of field and the shape of the curves P_1 and P_2 is approximately that expected for a total temperature increase along the x-axis of 20 K. Thermal runaway does not occur as long as the heat loss line which is proportional to ΔT intersects the power-temperature curve (P_1, P_2 etc.). For the curves P_1 and P_2 the stable temperatures eventually attained are T_1 and T_2. The temperature-time plot (diagram c) is derived from dT/dt (diagram b). The derivative as shown in fig. 6.29 (b) may be described approximately by an equation:

$$C \frac{dT}{dt} = P_0 - bT \qquad \ldots\ldots 6.22$$

where P_0 is the value of the derivative term at T_a

and b is approximately constant. In general,

$$b < \frac{\Gamma}{A d} \qquad \ldots\ldots 6.23$$

and this inequality becomes more pronounced for large values of T.

It may also be expressed as

$$b = \frac{\Gamma_1}{A d}$$

with $\Gamma_1 < \Gamma$

If there were no current increase with temperature then Γ and Γ_1 would be identical.

Fig. 6.29

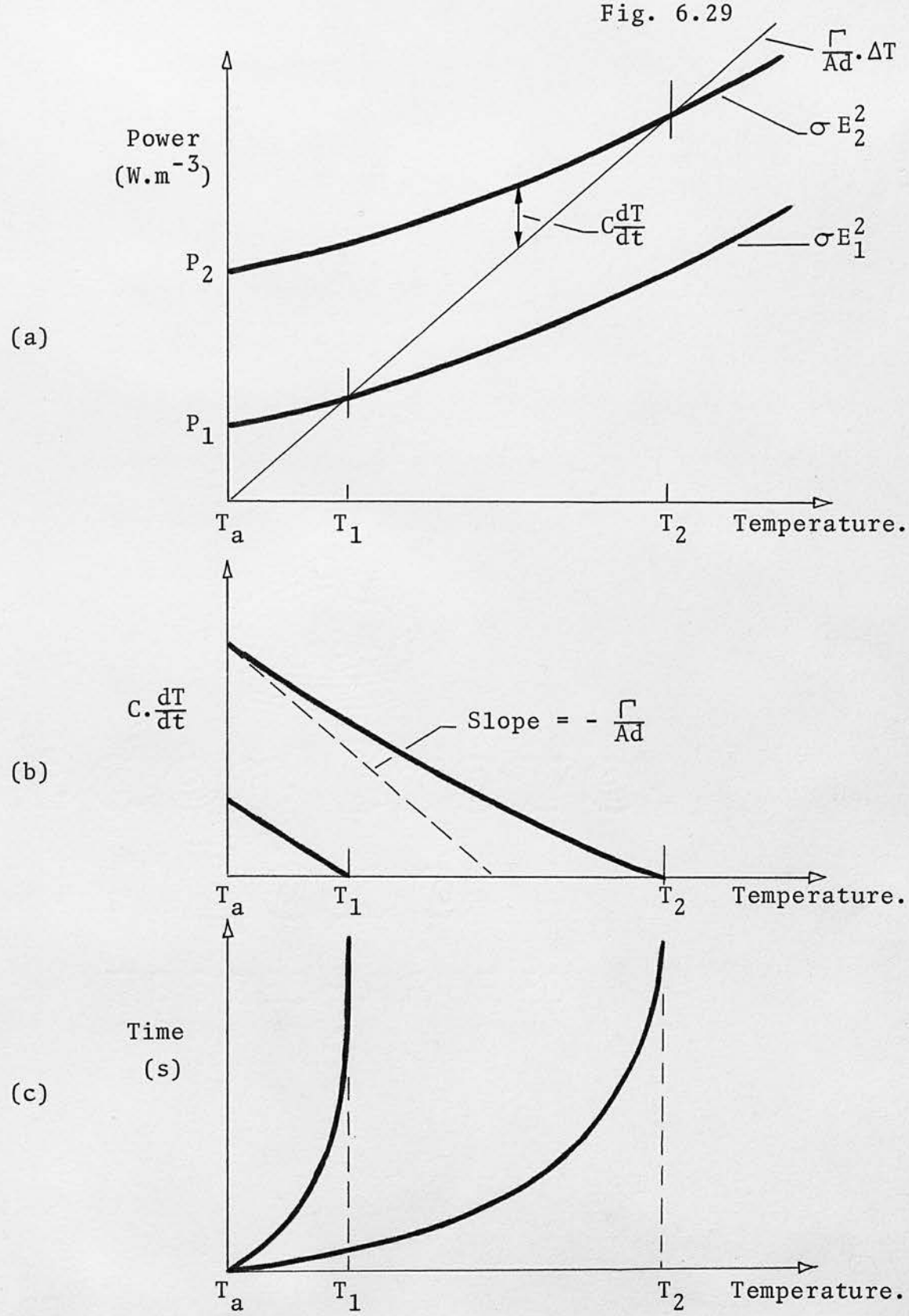

Graphical representation of the solution of the energy-balance equation.

The solution of equation 6.22 is:

$$T = \frac{P_0}{b}(1 - \exp - t/\tau_s) \quad \ldots\ldots 6.24$$

where τ_s is a time constant; $\tau_s = \frac{C}{b}$ 6.25

It is equation 6.24 which is represented in fig. 6.29 (c).

When the voltage is removed from a sample, the temperature within the material falls to the ambient value, T_a. The time for this temperature drop to occur may be found from equation 6.21 with E = 0.

i.e. $$C\frac{dT}{dt} = \frac{\Gamma}{Ad} \cdot \Delta T$$

This has a solution:

$$\Delta T = \Delta T_{max} \exp - t/\tau_d \quad \ldots\ldots 6.26$$

where ΔT_{max} is the sample internal temperature when the voltage pulse ends. τ_d is a time constant,

$$\tau_d = \frac{CAd}{\Gamma} \quad \ldots\ldots 6.27$$

When this time constant is compared with that for the current increase (equation 6.25) :

$$\frac{\tau_s}{\tau_d} = \frac{\Gamma}{\Gamma_1} > 1 \text{ since } \Gamma > \Gamma_1 \quad \ldots\ldots 6.28$$

This relationship, however, is only valid for temperature-time curves. Experimentally only current variation with time can be easily measured, so temperatures have to be deduced from current

values.

The shape of the current waveform was measured as part of the routine assessment of each thin film sample. A low repetition rate double voltage pulse was applied and the current pulse shape was given by the voltage across a resistor in series with the sample. Voltage-time and current-time pulse shapes are shown in fig. 6.30. Voltage amplitude, pulse width and pulse separation are independently variable.

The variation of I_{01} (the current at t = 0) with voltage has been discussed in sections 6.4.2.- 5. and characteristics for I_{01} - V and I_{11} - V are drawn in fig. 6.17. For the reasons given in section 6.4.1. the current increase above I_{01} or I_{02} during a pulse is due to Joule heating. It represents an increase over I_{01} of between 5 and 50% (before switching occurs). However, the current component due to heating can only be measured by substracting I_{01} from the current at any time during the pulse so experimental errors can be considerable, especially for high resistivity samples where I_{11} is only slightly greater than I_{01}.

The time constant for current rise can be measured directly from the current-time curve. As the pulse separation is increased, I_{02} falls from I_{11} to I_{01}. This gives a measure of the temperature fall with time. For small values of current increase due to heating, the current may be initially taken as proportional to temperature. The exact relationship between I and T for uniform heating is shown

Fig. 6.30

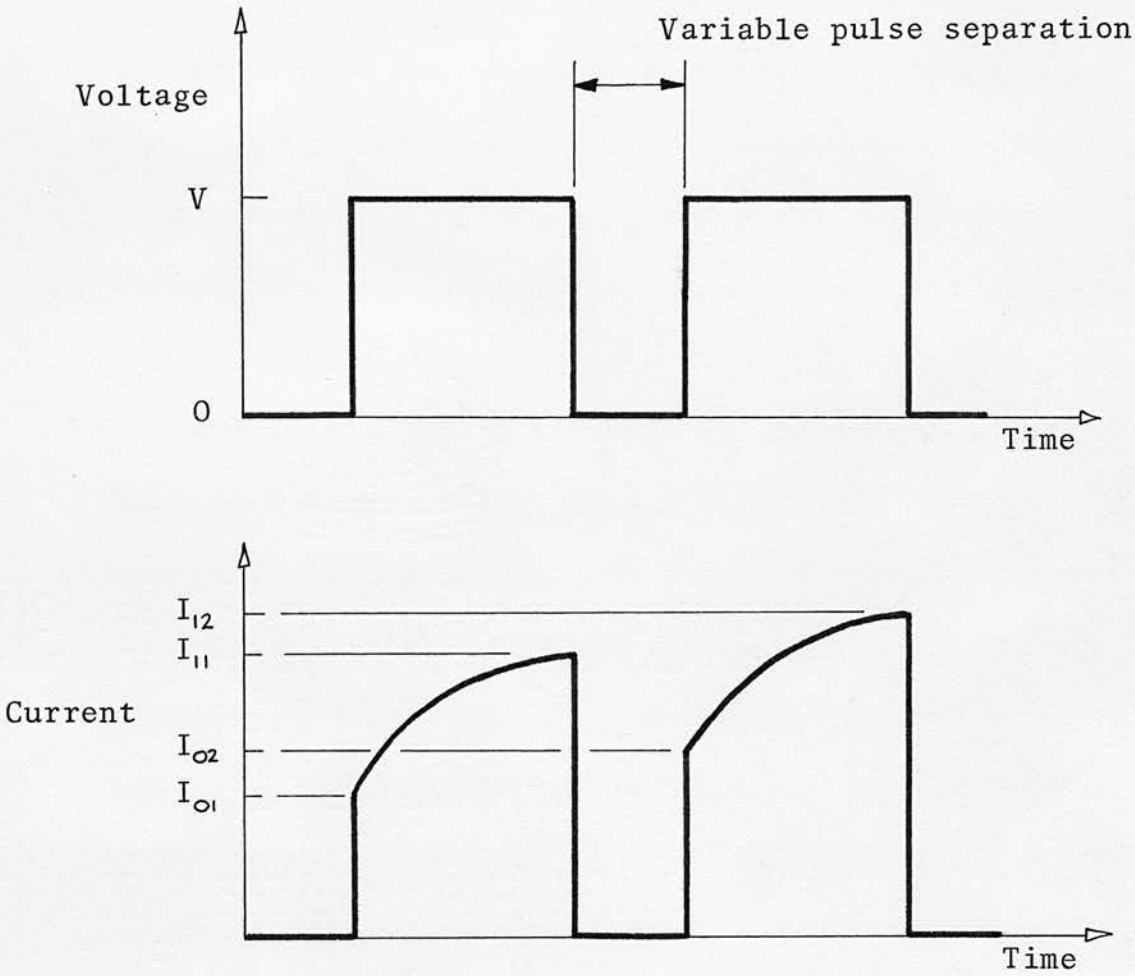

Voltage and current pulse shapes.

by curves P_1 and P_2 in fig. 6.29 (a). Samples were tested under a great variety of conditions and in all cases the rise and fall in temperature varied approximately exponentially with time.

As well as the standard crossover geometry, another electrode arrangement was also used. This consisted of a large bottom electrode of gold (1 - 2 cm square). then a layer of the chalcogenide film. The top contact was made with evaporated gold dots which were connected to the measuring equipment via an X - Y - Z probe. Variation of the diameter of the top contact gave samples of different area.

Substrates of silicon and 7059 glass gave exactly the same values for heating and cooling curves. The top and bottom electrodes were usually 0.3 μm thick, but they were varied between 40 nm and 0.5 μm with no effect on the time constant values. These comparison measurements were always made on samples of glass deposited at the same time. This indicates that the rate of heat dissipation required to give the thermal conductance term, Γ , can be achieved with thin electrodes ($\gtrsim$ 40 nm). Thicker electrodes or substrates of higher thermal conductivity do not improve the rate of heat transfer.

Other experimental results, however, were not as straightforward. Time constants varied with field, resistivity and sample area. From the treatment of thermal breakdown in section 3.3., the highest stable internal temperature which could be realised without thermal runaway was about 25 K above ambient. In a uniformly

heated sample this should mean that near V_{th} the current at the end of the voltage pulse, I_{11}, should be about three times greater than the value at the beginning of the pulse I_{01}. i.e. $\Delta I = I_{11} - I_{01} = 2I_{01}$. This was observed for only a few samples; in general the relation was $\Delta I = x I_{01}$ with x in the range 0.05 - 1.0. For values of $x < 0.05$, the increase in current was very difficult to measure.

The variation in the magnitude of the current component due to self-heating may be explained by non-uniform heating throughout the sample. Only a small region need be heated by 25 K to produce thermal runaway and this would imply a non-uniform current density across the sample in the pre-breakdown region. The 'hot' area may be considered initially to be at a uniform temperature (T_a + 25) and to have sharply defined boundaries with the rest of the sample at T_a. The area of the 'hot' region in terms of the 'cold' region is then given by:

$$\text{'Hot' area} = 0.3x.\text{'cold' area.}$$

where x is derived from the current-time curve and the sum of the 'hot' and 'cold' areas is equal to the geometrical area.

The non-uniform temperature distribution with a localized maximum value T_{max} may be represented by a uniform mean temperature T_{mean}, where $T_{mean} < T_{max}$. Both temperature distributions would give the same I - V characteristics but the onset of thermal runaway would occur at a smaller value of ΔI for the

non-uniform temperature distribution.

With the uniform temperature representation of non-uniform heating, the general shape of the diagrams in fig. 6.29. would not change but the curves P_1 and P_2 would be flatter. The thermal time constant for heating would approach the value for cooling, i.e. $\Gamma_1 \rightarrow \Gamma$ in equation 6.28.

In the more conducting chalcogenide films, the component of current due to self-heating (ΔI) was relatively much larger than for films of lower conductivity. This suggests that in the former case the temperature distribution before the onset of thermal runaway was more uniform than in the latter case, i.e. the effective heated volume was greater. The time constant given by equation 6.27 is:

$$\tau = \frac{CAd}{\Gamma}$$

If Γ is taken to be constant for given materials and device geometry, then τ depends on the effective heated volume, i.e. τ should increase as σ is increased. This is observed experimentally.

The proportion of a sample which is heated may be increased by reducing the geometrical area. The measured values for τ increase with sample area. Thus, experimentally $\tau \propto A\sigma$. This is shown in fig. 6.31. for values of τ obtained from cooling curves. Instead of $A\sigma$, the ratio of sample resistance to electrode separation, R/d, has been plotted. There is a large scatter in the experimental data but this is consistent with a non-uniform heating process which

Fig. 6.31

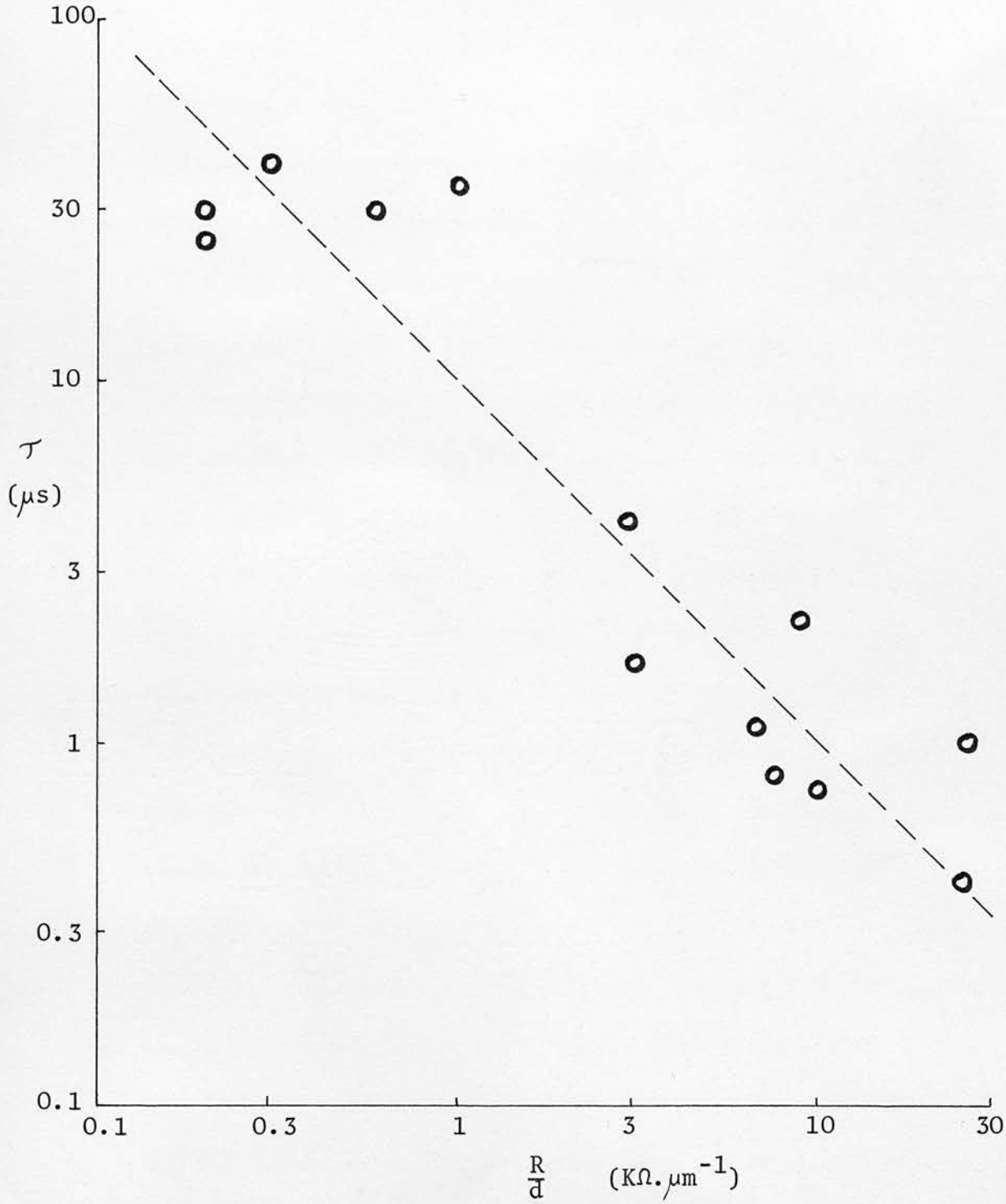

Cooling thermal time constant, τ : variation with resistance and electrode separation.

varies from sample to sample.

The numerical value for thermal time constant, τ , may be found from equation 6.27. The heat capacity, $C = 2.10^6$ J.m^{-3}.K^{-1}. For a relatively conducting chalcogenide film where almost uniform heating occurs, the experimental value of thermal conductance is: $\Gamma = 20$ mW.K^{-1}. For an area 2.10^{-7} m^2 and film thickness 2 μm, $\tau = 40$ μs. This is typical of the experimental values obtained for films produced from a glass of bulk composition $As_{20}Te_{70}Ge_{10}$. The thin film resistivity is 40Ω.m. Data points for such samples appear in the top corner of fig. 6.31.

Heating and cooling curves were measured as part of the routine assessment of each thin film. In fig. 6.32. the curves for two field values have been plotted as log $|\Delta I|$ against time. For heating, $|\Delta I| = I_{11} - I$ and the time scale refers to time elapsed since the beginning of the pulse (cf. fig. 6.30). For cooling, two pulses have to be used and $|\Delta I| = I_{11} - I_{02}$. The time scale refers to the separation between the two pulses.

The influence of field in fig. 6.32. may also be explained on the basis of non-uniform heating. At high fields the temperature distribution is much less uniform than in the low field case. The high field thermal time constant for heating is therefore shorter than the low field value. For cooling, however, the thermal conductance may limit the rate of heat loss from a small 'high-temperature' region so the high field cooling time constant is lower than the low

Fig. 6.32

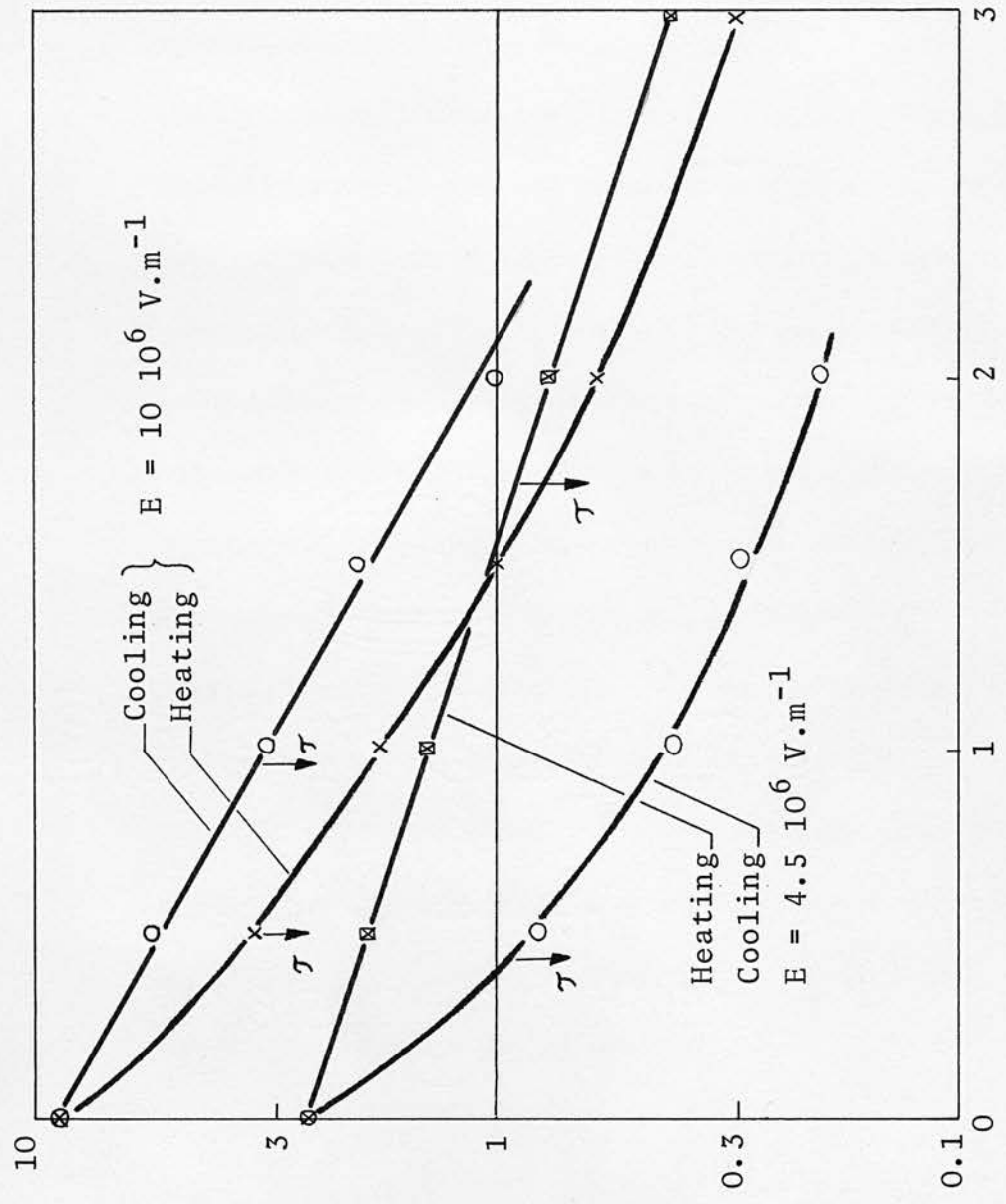

Heating and cooling curves. $|\Delta I| = I_{11} - I$ (heating)
$|\Delta I| = I_{11} - I_{\infty}$ (cooling)

field value.

Non-uniform heating also implies that when thermal breakdown occurs, it is localized. This determines the position of the high current filament of the on-state.

The interpretation of thermal time constant results has been limited by the errors of measurement and the scatter which arises from measurements on many different samples. However, it does appear that non-uniform heating can occur within sandwich samples and this is most marked for high resistivity materials. The thermal response time is of the order 0.5 - 40 μs and is shortest for samples with high resistivity and small area (fig. 6.31.). These are also the conditions which exist in chalcogenide switching devices so the performance of these devices must be examined from the viewpoint that some localized heating is almost certainly present. The thermal response time ~ 1 μs is also of the same order of magnitude as the delay time for switches operated under pulse conditions. It is reasonable therefore to consider that the switching process may be thermally initiated.

6.4.7. A.C. Admittance arising from thermal effects

One of the most unusual features of chalcogenide threshold switches is that when biased close to V_{th}, their capacitance changes sign. Vogel and Walsh (184) measured the capacitance of threshold switching devices as a function of d.c. bias voltage. Their results

are shown in fig. 6.33. Close to V_{th}, the capacitance decreases as the voltage is increased; it goes through zero and then towards $-\infty$ at V_{th}. Many explanations have been offered for this effect: space charge polarization, limited avalanche effects, phase changes, etc., but it can be shown that the graph in fig. 6.33. is to be expected if any Joule-heating occurs in the device.

A thin film of chalcogenide glass sandwiched between metal electrodes may be considered as a lossy capacitor and represented by a parallel R - C circuit - R_1 and C in fig. 6.34. When a voltage pulse is applied to the sandwich, a high current spike results. The peak current is limited by the current-measuring resistor or by the generator output resistance. The spike decays with a time constant $R_1 C$ and this is usually much shorter than the voltage pulse length: fig. 6.35. Internal self-heating increases the current above the steady-state level $I_{01} = V/R_1$. This response may be simulated with a series L - R circuit across R_1 where the resistor R_2 is determined by the current increase due to Joule heating; $R_2 = V/\Delta I$. The total equivalent circuit and its response to a voltage pulse are shown in figs. 6.34. and 6.35.

The thermal time constant, τ, is approximately constant for any given sample. It determines the value of the inductance;

$$L = R_2 \tau = \frac{V\tau}{\Delta I} \qquad \ldots\ldots 6.29$$

Under typical experimental conditions, the current increase due to Joule heating is zero until V is close to V_{th} then ΔI increases

Fig. 6.33

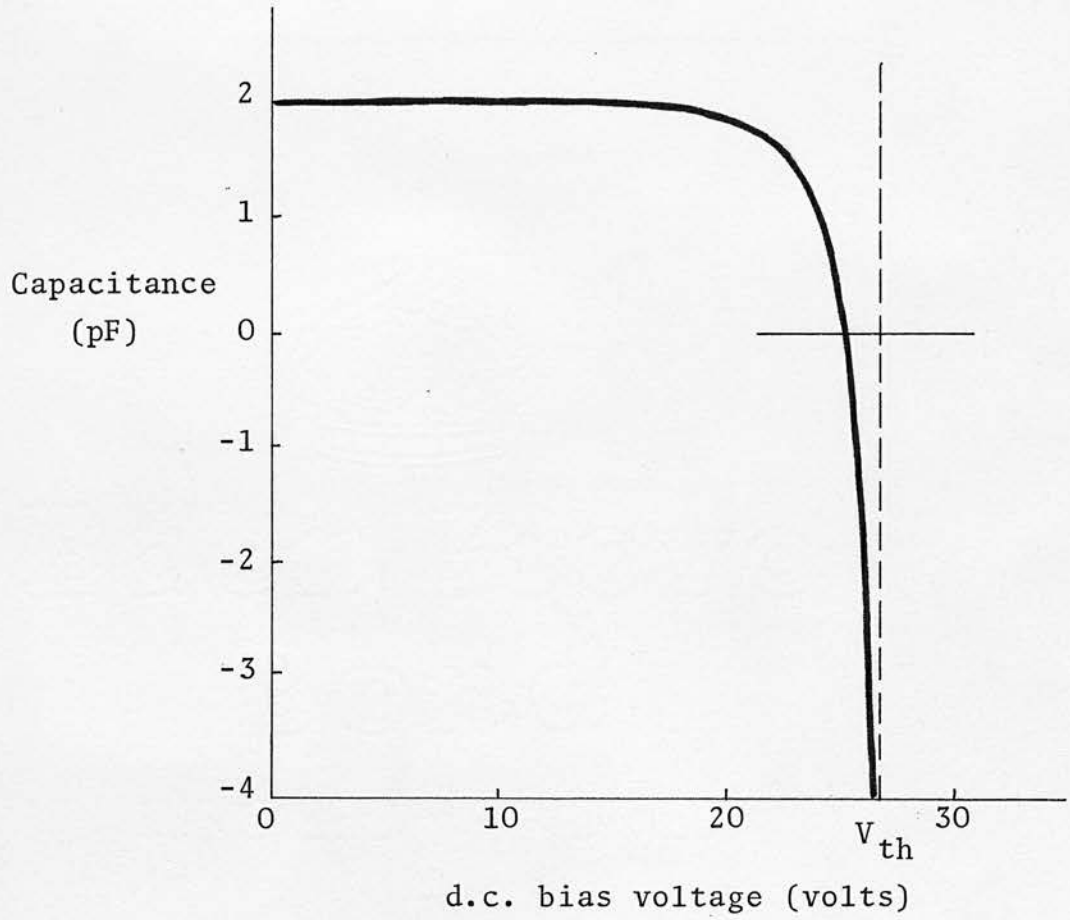

Variation of capacitance with bias voltage: results of Vogel and Walsh (184).

Fig. 6.34

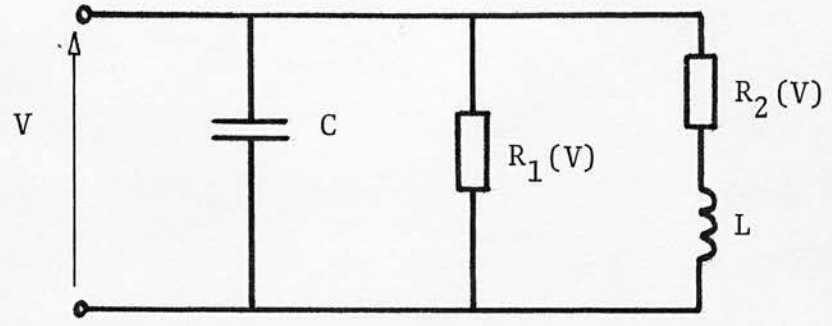

Equivalent circuit

Fig. 6.35

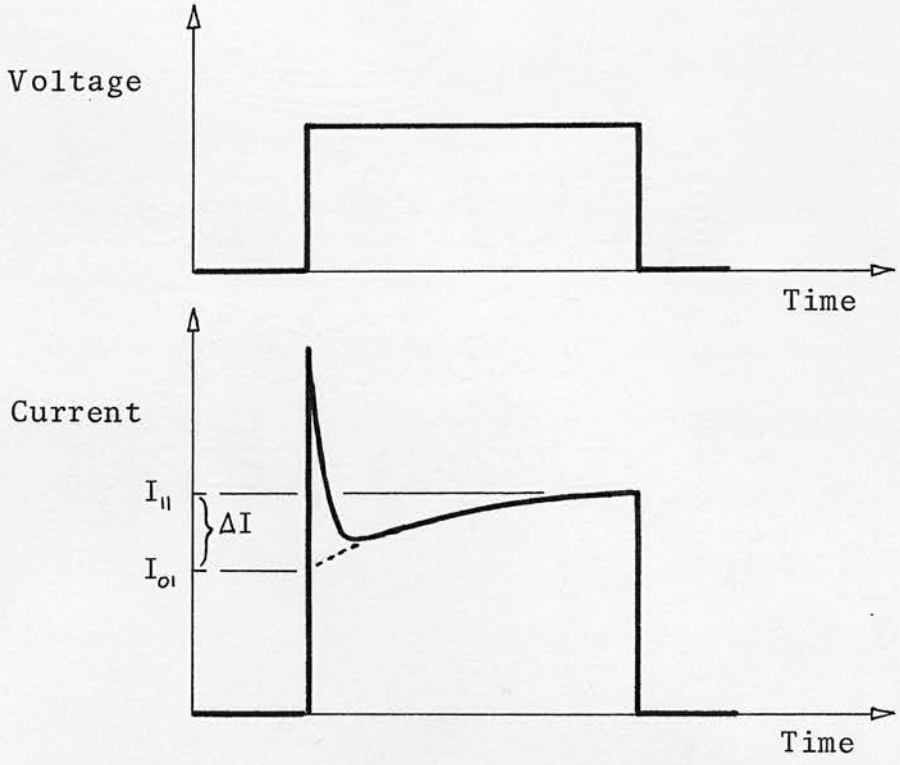

Response to a voltage pulse.

rapidly; ΔI therefore largely determines the variation of L with V. Qualitatively, this shows that the admittance of the R_2 - L combination is zero until V is close to V_{th}.

The principal features of the a.c. admittance of temperature-dependent circuit components have been treated in general terms in section 3.3.9. However, the equivalent circuit of fig. 6.34. is adequate for this analysis. The admittance as a function of voltage may be calculated on the basis of Joule heating. Constants appropriate to Vogel's devices are used so that a comparison can be made.

The current-voltage relation as a function of internal temperature (ΔT above ambient) is given by:

$$I = G_{\Omega} V \exp(a \Delta T) \exp(V/V_0) \quad \ldots\ldots 6.30$$

G_{Ω} is the low field conductance, taken as $10^{-7}\ \Omega^{-1}$. 'a' is a constant which depends on the resistance activation energy. For materials used in chalcogenide switches, $\Delta E = 0.45$ eV and $a = 0.04$. V_0 is a constant; from the analysis in section 6.4.3., $V_0 = 4$ volts for the 1.2 μm film used by Vogel. V_0 is slightly temperature-dependent ($\Delta E = 0.1$ eV) but since a temperature range of only 25 K is considered, V_0 may be taken to be independent of temperature. It must also be assumed that heating occurs uniformly throughout the sample.

The variation of ΔT and I with voltage is shown in fig. 6.36 (a) and (b). V_{th} occurs at 16 volts, but if slightly different constants were used in equation 6.30 and allowance were made for heat losses

Fig. 6.36

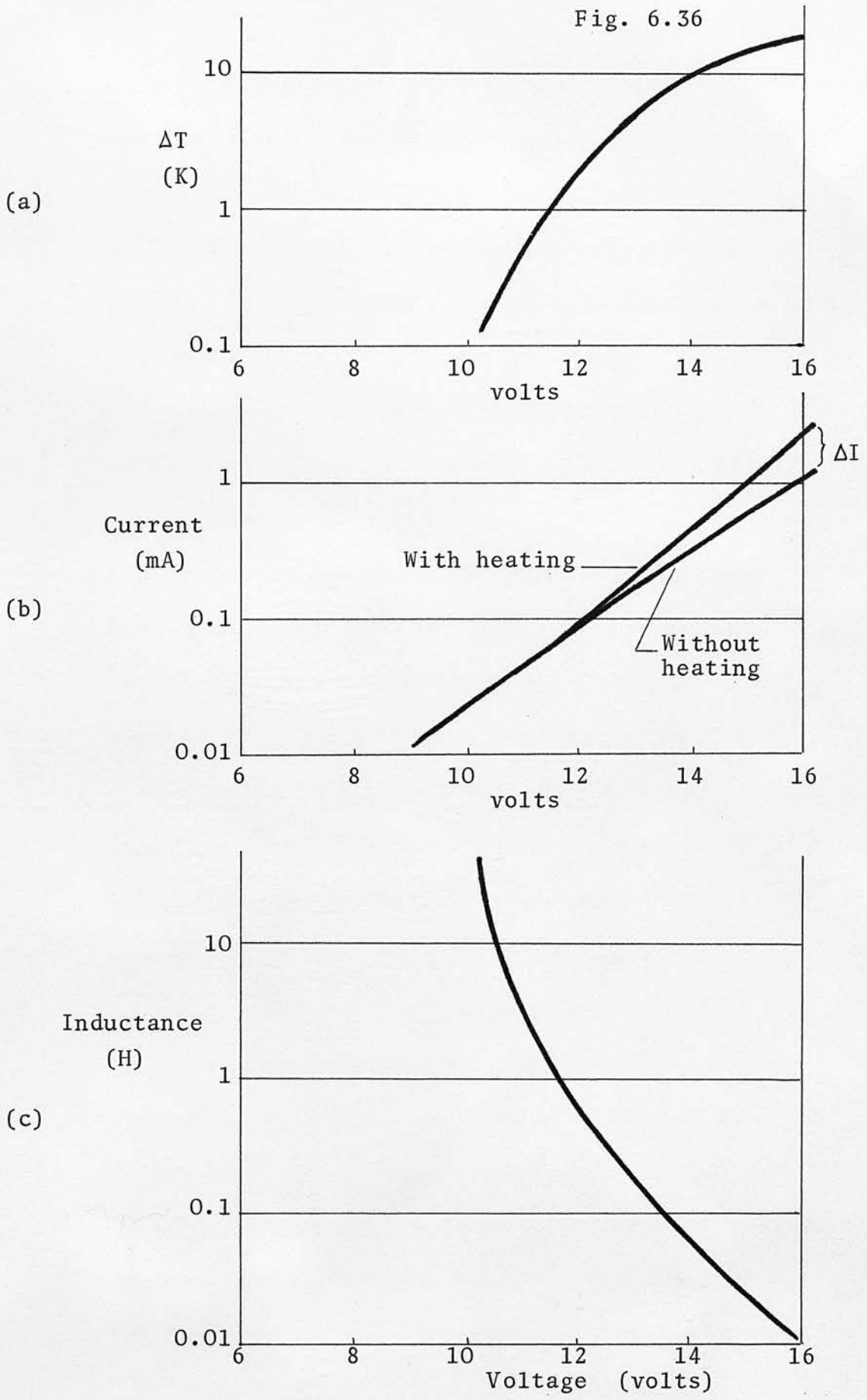

Variation of internal temperature, current and equivalent circuit inductance with bias voltage.

via the electrodes, then Vogel's experimental figure of V_{th} = 24 volts could easily result. The important feature of fig. 6.36 (a) is that the temperature rise is only significant in the four volts below V_{th} and in that region, the temperature rise is approximately uniform - 5 $K.V^{-1}$. For Vogel's devices, temperature effects are only likely to be significant for voltages above 20 - 22 volts.

The value of equivalent circuit inductance has been calculated from equation 6.29 for τ = 1 μs and is shown as a function of voltage in fig. 6.36 (c).

The sample capacitance, as measured on a bridge is derived from a measurement of the susceptance of the sample, i.e. $\omega C + (\omega L)^{-1}$. The capacitive term is not a function of voltage, but close to V_{th}, $(\omega L)^{-1}$ becomes the dominant term. This is shown in fig. 6.37. and is very similar to fig. 6.33. The rapid variation of L with V also means that the changeover from negative to positive susceptance will only be very weakly dependent on frequency. This is in agreement with Vogel's observations.

Vogel also observed that at low temperatures (below 0°C), the sample capacitance appeared to be negative even with no d.c. bias. Without information on the a.c. conductivity-frequency behaviour of these films, it is not possible to explain the effect quantitatively. However, if there were a peak in the a.c. loss curve at low temperature the power dissipated due to this loss could be of the order of 10 μW. The sample thermal conductance appears to be temperature dependent

Fig. 6.37

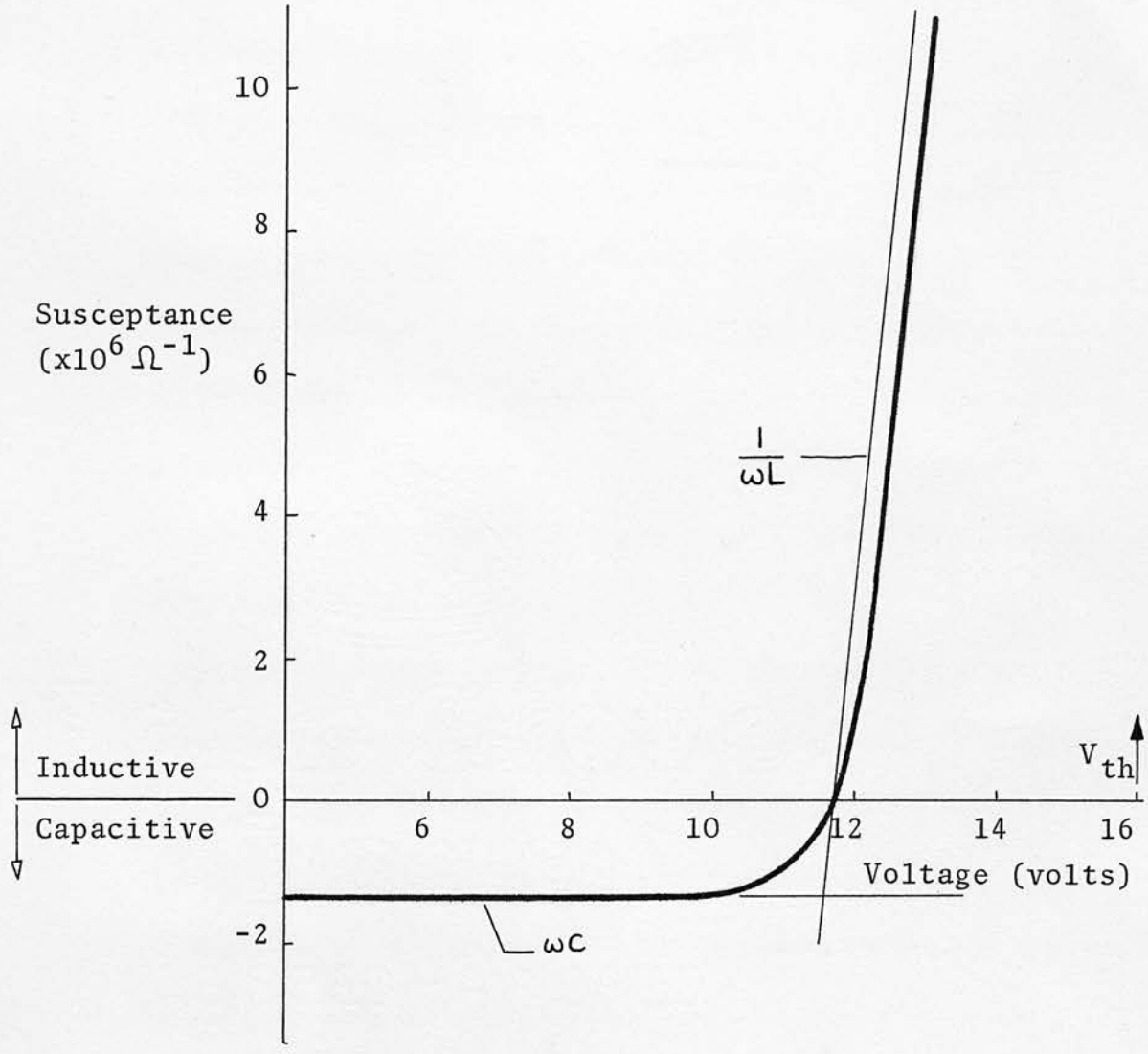

Predicted susceptance - voltage variation as a result of self-heating.

(this is discussed in the next section) and a value of $\Gamma = 10 \quad W.K^{-1}$. is possible for the small area device used by Vogel. A temperature rise of only a few degrees is all that is needed to give a susceptance which would completely swamp the capacitive value.

The heating which arises from dielectric loss depends on the loss-frequency curve which would vary slowly over a temperature range of 50 K or more. It would be expected therefore that the inductive character of the sample admittance would increase slowly as the temperature was reduced and there would be a much more gradual changeover than in the d.c. bias-room temperature case shown in fig. 6.37. These predictions are qualitatively in agreement with Vogel's observations.

Apart from the formal treatment of Burgess (35) and some application to Ge point-contact diodes (199), the problems of thermal admittance have not received much attention. It provides a straightforward explanation for negative capacitance in chalcogenide switches and it is consistent with the conduction and thermal processes which occur in these devices. The admittance measurements are very sensitive to temperature changes within the sample and along with data from a.c. loss measurements, could provide an accurate picture of the internal thermal behaviour of switching glasses.

6.4.8. Threshold switching

Threshold switching was observed in a large number of chalcogenide thin film samples. The primary objective of the experimental work was to ascertain whether a single mechanism could be used to explain all the switching observations. If so, then the variables which influence the process had to be determined so that in turn individual results could be explained in terms of the basic physical properties and geometry of the sample.

Chalcogenide glasses with 3 or more components all have similar activation energies for resistance and similar values of thermal conductivity. The biggest variable is resistivity. The effect of composition on resistivity has been discussed in chapter 5 and threshold switching was observed in samples with a wide range of low-field resistivities: $30\,\Omega.m$ - $10^6\,\Omega.m$. The upper limit implies that no monostable switching was observed in thin films of Se, As_2Se_3 or As_2S_3.

Switching may be considered under two groups of experimental conditions:

1. Steady state. This implies continuous cycling with low frequency square or sine waves.
2. Transient. Short, low repetition rate voltage pulses give information on the time taken for breakdown to occur.

Under steady-state conditions, the value of V_{th} is very dependent on the I - V characteristic at voltages just below V_{th}. The

experimental results of the preceeding sections have shown that close to V_{th}, current is described by an equation:

$$I = G(V).G(T).V$$

The exact expressions for G(V) and G(T) depend on the mechanisms used to explain the effect, but from section 6.4.3., G(V) may be described by

$$G(V) = G_{\Omega} \exp\left(\frac{E}{E_0}\right) = G_{\Omega} \exp\left(\frac{V}{V_0}\right) \quad \ldots\ldots 6.31$$

where the field E_0 is a constant for any material but it is slightly temperature-dependent ($\Delta E \doteqdot 0.1$ eV). The temperature dependence of I is dominated by $G_{\Omega}(T)$:

$$G_{\Omega}(T) = G_0 \exp - \frac{\Delta E}{kT} \qquad E \doteqdot 0.45 \text{ eV} \quad \ldots\ldots 6.32(a)$$

$$= G_1 \exp \frac{T}{T_1} \qquad T_1 = 24^{\circ} K \quad (b)$$

$$= G_{\Omega} \exp(a\ \Delta T) \qquad a \doteqdot 0.04\ K^{-1}$$

$$\Delta T = T - T_a \quad (c)$$

Over a small temperature range above ambient, T_a, the most convenient expression for the pre-breakdown current is:

$$I = G_{\Omega}\, V \exp\left(\frac{V}{V_0}\right) \exp(a\ \Delta T) \quad \ldots\ldots 6.33$$

Thermal breakdown occurs when $\Delta T = 25$ K (section 3.3.). A proportion of the total power dissipated will go towards increasing the internal temperature of the sample so it is important to examine how the VI product is affected by material and geometry.

For samples with a relatively high conductance or large electrode separation, significant self-heating can occur at voltages below V_0 ($E_0 \doteqdot 3 \times 10^6$ V.m^{-1}). Thus the temperature increase is dependent on a V^2 term. This is the case for the bulk samples discussed in section 6.2. Higher resistivity materials allow $V > V_0$ before significant heating occurs. Thus the temperature increase is determined by a term of the form $V^2 \exp V/V_0$ where the exponential term is dominant. When the temperature does start to increase (beyond about 1 K), it will do so much faster than in the low resistance case, so the whole runaway process will be much faster. This may also explain the non-uniform heating effect in high resistivity samples, discussed in section 6.4.6.

The mechanism of thermal breakdown with the current described by equation 6.33 gives a good qualitative explanation for the observed characteristics of a number of films with a wide range of resistivities. To assess numerical values expected for V_{th} by this mechanism, the expression developed in section 3.3.5. may be used:

$$V_{th}^2 \exp\left(\frac{V_{th}}{V_0}\right) = \frac{\Gamma R}{a e} \qquad \ldots\ldots 6.34$$

where Γ is the sample thermal conductance, R is the resistance, 'a' is a constant defined by equation 6.32(c) and e = 2.7.

The variation of V_{th} with thickness is shown in fig. 6.38. for 24 samples with resistivities between 40Ω.m and 4.10^5Ω.m. For a given resistivity value, $V_{th} \propto d$. This is also the theoretical result derived in section 3.3.5. For comparison, the result of Kolomiets (176) is also shown. With a wide spread in ρ values, the scatter of points in fig. 6.38. is confusing so it is more significant to test the validity of equation 6.34. The experimental details for the 24 samples used in fig. 6.38. may be applied to equation 6.34. The constants used were: a = 0.05, Γ = 8 $mW.K^{-1}$., $E_0 = 3.3 \times 10^6$ $V.m^{-1}$ and e = 2.7. In fig. 6.39. the value of breakdown field calculated from equation 6.34 is compared with the measured value for each of the 24 samples. The scatter of results is perhaps to be expected with such a wide range of samples. However, the points above the identity line belong to higher resistivity samples and points below the line are for the more conducting samples. This difference could result from the assumption of a constant value for Γ (although all samples had the same electrode area) and associated non-uniform heating.

The effect of ambient temperature on V_{th} can also be derived from equation 6.34. The relative importance of each of the temperature-dependent terms in equation 6.34 was discussed in section 3.3.5. The theoretical V_{th} - temperature curve was shown in fig. 3.8. and it has been redrawn in fig. 6.40. Experimental lines have also been drawn in

Fig. 6.38

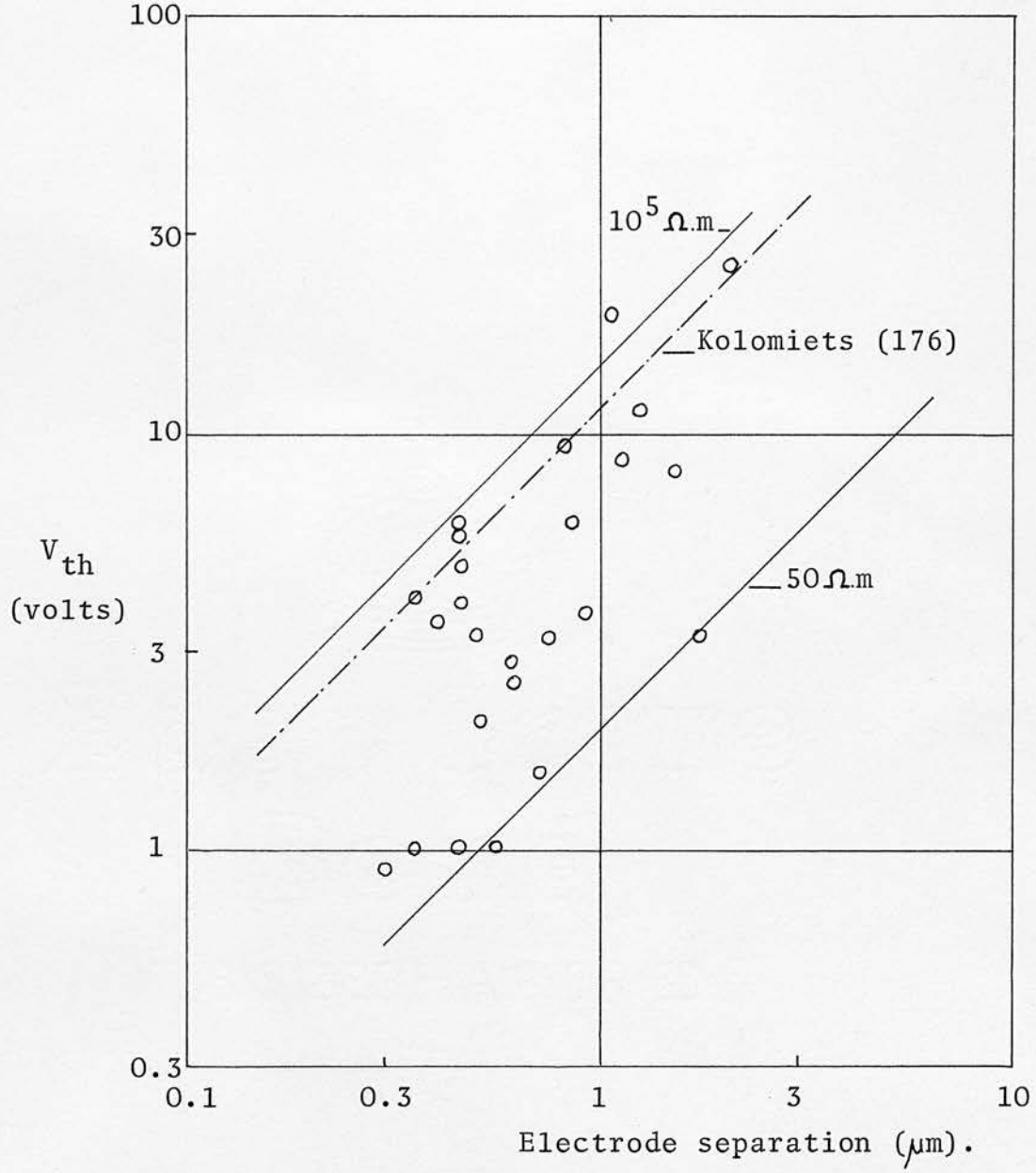

Variation of threshold voltage with electrode separation and film resistivity.

Fig. 6.39

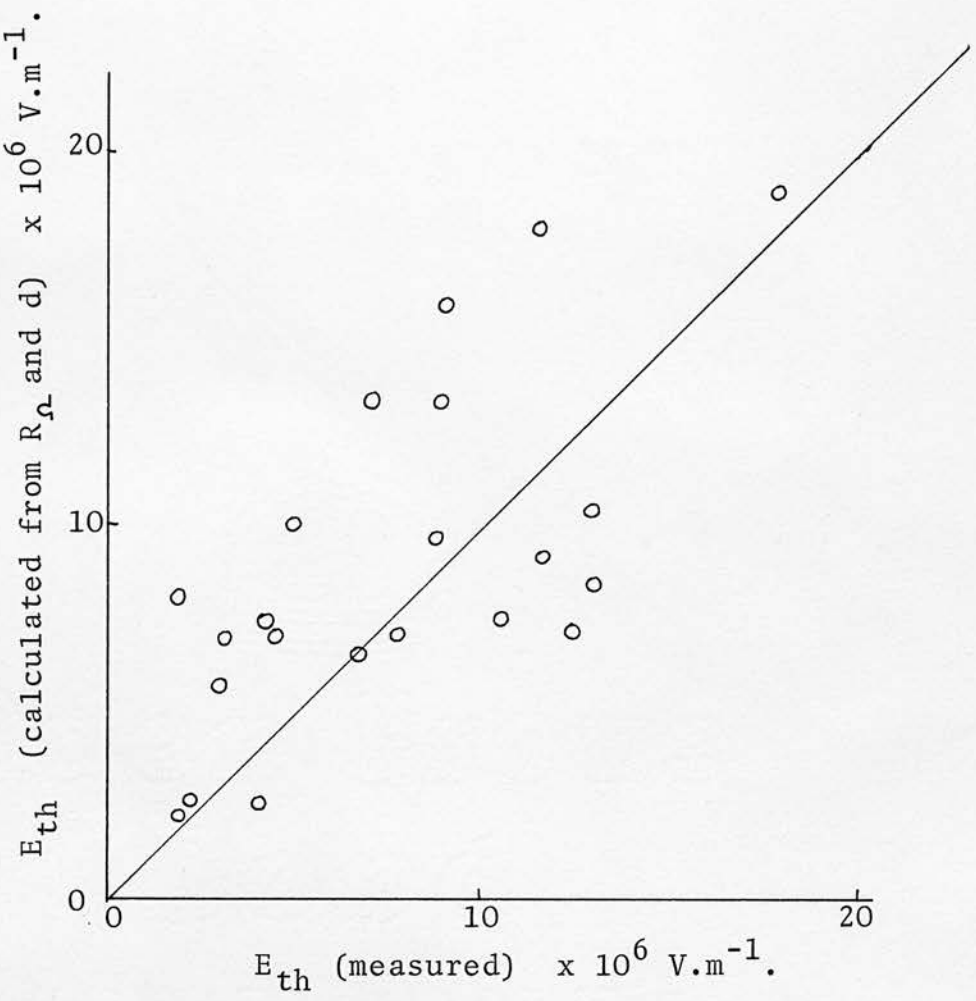

Comparison of calculated and measured values of breakdown field, E_{th}.

Fig. 6.40

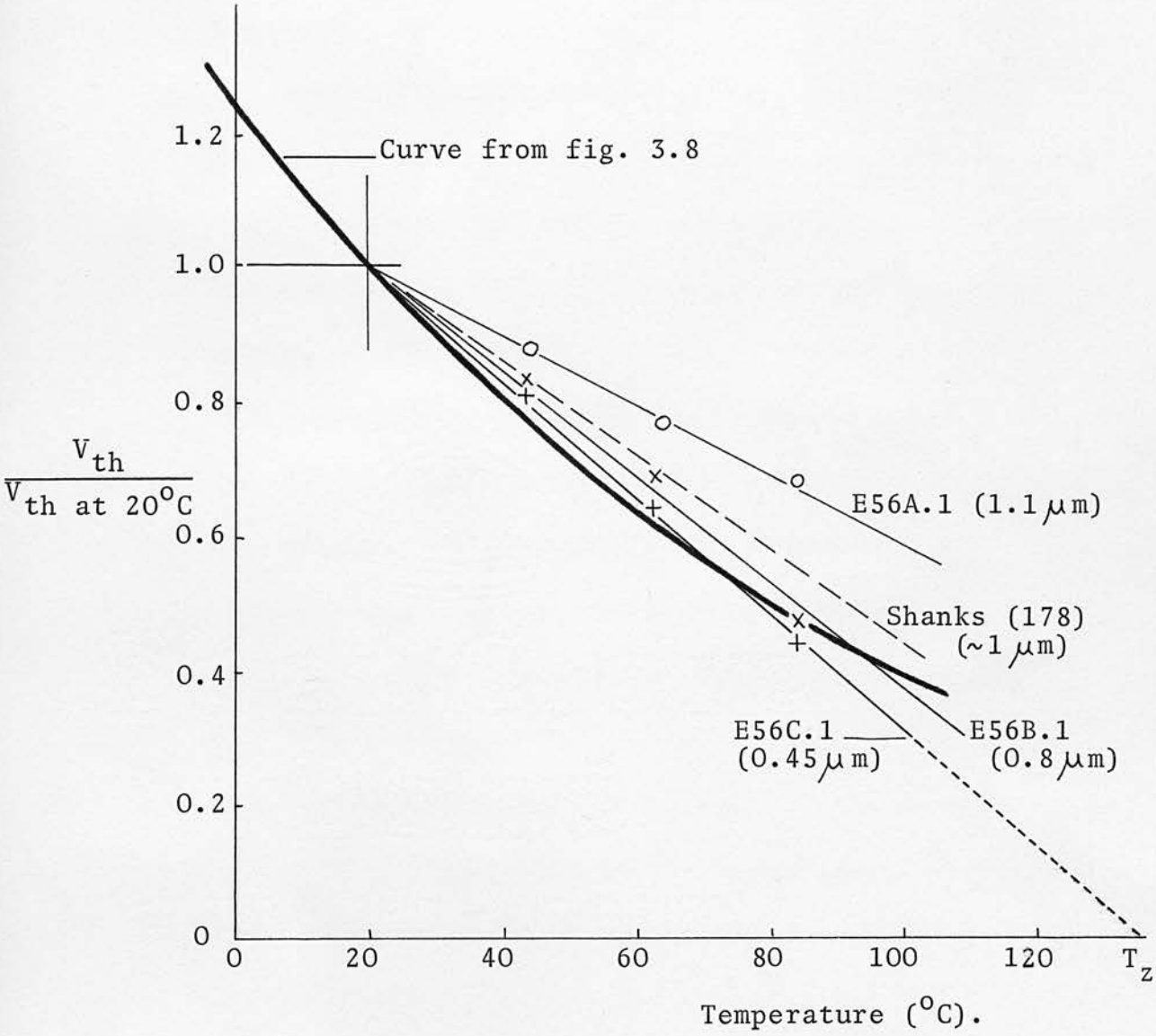

Variation of threshold voltage with temperature.

fig. 6.40. As expected from equation 6.34, the slope of the V_{th}-temperature lines depends on the sample thickness. The line given by Shanks (178) for a 1 μm thick film also fits the pattern of the E56 series.

The theoretical and experimental lines show good general correspondence in fig. 6.40. However, there is a slight difference in shape : the theoretical line has a distinct curvature, the experimental lines are straight. There are two possible explanations for this difference.

1. If V_0 is taken to be temperature independent, then $V_{th} \propto -a\,\Delta T$, i.e. lines of constant slope. However, the variation of V_0 with temperature for film E56 has been measured. It is significant and is shown in fig. 6.23. $V_0(T)$ should therefore be considered in any theoretical V_{th} - ΔT calculation.
2. In the derivation of data for fig. 3.8., it was assumed that Γ did not show any temperature-dependence. From detailed measurements of thermal breakdown in silicon monoxide, Klein has found that Γ increases with temperature (30). It has not been possible to make a quantitative measurement with thin chalcogenide films, but similar behaviour does appear to occur. The effect of this temperature-dependence of Γ is to offset the influence of $V_0(T)$ and therefore give $V_{th} \propto -\Delta T$.

In general terms, therefore, the steady state breakdown voltage conforms to the behaviour predicted by a thermal breakdown mechanism. If the effects of non-uniform heating and temperature dependent thermal conductance are considered, the variation of V_{th} with geometry, chalcogenide film properties and temperature can be predicted.

The experimental lines in fig. 6.40. may be extrapolated to give a temperature, T_z, at which $V_{th} = 0$. For sample E56 C 1 this occurs at 135°C. Walsh (194) has identified T_z with T_g the glass transition temperature of the chalcogenide glass used in the threshold switch. However, fig. 6.40 shows that T_z is thickness dependent so it is not uniquely determined by glass composition. In addition, although a value of T_g may be determined for the bulk glass which was evaporated to produce the thin film, it is much more difficult to ascribe a value of T_g to the thin film itself. Not only is the film composition likely to be different from the bulk glass, but the effective cooling rate which can be associated with a vapour deposition process is difficult to establish.

Under pulsed voltage conditions, each pulse may be considered as an isolated event if the repetition frequency is low. If a voltage pulse is applied to a sample so that it is close to the switching point, switching may be induced by widening the pulse if the initial length was of the same order or less than the thermal time constant for heating. A similar effect may be produced by decreasing the separation

between pulses to within a few multiples of the thermal time constant for cooling. Both effects are due to an increase in the sample internal temperature beyond the level at which an off-state can be maintained.

A typical current pulse shape for a device in the on-state is shown in fig. 6.41. The maximum current level is determined by the load resistor in series with the sample. The rise time for switching was faster than that for the oscilloscope amplifier (10 $ns.cm^{-1}$). The sample has a relatively low off-state resistance but a slight rise in the off-state current can be seen during the delay time, t_d, between application of the pulse and switching.

The conditions for impulse thermal breakdown in a sample which has field dependent conductivity were developed in section 3.3.7. The delay time, t_d, was related to the pulse voltage by the equation:

$$V^2 \exp\left(\frac{V}{V_0}\right) . t_d = \frac{C d^2 \rho_a}{a} \qquad \ldots\ldots 6.35$$

where the resistivity-temperature equation has the form given in equation 6.32(c) and $a = 0.04$. For typical chalcogenides, $C = 2.10^6\ J.m^{-3}.K^{-1}$.

As with the steady-state case, under impulse conditions the significance of the exponential term in equation 6.35 depends on geometry and composition. For thick or high conductivity samples where $V/V_0 < 1$ the relation $V^2 \propto t_d^{-1}$ occurs. This was the case

Fig. 6.41

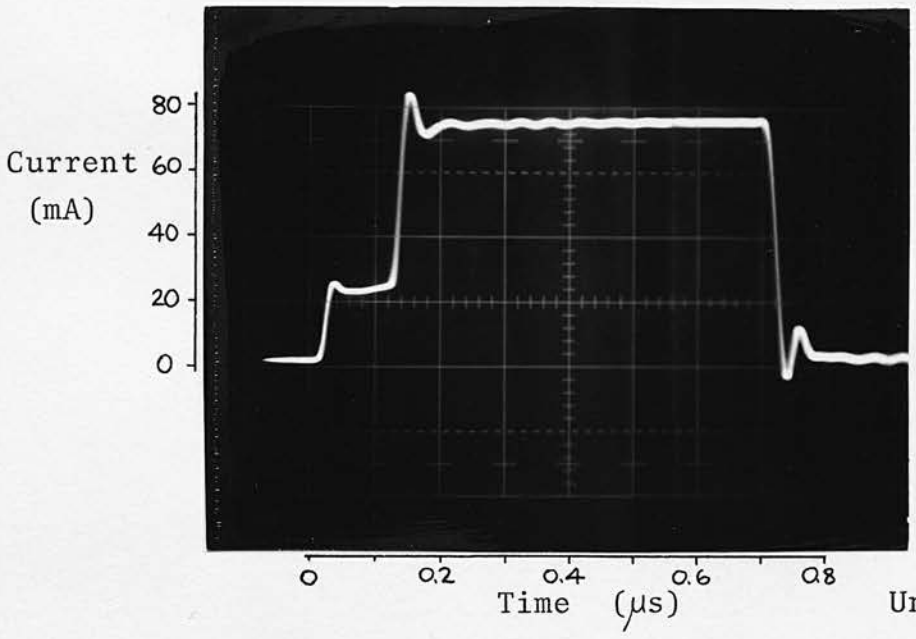

Switching under impulse conditions:
current through the device.

with thick bulk samples. When conditions allow $V > V_0$, the dependence approaches the form $V \propto \log t_d$. Results of variation of delay time with pulse voltage are shown in fig. 6.42. As the value of pulse voltage was reduced toward V_{th}, the delay time increased rapidly and when close to V_{th}, t_d fluctuated from cycle to cycle.

When two closely spaced voltage pulses were applied to a sample, the delay time of the second pulse depended on the separation between the two pulses: fig. 6.43. This may be taken as a measure of the time for a sample to recover from a switching operation. The variation of t_{d2} with pulse separation is shown in fig. 6.44. From this graph and that in fig. 6.42., the time for V_{th} to recover from a switching operation may also be derived.

The delay time recovery appears to be a two-stage process. It may be postulated that during the on-state of the first pulse, a high temperature filament exists in the sample. When the first pulse ends, the filament cools down. Recovery of t_d is very rapid to a point where the internal sample temperature is about 25 K above ambient. Up to this point (2 - 3 μs after the end of the first pulse) only a very low voltage is needed to heat or punch through the thin cool region of glass near the electrodes. In the second stage of the recovery process the internal sample temperature is only 0 - 25 K above ambient; the rate of heat loss is determined by the same process as in a sample biased in the pre-breakdown region. The second recovery

Fig. 6.42

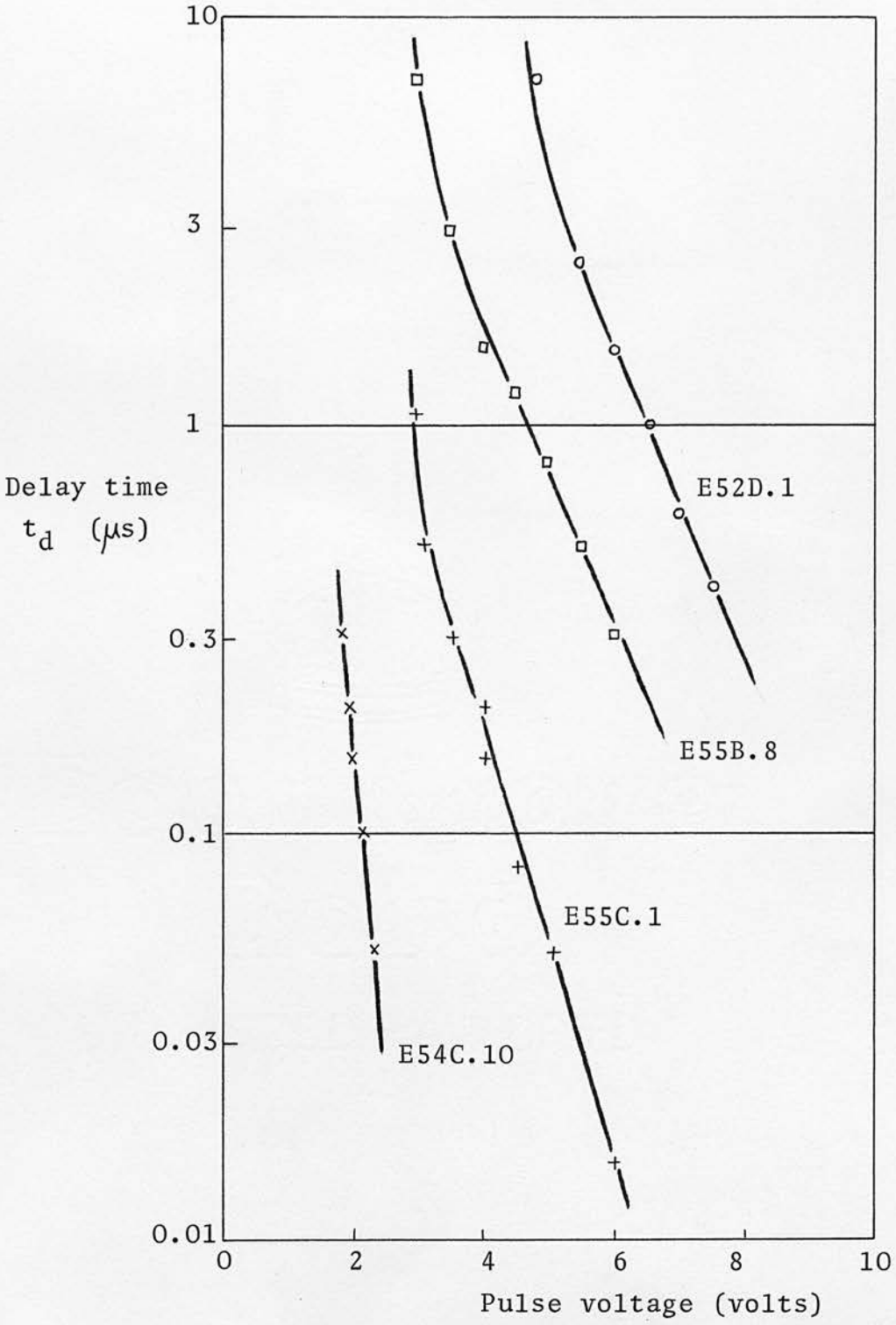

Influence of pulse voltage on delay time.

Fig. 6.43

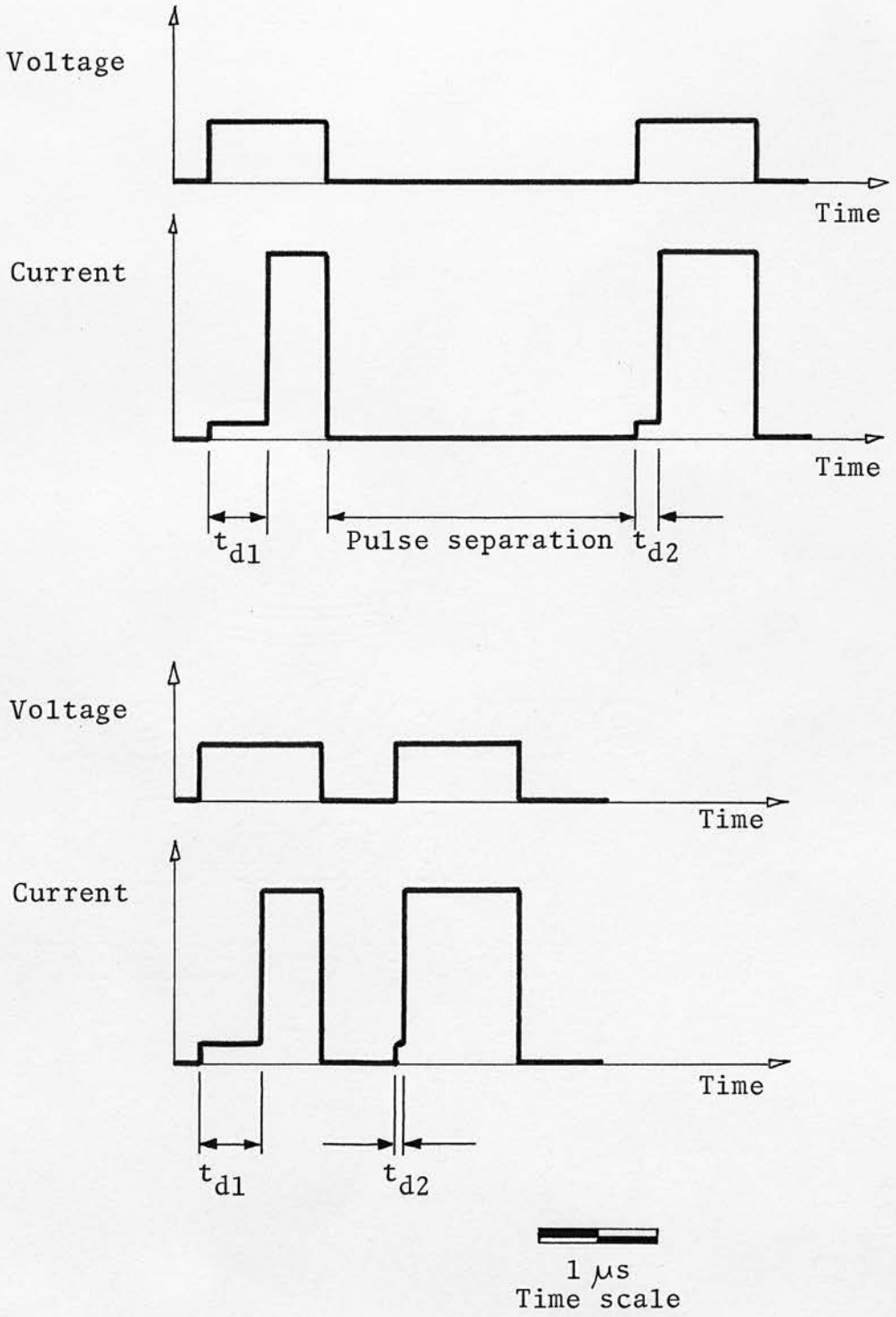

Recovery after switching: effect of pulse separation on delay time of second pulse.

Fig. 6.44

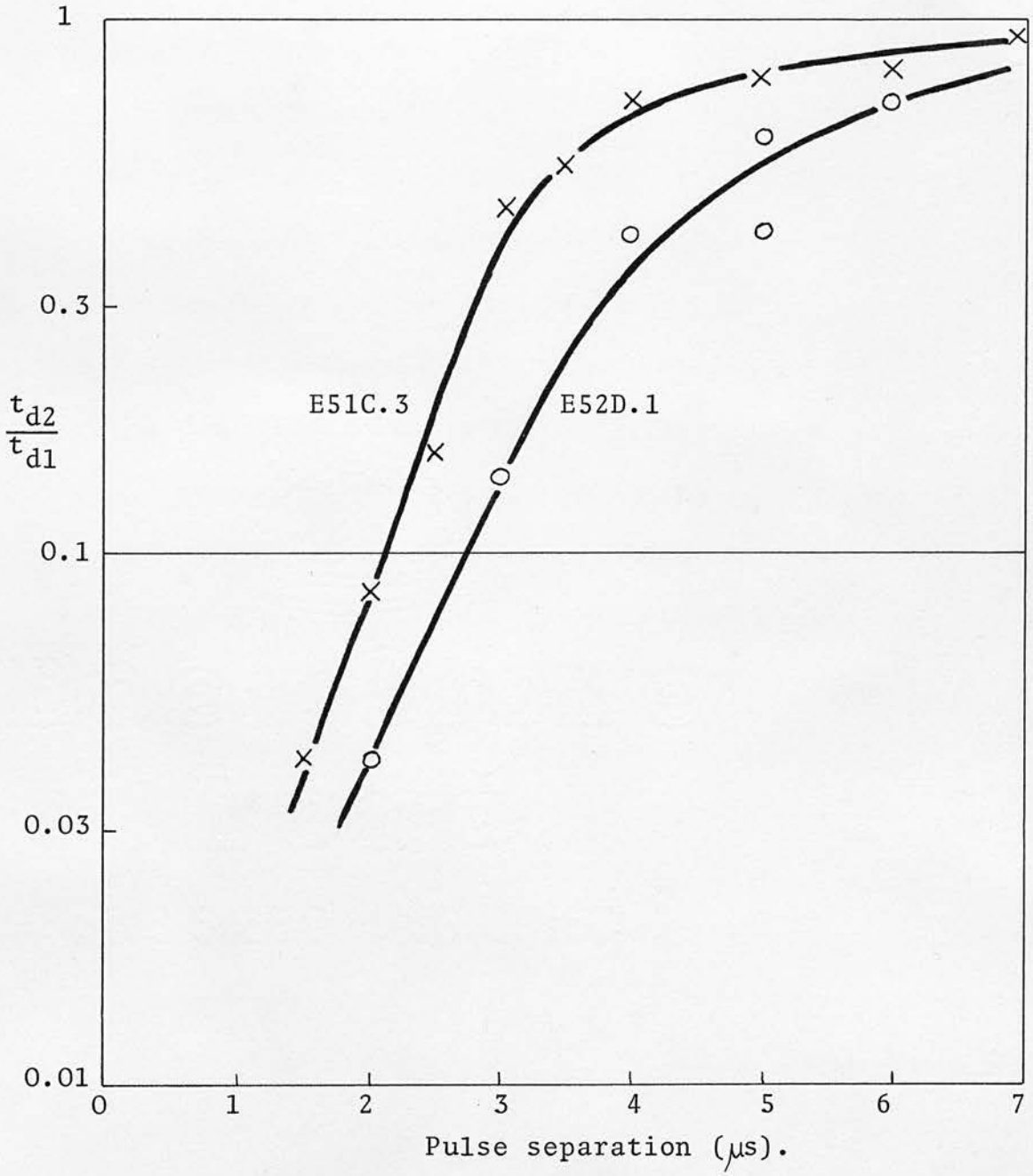

Recovery of delay time after switching.

stage should therefore occur over a time period which is similar to the cooling thermal time constant for the device. τ_d for E51 and E52 is approximately 20 μs. This is also the order of the recovery time in fig. 6.44.

The mechanism of thermal breakdown has been used to explain all the important features of threshold switching in thin films of chalcogenide glasses. However, there are two other processes which could also contribute to switching.

1. When a conducting path is formed between the electrodes, the capacitive energy of the sample will be discharged through it. This will have the effect of increasing the rate of thermal runaway and shortening the switching time.
2. As discussed in chapter 3, relatively cool, high resistance regions can exist near the electrodes. In these thin layers, tunnel currents may be significant or the high field could give an avalanche effect. In either case the result is the same as the capacitive discharge: the thermal runaway is assisted and a short switching time results.

The stability of the switching characteristics varied considerably from film to film. In high resistivity films where non-uniform heating occurred, the threshold voltage varied by as much as 50% between cycles. This may be due to a slight variation in the effective 'hot' area or in the filament position between cycles. Such effects are to

be expected with a simple crossover geometry where high fields can occur at the edges of the lower electrode. Films of relatively low resistivity gave much more stable results and also appeared to have more uniform heating across the whole area of the sample. For these units the variation in V_{th} was around 5%.

When threshold switches failed, they remained in the on-state. This is discussed in the next chapter in the context of memory switches.

6.4.9. The on-state

Thin chalcogenide films switch from the off-state to the on-state very rapidly. For the devices discussed in the preceeding sections the switching time, t_s, was shorter than 10 ns. This was the shortest time which could be measured with the equipment available. Published results, however, indicate that t_s is of the order of 100 ps (178). This is four orders of magnitude faster than typical delay time values.

In the bulk switching samples discussed in section 6.2.3., delay times were of the order of 1 s (fig. 6.7.) and switching times of the order of 0.1 ms (fig. 6.9.). However, the thermal breakdown analysis of section 3.3.7. indicates that the normalized rate of current increase at breakdown should not be geometry dependent. This is shown in fig. 3.11. The ratio $t_s : t_d$ would therefore be the same for both bulk and thin film samples so on the basis of a delay time of

1 μs, a switching time of 100 ps in thin films conforms to the thermal breakdown theory.

Fig. 3.11. shows a continuous curve for the increase in current with time. However, the formation of filaments, capacitive discharge and avalanche effects may all contribute to a more rapid rise in current. In addition, when t_s is measured on an oscilloscope, only the last order of magnitude increase in current is normally examined. This gives a minimum value for t_s, but even with times as short as 100 ps, the transition to the on-state remains consistent with thermal breakdown.

The on-state of a threshold switch is not very sensitive to experimental variables so it was not examined as closely as the off-state. The on-state is characterised by a holding voltage V_h which is approximately constant and a current which must be kept above a holding value I_h if the device is to remain in the on-state.

The on-state current does not depend on electrode area. This suggests that most of the current is confined to a small-area filament. This has been confirmed for threshold switches which can be locked into the on-state (4). Electrode separation and ambient temperature have no significant effect on on-state current or on V_h.

In order to obtain accurate measurements of on-state characteristics, stable reproducible devices are needed. Few of the thin film devices described in this chapter survived long in the high-current on-state so only superficial measurements and observations

were made. However, on-state properties provide a useful means of assessing the mechanism involved in switching. Accordingly, table 6.4 summarises on-state data obtained in this work and also that which has appeared in the literature. Figs. 6.45 and 6.46. show on-state I - V characteristics. Fig. 6.45. is from data published by Shanks (178). It is unique in giving current-voltage relations up to 1 amp. Fig. 6.46. is much more typical of low current level on-state characteristics (193). Above I_h there is a region of negative resistance and then an approximately constant V_h value.

Electronic mechanisms which could be used to explain threshold switching were reviewed in section 3.5.4. Although there are two mechanisms to describe the off-state, they give the same description for the on-state: energy barriers exist at each electrode so the on-state voltage should be approximately constant and equal to the band gap or (more accurately) the mobility gap. A current filament may exist and an increase in current is associated with an increase in filament diameter. A small decrease in V_h may also occur so the on-state characteristic would be like that of fig. 6.46. However, it is difficult to explain the high current characteristic of fig. 6.45. in terms of a purely electronic process.

The summary table indicates that V_h can have widely different values, even for electrodes of the same metal. In chalcogenide films the resistance activation energy is about 0.45 eV. This implies

Table 6.4

V_h (volts)	I_h (mA)	$V_h I_h$ (mW)	Electrodes	Reference
1.3	0.6	0.8	C	(178)
3	0.3	0.9	Mo	(193)
12	0.1	1.2	Mo	(193)
2.5	0.4	1	Au	(201)
4	-	-	Au	(201)
7	-	-	Au	(201)
3	-	-	-	(177)
2.8	0.4	1.1	Cu	(200)
3.0	0.4	1.2	Brass	(200)
1.8	0.3	0.6	V	(200)
1.3	1.9	2.5	C	(200)
20	0.06	1.2	Si	(200)
1 - 3	~1	1 - 2	Au,Mo	This project: thin films
10	~0.1	~1	Ag	This project: bulk glasses.

Note: the value of V_h has been taken at I_h.

Summary of experimental data for the on-state.

Fig. 6.45

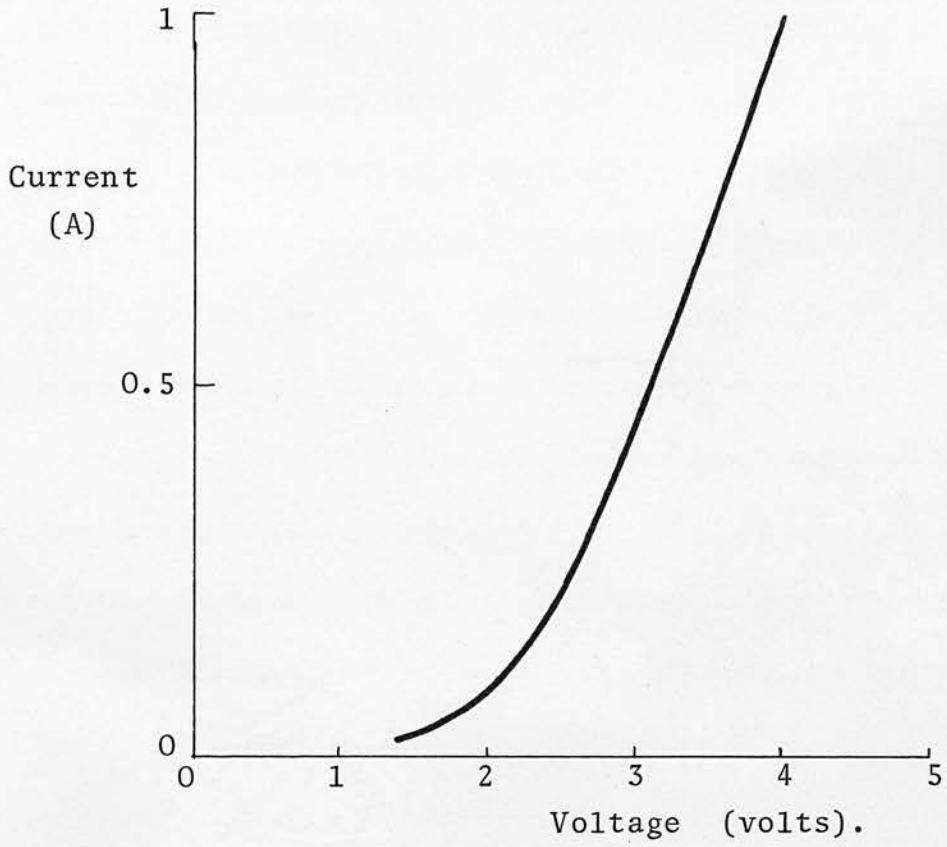

Fig. 6.46

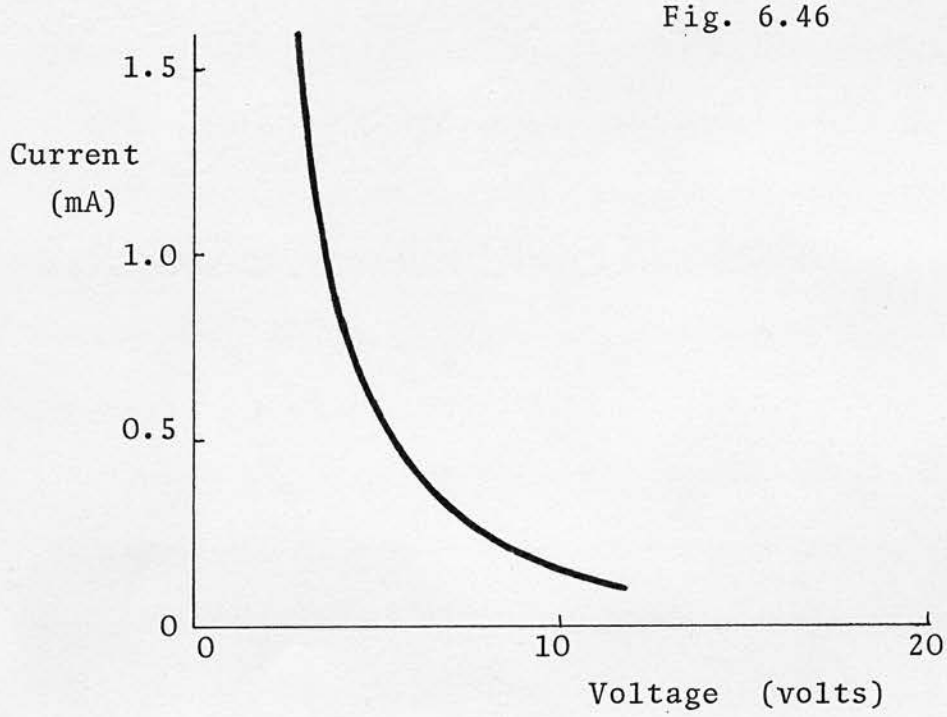

On-state current - voltage characteristics.

an energy gap of 0.9 eV if the material behaves as an intrinsic semiconductor. With carbon electrodes, V_h is close to the energy gap, but with other electrodes, particularly Au and Si where $V_h > 6$ volts, it is not possible to explain V_h in terms of a voltage across barrier layers. The electronic switching models therefore look reasonable only when applied to some types of glass-electrode combinations; they are not sufficiently flexible to explain all the results in table 6.4.

A current filament may be formed during thermal breakdown. A qualitative description of filament formation and its implications was given in section 3.3.6. The filament diameter is determined by current, voltage and internal temperature. In particular, the on-state voltage is determined by the temperature distribution between the electrodes, so V_h is not restricted to values in the range 1 - 2 volts. The temperature distribution is most easily varied in thick samples. In the bulk samples described in section 6.4. the on-state always has a near-zero dynamic resistance and V_h depends on the maximum current level. In thin films, the temperature distribution cannot be varied much so V_h remains approximately constant for any current level.

In fig. 3.10(a) there is a current level (marked B) below which a filament can no longer be sustained. This implies that the filament diameter and temperature have been reduced to a point where the rate of heat loss from the filament to the surrounding film and electrodes

is greater than the heat generated within the filament, i.e. there is a minimum power level needed to maintain a filament (and the on-state). Table 6.4 shows that the $V_h I_h$ product is approximately constant for a wide range of electrodes and geometries. The I - V characteristic just above I_h in fig. 3.10(a) (marked B - C) is very similar to the experimental curve in fig. 6.46.

In this work the thermal breakdown mechanism therefore gives a more accurate description of on-state characteristics than the electronic mechanisms of section 3.5.4.

If the on-state current filament is assumed to have an area of 10^{-10} m^2 when the current is 10 mA and V_h = 2 volts, the resistivity of the filament is 2.10^{-2} Ω.m. If the off-state resistivity is 10^4 Ω.m, resistivity changes by a factor 5.10^5 when switching occurs. This is equivalent to an increase in temperature within the filament of 330 K. Pearson has observed that if a low melting point metal such as lead is used as a top electrode in a sandwich device, the Pb film may melt locally (183). This may be taken as evidence of high temperatures associated with switching.

Many of the bulk chalcogenide glasses used to produce switching devices soften at temperatures below 350°C. If it is assumed that thin films have a glass transition temperature, T_g, which is similar to the value for bulk glasses of the same composition, then a temperature above T_g during the on-state could have several consequences:

1. Slow cooling may result in local crystallization.
2. Component separation within the film may occur.
3. Atoms of the electrode metal may diffuse into the chalcogenide film.

Threshold switches must not show any of these effects if good device lifetime is to be attained. It is therefore important to choose a chalcogenide glass which has a high thin film glass transition temperature and electrodes which provide a stable interface over a wide temperature range.

CHAPTER 7 MEMORY SWITCHING

7.1. INTRODUCTION

Some features of memory switches have already been discussed but it is useful to review the operation of these devices made from multicomponent chalcogenide glasses before discussing the experimental work done on them.

The glasses used for memory switches are chosen from compositions which lie close to the edge of glass-forming regions in the appropriate phase diagrams. In the amorphous phase, the resistivity is high and the switch is off. When energy is supplied to the glass, heating and possibly even local melting occurs. From this the on-state may be attained by one or both of two processes:

1. If the glass is allowed to cool slowly, crystallization may occur and usually the crystalline resistivity is much lower than that of the amorphous phase. Thus a conducting filament is formed between the electrodes.
2. Component separation may occur and a crystalline or metallic filament may be formed which has a composition which is quite distinct from the bulk of the glass.

In both cases the memory state is removed by supplying a sharply defined high-energy pulse which melts and rapidly quenches the region

around the conducting filament so that the glassy state is restored. It should be emphasised, however, that the glasses used in memory switches are very similar to those used for threshold switches but with a lower transition temperature and greater tendency to devitrification. As mentioned in section 1.1.3., there is a forming time necessary to establish a conducting filament in a memory glass. If pulses shorter than the forming time are applied, a memory switch shows typical threshold switch behaviour (4). Much of the work described in the previous two chapters is therefore relevant to memory switches as well as threshold switches.

Although it may be said that the basic mode of operation of memory switches is understood, there are serious technological problems which limit the development of reliable commercial devices. There is a difference in expansion coefficient of crystalline and amorphous materials. This can lead to voids, cracking and gross physical damage to devices. During switch-off, the whole filament may not be destroyed so on the next cycle, switching occurs at a lower threshold voltage. Similarly, the on-state may spread so that the filament size is increased. In turn this increases the pulse energy needed for switch-off. Volatile components such as As or Te may be vapourised with the result that the semiconductor composition changes slowly throughout the operational life of the switch.

All of these problems are associated with the switching process. Most memory applications would demand relatively few such operations

in the device lifetime. However, the device would be 'interrogated' much more frequently to ascertain whether it was in an off- or on-state. Since the glass composition was initially chosen so that it would easily devitrify, the cumulative effect of many interrogation pulses could be to precipitate devitrification and therefore switch the device on.

In order to make a more realistic assessment of the problems associated with memory switches, a preliminary investigation of the devices was made.

7.2. BULK MEMORY SWITCHING

7.2.1. Bulk memory glasses

The glass-forming regions of the ternary systems AsTeSi and AsTeGe are shown in figs. 5.1. and 5.2. respectively. The composition of a memory glass should be close to one of the boundaries. The composition used most was $As_{55}Te_{35}Ge_{10}$. (V38). This is in a small glass-forming region and has also been studied by Uttecht et al. (137). They observed component separation as a result of memory switching in this glass (fig. 3.30).

An unusual feature of V38 was that after it had been quenched, when the quartz tube was cut open, small shiny black platelets were found growing out from the material stuck to the walls near the (cooler) neck of the tube. The platelets were about 2 - 3 mm square and 15 μm thick. Their resistivity was 2.10^{-2} Ω.m. A similar type of growth has been observed with crystals of CdS (202). Chemical analysis indicated that in the case of V38, the platelets had an average composition : Ge 92%, Te 8% (by weight). The quantity of germanium in the platelets was small relative to that in the whole sample (< 5%). However, the result is important because it shows that even when glasses have been melted and rocked for 20 hours, complete mixing may not occur.

Another form of immiscibility was observed with samples composed of As, Te and Si. Where glasses were made up from As_2Te_3 + Si , a furnace temperature of 1000°C was sufficient to produce a melt and a

well-mixed glass resulted. In order to compare thin film properties with those of bulk glasses of similar composition, the mixtures $As_{20}Te_{75}Si_5$ and $As_{30}Te_{62}Si_8$ were sealed in capsules, put in a rocking furnace for 24 hours at 1000°C and then quenched. Inside the capsules were some glassy ingots but also some silicon powder which had not mixed with the As and Te.

It may therefore be necessary when producing memory-type glasses to use higher furnace temperatures and better agitation techniques than those which were standard in this work. There is also a need for more knowledge about the details of the phase diagrams of multicomponent chalcogenide glasses.

7.2.2. Memory switching in bulk samples

Flat bulk samples of the glass $As_{55}Te_{35}Ge_{10}$ (V38) were made by melting an ingot on a hot-plate (300°C) and then quenching it quickly while it was being pressed flat between two sheets of freshly cleaved mica. Typical dimensions were : 5 mm diameter and 0.5 mm thick. Contacts of silver paint and evaporated gold were used. Both gave similar results and the resistivity was $1.4.10^3\ \Omega.m$. This is lower than the value of $10^4\ \Omega.m$ reported by Uttecht et al. (137), but in V38 there was a slight loss of Ge due to the growth of small Ge platelets inside the melting capsule.

Crystallization of V38 could be induced by melting followed by slow cooling at about 1 - 5 $K.s^{-1}$ (as opposed to a cooling rate of $\sim 50\ K.s^{-1}$

which gives a glass). The crystalline resistivity was $10^{-2}\ \Omega$ .m which is in good agreement with the measurements of Uttecht. Strong pressure from a probe on the surface of the glass was also enough to convert some of the glass into the low-resistivity (crystalline) state.

Switching was observed in flat samples of V38 glass with two probes lightly positioned on the surface and an alternating voltage across them. The threshold voltage was not dependent on probe separation for distances of more than 1 mm.

With a high series resistor, threshold switching was observed. As the current-limiting resistor was reduced in value, the threshold voltage fell and eventually there was no evidence of any switching action. At this point there was a filament of melted material between the two probes. If the supply voltage were reduced quickly, the off-state returned and an increase in voltage produced threshold switching again. However, if the supply was reduced slowly (over about 10 s), the on-state remained even when the voltage was reduced to zero. To regain the off-state, a high current had to be passed and then cut off quickly.

Bulk memory switching was only examined with a 100 Hz supply. Over 10 - 20 memory operations and several thousand associated threshold operations, it gave consistent and repeatable results.

7.3. MEMORY SWITCHING IN THIN FILMS

The glass used in a memory switch should be readily devitrified. This in turn places requirements on the glass composition which are rather more exacting than those for threshold switching glasses. This is difficult to achieve experimentally since there is some difference between film and bulk compositions. The glass composition which showed memory action in the bulk material (section 7.2.2.) did not behave in the same way when it was evaporated to give a thin film device. The composition of a thin film could not be predicted accurately enough to give a memory-type film so the effect was only studied in films which happened to behave as memory switches rather than any which had been deliberately made as such.

Failure in threshold switches usually occurred with the device remaining in the on-state. This occurred more readily if the threshold switch were operated under 100 Hz a.c. conditions or if voltage pulses greater than V_{th} were applied, i.e. the delay time t_d was very short.

The high resistance off-state could be regained by applying a high current pulse or by passing a high current ($\sim$ 100 mA) in the on-state and then cutting off the supply quickly. The memory on-off cycle could be repeated about 10 times but it became more difficult to regain the off-state.

With films of As_2Te_3, memory switching occurred after only 1-10 threshold switching cycles and it was not possible to switch off with a high current pulse. As_2Te_3 exists in the bulk in a crystalline

phase and the amorphous phase can only be obtained with small rapidly quenched samples or with thin films. It is therefore reasonable to expect that the resistance change is due to crystallization of a portion of the As_2Te_3 film.

Crystalline and amorphous resistivities of As_2Te_3 were discussed in section 3.6.1. They are $3.10^{-3}\Omega.m$ and $10^{2}\Omega.m$ respectively. The as-prepared As_2Te_3 films had a low-field resistivity of $100\Omega.m$. This dropped at higher fields in a manner consistent with internal self-heating. The on-state resistance was not sensitive to electrode area, contact metal or temperature. However, the resistance value was much higher than that expected for uniform crystallization throughout the sample. It corresponded to local devitrification over a small region 10-20 μm diameter. This is approximately the filament size which has been observed in other memory switches (4) (203). Because of the stability of crystalline As_2Te_3 relative to the amorphous phase, it was not possible to switch off the small crystalline filament with a high current pulse.

The long-term stability of metal-glass contacts was not studied in detail. However, it is known that gold diffuses rapidly through chalcogenide glasses at temperatures above $300^{\circ}C$ and also that it is a good nucleating metal to help induce crystallization. In switches which operate by a thermal runaway mechanism, both diffusion and nucleation are likely to occur with gold electrodes and it is likely that the contacts played a significant part in the failure of threshold switches (into the

on-state).

To check the effect of high temperature on a device, a sandwich sample evaporated from a bulk ingot of $As_{30}Te_{48}Ge_{10}Si_{12}$ was heated for 2 hours at 170°C. The glass transition temperature for this bulk composition is around 250°C, but since the thin films are deficient in Si and Ge relative to the bulk glass, the effective glass transition temperature in the thin film is likely to be less than 250°C (cf. chapter 5). As a result of the heat treatment, the thin films resistivity dropped from 200 Ω.m to 10 Ω.m and the device still behaved as a threshold switch but with a lower off-state resistance. This suggests that gold diffusion from the electrodes was more important than crystallization for this particular case.

7.4. COMMENTS ON MEMORY SWITCHING

The investigation into memory switching has been very limited. However, the results are consistent with those published and indicate that local devitrification can produce a low-resistance filament which defines the on-state. The glass composition must be carefully chosen and to achieve predictable and repeatable thin film compositions, close control is needed over all stages of the deposition process. The principal factors which affect thin film deposition have been outlined in chapter 5.

Although gold is a very convenient contact metal to use, it has severe disadvantages for possible use in devices. More reliable operation could be achieved by using contacts of molybdenum or silicon which do not diffuse readily through chalcogenide glasses or help devitrification by providing nucleating centres.

CHAPTER 8 COMMENTS AND CONCLUSIONS

The literature on switching in amorphous semiconductors is extensive, but most publications have been restricted to small groups of experimental results. In particular there has been no attempt to examine the whole field of switching in relation to the general problem of dielectric breakdown. This thesis provides such a review. In practice most of the well-established dielectric breakdown processes require higher fields than are observed for switching in chalcogenide glasses.

Most of the experimental investigations on amorphous switches have been done over the past 2 - 3 years. Some of the work of this project was done independently of work which has since been published; this is an inevitable consequence of a rapidly developing subject. However, the work described in this thesis covers a wider range of experimental conditions than has been reported by any individual or group, so it has the advantage of experimental self-consistency and results can be compared since the experimental conditions are known.

There are several types of switching which have been observed in amorphous semiconductors. This project has concentrated on the chalcogenide glass switches because these devices are the closest to being commercially viable and because there is a degree of controversy

about their operating mechanism. The latter concerns the monostable or threshold switch and most experimental work was done on it. The mechanism of the memory or bistable switch is better understood so it was only studied briefly. However, the two types of switch share a common technology so much of the experimental effort and results for threshold switches can be easily applied to memory switches.

There are two schools of thought on the mechanism of threshold switching. One regards it as a purely electronic process; the other as a case of reversible thermal breakdown. The results and analysis of this project allow the two mechanisms to be compared and assessed.

The electronic switching mechanism proposed by Henisch (section 3.5.4.) can be used to explain qualitatively most of the features of threshold switching, e.g. the non-ohmic off-state characteristic, the delay time under impulse conditions, the very fast switching time, the constant on-state voltage and minimum holding current, the temperature dependence of V_{th} and V_h and the lack of any stable region of negative resistance between the off and on-states. However, the theory has not been developed much beyond a qualitative stage. Where it can be assessed quantitatively it is generally inadequate: the off-state characteristic cannot be described by a form of space charge limited current (section 6.4.2.); V_h is approximately constant but

it can be very much greater than the energy band gap (section 6.4.9.). The only point of potential agreement between theory and experiment is in the switching speed ($\sim 10^{-10}$s).

Application of thermal breakdown theory requires an accurate description of conductivity and thermal conductance. This has been done for a range of possible conditions and an accurate description of breakdown achieved for bulk, coplanar and sandwich samples. The former two, with electrode separations $> 10\ \mu$m, are accepted to show thermal breakdown. The sandwich samples produced by the same method as the coplanar also fit the theory if allowance is made for field-dependent conductivity. The origin of $\sigma = \sigma(E)$ has not been absolutely clarified, but it appears to arise from a form of hopping conduction with a temperature-activated jump distance.

A component of current can be identified as being due to Joule heating. With high resistivity samples, there appears to be non-uniform heating, but this is to be expected with a simple crossover-geometry. Thermal breakdown theory allows a quantitative prediction of V_{th}, t_d, t_s and their variation with temperature and geometry. It also gives a description of recovery from switching, thermal time constants, negative capacitance close to V_{th} and the non-ohmic I - V characteristic. If a high current filament is formed during switching, no region of negative resistance would exist, but the minimum on-state conditions would be described by a constant

power level (which is observed).

On the basis of this theory, the conditions needed for a good device can be established. There are also many problems which though not serious from a research viewpoint, would give poor device performance. The areas where more work is needed are:

1. General characterisation of chalcogenide glasses. This would include measurement of their basic transport properties, an understanding of their atomic structure, particularly in thin films and a more detailed description of the high field conduction mechanism.
2. The influence of composition on electrical properties.
3. An improved method of thin film deposition. The threshold voltage requirement for compatibility with transistor drive circuits limits the electrode separation to about 1 μm. The evaporation techniques used in this work gave films of different composition to the bulk starting material and in many cases it was difficult to achieve reproducible films easily. There are three techniques which could give improved results: an improved flash evaporation process, r.f. sputtering and sedimentation and firing of a suspension of glass in a suitable medium.
4. An improved device geometry with small area is required. This would give a high on: off resistance ratio. If the contact area were defined by a hole in an insulator film,

there would be a uniform field distribution in the chalcogenide film and probably fewer problems associated with non-uniform heating.

5. Stable contact metals are required. Internal temperatures greater than 300°C may occur in the on-state. The contacts must be stable and ohmic under these conditions. Gold was used in most of this work and though convenient is not suitable for extensive application. Nickel, molybdenum or silicon would appear to be better.
6. In the higher resistivity chalcogenide films, heating effects are only significant close to V_{th} because of the field-dependent conductivity. Thus as well as allowing a high off-resistance, such films should have more stable V_{th} values.
7. Commercial interest is needed to provide a goal and the incentive to solve the problems quickly.

REFERENCES

1 Fritzsche H., IBM Journal R. & D., 13, 1969, 515 - 521.

2 Fleming G.R., J. Non-Cryst. Solids, 2, 1970, 540 - 549.

3 Kobylarz T.J., J. Non-Cryst. Solids, 2, 1970, 515 - 527.

4 Neale R.G. et al., Symposium on Electrotechnical Glasses, Imperial College, London, 30th Sept. 1970.

5 Petz J.I. et al., J. Chem. Phys., 34, 1961, 526 - 529.

6 Zachariasen W.H., J. Amer. Chem. Soc., 54, 1932, 3841 - 3853.

7 Pearson A.D., J. Electrochem. Soc., 111, 1964, 753.

8 Hilton A.R. et al., Phys. & Chem. of Glasses, 7, 1966, 105 - 126.

9 Owen A.E., Glass Ind., 1967, 48, 637 - 642 and 695 - 699.

10 Marshall J.M., PhD Thesis, University of Edinburgh, 1970.

11 Owen A.E. & Robertson J.M., J. Non-Cryst. Solids, 2, 1970, 40 - 51.

12 Owen A.E., Contemp. Phys., 11, 1970, 257 - 286.

13 Uphoff H.L. & Healey J.H., J. App. Phys., 33, 1962, 2770 - 2773.

14 Cohen M.H., J. Non-Cryst. Solids, 4, 1970, 391 - 409.

15 Cohen M.H. et al., Phys. Rev. Letters, 22, 1969, 1065 - 1068.

16 Male J.C., Electronics Letters, 6, 1970, 91 - 92.

17 Croitoru N. et al., J. Non-Cryst. Solids, 4, 1970, 493 - 503.

18 Fagen E.A. & Fritzsche H., J. Non-Cryst. Solids, 2, 1970, 170 - 179.

19 Ridley B.K., Proc. Phys. Soc., 82, 1963, 954 - 966.

20 Burgess R.E., Can. J. Phys., 38, 1960, 369 - 374.

21 Wagner K.W., Trans. AIEE, 41, 1922, 288 - 298.

22 Fock V., Archiv. fur El., 19, 1927, 71 - 83.

23 Moon P.H., Trans. AIEE, 50, 1931, 1008 - 1021.

24 Becker J.A. et al., Trans. AIEE, 65, 1946, 711 - 725.

25 Sapoff M. & Oppenheim R., Proc. IEEE, 51, 1963, 1292 - 1305.

26 Collins F.M., J. Non-Cryst. Solids, 2, 1970, 496 - 503.

27 Jakob M., Heat Transfer vol.1., Wiley, 1955, 197.

28 Sze S.M., J. App. Phys., 38, 1967, 2951 - 2956.

29 Hartman T.E. et al., J. App. Phys., 37, 1966, 2468 - 2474.

30 Klein N., Trans. IEEE Electron Devices, ED 13, 1966, 281 - 289.

31 Burton P. & Brander R.W., Int. J. Electronics, 27, 1969, 517 - 525.

32 Brander R.W., Private communication.

33 Fishenden M., Introduction to Heat Transfer, Oxford, 1961, 47.

34 Klein N. & Burstein E., J. App. Phys., 40, 1969, 2728 - 2740.

35 Burgess R.E., Proc. Phys. Soc., 68B, 1955, 766 - 774.

36 Klein N. & Levanon N., J. App. Phys., 38, 1967, 3721 - 3728.

37 Stratton R., Progress in Dielectrics, 3, 1961, 234 - 292.

38 Frohlich H., Proc. Roy. Soc., A160, 1937, 230 - 245.

39 Seitz F., Phys. Rev., 76, 1949, 1376 - 1393.

40 O'Dwyer J.J., J. Phys. Chem. Solids, 28, 1967, 1137 - 1144.

41 Forlani F. & Minnaja N., Phys. Stat. Sol., 4, 1964, 311 - 324.

42 McKay K. & McAfee K., Phys. Rev., 91, 1953, 1079 - 1084.

43 McKay K., Phys. Rev., 94, 1954, 877 - 884.

44 Loeb L.B., Encyclopaedia of Physics, Springer, Berlin, 22, 1956, 445 - 530.

45 Chynoweth A.G., Phys. Rev., 109, 1958, 1537 - 1548.

46 Chynoweth A.G., J. App. Phys., 31, 1960, 1161 - 1165.

47 Baraff G.A., Phys. Rev., 128, 1962, 2507 - 2517.

48 Chynoweth A.G. & McKay K., Phys. Rev., 102, 1956, 369 - 376.

49 Senitzky B. & Moll J., Phys. Rev., 110, 1958, 612 - 620.

50 Muller M. & Guckel H., Trans. IEEE Electron Devices, ED 15, 1968, 560 - 568.

51 Rose D.J., Phys. Rev., 105, 1957, 413 - 418.

52 Martirosov I.M., Sov. Phys. - Semiconductors, 1, 1968, 899 - 903.

53 Ruge I. & Keil G., J. App. Phys., 34, 1963, 3306 - 3308.

54 Haitz R.H., Solid State Electronics, 7, 1964, 439 - 444.

55 Nield M. & Leck J., Brit. J. App. Phys., 18, 1967, 185 - 191.

56 Champlin K.S., J. App. Phys., 30, 1959, 1039 - 1050.

57 McIntyre R.J., J. App. Phys., 32, 1961, 983 - 995.

58 Haitz R.H., J. App. Phys., 36, 1965, 3123 - 3131.

59 McIntyre R.J., Trans. IEEE Electron Devices, ED 13, 1966, 164 - 168.

60 Main C., Private communication.

61 Crowell C. & Sze S.M., App. Phys. Lett., 9, 1966, 242 - 244.

62 Tyagi M., Solid State Electronics, 11, 1968, 99 - 128.

63 Simmons J., J. App. Phys., 34, 1963, 1793 - 1803.

64 Gunn J.B., Proc. Phys. Soc., 69, 1956, 781 - 790.

65 Koenig S.H., J. Phys. Chem. Solids, 2, 1957, 268 - 276.

66 Melngailis I. & Milnes A. J. App. Phys., 33, 1962, 995 - 1000.

67 Steele M.C. et al., Proc. IRE, 47, 1959, 1109 - 1117.

68 McWhorter A. & Rediker R., Proc. IRE, 47, 1959, 1207 - 1213.

69 Shockley W., Bell Syst. Tech. J., 33, 1954, 799 - 826.

70 Read W., Bell Syst. Tech. J., 37, 1958, 401 - 446.

71 Hines M.E., Trans. IEEE Electron Devices, ED 13, 1966, 158 - 163.

72 Lee C.A. et al., Trans. IEEE Electron Devices, ED 13, 1966, 175 - 180.

73 Lampert M.A., Reports on Progress in Physics, 27, 1964, 329 - 367.

74 Rose A., J. App. Phys., 35, 1964, 2664 - 2678.

75 Mott N.F. & Gurney R., Electronic Processes in Ionic Crystals, Oxford, 1940, 172.

76 Lampert M.A., Phys. Rev., 103, 1956, 1648 - 1656.

77 Rose A., Phys. Rev., 97, 1955, 1538 - 1544.

78 Hartke J.L., Phys. Rev., 125, 1962, 1177 - 1185.

79 Ashley K. & Milnes A., J. App. Phys., 35, 1964, 369 - 374.

80 Mayer J.W. et al., Phys. Rev., 137A, 1965, 286 - 301.

81 Wagener J. & Milnes A., Solid State Electronics, 8, 1965, 495 - 507.

82 Henderson H.T., Proc. IEEE, 57, 1969, 1677.

83 Lebedev A. & Sultanov N., Sov. Phys. Semicond., 3, 1969, 276 - 277 and 108 - 109.

84 Jordan A. & Knepper R., App. Phys. Lett., 6, 1965, 126 - 128.

85 Iida M. et al., Jap. J. App. Phys., 7, 1968, 1078 - 1083.

86 Lebedev A. & Sultanov N., Sov. Phys. Semicond., 2, 1969, 1295 - 1296.

87 Chino K. et al., Jap. J. App. Phys., 8, 1969, 314 - 318.

88 Lebedev A. & Sultanov N., Sov. Phys. Semicond., 3, 1969, 530 - 531.

89 Ferro A.P., App. Phys. Lett., 16, 1970, 196 - 198.

90 Barnett A.M., IBM Journal R & D., 13, 1969, 522 - 528.

91 Henisch H.K. et al., J. Non-Cryst. Solids, 4, 1970, 538 - 547.

92 Mott N.F., Contemp. Phys., 10, 1969, 125 - 138.

93 Mott N.F., Festkorperprobleme, 9, 1969, 22 - 45.

94 Lindmayer J. & Slobodskoy A., Solid State Electronics, 6, 1963, 495 - 503.

95 Bowers H.C., Trans. IEEE Electron Devices, ED 15, 1968, 343 - 350.

96 Tillman J.R. & Henderson J.C., Phil. Mag., 44, 1953, 677 - 696.

97 Benzer S., J. App. Phys., 20, 1949, 804 - 815.

98 Hunter L.P., Phys. Rev., 1951, 151 - 152, 81.

99 Burgess R.E., Proc. Phys. Soc., 68B, 1955, 908 - 917.

100 Cutler M., Trans. IRE., Electron Devices, ED 5, 1957, 201 - 206.

101 Schafft H. & French J., Trans. IEEE Electron Devices, ED 13, 1966, 613 - 618.

102 English A.C., Solid State Electronics, 6, 1963, 511 - 521.

103 Melchior H. & Strutt M., Proc.IEEE, 52, 1964, 439 - 446.

104 Popescu C., Solid State Electronics, 13, 1970, 887 - 901.

105 Khuranu B.S. et al., Trans. IEEE Electron Devices, ED 13, 1966, 763 - 770.

106 Weitzsch F., Trans. IEEE Electron Devices, ED 13, 1966, 731 - 734.

107 Pamplin B.R., Contemp. Phys., 11, 1970, 1 - 19.

108 Gaylord T.K. et al., Trans. IEEE Electron Devices, ED 15, 1968, 777 - 788.

109 Simmons J. & Verderber R., Proc. Roy. Soc., A301, 1967, 77 - 102.

110 Dearnaley G. et al., J. Non-Cryst. Solids, 4, 1970, 593 - 612.

111 Pearson A.D., J. Eletrochem. Soc., 111, 1964, 753 - 755.

112 Roy R. & Caslavska V., Solid State Commun., 7, 1969, 1467 - 1473.

113 Vengel T. & Kolomiets B., Sov. Phys. Tech. Phys., 2, 1957, 2314.

114 Bagley B.G., J. Non-Cryst. Solids, 2, 1970, 155 - 169.

115 Adler D. et al., J. Non-Cryst. Solids, 4, 1970, 330 - 337.

116 Mott N.F., Phil. Mag., 17, 1968, 1259 - 1284.

117 Gildart L., J. Non-Cryst. Solids, 2, 1970, 240 - 249.

118 Price B.L., M.Sc. Thesis, Fairleigh Dickinson University, Taeneck, N.J., 1967.

119 Mattis D. & Landovitz L., J. Non-Cryst. Solids, 2, 1970, 454 - 473.

120 Mattis D., Phys. Rev. Lett., 22, 1969, 936 - 939.

121 Lipsicas M. et al., J. Non-Cryst. Solids, 2, 1970, 550 - 557.

122 Bongers P. & Enz U., Philips Res. Reports, 21, 1966, 387 - 389.

123 Futaki H., Jap. J. App. Phys., 4, 1965, 28 - 41.

124 Drake C.F. et al., Phys. Stat. Sol., 32, 1969, 193 - 208.

125 Drake C.F. & Scanlan I., J. Non-Cryst. Solids, 4, 1970, 234 - 247.

126 Eisenberg A., Inorg. Macromol. Rev., 1, 1970, 75 - 88.

127 Gupta Y., J. Non-Cryst. Solids, 3, 1970, 148 - 154.

128 Chan W. & Jonscher A.K., Phys. Stat. Sol., 32, 1969, 749 - 761.

129 Frank S., PhD Thesis, University of Sheffield, 1967.

130 Vasko A., Private communication.

131 Avetikyan G.B. et al., Inorg. Materials (Consultants Bureau Translation), 5, 1969, 1411 - 1413.

132 Park K.C. & Basaviah S., J. Non-Cryst. Solids, 2, 1970, 284 -291.

133 Klein N., Trans IEEE Electron Devices, ED 13, 1966, 788 - 805.

134 Gibbons J. & Beadle W., Solid State Electronics, 7, 1964, 785 -797.

135 Puddy D.C., M.Sc. Thesis, University of Manchester, 1965.

136 Bruyere J. & Chakraverty B., App. Phys. Lett., 16, 1970, 40 - 43.

137 Uttecht R. et al., J. Non-Cryst. Solids, 2, 1970, 358 - 370.

138 Kikuchi M. & Iizima S., App. Phys. Lett., 15, 1969, 323 - 325.

139 Gildart L., J. Non-Cryst. Solids, 2, 1970, 240 - 249.

140 Silva P.O. et al., J. Non-Cryst. Solids, 2, 1970., 316 - 333.

141 Chapman R., Electronics Letters, 5, 1969, 246 - 247.

142 Shanefield D. & Lighty P., App. Phys. Lett., 16, 1970, 212 - 214.

143 Evans E.J., J. Non-Cryst. Solids, 2, 1970, 334 - 346.

144 Holonyak N., Proc. IEEE, 50,1962, 2421 - 2428.

145 Braunstein M., App. Phys. Lett., 10, 1967, 313 - 315.

146 Kuwano H. et al., Jap. J. App. Phys., 4, 1965, 383 - 384.

147 Nimtz G. & Seeger K., App. Phys. Lett., 14, 1969, 19 - 21.

148 Konyaev S.I. et al., Sov. Phys. Semicond., 2, 1969, 1395 - 1396.

149 Feldman C. & Gutierrez W., J. App. Phys., 39, 1968, 2474 - 2476.

150 Feldman C. & Moorjani K., J. Non-Cryst. Solids, 2, 1970, 82 - 90.

151 Feldman C. & Moorjani K., Thin Solid Films, 5, 1970, R1 - R4.

152 Hughes W.E., Proc. IEEE, 56, 1968, 1715.

153 Pervova L.Y. et al., Sov. Phys. Semicond., 3, 1969, 254 - 255.

154 Ogorodnik A.D. et al., Sov., Phys. Semicond., 3, 1969, 717 - 719.

155 Lee P.A. et al., Solid State Commun., 7, 1969, 1359 - 1361.

156 Bullock D. & Epstein D., App. Phys. Lett., 17, 1970, 199 - 201.

157 Monk J.S. & Learn A., Proc. IEEE, 56, 1968, 68.

158 Robertson J., M.Sc. Thesis, University of Dundee, 1968.

159 Chopra K., Proc. IEEE, 51, 1963, 1242.

160 Eastman L.F., Trans. IEEE Electron Devices, ED 13, 1966, 117 - 121.

161 Baev I.A., Sov. Phys - Solid State, 6, 1965, 3007 - 3008.

162 Wei L. & Shewchun J., Proc. IEEE, 51, 1963, 946.

163 Hickmott T. & Hiatt W., Solid State Electronics, 13, 1970, 1033 - 1047.

164 Chopra K.L., Proc. IEEE, 51, 1963, 941 - 942.

165 Lo S-F., Proc. IEEE, 52, 1964, 609 - 610.

166 Hed A. & Freud P., J. Non-Cryst. Solids, 2, 1970, 484 - 495.

167 Argall F., Solid State Electronics, 11, 1968, 535 - 541.

168 Pearson A.D. et al., J. Electrochem. Soc., 109, 1962, 243C.

169 Pearson A.D. et al., Adv. Glass Technology, Plenum, N.Y., 1962, 357 - 365.

170 Eaton D.L., J. Amer. Ceram. Soc., 47, 1964, 554 - 558.

171 Kolomiets B. & Lebedev E., Radio Eng. & Elect. Phys., 1963, 1941 - 1943.

172 Busch G. et al., Phys. Lett., 33A, 1970, 64 - 65.

173 Ovshinsky S.R., Phys. Rev. Lett., 21, 1968, 1450 - 1453.

174 Ovshinsky S.R., J. Non-Cryst. Solids, 2, 1970, 99 - 106.

175 Servini A. & Jonscher A.K., Thin Solid Films, 3, 1969, 341 - 365.

176 Kolomiets B.T. et al., Sov. Phys. Semicond, 3, 1969, 267 - 268.

177 Kolomiets B.T. et al., Sov. Phys. Semicond., 3, 1969, 621 - 624.

178 Shanks R.R., J. Non-Cryst. Solids, 2, 1970, 504 - 514.

179 Boer K.W. et al., J. Non-Cryst. Solids, 4, 1970, 573 - 582.

180 Ovshinsky S.R. et al., Trans. IEEE Nuc. Sci., NS15, 1968, 311 - 321.

181 Fritzsche H., J. Non-Cryst. Solids, 2, 1970, 343 - 405.

182 Stocker H.J., J. Non-Cryst. Solids, 2, 1970, 371 - 381.

183 Pearson A.D. & Miller C.E., App. Phys. Letters, 14, 1969, 280 - 282.

184 Vogel R. & Walsh P., App. Phys. Letters, 14, 1969, 216 - 218.

185 Warren A.C., Electronics Letters, 5, 1969, 461 - 462.

186 Stocker H.J. et al., J. Non-Cryst. Solids, 4, 1970, 523 - 535.

187 Warren A.C. & Male J.C., Electronics Letters, 6, 1970, 567 - 569.

188 Csillag A. & Jager H., J. Non-Cryst. Solids, 2, 1970, 133 - 140.

189 Hilton A.R. & Brau M., Infra-red Physics, 3, 1963, 69 - 76.

190 Pliskin W. & Conrad E., Electrochem. Tech., 2, 1964, 196 - 200.

191 Dienst J. et al., RCA Review, 28, 1967, 585 - 594.

192 Honig R. & Kramer D., RCA Review, 30, 1969, 285 - 305.

193 Neale R.G., J. Non-Cryst. Solids, 2, 1970, 558 - 574.

194 Walsh P.J. et al., Phys. Rev., 178, 1969, 1274 - 1279.

195 Hartke J.L., J. App. Phys., 39, 1968, 4871 - 4872.

196 Jonscher A.K., Thin Solid Films, 1, 1967, 213 - 234.

197 Mark P. & Hartman T.E., J. App. Phys., 39, 1968, 2163 - 2164.

198 Yeargan J.R. & Taylor H.L., J. App. Phys., 39, 1968, 5600 - 5604.

199 Hyde F.J., J. Electronics & Control, 1, 1955, 303 - 312.

200 Altunyan S.A. & Stafeev V.I., Sov. Phys. Semicond., 4, 1970, 431 - 433.

201 Wisbey P.H., Symp. on Amorphous Materials, Chelsea College, London, 28/29th March 1969.

202 Fochs P.D., J. App. Phys., 31, 1960, 1733 - 1734.

203 Coward A., J. Non-Cryst. Solids, To be published 1971.

LIST OF SYMBOLS

Symbol	Section where defined	Units	Meaning
a	2.3.	K^{-1}	Constant in σ - T equation
a	6.4.3.	m	Distance between trapping sites
A	3.3.3.	m^2	Electrode area
A	3.4.1.	W	Rate of energy transfer from field to electron
b	6.4.6.	$W.m^{-3}.K^{-1}$	Constant
b	3.2.	-	Fraction of total area
B	3.4.1.	W	Electron-phonon energy transfer rate
B	3.3.7.	-	Parameter depending on pulse length
C	2.2.3.	$J.K^{-1}.m^{-3}$	Heat capacity
C	3.5.3.	F	Capacitance
CCNR	1.1.1.	-	Current controlled negative resistance
d	3.3.3.	m	Electrode separation
e	3.4.1.	C	Electronic charge
E	3.2.	$V.m^{-1}$	Electric field
E_{opt}	2.2.3.	eV	Optical energy gap

Symbol	Section	Units	Meaning
E_0	3.3.4.	$V.m^{-1}$	Constant in field-dependent conductivity expression
E_t	3.5.3.	eV	Trap depth below conduction band
g	3.3.1.	Ω^{-1}	Incremental conductance
G_Ω	6.4.7.	Ω^{-1}	Ambient low field conductance ($= R_\Omega^{-1}$)
h	3.3.1.	$A.K^{-1}$	Temperature coefficient of current
h	3.4.1.	J.s	Planck's constant
H	3.3.7.	m	Substrate thickness
i, I	3.3.3.	A	Current
I_h	1.1.2.	A	Minimum on-state holding current
I_0	3.3.3.	A	Pre-exponential parameter
J	3.2.	$A.m^{-2}$	Current density
k	2.3.	$eV.K^{-1}$	Boltzmann's constant
K	3.3.7.	$W.m^{-1}.K^{-1}$	Thermal conductivity of substrate
M	3.4.3.	-	Avalanche multiplication factor
n	3.5.3.	m^{-3}	Free carrier density
n_t	3.5.3.	m^{-3}	Trapped carrier density
N_c	3.5.3.	m^{-3}	Density of states at the bottom of the conduction band
N_t	3.5.3.	m^{-3}	Trap density

Symbol	Section	Units	Meaning
p	6.4.3.	-	Probability of hopping
P	3.3.1.	W	Power
P_{th}	6.2.2.	W	Power at threshold ($V_{th}.I_{th}$)
Q	3.5.3.	C	Charge
R	3.3.1.	Ω	Resistance
R_L	3.2.	Ω	Load resistor
R_n	3.2.	Ω	Slope in negative resistance region of I - V curve
R_Ω	6.2.2.	Ω	Low field ohmic resistance ($= G_\Omega^{-1}$)
RMM	1.1.3.	-	Read-mostly-memory
ROM	1.2.3.	-	Read-only-memory
$\dot{s}$	3.2.	$W.m^{-3}.K^{-1}.s^{-1}$	Entropy production rate
t	6.4.2.	$m.V^{-1}$	Trapping parameter
t_d	1.1.2.	s	Delay time
t_f	1.1.3.	s	Forming time
t_0	4.3.2.	s	Constant in $V_p - t_d$ expression
t_s	1.1.2.	s	Switching time
T_c	3.5.3.	K	Parameter which characterises a trap distribution
T_g	2.1.	K	Glass transition temperature
T_m	2.1.	K	Crystal melting point
T_0	3.4.1.	K	Lattice temperature
T_s	6.3.1.	K	Surface temperature

Symbol	Section	Units	Meaning
T_z	6.4.8.	K	Temperature at which $V_{th} = 0$
$\bar{v}$	6.4.3.	$m.s^{-1}$	Mean drift velocity
V	1.1.1.	V	Voltage
V_2	3.3.3.	V	Constant in I - V expression
VCNR	1.1.1.	-	Voltage controlled negative resistance
V_h	1.1.2.	V	On-state holding voltage
V_0	4.3.2.	V	Constant in V_p - t_d expression
V_{th}	1.1.2.	V	Switching threshold voltage
V_{th0}	4.3.2.	V	Constant in V_{th} - T expression
W	6.3.1.	m	Width of contact strip
x(y and z)	3.3.3.	m	Dimensions
x	3.3.1.	-	Constant
x_m	6.4.4.	m	Distance to field maximum
y	3.3.1.	-	Constant
$Y(\omega)$	3.3.9.	Ω^{-1}	Admittance
Z	3.3.1.	Ω	Impedance
α	6.3.1.	$m^2.s^{-1}$	Ratio of thermal conductivity to heat capacity
α	2.2.3.	m^{-1}	Optical absorption coefficient
α	3.4.3.	m^{-1}	Avalanche ionization rate
β	6.4.4.	$C\,(V.m)^{\frac{1}{2}}$	Poole-Frenkel coefficient
Γ	3.3.1.	$W.K^{-1}$	Thermal conductance

Symbol	Section	Units	Meaning
Γ_w	3.3.9.	$W.K^{-1}$	Frequency-dependent thermal conductance
δ	3.5.4.	-	Normalized current density
ΔE	2.3.	eV	Activation energy
ΔT	2.3.	K	Temperature increase above ambient
$\Delta\phi$	6.4.4.	eV	Reduction in barrier due to field
ϵ	3.3.3.	K^{-1}	Temperature coefficient of resistance
ϵ_0	3.5.3.	$F.m^{-1}$	Primary electric constant
$\mathcal{E}$	3.4.1.	J	Electron energy
ξ	3.3.3.	-	Normalized distance from electrode
θ	3.5.3.	-	Free : trapped charge ratio
κ	2.2.3.	$W.K^{-1}.m^{-1}$	Thermal conductivity
κ_i	3.3.4.	-	Dielectric constant
Λ	3.3.3.	-	Parameter describing temperature distribution
μ	3.4.1.	$m^2.V^{-1}.s^{-1}$	Carrier mobility
ν	3.4.1.	s^{-1}	Phonon frequency
ν_0	6.4.3.	s^{-1}	Vibration frequency of carrier in a well
ρ	3.3.3.	$\Omega.m$	Resistivity (= σ^{-1})
ρ_a	3.3.3.	$\Omega.m$	Resistivity at ambient temperature

Symbol	Section	Units	Meaning
σ	2.3.	$(\Omega.m)^{-1}$	Conductivity ($= \rho^{-1}$)
σ_a	2.3.	$(\Omega.m)^{-1}$	Conductivity at ambient temperature
σ_0, σ_1	2.3.	$(\Omega.m)^{-1}$	Constant in σ - T expression
$\sigma_{p,n}$	3.5.3.	m^2	Capture cross section for holes, electrons
τ	3.3.9.	s	Thermal time constant
τ_t	3.5.3.	s	Transit time
ϕ	6.4.3.	eV	Depth of potential well
ϕ_1	3.3.4.	eV	Poole-Frenkel trap depth
ψ	6.4.3.	eV	Jump distance activation energy
ω	3.3.9.	$rad.s^{-1}$	Angular frequency

APPENDIX EXPERIMENTAL DATA

1. Bulk glasses

Nomenclature

Each melt was given a number for identification. The number is preceeded by the letter 'V' to indicate that the glass was melted under vacuum. All compositions are expressed in atomic %.

Details of glasses

Number	Composition	Resistivity (Ω.m)	Comments
V9	$Ge_5 Se_{95}$	10^9	MELTED AT 930°C
V12	"	$1.5\ 10^0$	870
V18	"	$5\ 10^9$	700
V19	"	$3\ 10^9$	600
V20	$As_{30} Te_{48} Si_{12} Ge_{10}$	10^4	BULK SWITCHING.
V22	$(As_2Te_3)_{60} . Si_{40}$	10^8	USED FOR EVAPORATION MAINLY
V28	$(As_2Te_3)_{60} . Si_{40}$	10^8	
V29	$(As_2Te_3)_{70} . Si_{30}$	$6\ 10^6$	
V30	$(As_2Te_3)_{80} . Si_{20}$	$7\ 10^4$	
V31	$As_{20} Te_{70} Ge_{10}$	250	
V33	$As_{30} Te_{48} Si_{12} Ge_{10}$	$1.2\ 10^4$	
V37	$(As_2Te_3)_{65} . Si_{35}$	$3\ 10^7$	
V38	$As_{55} Te_{35} Ge_{10}$	$1.5\ 10^3$	
V39	$As_{20} Te_{75} Si_5$		
V40	$As_{30} Te_{62} Si_8$		
V41	$(As_2Te_3)_{90} . Si_{10}$	$2\ 10^3$	

fig 3.28.

2. Properties of thin films

Nomenclature

Each glass evaporation was denoted by the letter 'E' followed by a number which identified the run, i.e. experimental conditions, glass composition, etc. When a film was evaporated on more than one substrate during a run, the substrates were labelled, A, B, C.... Each device on a substrate was given a number. Thus a typical notation would be: E56A.10. This is the 10th device on substrate A produced during evaporation no. 56.

Details of films

NUMBER	BULK GLASS	EVAPORATION TECHNIQUE	SANDWICH RESISTIVITY ρ_a (KΩ.m)	ΔE (eV)	THICKNESS (μm)	V_{th} (volts)	τ, THERMAL TIME CONSTANT (μs).
E51C	V31	BOAT	0.2	0.44	1.6		35
E52C	V31	BOAT	0.05	0.42	1.7	3.1	40
E53C	V29	BOAT	0.4	0.40	0.5	3.3	0.4
E54B	V33	BOAT	0.3	0.43	0.35	1	
E55C	V33	BOAT	2	0.43	0.9	3.7	2
E56A	V29	BOAT	3	0.46	1.1	8.5	0.7
E56B			2.5	0.46	0.8	9.3	0.8
E56C			3.6	0.46	0.45	6	1.1
E57A	V29	BOAT	0.8	0.48	0.45	4.7	
E57B			0.8	0.48	0.75	3.3	1
E58B	V37	BOAT	2	0.45	0.45	3.9	
E58C			2	0.45	0.45	6	
E64A	V31	BOAT	0.04		0.5	2	25
E64B			0.04		0.7	1.5	30
E68A	V28	FLASH	220		1.05	19	
E70A	V28	ELECTRON BEAM	250		1.2	11	
E71B	V33	ELECTRON BEAM	1.2	0.49	0.55	1	
E73B	V37	FLASH	30	0.49	0.85	6	
E74C	V38	FLASH	60	0.46	0.35	4	
E75B	V41	FLASH	0.5	0.40	0.6	2.5	
E77C	V30	FLASH	2.5	0.43	0.3	0.9	
E78C	V38	FLASH	3	0.49	0.6	2.8	
E84E	V38	BOAT	10	0.42	2.0	25	
E86B	V38	BOAT	10	0.42	0.4	3.5.	

3. Bulk current - voltage - temperature data

V 20 glass figs. 6.2. - 6.4.

0°C		20°C		35°C		50°C		75°C		100°C.	
V VOLTS	I μA	V VOLTS	I μA	V VOLTS	I μA	V VOLTS	I μA	V VOLTS	I μA	V VOLTS	I μA
160	4	60	5	10	2	5	2	5	5	5	10
180	5	80	6	20	4	10	4	10	12	10	20
200	6	100	8	30	5	20	8	20	27	20	50
220	7	120	10	40	7	30	12	30	45	30	90
240	7	140	12	50	9	40	17	40	70	40	160
260	8	160	16	60	11	50	23	50	100	50	280
280	9	180	20	70	14	60	29	60	160		
300	10	200	25	80	16	70	37				
320	12	220	30	90	19	80	46				
340	14	240	34	100	22	90	60				
360	16	260	40	120	32	100	75				
400	22	280	46	140	45	110	95				
440	35	300	60	160	65	120	150				

TEMPERATURE (°C)	R_Ω (MΩ)	V_{th} (VOLTS)	V_0	I_{th} (μA)	I_0	$V_{th}I_{th}$ (mW).
−10	67	>600				
0	42	450	139	40	1.3	18
10	25	330		50		17
20	16	260	97	100	3	26
27	11	220		100		22
31	9	200		100		20
35	5.7	170	58	120	4	20
41	4.4	150		150		23
48	2.95	135		200		27
51	2.75	130	41	200	7	26
55	2.5	115		200		23
60	2.1	105		220		23
65	1.74	96		300		29
70	1.43	78		300		23
75	1.33	80	22.6	400	11	32
80	0.95	75		450		34
85	0.80	72		500		36
90	0.77	67		500		33
95	0.62	63		600		38
100	0.50	56	17.4	800	15	45

4. Coplanar electrode/thin film current - voltage - temperature data

Sample E84A.2 figs. 6.11. - 6.13.

293K		310K		320K		330K	
V VOLTS	I μA	V VOLTS	I μA	V VOLTS	I μA	V VOLTS	I μA.
50	6	30	10	20	10	10	8
80	10	50	16	40	20	20	16
100	13	60	19	60	30	40	36
120	15	75	25	80	44	60	55
140	19	90	30	100	60	80	80
200	32	100	33	120	80	100	105
250	44	120	39	140	105	120	135
300	65	140	48	160	135	140	180
		160	68	180	190	150	250
		180	90				
		200	110				

340K		350K		360K	
V VOLTS	I μA	V VOLTS	I μA	V VOLTS	I μA
20	28	10	17	10	25
40	58	20	36	20	54
50	70	30	52	30	85
60	85	40	72	40	115
80	125	50	95	50	150
100	180	60	125	60	190
110	250	70	160	70	240
120	350	80	200	80	310
		90	250	90	450
		100	320		

TEMPERATURE (K)	$R_\square$ (MΩ)	V_{th} (VOLTS)	V_o	I_{th} (μA)	I_o
293	8.0	350	120	150	5.7
310	3.0	210	83	200	10
320	2.0	190	72	250	14
330	1.25	160	62	300	21
340	0.71	130	50	350	26
350	0.59	110	44	400	33
360	0.40	100	42	600	44

5. Sandwich electrode/thin film current - voltage - temperature - thickness data

Samples E56A.1 1.1 μm thick (Joule heating component
E56B.1 0.8 μm of current removed)
E56C.1 0.45 μm

	296K		320K		340K		360K	
	V VOLTS	I mA	V VOLTS	I mA	V VOLTS	I mA	V VOLTS	I mA.
E56A.1	1	0.065	0.5	0.13	0.18	0.17	0.17	0.32
	1.5	0.09	1	0.30	0.55	0.48	0.5	1.0
	2	0.13	1.5	0.45	0.9	0.7	0.82	1.8
	2.5	0.17	2	0.65	1.8	1.8	1.65	3.5
	3	0.21	2.4	0.80	2.3	2.3	2.1	4.2
	3.5	0.26	2.9	0.95	2.7	2.8	2.5	4.6
	4	0.30	3.4	1.2	3.2	3.3	2.9	6.0
	4.5	0.36	3.9	1.4	3.6	3.8	3.3	6.8
	5	0.40	4.4	1.6	4.1	4.4	3.7	8.0
V_{th} →	5.8	0.50	4.8	1.9	4.5	5.2	4.0	10
E56B.1	1	0.17	0.5	0.4	0.3	0.9	0.24	1.6
	1.5	0.28	1.4	1.5	0.6	1.8	0.48	3.2
	2	0.42	1.8	2.25	1.2	3.4	0.62	3.8
	2.7	0.60	2.2	2.8	1.9	5.8	1.0	5.8
	3	0.65	2.7	3.5	2.3	6.8	1.3	7.4
	3.4	0.80	3.1	4.2	2.6	8.5	1.5	10
	3.9	1.0	3.5	5.2	2.9	11	1.8	12
	4.4	1.2	3.9	6.2	3.2	13	2.05	14.5
V_{th} →	4.85	1.5	4.3	7.2	3.4	16	2.25	17.5
E56C.1	1	0.48	0.4	0.75	0.14	0.64	0.1	1
	1.4	0.84	0.85	1.5	0.27	1.3	0.18	2.2
	1.9	1.2	1.3	2.4	0.55	2.5	0.27	3.3
	2.3	1.65	1.6	4	0.68	3.2	0.36	4.4
	2.8	2.2	2.0	5	1.0	4.8	0.50	5.2
	3.2	2.7	2.4	6	1.35	6.5	0.7	7.8
	3.6	3.5	2.7	7.7	1.6	8.8	1	10
	4.1	4.4	3.1	9	1.9	11	1.15	13.5
	4.4	5.5	3.4	11	2.2	13	1.4	16
			3.7	13	2.4	15.5	1.6	19
					2.7	18	1.8	22
V_{th} →	4.4	5.5	3.7	13	2.8	22	1.9	26

6. Sandwich electrode/thin film current - voltage - temperature - thickness data

Samples E57A.10 0.45 μm thick (Joule heating component
E57B.7 0.75 μm of current removed)
E57C.2 0.2 μm

298K

E57A.10		E57B.7		E57C.2	
V VOLTS	I mA	V VOLTS	I mA	V VOLTS	I mA
0.19	0.12	0.48	0.2	0.18	0.15
0.38	0.24	0.96	0.4	0.37	0.34
0.56	0.40	1.4	0.68	0.54	0.55
0.74	0.57	1.9	0.9	0.7	0.8
0.93	0.70	2.4	1.25	0.9	1.0
1.4	1.2	2.8	1.6	1.3	2.0
1.8	1.7	3.3	2.0	1.7	3.0
2.3	2.4			2.0	4.6
2.7	3.2			2.4	6.4
3.1	4.1			2.6	8.8
3.5	5.0			2.9	11
3.9	6.3				
4.2	8.2				

E57A.10

310K		330K		350K		370K	
V VOLTS	I (mA)	V VOLTS	I mA	V VOLTS	I mA	V VOLTS	I mA
0.18	0.24	0.15	0.5	0.1	0.9	0.07	1.3
0.35	0.52	0.28	1.2	0.2	1.9	0.12	2.8
0.51	0.85	0.41	1.9	0.3	2.8	0.19	4.1
0.68	1.25	0.53	2.7	0.4	3.8	0.24	5.6
0.84	1.55	0.65	3.5	0.54	4.6	0.3	7.0
1.25	2.5	1.0	5.2	0.8	7.2	0.45	10
1.65	3.5	1.3	6.6	1.0	10	0.65	13
2.0	4.6	1.6	8.8	1.25	12.5	0.8	17
2.4	5.6	1.9	11	1.45	15.5	0.9	21
2.8	7.0	2.2	13	1.6	19	1.0	25
3.1	8.8	2.4	16	1.8	22	1.1	29
3.4	11	2.6	19	1.9	26		
3.7	13.5	2.8	22	2.0	30		

APPENDIX 2 (related to paras. 6.4.2 - 6.4.5)

Hopping Processes in Amorphous Semiconductors

In an amorphous semiconductor which has a high density of localized states there are 3 possible processes of one-carrier charge transport, each of which has been described in the literature as hopping.

1. Thermally assisted tunnelling.

The carriers jump by quantum mechanically tunnelling between two relatively close sites which are separated by only a small energy, W. The conductivity is given by an expression of the form:

$$\sigma = \sigma_1 \exp\left(-\frac{W}{kT}\right) \exp\left(-2\alpha a\right)$$

where σ_1 is a constant, a is the jump distance and α is a tunnelling parameter which is determined by the trap depth below the conduction band.

This form of hopping is important in a.c. conductivity measurements, but is probably not significant in d.c. measurements.

2. Hopping from neutral traps.

A carrier is released from a trap (leaving the trap uncharged) and retrapped at another site. The carrier must be excited into a region of the gap when the mobility is relatively high. For deep traps close to the Fermi level, this implies a relatively large activation energy, E. This process is field dependent

and is described by a sinh-expression as in equation 6.12.

3. The Poole-Frenkel process.

A high field lowers the coulombic potential barrier around a centre which is charged when not occupied by a carrier. Although it is usually implied that carriers are excited into the conduction band, this is not essential; they only need to be excited into a region where the mobility is relatively large.

Comment

Unless the nature of the trapping site can be identified, i.e. whether it is charged or uncharged when full, then it may be difficult to distinguish between processes 2 and 3. Superficially both give similar current-voltage relations. However, to obtain the field dependence observed in the experimental work, process 2 does require the jump distance to be exceptionally large ($\sim$10 - 20 nm.).

With the results available, a specific conduction process cannot be uniquely identified. This does not affect the thermal breakdown analysis which requires only an expression for (E,T).